NON-OHMIC EFFECTS AND GALVANOMAGNETIC PHENOMENA IN QUANTUM CONFINED SEMICONDUCTOR STRUCTURES AT LOW AND SOME OTHER LATTICE TEMPERATURES

THESIS SUBMITTED FOR THE DEGREE OF
DOCTOR OF PHILOSOPHY IN SCIENCE (PHYSICS)
OF
JADAVPUR UNIVERSITY
2023

BY

BITTU ROY
DEPARTMENT OF PHYSICS
JADAVPUR UNIVERSITY
KOLKATA-700 032

যাদবপুর বিশ্ববিদ্যালয়
কলকাতা-৭০০ ০৩২, ভারত

*JADAVPUR UNIVERSITY
KOLKATA-700 032,INDIA

FACULTY OF SCIENCE : DEPARTMENT OF PHYSICS

TO WHOM IT MAY CONCERN

This is to certify that the thesis entitled "**NON-OHMIC EFFECTS AND GALVANOMAGNETIC PHENOMENA IN QUANTUM CONFINED SEMICONDUCTOR STRUCTURES AT LOW AND SOME OTHER LATTICE TEMPERATURES**" submitted by Sri. **Bittu Roy**, who got his name **registered on 30.01.2018** for the award of **Ph.D. (Science) degree of Jadavpur University**, is absolutely based upon his own work under the Supervision of **Dr. (Mrs.) Sulava Bhattacharyya** and that neither this thesis nor any part of it has been submitted for either any degree/diploma or any other academic award anywhere before.

Sulava Bhattacharyya
.....

26/09/2023

Dr. (Mrs.) Sulava Bhattacharyya
Associate Professor
Department of Physics
Jadavpur University
Kolkata 700 032

Dr. (Mrs.) Sulava Bhattacharyya
Associate Professor
Dep[illegible] of Physics
Jadavpur University
Kolkata-700 032

Dedicated to

The memory of my deceased father

And to my mother

ACKNOWLEDGEMENTS

This thesis would be absolutely incomplete without my sincere expression of gratitude to one and all who helped me in my endeavour in some way or other.

The very first one to mention is my supervisor, Dr. Sulava Bhattacharyya for her invaluable guidance and support throughout my Ph.D. journey. She has guided me steadfastly throughout my research studies with her patience and knowledge, and always encouraged me to work in my own way. Her untiring support through illuminating discussions and invaluable advice have inspired me to work with determination.

I thankfully acknowledge the financial support from the University Grants Commission, New Delhi, India, in the form of UGC-NET-JRF. I would also like to thank Jadavpur University for providing me the infrastructural support that I needed to complete this thesis.

I am also grateful to my senior Dr. S. Nag for helpful discussions and to my colleagues who have supported me in numerous ways, both professionally and personally. Their camaraderie and encouragement have made the long hours of my research work more bearable. The help rendered by Prof. D.P. Bhattacharya is duly acknowledged.

Finally, I would like to thank my family for their unconditional love and unwavering support throughout my academic journey. Their belief in me and my abilities has been a constant source of motivation.

Department of Physics
Jadavpur University
Kolkata 700 032
India

Bittu Roy 26.09.2023

BITTU ROY

CONTENTS

		Page No
List of publications		viii-ix
Conferences attended		x
List of symbols		xi-xv
Chapter I	**Introduction, basic assumptions and scope of the thesis**	1-19
1.1	Introduction	1
1.2.1	Basic assumptions	10
1.2.2	Concepts and specific features of low lattice temperature	13
1.3	Scope of the thesis	16
Chapter II	**Some basic physics and properties of quantum confined semiconductor structure**	20-41
2.1	Introduction	20
2.2	Electron confinement by the quantum well in a semiconductor structure	20
2.3.1	Types of quantum wells in semiconductor structure	20
2.3.2	Envelope functions for different wells and energy eigenvalues	21
2.4	Low dimensional semiconductor structure	24
2.4.1	Electron fundamental lengths in solids	24
2.4.2	(a) Wave function, energy dispersion, wave vector element, (b) Density of states function for different structures, subband energy, (c) Equilibrium carrier concentration, (d) Current density	25
2.4.3	Importance of low dimensional structures from the view point of device applications	32
2.5	Heterostructures	32
2.5.1	Subband energy	32

2.5.2	Modulation doping	33
2.5.3	Phenomenon of screening	35
2.5.4	General properties	35
2.6	Some widely used structures which support 2DEG	36
2.7	Scattering mechanisms	40
Chapter III	**Non-ohmic two-dimensional electron ensemble in a quantum well of a compound semiconductor**	42-69
3.1	Introduction	42
3.1.1	Types of electron ensemble	42
3.1.2	Effect of high D.C. electric field on the energy distribution of an electron ensemble	44
3.1.3	Concept of effective temperature of an electron ensemble	45
3.1.4	Applicability of the effective temperature approximation	46
3.2	Method of calculation of the electron temperature characteristics	47
3.2.1	Energy balance condition for the electron-phonon system	47
3.3	Calculation of the collision integrals	47
3.4	Matrix elements for various interactions of the two-dimensional electrons with lattice imperfections	48
3.5	Calculation of the rate of change of the isotropic part of the high-field distribution function of the electrons in a degenerate ensemble of 2DEG for interaction with phonons	51
3.5.1	Interaction with deformation potential acoustic phonons	52
3.5.2	Interaction with piezoelectric acoustic phonons	53
3.6	Calculation of the rate of change of the isotropic part of the high-field distribution function of the electrons in a degenerate ensemble of 2DEG due to an applied field	54
3.7	Calculation of the field dependence of the electron temperature of different surface layers for interaction with phonons	54

3.7.1	Case of a moderately degenerate layer under different conditions	55
(i)	When the electrons interact only with the deformation potential acoustic phonons	55
(ii)	When the electrons interact only with the piezoelectric acoustic phonons	55
(iii)	For the combined interaction with both the deformation potential acoustic and the piezoelectric acoustic phonons	56
3.7.2	Case of a highly degenerate layer of an ensemble of 2DEG under the condition of the combined interaction of the electrons with the deformation potential acoustic and the piezoelectric acoustic phonons	56
3.7.3	Case of a non-degenerate layer of an ensemble of 2DEG	57
(i)	When the electrons interact only with the deformation potential acoustic phonons	57
(ii)	When the electrons interact only with the piezoelectric acoustic phonons	58
(iii)	For the combined interaction with both the deformation potential acoustic and the piezoelectric acoustic phonons	58
3.8	Results for the field dependence of the effective electron temperature for the quantum confined surface layers of 2DEG in InSb, GaAs and GaN, with different levels of degeneracy, and their comparison with the theoretical and the experimental results which are available from other studies	58
3.9	Discussions	66
Chapter IV	**Energy loss rate and non-ohmic mobility of a degenerate two-dimensional ensemble in a quantum well of compound semiconductors**	70-93
4.1	Introduction	70

4.2	Brief review of the studies on the energy loss rate of electrons in quantized surface layer	71
4.3	Method of calculation of energy loss rate of the electrons in surface layers of compound semiconductors	74
4.4	Calculation of the rate of loss of energy of non-equilibrium 2DEG in different surface layers	74
4.4.1	Case of a moderately degenerate layer under different conditions	74
(i)	When the electrons interact only with the deformation potential acoustic phonons	74
(ii)	When the electrons interact only with the piezoelectric acoustic phonons	75
(iii)	For the combined interaction with both the deformation potential acoustic and the piezoelectric acoustic phonons	75
4.4.2	Case of a highly degenerate surface layer for the combined interaction of the electrons with both the deformation potential acoustic and the piezoelectric acoustic phonons	75
4.4.3	Case of a non-degenerate surface layer under different conditions	76
(i)	When the electrons interact only with the deformation potential acoustic phonons	76
(ii)	When the electrons interact only with the piezoelectric acoustic phonons	76
(iii)	For the combined interaction with both the deformation potential acoustic and the piezoelectric acoustic phonons	77
4.5	Results for the dependence of average ELR of an electron in a non-equilibrium ensemble of 2DEG upon the normalised electron temperature on the surface layers of InSb, GaAs and GaN with different levels of degeneracy	77
4.6	Discussions	81

4.7	Brief review of the studies on the non-ohmic mobility characteristics of electrons in quantized surface layer	82
4.8	Method of calculation of non-ohmic mobility characteristics	84
4.9	Calculation of non-ohmic mobility characteristics of an ensemble of 2DEG from the expression for the average ELR	85
4.10	Calculation of non-ohmic mobility characteristics of 2DEG from the expression for the current density	87
4.10.1	Case of a moderately degenerate layers under different conditions	87
(i)	When the electrons interact only with the deformation potential acoustic phonons	87
(ii)	When the electrons interact only with the piezoelectric acoustic phonons	88
(iii)	For the combined interaction with both the deformation potential acoustic and the piezoelectric acoustic phonons	88
4.10.2	Case of a highly degenerate layer for the combined interaction of the electrons with both the deformation potential acoustic and the piezoelectric acoustic phonons	88
4.10.3	Case of a non-degenerate layers under different conditions	88
(i)	When the electrons interact only with the deformation potential acoustic phonons	88
(ii)	When the electrons interact only with the piezoelectric acoustic phonons	89
(iii)	For the combined interaction with both the deformation potential acoustic and the piezoelectric acoustic phonons	89
4.11	Results for the field dependence of non-ohmic mobility of the non-equilibrium electrons which are confined to the quantum wells on the surface layers of InSb, GaAs and GaN with different levels of degeneracy	89
4.12	Discussions	93

Chapter V	**Microwave harmonic generation in a quantum well of compound semiconductors**	94-110
5.1	Introduction	94
5.2	Brief review of the studies on the characteristics of Harmonic Generation in semiconductor structures	95
5.3	Method of calculation of the efficiency of SHG in an ensemble of 2DEG	96
5.4	Results for the dependence of the efficiency of SHG upon the biased field in quantum surface layers of InSb, GaAs and GaN with different levels of degeneracy	98
5.5	Discussions	107
Chapter VI	**Galvanomagnetic phenomena in a two-dimensional ensemble of electrons in a quantum well of a heterostructure of compound semiconductors**	111-133
6.1	Introduction	111
6.2	Brief review of the studies on the Hall mobility of two-dimensional electrons in quantum well structures	111
6.2.1 (i)	The case of an ohmic ensemble	113
6.2.2	Method of calculation of temperature dependence of Hall mobility for an ohmic and degenerate ensemble of Q2D in a modulation-doped heterostructure	114
6.2.3	The transition probability for interaction with different lattice imperfections	115
6.2.3.1	Deformation potential acoustic scattering	116
6.2.3.2	Piezoelectric acoustic phonons scattering	117
6.2.3.3	Remote ionized impurity scattering	118
6.2.3.4	Background ionized impurity scattering	118
6.2.3.5	Surface roughness scattering	118

6.2.4	Results for the dependence of Hall mobility of an ohmic degenerate ensemble of Q2D upon the lattice temperature in AlGaAs/GaAs, AlGaN/GaN and AlInSb/InSb heterostructures	118
6.2.5	Discussions	124
6.3.1 (ii)	The case of a non-ohmic ensemble	125
6.3.2	Method of calculation of the Hall mobility of a non-ohmic ensemble of Q2D in a modulation-doped heterostructure	126
6.3.3	Energy loss rate of the non-equilibrium electrons due to interaction with the deformation potential acoustic phonons	127
6.3.4	Energy loss rate of the non-equilibrium electrons due to the interaction with the piezoelectric acoustic phonons	128
6.3.5	Results for the field dependence of the Hall mobility of a non-ohmic degenerate Q2D in AlGaAs/GaAs, AlGaN/GaN and AlInSb/InSb heterostructures	128
6.3.6	Discussions	132

Appendix A 134

Appendix B 136

Appendix C 138

Appendix D 140

Appendix E 141

Appendix F 142

Appendix G 146

Appendix H 149

Appendix I 152

References 155

LIST OF PUBLICATIONS

Journal papers:

[1] Heating of a degenerate electron ensemble in a well of compound semiconductors at low lattice temperatures
B. Roy, S. Bhattacharyya, D.P. Bhattacharya
Applied Physics A 125: 223 (2019).
https://doi.org/10.1007/s00339-019-2494-z

[2] Energy loss rate and non-ohmic characteristics of a degenerate surface layer of compound semiconductors at low lattice temperatures
B. Roy, S. Bhattacharyya, D.P. Bhattacharya
Physica E: Low-dimensional Systems and Nanostructures 126, 114465 (2021).
https://doi.org/10.1016/j.physe.2020.114465

[3] Generation of microwave harmonics by non-ohmic surface layers in quantum wells of compound semiconductors at low lattice temperatures
B. Roy, S. Bhattacharyya, D.P. Bhattacharya
Journal of Physics and Chemistry of Solids 169, 110858 (2022).
https://doi.org/10.1016/j.jpcs.2022.110858

[4] A comprehensive study on the Hall mobility of an ohmic ensemble of two-dimensional electrons confined in a quantum well of a heterostructure at low lattice temperatures
B. Roy, S. Bhattacharyya, D.P. Bhattacharya
Canadian Journal of Physics 101(6), 262-274 (2023).
https://doi.org/10.1139/cjp-2022-0144

Conference papers:

[1] Non-Ohmic Characteristics of a Quantum Confined Degenerate Ensemble of Carriers in a Well of GaAs at Low Lattice Temperature
B. Roy, S. Bhattacharyya, D.P. Bhattacharya
In: Das N.R., Sarkar S. (eds) Computers and Devices for Communication. CODEC 2019. Lecture Notes in Networks and Systems, Vol 147. Springer, Singapore.
https://doi.org/10.1007/978-981-15-8366-7_55

[2] An inclusive theory of the Hall mobility of a non-ohmic degenerate ensemble of two-dimensional electrons in a modulation-doped AlGaN/GaN heterostructure at low lattice temperature

B. Roy, S. Bhattacharyya, D.P. Bhattacharya

AIP Conference Proceedings (In Press)

CONFERENCES ATTENDED

[1] National Conference on Condensed Matter Physics 'Condensed Matter Days-2019' (CMDAYS19)

Organized by Department of Physics, Vidyasagar University, Midnapore-721102, West Bengal, India.

Held on August 29-31, 2019 at Vidyasagar University, Midnapore, West Bengal, India.

[2] 7th International Conference on Computers and Devices for Communication (CODEC-2019)

Organized by Institute of Radio Physics and Electronics, University of Calcutta.

Held on 19-20, 2019 at Hotel Vivanta, Kolkata, India.

[3] 66th DAE Solid State Physics Symposium

Organised by Bhabha Atomic research centre, Mumbai.

Sponsored by Board of Research in Nuclear Science (BRNS), Department of Atomic Energy, Government of India.

Held on 18-22 December 2022 at Birla Institute of Technology Mesra, Ranchi, India.

LIST OF SYMBOLS

a	lattice constant
ac	acoustic
A	surface area
$A_i(z)$	Airy function of first kind
b	variational parameter associated with Fang-Howard wave function
bg	background impurities
$\vec{B}$	applied magnetic field
B_m	Bernoulli number
$B_i(z)$	Airy function of second kind
d	width of the layer of lattice atoms with which the electrons can interact
d_s	spacer layer width
deg	degenerate
$D_n(\varepsilon_{\vec{k}})$	density of states function of electrons in the nth dimensional structure
e	electronic charge
eff	effective
E_a	deformation potential
$E_1(z)$	exponential integral function
$\vec{E}$	applied electric field
E_s	surface electric field
E_0	high d.c. electric field
E_1	amplitude of microwave electric field
f	frequency of the a.c. microwave field
$f(\vec{k})$	carrier distribution function in wave vector space
$f_0(\vec{k})$	isotropic part of the distribution function of the electrons
$f_0(\varepsilon_{\vec{k}})$	Fermi-Dirac distribution function
$f_0^n(\varepsilon_{\vec{k}})$	n^{th} derivative of the Fermi function with respect to the electron energy

$F_1(q)$	form factor for the supplementary material
$F_2(q)$	form factor for the core material
$F_j(x)$	Fermi integral of jth order
g_v, n_v	valley degeneracy factor
$G(q_z)$	form factor
h	Planck's constant
$\hbar$	reduced Planck's constant
$H(x)$	Heaviside step function
H'	perturbing potential
$\vec{J}$	current density
J_m	amplitude of the mth harmonic
J_1	fundamental component of current density
J_2	second harmonic component of current density
k_m	piezoelectric coupling constant
$\vec{k}$	in-plane wave vector of a carrier before scattering
$\vec{k}'$	in-plane wave vector of a carrier after scattering
k_x, k_y, k_z	components of $\vec{k}$ along x, y and z directions respectively
K_B	Boltzmann constant
L_x, L_y, L_z	dimensions of the semiconductor structure along x, y and z directions respectively
m_0	free mass of an electron
m^*	effective mass of an electron
m_1, m_2	effective mass of an electron along x and y directions respectively
$m_{\parallel}^*$	effective mass of an electron parallel to the surface
$m_{\perp}^*$	effective mass of an electron perpendicular to the surface
$\overleftrightarrow{M}$	reciprocal effective mass tensor of an electron
$M(\vec{k},\vec{k}')$	matrix element for scattering by crystal imperfections
non-deg, nd	non-degenerate

N_c	effective density of states in the conduction band
$N_i,\ n_{2D},\ n$	surface layer concentration
N_i^B	background ionized impurities density
N_i^r	remote ionized impurities density
$N_{\vec{q}},\ N_{\vec{Q}}$	phonon population
pz	piezoelectric
$P\left(\varepsilon_{\vec{k}}\right)$	net scattering rate of an electron
$P_i\left(\varepsilon_{\vec{k}}\right)$	scattering rates of an electron for the ith scattering
$\vec{q}$	two-dimensional phonon wave vector
$\vec{Q}$	three-dimensional phonon wave vector
q_z	transverse component of phonon wave vector
$\vec{r}$	position vector
rm	remote impurities
sr	surface roughness
$S\left(\vec{q}\right)$	screening factor
T_e	effective electron temperature
T_L	lattice temperature
u_l	average acoustic velocity
u_{th}	average thermal velocity of an electron in thermodynamic equilibrium
w	$\left(=\varepsilon_{\vec{k}}/K_BT_L\right)$
X	$\left(=\hbar\omega_{\vec{Q}}/K_BT_L\right)$, normalized phonon wave vector
α	screening length
β_1	$\left(=1-K_BT_L/\varepsilon_F\right)$
β_2	$\left(=1+K_BT_L/\varepsilon_F\right)$
γ_n	roots of the equation $A_i\left(-\gamma_n\right)=0$
$\delta\left(x\right)$	Dirac delta function

Δ	average height of the roughness in the z-direction
$\varepsilon_{\vec{k}}$	energy of a carrier in the wave vector state $\vec{k}$ before scattering
$\varepsilon_{\vec{k}'}$	energy of a carrier in the wave vector state $\vec{k}'$ after scattering
ε_F	Fermi energy
ε_g	energy bandgap
ε_e	$\left(= K_B T_e\right)$
ε_L	$\left(= K_B T_L\right)$
ε_{ph}	phonon energy
ε_s	$\left(= m_{\|\|}^* u_l^2 / 2\right)$
ε_n	energy eigenvalue of the nth subband
ε_0	energy of the lowest subband
$\in_{sc}$	permittivity of the material
η	efficiency of second harmonic generation
η_D	$\left(= \varepsilon_F / K_B T_L\right)$, normalized Fermi energy
λ	de Broglie wavelength
λ_0	de Broglie wavelength of free electron
Λ	spatial extent of the roughness in the direction parallel to the interface
θ	angle between $\vec{k}$ and $\vec{E}$
$\theta_{\vec{k}}$	angle between the states $\vec{k}$ and $\vec{k}'$
$\theta_{\vec{k}\vec{q}}$	angle between $\vec{k}$ and $\vec{q}$
μ_{eff}	effective mobility
μ_0	low-field mobility
$\left(\mu_0\right)_{ac}$	low-field mobility for interaction with the deformation potential acoustic phonons
$\left(\mu_0\right)_{pz}$	low-field mobility for interaction with the piezoelectric acoustic phonons
$\mu\left(E\right)$	high-field mobility
μ_H	Hall mobility

$(\mu_H)_{ac}$	Hall mobility for interaction with the deformation potential acoustic phonons
$(\mu_H)_{bg}$	Hall mobility for interaction with the background ionized impurities
$(\mu_H)_{pz}$	Hall mobility for interaction with the piezoelectric acoustic phonons
$(\mu_H)_{rm}$	Hall mobility for interaction with the remote ionized impurities
$(\mu_H)_{sr}$	Hall mobility for interaction with the surface roughness
μ_{xx}, μ_{xy}	anisotropic mobilities
$\mu_{xx}(0)$	value μ_{xx} of in the absence of the magnetic field $\vec{B}$
$\xi_x(\varepsilon_{\vec{k}})$	perturbation function in x-direction
$\xi_y(\varepsilon_{\vec{k}})$	perturbation function in y-direction
$\zeta_n(z)$, $F(z)$	envelope wave function
ρ_v	volume mass density
σ	electrical conductivity
τ, τ_{eff}	effective relaxation time of the collision
τ_e	energy relaxation time
τ_m	momentum relaxation time
τ_n	$(=\tau_{acm}/\tau_{pzm})$
$\phi(z)$	surface potential
$\psi_{\vec{k}}$	wave function of the electron
ψ_{1e}, ψ_{2e}	wave functions of the ground state and next higher energy state of the electron respectively
$\Psi_{F-H}(z)$	Fang-Howard wave function
ω	angular frequency
ω_B	$(=eB/m_{\parallel}^*)$ cyclotron resonance frequency
$\omega_{\vec{q}}$	frequency of lattice vibration for any wave vector $\vec{q}$
$\omega_{\vec{Q}}$	frequency of lattice vibration for any wave vector $\vec{Q}$

CHAPTER I

INTRODUCTION, BASIC ASSUMPTIONS AND SCOPE OF THE THESIS

The use of electronic gadgets has become indispensable for our daily life. The technological advancement of the process of designing and fabrication of semiconductor devices is already quite phenomenal. It is now possible to fabricate elegant quantum well devices which are not only practically more useful but are also economically more viable. This in turn has resulted in quite significant boost of the electronics industry and hence of the world economy.

The comprehension of the performance of a semiconductor device structure and subsequently to strive for its improvement, demands the knowledge of the physics of the constituent semiconductor materials the device is made of. In course of achieving such knowledge newer ideas, theories etc. have been developed. That in turn led to numerous newer devices and circuits which possesses more useful and challenging applications and paves the way for more exciting developments in this rapidly growing field. Almost insatiable demand for faster and faster devices, which again operate at smaller and smaller input power demands scaling down the device sizes. All these have led to realisation of quantum-confined, low-dimensional semiconductor structures. Hence, to work in this field is a challenging task and thus inspires future worker in this field.

1.1 Introduction

Moderate doping of a sample of bulk semiconductor gives rise to discrete energy levels, so to speak, the impurity levels, in the band gap. The carriers within the bulk material are not confined in any way, and thus they have three degrees of freedom. They move freely along the three dimensions.

Apart from that, discrete energy levels for electrons and holes may also be created, when these carriers are confined to various quantum wells (QW), which can be fabricated in different semiconductor structures. Thus, on being confined to such QW's, the carriers may lose one or more degrees of freedom, depending upon the number and relative orientation of these fabricated wells. Under these conditions, the carriers can no longer move freely along all the three dimensions. Consistent with the lesser number of degrees of freedom, their free motion

is now limited by the constraints arising from the quantum wells. In such semiconductor structures, the electrons move freely, either on a specific surface only, or along a specific direction. Whereas their motion along the transverse direction(s) is now quantised.

All these make the electrical transport of the carriers in such quantum-confined structures, characteristically much different from what follows for the bulk materials [1-5].

The great advancement in the crystal growth techniques, like that of molecular beam epitaxy (MBE) or that of metal-organic vapour-phase epitaxy (MOVPE) has made it possible to grow multi-layered, continuous single crystal, in which the adjacent layers have different band gap $\left(\varepsilon_g\right)$. This results in a quantum well in the structure, where the carriers may get confined. As an example, a simple quantum well may be produced by growing a multi-layered structure, consisting of a thin layer of GaAs $\left(\varepsilon_g = 1.43\ eV\right)$, sandwiched between two layers of AlGaAs $\left(\varepsilon_g = 1.85\ eV\right)$. The Figures 1.1 and 1.2 represent a rough sketch of such a prototype structure along with its approximate band model.

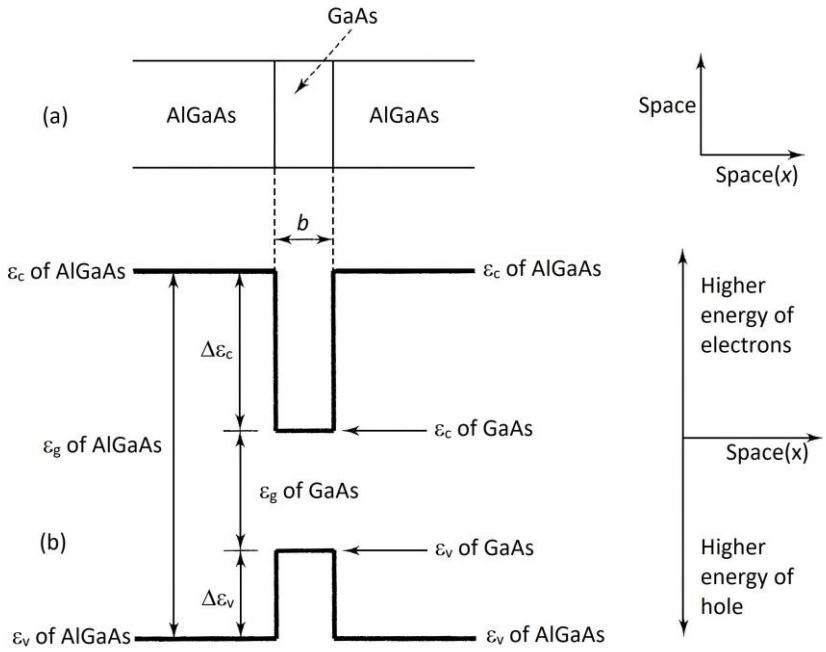

Figure 1.1 (a) Material structure and (b) band model of GaAs/AlGaAs Quantum well (QW). ε_c is lower edge of conduction band and ε_v is upper edge of valence band. ε_g is band gap. $\Delta\varepsilon_c$ is conduction band offset and $\Delta\varepsilon_v$ is valence band offset. There is a QW for electrons in CB and there is a QW for holes in valence band. We often taken $\Delta\varepsilon_c : \Delta\varepsilon_v = 65:35$.

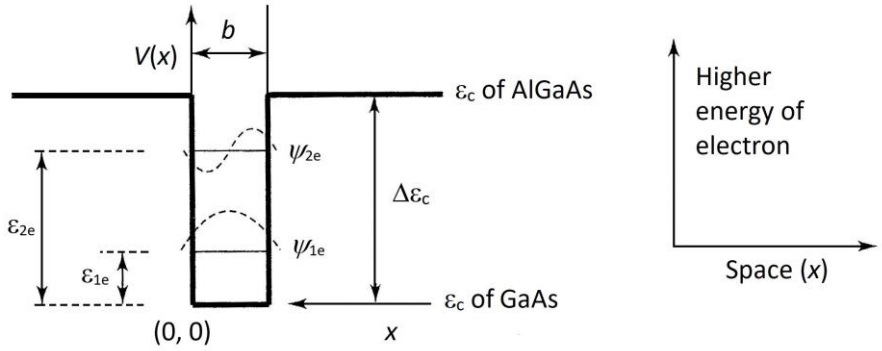

Figure 1.2 Showing electronic structure of QW for electrons in conduction band. ε_{1e}, ε_{2e} are allowed values of kinetic energy as well as total energy of electron for motion only along x direction i.e., perpendicular to GaAs/AlGaAs interfaces inside the QW. Potential energy is zero inside the QW by choice of origin. Space part of ψ_{1e} and of ψ_{2e} associated with ε_{1e}, ε_{2e} are shown by dotted curves. Tails of ψ_{1e} and of ψ_{2e} extend outside the QW to some extent.

The figure displays how does the difference in the band gaps of the adjacent materials of the structure results in quantum wells for the electrons in the conduction band and for the holes in the valence band of GaAs. It may be pointed out here that due to charge redistribution at the interfaces, there would be some bending of band edges. However, such band bending may be usually neglected in the first approximation for all practical purposes.

The remarkable conjecture made by Esaki and Tsu [6], that the quantum confinement of the carriers in different semiconductor set-ups, may exhibit some novel and interesting properties from the viewpoints of both the basic physics and the subsequent device applications. Their presumption has earned great attention.

Hence, such a conjecture motivated extensive research, and development of so many quantum-confined semiconductor structures of substantial practical importance. Amongst so many set-ups one can refer to various heterostructures, the superlattices, the multi-quantum wells (MQW), the high electron mobility transistors (HEMT), the modulation-dope field-effect transistors (MODFET), the metal-oxide-semiconductor field-effect transistors (MOSFET), the quantum wires, the quantum dots, etc. The niceties of all these set-ups are adequately illustrated in [1-5]. However, since the present treatise mainly deals with quantum wells in heterostructures, the requisite description of the same may be outlined in what follows.

It is well known that a heterostructure consists of alternate ultrathin layers of two semiconductors having different band gaps. One can evaluate the electronic states in the structure by supposing that the bulk band structures may be applicable for the constituents, even when the dimension in one or more directions may be of the same order as that of the lattice constant.

A heterostructure gives rise to a periodic potential with a period commensurate with the sum of the widths of two successive layers.

For the layer thicknesses in the nanometre range, the wavelength, as well as the mean free path of the electrons, are now spread over several layers. The energy bands of the host lattice is now changed into mini bands.

It has been experimentally demonstrated by Störmer and others [7] that the electrons on the GaAs surface being confined to the QW at the interface of the AlGaAs/GaAs heterojunction, lose one degree of freedom, and thus forms an ensemble of two-dimensional electron gas (2DEG). In fact, 2DEG is not practicably realisable. What is realisable is a quasi-two-dimensional electron gas usually referred to as Q2D [2].

Under the condition, when the GaAs layer is taken to be quite undoped, but the AlGaAs layer is doped n-type, the electrons on being migrated to the low-lying conduction band of GaAs, form a layer of space charge at the interface. It is quite interesting to note here, that due to such segregation of the impurity atoms, which are confined to the barrier layer, the electrons in GaAs layer hardly suffer collision with the impurity atoms. This results in significantly higher values of the electron mobility there. This, in turn produces negative differential mobility at lower fields.

The present advancement in the crystal growth techniques has made it possible to grow heterostructures of any composition with crystalline perfections at the interfaces.

As has already been mentioned, the superlattice is one of the pre-eminent quantum-confined structure, which again exhibits novelty. Based on the idea floated by Esaki and Tsu [6], a superlattice structure may be fabricated by growing with sufficiently pure and perfect samples of n layers of GaAs and m layers of AlAs periodically. The novelty here lies in that, the Bloch oscillations may be observed in the superlattice structures having a very narrow Brillouin zone. Actually, the Bloch oscillation takes place, when, in the presence of a quite high electric field, the electrons, on being accelerated, reach the Brillouin zone edge without suffering any

collision, at sufficiently low temperatures. It may be mentioned here that a bulk structure cannot withstand such a high electric field and electrical breakdown readily takes place. However, on reaching the zone boundary in the superlattice, the electron suffer reflection there and begins to transit the zone in the reverse direction just to be reflected again from there. The process continues repeatedly. The resultant unimpeded motion of the electrons is thus oscillatory, and are termed Bloch oscillations.

Now some details of the quantum-confined structures needs to be elaborated. The physical dimensions of a semiconductor structures may produce significant effects on their electronic properties, when these dimensions are so reduced as to be comparable with the de Broglie wavelength λ. When the free carriers are confined along some direction(s) by means of a potential, they may lose some of their degrees of freedom. The dimensionality of the confinement may be described on comparing the geometrical sizes L_x, L_y and L_z along the x, y and z axes respectively with the de Broglie wavelength λ. The categorization of the semiconductor structures can be made as follows:

(a) Bulk structures: In such structures when $\lambda \ll L_x, L_y, L_z$, the electrons move as free particles in all the three directions. The electron ensemble in such structures is termed three-dimensional electron gas (3DEG).

(b) Quantum well structures: In such structures when $\lambda \sim L_z$ but $\lambda \ll L_x, L_y$, the motion of the electrons get quantized along the z-direction, but still they are free to move along the x and y directions. Hence, the electrons lose one degree of freedom. The electron ensemble in such structures is termed two-dimensional electron gas (2DEG).

(c) Quantum wire structures: In such structures when $\lambda \sim L_z, L_y$ but $\lambda \ll L_x$, the motion of the electrons get quantized along the y and z directions, but still, they are free to move only along the x direction. Hence, the electrons lose two degrees of freedom. The electron ensemble in such structures is termed one-dimensional electron gas (1DEG).

(d) Quantum dot structures: In such structures when $\lambda \sim L_x, L_y, L_z$, the motion of the electrons get quantized along all the three directions, and are not free to move freely in any of the directions. Hence, the electrons lose all the three degrees of freedom. The electron ensemble in such structures is termed as zero-dimensional electron gas (0DEG).

It has already been pointed out with little elaboration as regards how such quantum-confined structures can be realised in practice by exploiting the advanced epitaxial growth techniques. However, a little more elaboration is added in what follows now.

Several fabrication techniques can be applied to obtain quantum wire and dot structures. They include etching techniques, focused ion beam implantation, self-assembled growth techniques and area selective growth.

A standard quantum well layer can be patterned with photolithography technique, and etched to leave a free-standing strip of quantum well material. The latter may or may not be filled in with an overgrowth of the barrier material. The charge carriers are still confined along the heterostructure growth (z) axis. Moreover, provided the strip is narrow enough, they may now be confined along an additional direction, say the y axis, depending upon the lithography [8, 9].

Another class of quantum wires can be formed by patterning the substrate before growth. This leads to the formation of the so-called V-grooved quantum wires [10, 11].

Quantum dots can be formed when a quantum well sample is etched to leave pillars-like rather than wires structure, combining the area selective epitaxy and self-assembled growth technique well controlled quantum dots where a charge carrier become confined in all three dimensions can be achieved by using Selective Area Metalorganic Vapor Phase Epitaxy (SA-MOVPE) [12] and MBE [13].

Next, the question that arises in respect of the benefits which may be acquired due to the quantum confinement of carriers in such low-dimensional semiconductor structures. The practical benefits which can be accrued from a quantum-confined structure depend on the properties of the confined electron wave functions and their resulting energy levels. In principle, semiconductor structures of all sizes feature confined electronic states, but only in quantum-confined structures, the separation of these energy levels is so large as to be experimentally useful. The large energy separation between the energy levels is useful for applications in the areas like optoelectronics, nanophotonics, nanoelectronics, quantum computing, and bio-nanotechnology etc.

Since in quantum confined structures it is possible to segregate carriers from impurities, hence a large carrier concentration can be realised, unlike in bulk structures where the carrier concentration can be increased only with the increase in doping at the cost of the decrease in

the mobility values of the carriers. A larger carrier concentration in quantum-confined structures has enormous applications. From the device point of view the larger values of both the transport parameters, like the conductivity and the mobility, observed in low-dimensional structures would provide higher switching speeds and higher transconductance, and thus seem to be an ideal system for ultrafast and new ballistic devices [14, 15]. Such benefits of quantum-confined carriers have been observed in a number of low-dimensional devices. The advancement of the MBE techniques has made it possible to realise AlGaAs/GaAs heterostructures with low temperature mobility values exceeding $1\times10^{3}\ m^{2}/V.s$ [16-18]. The superior opto-electronic and transport properties of quantum well structures have been utilized to realize better performance characteristics of transistors, lasers and nonlinear optic devices.

Quantum wires and dots are already known to be promising structures for the future generation of nanoelectronic devices. Thin films with thicknesses approaching the few monolayer range are already in use in conventional devices in the microelectronics industry. But the quantum confinement of the electrons in the quantum dots makes the devices operate in entirely new ways. It has been physically possible that the single electron transistors, e.g., could take the advantage not only of the discrete spectrum of the energy levels in nanostructures, but also of the so-called Coulomb blockade, whereby charging of the structures is electrostatically limited to one or a few electrons at a time [19]. The Coulomb interaction in quantum dots also forms the basis on which some quantum computing devices would operate [20]. New applications of quantum dots in computing are still being conceived, and only a few applications have been possible.

Quantum dots so far could be used mainly in applications related to optical electronics. These applications include laser sources [21], active elements in nanophotonics [22], and in photodetectors [23]. But the quantum dots hold more significant promise compared to the quantum wires and thin films due to their delta-function-like density of states, which allows for narrow line widths in the optical spectra of the devices.

The fabrication of quantum-confined semiconductor structures and the experimentations for the electrical characterization of the same, require technologically quite sophisticated set ups. However, most of the physics of such structures can be understood on the basis of relatively straightforward concepts.

In the present thesis, the theory of the non-ohmic effects and galvanomagnetic phenomena in the quantum wells of some widely used heterostructures at low and some other lattice

temperatures have been developed to understand and to explore the practicability of the characteristics of the devices, which are made of the above-mentioned structures.

It is well known that ensemble of electrons in a structure may exhibit non-ohmicity and the mobility may turn field dependent in the presence of a relatively high electric field. The field, at which the electrical nonlinearity of the current density $(\vec{J})$ vs. electric field $(\vec{E})$ characteristics of the ensemble sets in depends upon the lattice temperature. If the lattice temperature is low, a seemingly low field may turn out to be effectively high, and the high-field features may be observed [24-26].

The galvanomagnetic phenomenon may be observed when the structure is subjected to a magnetic field $(\vec{B})$ along with the electric field.

In quantum wells, the average energy of the electrons may exceed the barrier potential and then the electrons do not remain confined within the wells, but may move about in the barrier layers. This so-called electron transfer effect [27, 28] causes a decrease of velocity with increasing field since the mobility in the barrier material is lower than that in the well. Even for those electrons which still remain confined in the well, their wave functions assume different form.

When the field is effectively high, the semiconductor structure may exhibit negative-differential-resistance (NDR) in the current-voltage characteristic. The negative resistance of a structure can be utilized to design an amplifier, or an oscillator, or a harmonic generator or a switching device.

The theoretical analysis which has been made here mostly assumes that the lattice temperature is low $T_L \leq 20K$. It may be pointed out that the region of low temperature has distinctive, complicated features which are quite interesting from the viewpoints of both the basic physics and the device applications. These features are either absent at higher temperatures or are ignored for the theoretical studies to make the problem easily tractable.

In a semiconductor structure the impurity scattering limits the mobility of the electrons at low lattice temperatures when there are few phonons present. In a heterostructure the segregation of the carriers from the impurities may be accomplished through the well-known process of modulation-doping. This significantly enhances the value of the electron mobility at the low temperatures [16-18].

Moreover, it is at the low lattice temperatures, in high mobility quantum well structures, novel and interesting phenomena like Quantum Hall Effect (QHE) [29] and Fractional Quantum Hall Effect (FQHE) [30] are observed at high magnetic fields. Since the discovery of such phenomena in quantum well structures, many studies have been carried out to understand the salient physics associated with these phenomena. Hence, the study of the quantum well structures at low lattice temperatures is no doubt interesting.

Due to the advancement of fabrication techniques, one can now precisely control the compositions of modern semiconductor heterostructures in the atomic scale to develop low-dimensional systems. This has led to design different semiconductor devices with extraordinary electrical and optical properties. The emergence of these devices has prompted the detailed study of the carrier transport in low-dimensional structures.

The high-field transport properties of an ensemble of electrons are calculated by a solution of the Boltzmann transport equation. Although there are certain limitations in the application of the Boltzmann equation to transport problems, it is almost the only method for a description of a system far from equilibrium. Due to the complicated nature of the Boltzmann transport equation, it is usually not possible to solve it analytically without making some simplifying approximations. These approximations very often compromise with the validity of the theoretical results over a quite considerable regime of the prevalent experimental conditions. However, an approximate analysis of the high-field transport properties may be made by assuming a heated Fermi-Dirac or Maxwellian distribution at a field dependent effective temperature T_e of the carriers. The results thus obtained from such theoretical analysis mostly agree with what the experiments predict.

The electron temperature approximation is known to be more justified for the low-dimensional structures where a considerably higher carrier concentration can be realized.

The high-field transport phenomena in semiconductors form the basis of many ultrafast electronic and optoelectronic devices. Extensive experimental and theoretical studies in the field of electronic transport in semiconductor quantum well structures have been carried out over the last few decades. As a result of these studies [31-40], there have been lots of advancement in the field of Solid-State devices and sophisticated experimental methods are now producing more and more accurate results.

The central problem of the electron transport theory in any structure is to know the energy distribution function of the free carriers. Once the distribution function of the free carriers is known from the solution of the Boltzmann transport equation, the current can be calculated, and thus the important parameters of the electron transport in the semiconductor structure, viz. the mobility and the diffusion coefficient etc. can be obtained. The solution of the transport equation is determined by the prevalent scattering rates of the free charge carriers as they interact with various static and dynamic lattice imperfections in course of their motion through the material. Different collision processes become significant in different materials at a particular temperature and in a particular material at different temperatures.

Considering some quantum-confined ensembles of 2DEG in a heterostructure, a comprehensive theoretical analysis of the electron transport under the condition of low lattice temperatures and at effectively high electric fields has been carried out in the present thesis.

1.2.1 Basic assumptions

In order to develop the mathematical theory of any system, often some simplifying assumptions may have to be made so that the problem becomes amenable to a solution. These assumptions need to be physically realistic so that the results that follow from the subsequent theoretical analysis can indeed describe the characteristics of the real system under the prevalent condition without significant loss of accuracy. In the present thesis, to carry out the theoretical investigations of the electrical transport parameters of an ensemble of electrons which is confined to a quantum well of some widely used heterostructures, the principal basic assumption that have been made are pointed out in what follows now.

For a theoretical analysis, different shapes of the quantum wells in the heterostructures are assumed. The infinitely deep square well potential are sometimes used to mitigate the mathematical problem for the analysis. But such a potential well can hardly be experienced in practice. A square well potential with finite depth seems to be a better representation for the well. Parabolic wells are known to be encountered under the condition when the composition of the semiconductor may change continuously. But the widely used, simple model of the infinite triangular well potential represents a more realistic and easily workable model for a theoretical analysis [3].

When the electrons in the heterostructures of consideration here are assumed to be confined to such an infinite triangular potential well, the eigenvalues of the electron energy are quantized in the z - direction. However, they move like free particles in the $x-y$ plane. The energy of

this confined electrons now have discrete values, and the energy bands, as said earlier, turn into subbands. Under the condition of low temperature considered here it can be assumed that almost all the electrons are in the lowest subband and the higher subbands are essentially unoccupied.

As has already been explained the ensemble of quantum-confined electrons in a heterostructure constitute an ensemble of 2DEG. However, the phonon system is essentially three-dimensional. Many theoretical analyses have been made considering the phonon ensemble also to be two-dimensional for mathematical simplicity. The results thus obtained are seen to be in good agreement with the experimental results [41-45]. Thus, it is also assumed here that, even though the lattice wave is three-dimensional, the interaction of the quantised conduction electrons will also be confined to two-dimensions. However, the effect of the transverse component of the phonon wave vector have also been considered subsequently.

The electrical transport coefficients of the quantum-confined electrons have been obtained for the widely used heterostructures like AlGaAs/GaAs, AlGaN/GaN and AlInSb/InSb. These heterostructures are utilized in fabricating several electrical and opto-electronic devices. Such devices are usually made of n-type materials owing to several benefits. Thus, the analysis that have been carried out in this thesis have been made for the n-type materials only.

In a compound semiconductor which lacks inversion symmetry, the conduction electrons interact simultaneously with the intrinsic deformation potential acoustic phonons and the piezoelectric phonons along with the impurity atoms and other lattice defects. The effectiveness of each scattering mechanism depends upon the lattice temperature and the amount of doping, which may be monitored using the process of modulation-doping in the heterostructures.

At low lattice temperatures, the average thermal energy of the electrons would not be sufficient enough to excite optical mode lattice vibrations and thus the optical phonons hardly control the electron transport characteristics. The electronic collision processes which have been taken into account in the present work include that with the deformation potential acoustic phonons, the piezoelectric phonons and the ionized impurities in the quantum well, the remote ionized impurities at the adjacent layer of the well and the impurities at the interface of two semiconductor layers forming the quantum well. It may be mentioned here that the impurity scatterings may be neglected when the material is ultra-pure.

In the domain of low lattice temperatures $\left(T_L \le 20K\right)$ of interest here, the ensemble of carriers may be significantly perturbed from the state of thermodynamic equilibrium with the lattice atoms, and their average thermal energy may exceed the thermal equilibrium value $K_B T_L$, in the presence of a relatively weak fields, sometimes of the order of a fraction of a $volt/cm$. The energy distribution function of these non-equilibrium carriers can no longer be represented by the equilibrium F.D. function at a temperature T_L. In principle, the solution of BTE under these conditions may be worked out to obtain the energy distribution of the non-equilibrium electrons. But usually for an analytical solution of BTE, one needs to make some approximations which very often compromise with the accuracy of the analysis. Hence, one may take recourse to the well-known electron temperature approximation and assume that the effective temperature of the electrons T_e of the ensemble now exceeds the lattice temperature T_L, and turns field dependent: $T_e\left(E\right) > T_L$. The energy distribution function may now be represented by the 'heated' F.D. distribution replacing T_L by $T_e\left(E\right)$. The field dependence of the electron temperature $T_e\left(E\right)$ may be calculated from the energy balance equation of the electron-phonon system [24-26, 46-49].

At the low lattice temperatures, normally $T_e\left(E\right)$ can hardly reach a value above some ten to hundred times the lattice temperature. Hence under this condition the electrons are confined to a short segment of the energy dispersion curve near the minimum of the lowest subband, where the band is assumed to be essentially parabolic, without any serious loss of accuracy.

The strength of the electric field which the microstructure system is subjected to is assumed to be such, that it only changes the form of the energy distribution of the carriers and does not trigger the impact ionization process. As such, the carrier concentration essentially remains independent of the applied field.

The maximum value of the field is thus limited, so that the average crystal momentum of the carriers falls within the Brillouin zone. As such, the theoretical investigation of interest here may be carried out in the semi-classical framework. In this framework, the carriers are considered to be moving between successive collisions in accordance with the classical mechanics, while the scattering rates, in the host crystal are derived from the quantum theory.

The mechanism of interaction of the charge carriers with the lattice imperfections is assumed to be independent of the applied field, and the collisions are assumed to occur almost instantaneously, compared to the average time between two successive collisions. The scattering rates may be calculated using the first order perturbation theory, and consequently only two body interactions need to be analysed.

A number of interactions may be simultaneously effective under any prevalent conditions of the experiment. Then in calculating the total transition probability the interaction processes are taken to be uncorrelated.

The calculations have been carried out here considering a degenerate ensemble of electrons which is confined to the quantum wells of a heterostructure. To assess the effect of degeneracy, results have also been obtained for a similarly quantum-confined non-degenerate ensemble.

The theoretical investigations carried out here making use of all these basic assumptions would usually give the qualitative aspects of some of the characteristics of the two-dimensional structures formed at the interface of a heterostructure made of widely used compound semiconductors and mostly under the condition when the lattice temperature is low.

The concept and various features of the low lattice temperature are described in the next section.

1.2.2 Concepts and specific features of low lattice temperature

The problem of characterization of semiconductor structures and devices at and around the room temperature have already received much attention. As such, the amount of research that have already been reported in this field is quite large. This indicates that the electron transport characteristics are well understood at such temperatures. But such characteristics are significantly altered at the low lattice temperatures, for $T_L \leq 20K$. Some theoretical studies have been made under the condition of such low lattice temperatures. But usually, the specific features of the low lattice temperatures have been ignored in such studies, principally for mathematical simplicity. The problem for a comprehensive study of the electron transport in any semiconductor structure taking due account of the features of low lattice temperature, is important as it provides a good understanding of the electrical response of many devices when operated under the similar low temperature conditions. Such studies are useful in many fields where one is required to use the semiconductor devices at low temperatures, like in the field of

cryogenics and in space ships etc. The various features of the low lattice temperature that are frequently encountered in this thesis are specified below.

(i) The frequently used simple equipartition approximation of the Bose-Einstein (B.E.) distribution function for the phonons may hardly be valid at the low lattice temperatures. The energy distribution for the phonons is well-known to be given by the expression

$$N_{\bar{Q}} = \frac{1}{\exp\left(\frac{\hbar\omega_{\bar{Q}}}{K_B T_L}\right) - 1} \tag{1.1}$$

Under the condition when the lattice temperature is high, so that the average thermal energy of the free carriers which are at thermodynamic equilibrium largely exceeds the phonon energy i.e., $K_B T_L \gg \hbar\omega_{\bar{Q}}$ the expression (1.1) simplifies to $N_{\bar{Q}} = K_B T_L / \hbar\omega_{\bar{Q}}$. However, at the low lattice temperatures $\left(T_L \leq 20K\right)$, the true phonon distribution $N_{\bar{Q}}$ may be expressed by Laurent expansion [25]

$$N_{\bar{Q}}(X) = \begin{cases} \sum_{m=0}^{\infty} \frac{B_m}{m!} X^{m-1} \text{ for } X \leq \overline{X} \\ 0 \text{ for } X > \overline{X} \end{cases} \tag{1.2}$$

where B_m are the Bernoulli numbers, X is the normalized phonon wave vector, given by $X = \hbar u_l Q / K_B T_L$, $\overline{X}$ for all practical purposes may be taken to be 3.3.

(ii) Under the condition, when the lattice temperature is low, so that the phonon energy becomes comparable with the average thermal energy of the electrons, the electron-phonon interaction turns out to be inelastic. The phonon energy can no longer be neglected in comparison to the electron energy. However, when T_L is high, the analyses neglect the phonon energy $\left(\varepsilon_{ph}\right)$ compared to the electron energy $\left(\varepsilon_{\bar{k}}\right)$. Hence, the electron-phonon collisions are treated to be elastic. The ratio $\varepsilon_{ph} / \varepsilon_{\bar{k}}$ is of the order of $2u_l / u_{th}$. At higher temperatures, the ratio being very small, the phonon energy is indeed only a negligible fraction of the carrier energy. But with the lowering of T_L, the ratio increases, eventually that makes the phonon energy comparable with the electron energy. However, the interaction of the electron-phonon system may still assume to be elastic even at low

temperatures in order to overcome the mathematical difficulties in solving a problem. But such study would indeed incur some errors in subsequent analysis.

(iii) The electrons which are confined to the quantum wells of heterostructures, represent an ensemble of indistinguishable, non-interacting, identical particles, which occupy quantum states in accordance with the Pauli's exclusive principle. It is well-known that the thermal equilibrium energy distribution is given by the Fermi-Dirac distribution $f_0\left(\varepsilon_{\vec{k}}\right)$, where

$$f_0\left(\varepsilon_{\vec{k}}\right)=\frac{1}{1+\exp\left(\dfrac{\varepsilon_{\vec{k}}-\varepsilon_F}{K_BT_L}\right)} \tag{1.3}$$

The normalized Fermi energy $\eta_D\left(=\varepsilon_F/K_BT_L\right)$ in the 2DEG system is given by [5, 24, 42]

$$\eta_D=\frac{\varepsilon_F}{K_BT_L}=\ln\left[\exp\left(\frac{\pi\hbar^2N_i}{m_{\|}^*n_vK_BT_L}\right)-1\right]+\frac{\varepsilon_0}{K_BT_L} \tag{1.4}$$

Under the condition when the lattice temperature is high and the concentration of the carriers is low, so that $\left(\varepsilon_{\vec{k}}-\varepsilon_F\right)\gg K_BT_L$, then the distribution function (1.3) can be approximated by $f_0\left(\varepsilon_{\vec{k}}\right)=\exp\left[-\left(\varepsilon_{\vec{k}}-\varepsilon_F\right)/K_BT_L\right]$, which represents the classical, Maxwell-Boltzmann distribution function. Hence, the electron ensemble under these conditions turns out to be quite non-degenerate. However, as has just been pointed out, that the low lattice temperatures, and for sufficiently high carrier concentration, the electron ensemble behaves like a degenerate gas. The level of degeneracy is decided by the value of η_D. As the temperature is lowered more and more or the concentration is made higher and higher, the material becomes more and more degenerate. Again, as the temperature decreases, a lower value of the layer concentration may be quite sufficient to attain the same level of degeneracy.

(iv) It is well-known that any crystalline imperfection gives rise to a perturbing potential with which the electrons interact. This potential is again screened by the electron ensemble. For an ensemble of 2DEG that is in thermodynamic equilibrium with the lattice, the screening constant α may be expressed as $\alpha=\left(e^2N_i/2\in_{sc}\right)\left[K_BT_L\left(1+\exp\left(-y\right)\right)\ln\left(1+\exp\left(y\right)\right)\right]^{-1}$ where $y=\left(\varepsilon_F-\varepsilon_0\right)/K_BT_L$ [46]. Obviously, the effect of screening becomes significant for the higher carrier concentrations and at the lower lattice temperatures. Thus, under the

condition of low temperature, besides considering the features like the finite value of the energy of the intravalley acoustic phonons, the degeneracy of the carrier ensemble, the screening effect should also be taken into account in the theoretical analysis of the problems of electronic transport. The study of the effects of such screening would be important from the device point of view, because, as the process of miniaturization advances more and more, the sizes of the solid-state devices are gradually becoming smaller and smaller. This in turn results in higher and higher concentration of the carriers of the ensemble.

1.3 Scope of the thesis

The physical system under consideration in the present thesis comprises a degenerate ensemble of 2DEG under the condition mostly of the low lattice temperatures. The ensemble is assumed to be confined to an infinite triangular potential well of a heterostructure of some widely used compound semiconductors.

Based on the basic assumptions which have been elaborated in the paragraph 1.2.1, and taking due account of the specific features of the low lattice temperatures as described in the paragraph 1.2.2, theories have been developed on some aspects of the electron transport in the presence of an effectively high electric field. The theories have also been developed for the case when the ensemble is subjected simultaneously to an electric field and a transverse, non-quantising magnetic field. The results of the electron transport characteristics as theoretically obtained here, have been compared with available experimental data.

The aspects of the electronic transport that have been dealt with include:

(i) The effective electron temperature characteristics of the electron ensemble taking due account of the degeneracy of the ensemble and the piezoelectric interaction of the electrons.
(ii) The energy loss rate and the non-ohmic mobility characteristics of the electrons considering the degeneracy of the ensemble and the piezoelectric interaction of the electrons.
(iii) The efficiency of the second harmonic generation of microwaves due to the electrical nonlinearity of the electron ensemble.
(iv) The ohmic and the non-ohmic Hall mobility characteristics considering all the major scatterings of the electrons.

The thesis contains in all six chapters. The chapter-wise orientation is as follows:

In chapter II a brief introduction has been made on the quantum confinement of the electrons in semiconductor structures. Some structures which support the 2DEG system are then discussed. The basic properties of the 2DEG systems, like the subband energy, the density of states, the envelope functions for different quantum wells, the types of the scattering mechanisms and the phenomenon of screening are also discussed. The process of modulation-doping is also described.

In chapter II a brief introduction has been made on the quantum confinement of the electrons in semiconductor structures. Different types of quantum well and their envelope functions and energy eigenvalues have been discussed. The electron fundamental length in different semiconductors have been calculated.

The basic properties like the (a) wave function, energy dispersion, wave vector element, (b) density of states function for different structures, subband energy, (c) Equilibrium carrier concentration, (d) current density have been obtained. Structures which support the 2DEG system are then discussed. The types of the scattering mechanisms and the phenomenon of screening are also discussed. The chapter also includes the concept of modulation doping. All these details would serve as the foundation for the studies that are made in subsequent chapters.

Chapter III starts with the calculation of the concentration for an ensemble of two-dimensional carriers, the fermi energy level and the average carrier energy for (i) a non-degenerate, (ii) a moderately degenerate and (iii) an extremely degenerate ensemble. Then the effects of high d.c. electric fields on the carrier ensemble have been discussed. The concept of the effective electron temperature is then introduced and their applicability is discussed. Next the method of calculation of the effective electron temperature has been explained. To calculate the effective electron temperature of an ensemble and other transport coefficients, the knowledge of the matrix elements for various interaction of the two-dimensional electrons with different lattice imperfections is essential. Hence, the matrix elements for such interactions have been discussed. Next the calculation of the collision integrals and rate of change of the isotropic part of the high-field distribution function of the electrons in a degenerate 2DEG for interaction with phonons and due to applied field have been discussed. The calculation of the field dependent effective electron temperature have been carried out from the energy balance condition of the electron-phonon system, under the conditions when the electrons interact exclusively with the deformation potential acoustic phonons. Similar calculation is then carried

out for the interaction with the piezoelectric phonons. The results have been obtained for the combined interaction at the low and some other specific temperatures. The calculations have been carried out for different electron ensembles i.e., like the moderately degenerate, the extremely degenerate and the non-degenerate ensembles. The numerical results have been obtained for the ensemble of two-dimensional electrons in the quantum wells of InSb, GaAs and GaN for different levels of degeneracy and at different lattice temperatures. The results have been compared with other experimental and theoretical data.

In chapter IV, a short review of the energy loss rate (ELR) of the non-equilibrium electron in quantized surface layer have been made. Then the method of calculation of the ELR of the electrons on the surface layers of compound semiconductors have been presented. The characteristics of the energy loss rate of the conduction electrons on the surface layer has been calculated separately when the electrons interact with (i) the deformation potential acoustic phonons, and (ii) the piezoelectric phonons and for the combined interaction, under the conditions of low lattice temperatures. Here again, different electron ensembles like the moderately degenerate, the extremely degenerate and the non-degenerate ensembles have been considered. The numerical results have been obtained for the quantum surface layers on InSb, GaAs and GaN at different lattice temperatures and for different levels of the degeneracy.

In this chapter the non-ohmic mobility of the non-equilibrium ensemble of electrons which are confined to the quantum wells of compound semiconductors have also been studied. A brief review of the studies of the non-ohmic mobility characteristics of the ensembles of electrons on the quantized surface layers have been made first. The non-ohmic mobility characteristics have been then obtained using two methods: (i) from the expression for average ELR and (ii) from the expression for the current density. The method of calculation of the non-ohmic mobility characteristics from both the methods are then presented. The characteristics of the non-ohmic mobility of the electron ensemble on the surface layer have been calculated separately, when the electrons interact with the deformation potential acoustic phonons, and with the piezoelectric phonons and then for the combined interaction, under the conditions of low lattice temperature using both the methods. Here again different electron ensembles viz. the moderately degenerate, the extremely degenerate and the non-degenerate ensembles have been considered. The numerical results thus obtained using both the methods, for the two-dimensional electrons in the quantum wells on InSb, GaAs and GaN, for different levels of degeneracy and at different lattice temperatures have been compared with other experimental and theoretical data.

Chapter V deals with the generation of harmonics of the input microwave signal in the quantum well of heterostructure of compound semiconductors, due to the electrical nonlinearity of current-voltage characteristics of the ensemble of the non-equilibrium electrons which is confined to the well. The chapter starts with a brief review of the microwave harmonic generation in semiconductor structures. This is followed by the method of calculation of the efficiency of Second Harmonic Generation (SHG) in the quantum confined of 2DEG ensemble. The numerical results for the efficiency of microwave harmonic generation of SHG upon the biased field on the surface layers of InSb, GaAs and GaN have been obtained for different levels of degeneracy and for different lattice temperatures. Then a comparative discussion of the results for the different materials have been made.

Chapter VI deals with the galvanomagnetic phenomena in an ensemble of two-dimensional electrons in a quantum well of a heterostructure of compound semiconductors at the low lattice temperatures. A comprehensive analysis of the Hall mobility characteristics of the ensemble is carried out considering the two cases, viz. (i) the case of an ohmic ensemble and (ii) the case of a non-ohmic ensemble in some reasonable details. The characteristics have been obtained considering some of the low temperature features and relevant scattering mechanisms. The numerical results have been obtained for the ensembles of 2DEG which are confined to the wells of the heterostructures like AlGaAs/GaAs, AlGaN/GaN and AlInSb/InSb. The temperature dependence of the Hall mobility for these structures shows that the consideration of the above details significantly changes the overall characteristics, and makes them agree quite well with the experimental data. The results for the electric field dependence of the Hall mobility of the non-ohmic ensemble of 2DEG reveals the limits of the Hall mobility under the high-field conditions, which controls the transconductance and consequently the switching speed of a transistor.

CHAPTER II

SOME BASIC PHYSICS AND PROPERTIES OF QUANTUM CONFINED SEMICONDUCTOR STRUCTURE

2.1 Introduction

Prior to making a detailed enumeration of the comprehensive theoretical analysis of some of the aspects of the electron transport characteristics of a quantum confined ensemble of 2DEG in a heterostructure, under the condition of low lattice temperature and at effectively high electric field, it is worth to highlight a short review of the basic physics of the structure that is under consideration here.

2.2 Electron confinement by the quantum well in a semiconductor structure

By growing epitaxially a semiconductor material on the top of a crystal of a different semiconductor, a semiconductor heterostructure can be realised. The relative positions of the energy gaps of the two materials constitute the band offset of the heterojunction. In AlGaAs/GaAs heterostructures, when a heavily doped n-type AlGaAs is grown on a lightly or undoped GaAs, the discontinuity in the conduction band allows electrons to spill over from the N^+-AlGaAs into the GaAs, where they become trapped in the potential well. As a result, the electrons get collected on the GaAs side of the heterojunction and the Fermi level moves above the conduction band in the GaAs near the interface. The electrons in such a potential well form a two-dimensional electron gas [7, 14]. There are different types of quantum wells that can be formed in the semiconductor structures.

2.3.1 Types of quantum wells in semiconductor structure

Depending upon the fabrication technique, different shapes of the quantum wells can be confronted in semiconductor structures. In order to make the theoretical analysis tractable, some simplified models for the well are frequently assumed. Though hardly encountered in practice, an infinitely deep square well potential is often used. Actually, a square well of finite depth seems to be a better representation of the quantum wells. This additional feature of finite depth, no doubt, gives rise to much difficulties for the theoretical analysis. A parabolic shaped well can be encountered through changing the composition of the semiconductor continuously.

The model of infinite triangular well on the other hand, is known to be a more realistic model, which presents a simple description of the well found in MOSFET or in modulation doped heterojunctions [3].

2.3.2 Envelope functions for different wells and energy eigenvalues

The characteristics of the quantum-confined structures are determined by the properties of the wave functions of the confined electrons. The subband energy levels can be calculated from a self-consistent solution of the coupled Schrödinger and Poisson's equations.

In the effective-mass approximation, the electronic wave function for the nth subband may be written as [42, 46]

$$\psi_{\vec{k}} = \zeta_n(z)\exp(i\beta z)\exp\left[i\left(k_x x + k_y y\right)\right] \tag{2.1}$$

β depends only on k_x and k_y and is zero if the effective mass tensor is diagonal. $\zeta_n(z)$ is the envelope wave function that satisfies the equation

$$\frac{d^2\zeta_n(z)}{dz^2} + \frac{2m_\perp^*}{\hbar^2}\left[\varepsilon_n + e\phi(z)\right]\zeta_n(z) = 0 \tag{2.2}$$

where $m_\perp^*$ is the effective mass of an electron in the direction of quantization, $\phi(z)$ is the surface potential and ε_n is the energy eigenvalue of the nth subband.

The envelope wave function satisfies the boundary conditions $\zeta_n(z) = 0$ at $z = 0$ and $z = \infty$.

For the spherical constant energy surfaces in the wave vector space the total energy may be expressed as [3, 42, 50]

$$\varepsilon = \frac{\hbar^2 k_x^2}{2m_1^*} + \frac{\hbar^2 k_y^2}{2m_2^*} + \varepsilon_n = \frac{\hbar^2 k^2}{2m_\parallel^*} + \varepsilon_n = \varepsilon_{\vec{k}} + \varepsilon_n \tag{2.3}$$

Here $m_\parallel^* = \left(m_1^* m_2^*\right)^{1/2}$ is the effective mass of an electron parallel to the surface of $x - y$ plane.

The envelope function $\zeta_n(z)$ and the subband energy eigenvalue ε_n are determined by the surface potential $\phi(z)$. Their forms are given in the next paragraph for different wells [3].

It may be mentioned here that under the condition of low lattice temperature, almost all the electrons occupy the lowest subband and the higher subbands are essentially unoccupied.

(a) Infinitely deep square well

In this case, the potential inside the well of thickness d is approximated as $\phi(z)=0$ and Eq. (2.2) takes the form

$$\frac{d^2\zeta_n(z)}{dz^2}+\frac{2m_\perp^*\varepsilon_n}{\hbar^2}\zeta_n(z)=0 \tag{2.4}$$

Therefore, the envelope function as given by the solution of (2.4) and is

$$\zeta_n(z)=\sqrt{\frac{2}{d}}\begin{matrix}\cos\\ \sin\end{matrix}\left(\frac{\pi nz}{d}\right);\ \begin{matrix}n=1,3,5...\\ n=2,4,6...\end{matrix} \tag{2.5}$$

And the energy eigenvalue for the nth subband is given by

$$\varepsilon_n=\frac{\hbar^2}{2m_\perp^*}\left(\frac{n\pi}{d}\right)^2;\ n=1,2,3... \tag{2.6}$$

(b) Infinite Triangular well

The potential $\phi(z)$ in such a triangular well may be represented by

$$\phi(z)=\begin{cases}-E_s z & \text{for } z>0\\ \infty & \text{for } z<0\end{cases} \tag{2.7}$$

Here the surface electric field E_s is given by $E_s=eN_i/\in_{sc}$. Thus the Eq. (2.2) becomes

$$\frac{d^2\zeta_n(z)}{dz^2}+\frac{2m_\perp^*}{\hbar^2}\left[\varepsilon_n-eE_s z\right]\zeta_n(z)=0 \tag{2.8}$$

The two independent solutions of (2.8) are given the Airy functions $A_i(z)$ and $B_i(z)$ [51]. We require a wave function that is well behaved as $z\to\infty$. The Figure 2.1 shows the Airy functions $A_i(z)$ and $B_i(z)$. One can note that as $z\to\infty$, $A_i(z)$ retains a finite value, whereas $B_i(z)\to\infty$. Hence the solution $B_i(z)$ can be rejected.

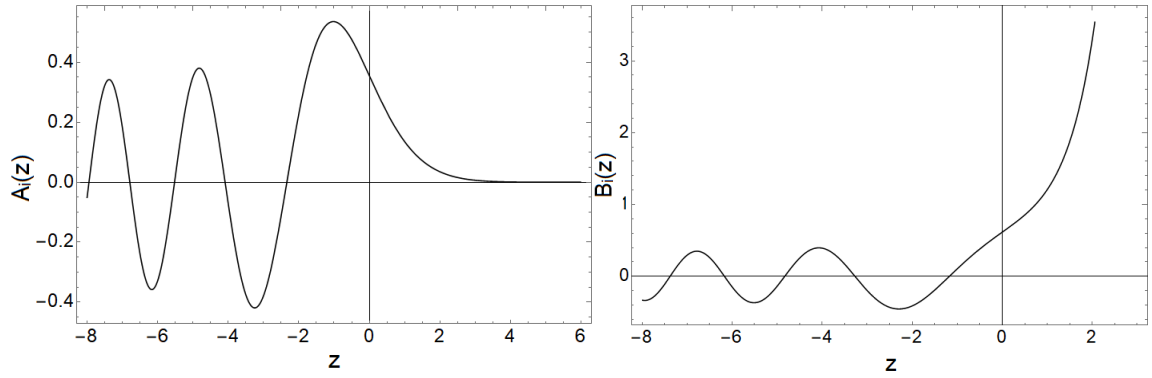

Figure 2.1 Plots of the Airy functions $A_i(z)$ and $B_i(z)$.

The expression for $\zeta_n(z)$ and ε_n that now follows are

$$\zeta_n(z) = KA_i\left[a(z - z_n)\right];\ n = 0,1,2... \tag{2.9}$$

$$\varepsilon_n = \left[\frac{3}{2}\pi\left(n + \frac{3}{4}\right)\right]^{2/3}\left[\frac{(e\hbar E_s)^2}{2m_\perp^*}\right]^{1/3};\ n = 0,1,2... \tag{2.10}$$

where, the normalization factor K is given by $K = a/A_i^2(-az_n)$, $a = \left[2m_\perp^* eE_s/\hbar^2\right]^{1/3}$, $z_n = \varepsilon_n/eE_s$.

The envelope functions and the subband energies are shown in the next Figure 2.2.

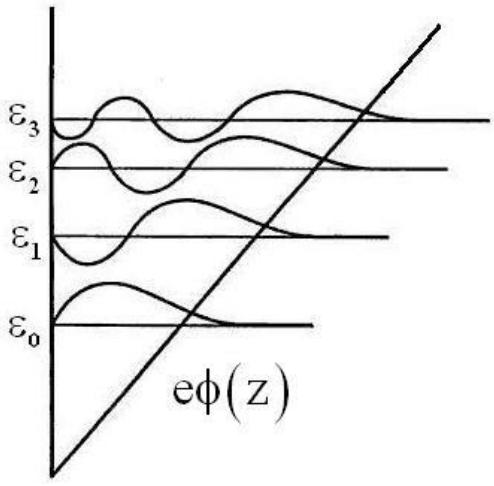

Figure 2.2 Envelope functions and subband energies in an infinite triangular quantum well.

(c) Parabolic well

The potential for the parabolic well is given by

$$\phi(z) = -\frac{1}{2e}C^2 z^2 \tag{2.11}$$

where C is the proportionality constant. Now, the Eq. (2.2) can be written as

$$\frac{d^2\zeta_n(z)}{dz^2} + \frac{2m_\perp^*}{\hbar^2}\left[\varepsilon_n - \frac{1}{2}C^2 z^2\right]\zeta_n(z) = 0 \tag{2.12}$$

The above equation becomes identical with the equation of a simple harmonic oscillator [52] by substituting $\omega^2 = C/m_\perp^*$. Thus, the envelope function takes the form of Hermite polynomials and the energy eigenvalues are

$$\varepsilon_n = \left(n + \frac{1}{2}\right)\hbar\omega \;;\; n = 0,1,2... \tag{2.13}$$

2.4 Low dimensional semiconductor structure

It has already been explained earlier what a low dimensional semiconductor structure is, and how can that be realised in principle.

2.4.1 Electron fundamental lengths in solids

The dimensionality of a structure is determined by comparing the dimensions of the structure with the de Broglie wavelength λ of the electrons in the material. When any of the dimensions is miniaturized to the order of λ, the electronic properties of the carrier ensemble get significantly influenced. Hence, the knowledge of this fundamentally important length λ is required.

The de Broglie wavelength λ_0 for a free electron is given by $\lambda_0 = 2\pi\hbar/\sqrt{2m_0\varepsilon}$, where ε is the electron energy and m_0 is the mass of an electron in vacuum. As such, the de Broglie wavelength λ of an electron in the material is given by $\lambda = 2\pi\hbar/\sqrt{2m^*\varepsilon}$. Since $m^* < m_0$, then $\lambda > \lambda_0$.

For a thermodynamically equilibrium ensemble of 2DEG around the room temperature $(T = 300K)$, using the average thermal energy of an electron $\varepsilon \sim K_B T$, one can calculate the value of λ for InSb, GaAs and GaN. The effective masses (m^*/m_0) of these materials are 0.014, 0.072 and 0.2 and their lattice constants in $\AA$ are ~ 6.479, 5.653 and $a = 3.189$, $c = 5.182$ respectively [1]. Thus, one can see that at $T = 300K$, the value of λ of these materials $\sim 10^2 \AA$ i.e., much larger than their lattice constants.

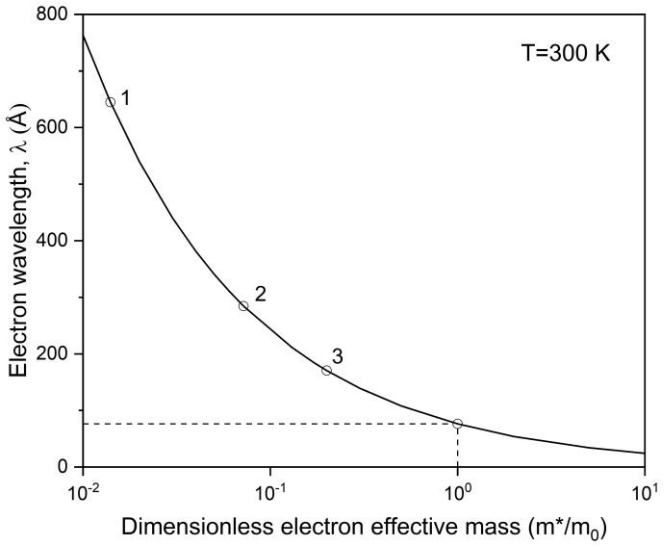

Figure 2.3 Electron wavelength versus the electron effective mass for room temperature $(T = 300K)$. Points 1 through 3 correspond to InSb, GaAs and GaN respectively.

The Figure 2.3 shows the variation of the electron wavelength λ with (m^*/m_0). Now if the temperature is lowered by 10^{-2}, λ becomes comparable with the sizes of the semiconductor nanostructure. Hence the devices using such structures can be fabricated using advanced nanofabrication technology [4].

2.4.2 (a) Wave function, energy dispersion, wave vector element, (b) Density of states function for different structures, subband energy, (c) Equilibrium carrier concentration, (d) Current density

Some of the specific electrical transport related factors which frequently occur in the present analysis are described for different structures in what follows now.

(a) Wave function, energy dispersion, wave vector element

(i) Bulk structure:

The wave function of an electron for this structure is

$$\psi_{\vec{k}}(\vec{r}) \sim \exp\left(i\vec{k}.\vec{r}\right) \tag{2.14}$$

where in rectangular coordinates the wave vector may be represented as $\vec{k} = \hat{i}k_x + \hat{j}k_y + \hat{k}k_z$ and $\vec{r} = \hat{i}x + \hat{j}y + \hat{k}z$.

For the parabolic band structure

$$\varepsilon_{\vec{k}} = \frac{\hbar^2}{2m^*}\left(k_x^2 + k_y^2 + k_z^2\right) = \frac{\hbar^2 k^2}{2m^*} \tag{2.15}$$

This proves to be a good approximation particularly near the bottom of the conduction band or the top of the valance band.

$d\vec{k}$, the 'volume' element in three dimensional $\vec{k}$ space given by the space between two concentric spheres of radii $\vec{k}$ and $\vec{k} + d\vec{k}$. Thus

$$d\vec{k} = 4\pi k^2 dk \tag{2.16}$$

(ii) Two-dimensional structures (quantum well)

Let the quantum well be along the $z-$axis. The $\vec{k}$ space is now two-dimensional: $\vec{k} = \hat{i}k_x + \hat{j}k_y$

If the well is an infinite well, the wave function of an electron now assumes a form

$$\psi_{\vec{k}}(\vec{r}) \sim \sin\left(\frac{m\pi z}{L_z}\right)\exp\left(i\vec{k}\vec{r}\right) \tag{2.17}$$

Here $\vec{k}.\vec{r} = k_x x + k_y y$.

$$\varepsilon_{\vec{k}} = \frac{\hbar^2 k_x^2}{2m_1^*} + \frac{\hbar^2 k_y^2}{2m_2^*} + \varepsilon_m \tag{2.18}$$

$$\varepsilon_{\vec{k}} = \frac{\hbar^2 k^2}{2m_{||}^*} + \varepsilon_m, \quad m_{||}^* = \left(m_1^* m_2^*\right)^{1/2} \tag{2.19}$$

where ε_m is the m[th] energy eigenvalues for the well of width L_z, and is given by

$$\varepsilon_m = \frac{m^2\hbar^2\pi^2}{2m_w^* L_z} \tag{2.20}$$

m_w being the effective mass of an electron in the well. Thus, for each m one gets a subband.

$\vec{k}$ is now two-dimensional and the 'volume' element in the two-dimensional $\vec{k}$ space is the annular region between two concentric circles of radii $\vec{k}$ and $\vec{k} + d\vec{k}$. Thus

$$d\vec{k} = 2\pi k dk \tag{2.21}$$

(iii) One-dimensional structure (quantum wire)

Let there be two infinite quantum wells, one along the $y-$axis of width L_y and the other along the $z-$axis, of width L_z respectively.

The wave vector $\vec{k}$ is now one-dimensional: $\vec{k} = \hat{i}k_x$.

The wave function of an electron now assumes the form

$$\psi_{\vec{k}}(\vec{r}) \sim \sin\left(\frac{n\pi y}{L_y}\right)\sin\left(\frac{m\pi z}{L_z}\right)\exp\left(i\vec{k}\vec{r}\right) \tag{2.22}$$

Here $\vec{k}.\vec{r} = k_x x$ and

$$\varepsilon_{\vec{k}} = \frac{\hbar^2 k_x^2}{2m_1^*} + \varepsilon_n + \varepsilon_m \tag{2.23}$$

where ε_n and ε_m are respectively the n[th] and m[th] energy eigenvalues for the wells along the y and z axes respectively.

$\vec{k}$ is now one-dimensional, and $d\vec{k}$ is the space element between lines of lengths $\vec{k}$ and $\vec{k} + d\vec{k}$. Thus

$$d\vec{k} = 2dk \tag{2.24}$$

(iv) Zero-dimensional structure (quantum dot)

In the quantum dot structure, the electrons are confined in all the three directions. As such the total energy of an electron in the quantum dot taking together all the three directions is completely discrete, having no continuous part. Hence, quantum dots are often called an artificial atom or a giant-atom.

If we take the confining potential of a quantum dot similar to that a particle in a 3D potential box, of width L_x, L_y and L_z along x, y and z directions respectively, the energy eigenvalues of an electron may be expressed as

$$\varepsilon_{n_x,n_y,n_z} = \frac{\hbar^2\pi^2}{2m^*}\left(\frac{n_x}{L_x^2}+\frac{n_y}{L_y^2}+\frac{n_z}{L_z^2}\right);\ n_x,n_y,n_z = 0,\pm1,\pm2... \tag{2.25}$$

(b) Density of states function [53]

In a unit volume of a structure, the number of $\vec{k}$ states in the "volume" element $d\vec{k}$ of the $\vec{k}$ space for a p dimensional structure is given by [53]

$$dg = \frac{2g_v}{(2\pi)^p}d\vec{k} \tag{2.26}$$

where p stands for the dimensionality of the structure. It assumes the values 3, 2 and 1 respectively for the bulk, the quantum well and quantum wire structure. g_v is the valley degeneracy factor. The factor 2 at the numerator takes into account the spin degeneracy. Now using energy dispersion relation $\varepsilon \equiv \varepsilon(\vec{k})$ for any structure, one can obtain $D(\varepsilon_{\vec{k}}) = dg/d\varepsilon_{\vec{k}}$. Thus $D(\varepsilon_{\vec{k}})$ gives us the number of quantum states per unit energy interval. Hence, one can obtain

(i) For the bulk structure:

$$D_3(\varepsilon_{\vec{k}}) = g_v\frac{\sqrt{2}}{\pi^2}\left(\frac{m^*}{\hbar^2}\right)^{3/2}\varepsilon_{\vec{k}}^{1/2} \sim \varepsilon_{\vec{k}}^{1/2} \tag{2.27}$$

(ii) For the quantum well structure:

$$D_2(\varepsilon_{\vec{k}}) = \sum_{n=0}^{\infty}\frac{g_v m_{\|}^*}{\pi\hbar^2}H(\varepsilon_{\vec{k}}-\varepsilon_n) \sim \varepsilon_{\vec{k}}^0 \tag{2.28}$$

where ε_n is the lowest energy of the nth subband and $H(x)$ is the Heaviside step function [51].

(iii) For the quantum wire structure:

$$D_1\left(\varepsilon_{\vec{k}}\right)=\sum_{n_y,n_z=0}^{\infty}\frac{g_v\sqrt{2m^*}}{\pi\hbar}\left(\varepsilon_{\vec{k}}-\varepsilon_{n_y,n_z}\right)^{-1/2}H\left(\varepsilon_{\vec{k}}-\varepsilon_{n_y,n_z}\right)\sim\varepsilon_{\vec{k}}^{-1/2} \tag{2.29}$$

(iv) For the quantum dot structure:

What follows from (2.25) the density of states for an electron in a single quantum dot consists of a set of Dirac delta functions at the discrete allowed values of energy of the electron.

The density of states of electrons in different structures are depicted in Figure 2.4. It may be noted that the density of states function for 1D and 0D exhibit singularities in energy. This has important implications for semiconductor devices [53].

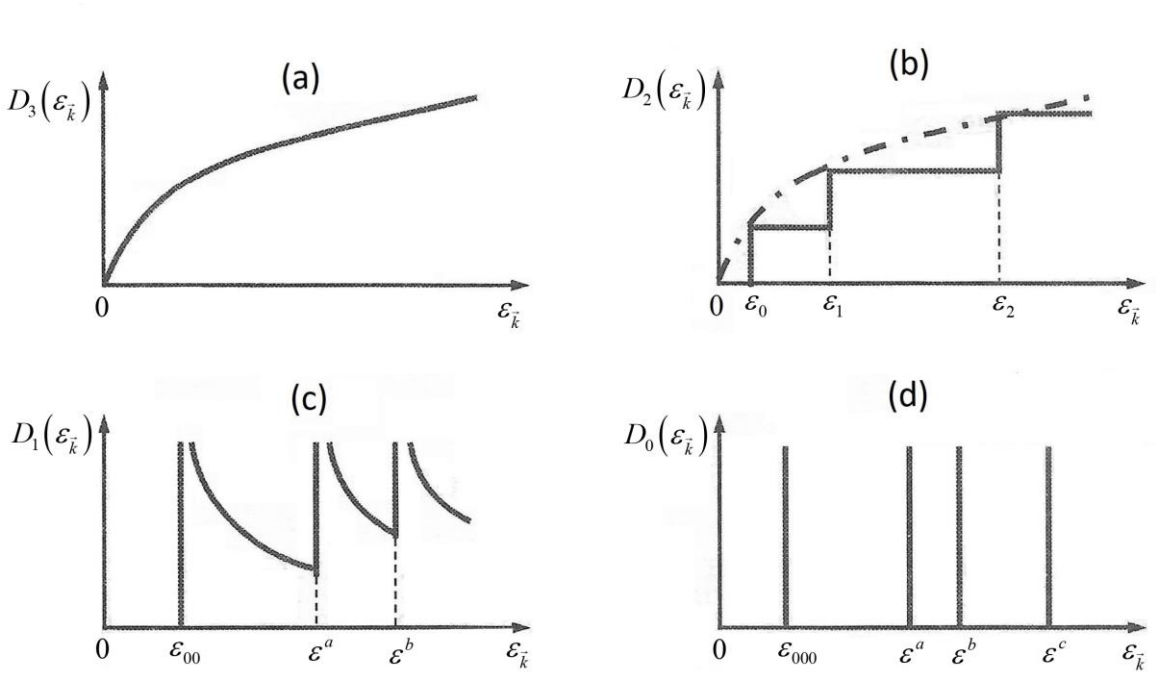

Figure 2.4 The density of states function of electrons $D(\varepsilon)$ in structures of different dimensionalities: (a) bulk structure, (b) a quantum well structure, (c) a quantum wire structure and (d) a quantum dot structure. Here ε_0, ε_{00} and ε_{000} are the ground states in quantum well, quantum wire and quantum dot respectively; ε_1 and ε_2 are higher states in a quantum well and ε^a, ε^b and ε^c are higher states in a quantum wire and in a quantum dot [4].

(c) Equilibrium carrier concentration [53]

The equilibrium carrier concentration n_p of a ' p ' dimensional structure may be calculated from the integral

$$n_p = \frac{2}{(2\pi)^p} \int f(\vec{k}) d\vec{k} \tag{2.30}$$

where $f(\vec{k})$ is the equilibrium distribution function of the carriers. Assuming F.D. distribution for $f(\vec{k})$ one can obtain

(i) For the bulk structure $(p = 3)$:

$$n_3 = 2\left(\frac{2\pi m^* K_B T}{h^2}\right)^{3/2} F_{1/2}(\eta_D) \tag{2.31}$$

(ii) For the quantum well structure $(p = 2)$:

$$n_2 = 2\left(\frac{2\pi m^* K_B T}{h^2}\right) F_0(\eta_D) \tag{2.32}$$

(iii) For the quantum wire structure $(p = 1)$:

$$n_1 = 2\left(\frac{2\pi m^* K_B T}{h^2}\right)^{1/2} F_{-1/2}(\eta_D) \tag{2.33}$$

where $w = \varepsilon / K_B T$, $\eta_D = \varepsilon_F / K_B T$, ε_F being the Fermi energy and $F_j(\eta_D)$ is the Fermi integral of j[th] order and is given by $F_j(\eta_D) = \frac{1}{\Gamma(j+1)} \int_0^\infty \frac{w^j dw}{1 + \exp(w - \eta_D)}$ [54].

(d) Current density

The expression for the current density is given by [55]

$$\vec{J} = \frac{e}{\hbar} \int (\nabla_{\vec{k}} \varepsilon_{\vec{k}}) f(\vec{k}) d\vec{k} \tag{2.34}$$

here $f(\vec{k})$ is the distribution function of the free carrier and may be obtained from the solution of the Boltzmann transport equation (BTE). The unknown distribution function $f(\vec{k})$ may be expanded in a series neglecting the higher order terms as [55]

$$f(\vec{k}) = f_0(\varepsilon_{\vec{k}}) + \vec{k}.f_1(\varepsilon_{\vec{k}}) \tag{2.35}$$

$f_0(\varepsilon_{\vec{k}})$ is the isotropic part of the distribution function.

Let us assume that a d.c. field of magnitude E is applied to a homogeneous sample having an electron concentration of n. The force on the electron due to the applied electric field is $e\vec{E}$. In the steady state the BTE in relaxation time approximation can be written as

$$\frac{e\vec{E}}{\hbar}.\nabla_{\vec{k}} f = \left.\frac{\partial f}{\partial t}\right|_{coll} = -\frac{f - f_0}{\tau} \tag{2.36}$$

where τ is the effective relaxation time of the collision. Replacing f by $f_0(\varepsilon_{\vec{k}}) + \vec{k}.f_1(\varepsilon_{\vec{k}})$ from Eq. (2.35) and neglecting higher order terms in the left-hand side, we obtain

$$-\frac{\vec{k}.f_1(\varepsilon_{\vec{k}})}{\tau} = \frac{e\vec{E}}{\hbar}.\nabla_{\vec{k}} f_0 = \frac{e\vec{E}}{\hbar}.\nabla_{\vec{k}}\varepsilon_{\vec{k}}\frac{\partial f_0}{\partial \varepsilon_{\vec{k}}} \tag{2.37}$$

But $\vec{E}.\nabla_{\vec{k}}\varepsilon_{\vec{k}} = \hbar^2\vec{E}.\overleftrightarrow{M}.\vec{k} = \hbar^2\vec{k}.\overleftrightarrow{M}.\vec{E}$.

Eq. (2.36) thus yields for $f_1(\varepsilon_{\vec{k}}) = -\hbar e\tau\left(\overleftrightarrow{M}.\vec{E}\right)\frac{\partial f_0}{\partial \varepsilon_{\vec{k}}}$.

Now, replacing the value of $f(\vec{k}) = f_0(\varepsilon_{\vec{k}}) - \hbar e\tau\left(\vec{k}.\overleftrightarrow{M}.\vec{E}\right)\frac{\partial f_0}{\partial \varepsilon_{\vec{k}}}$ in Eq. (2.34), we get the current density

$$\vec{J} = -e^2\int\left(\nabla_{\vec{k}}\varepsilon_{\vec{k}}\right)\left(\vec{k}.\overleftrightarrow{M}.\vec{E}\right)\tau\frac{\partial f_0}{\partial \varepsilon_{\vec{k}}}d\vec{k} \tag{2.38}$$

When constant energy surfaces are spherical in k - space, the reciprocal effective mass tensor $\overleftrightarrow{M}$ can be reduced to a scalar $1/m^*$ and the integrand may be expressed in polar coordinates with the direction of the applied field as the reference. One then obtains

$$\vec{J} = -\frac{e^2E}{m^*}\int\frac{\hbar^2k^2}{m^*}\cos^2\theta\tau\frac{\partial f_0}{\partial \varepsilon_{\vec{k}}}d\vec{k} \tag{2.39}$$

On carrying out the integral (2.39) one can obtain the expression for the current density.

2.4.3 Importance of low dimensional structures from the view point of device applications

Low-dimensional semiconductor structures are nowadays used as the centrepiece of many electronic and optoelectronic devices. This ensues from their interesting properties, like the carrier confinement and localization, the tunability of electronic energies by geometric dimension, or the spectrally narrow and high density of states etc.

Some of the novel quantum well devices include: the Modulation-doped field-effect transistors [7, 14, 56], the injection quantum-well laser [57], the microwave DBRTD (Double Barrier Resonant Tunnel Diode) oscillator [58], the hot electron transistor [59, 60], the sub-terahertz III-V compound nanoscale field-effect transistor, the sub-terahertz InP and SiGe bipolar transistors [4] etc. Low dimensional semiconductor structures, in particular, the heterostructures provide new means to enhance the consequences of many optical and electro-optical effects. For example, the performance of both of the most widely used light sources-light-emitting diodes and laser diodes may be improved significantly when quantum wells, quantum wires and quantum dots are exploited as active optical elements [3, 5].

The system which has been taken up for an analysis in the present thesis, consists of an ensemble of 2DEG, confined in a quantum well of a heterostructure. As such, though some general aspects of a quantum confined structure have already been discussed, henceforth, the discussions which follow now will mostly involve the system under consideration here.

2.5 Heterostructures

A heterostructure is grown with two or more abrupt interfaces at the boundaries between the regions of different materials. With the modern techniques for growth of materials, it is possible to grow structures with transition regions between materials that may have thickness of only one or two atomic monolayers. Although effort was initially concentrated on materials of nearly identical lattice constants, current applications may require properties that can be met only by mismatched materials, which in turn result in strained layers [3]. Heterostructures serve as the fundamental building block for the low dimensional devices. A huge variety of devices have been fabricated from heterostructures, for both electronic and optical applications.

2.5.1 Subband energy

It has already been seen that for a two-dimensional structure (quantum well) the energy dispersion relation as given by (2.19) $\varepsilon_{\vec{k}} = \hbar^2 k_x^2 / 2m_1^* + \hbar^2 k_y^2 / 2m_2^* + \varepsilon_m = \hbar^2 k^2 / 2m_{\|}^* + \varepsilon_m$ where

$m_{\|}^{*} = \left(m_1^{*} m_2^{*}\right)^{1/2}$. Thus, the energy spectrum for this system depends upon three parameters, two continuous, k_x and k_y and one, the discrete number m. Such a spectrum is interpreted as a set of subbands. This can be represented by a set of paraboloids, with minima at the quantised energy ε_m as depicted in the figure below.

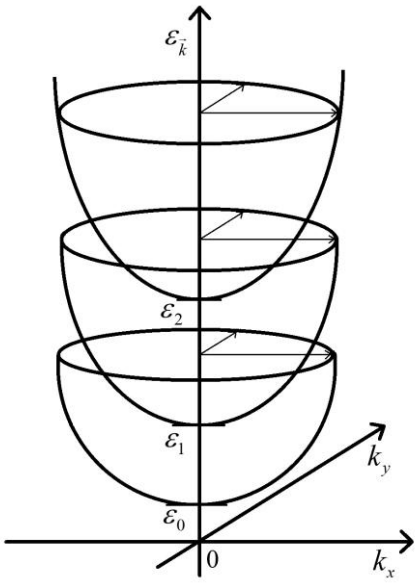

Figure 2.5 An example of two-dimensional subbands. The subbands are represented by the paraboloids in $\left\{\varepsilon_{\bar{k}}, k_x, k_y\right\}$-space; ε_0, ε_1 and ε_2 indicate the bottoms of subbands [4].

Thus, according to Eq. (2.19), the electron characterized by a given quantum number m, may be viewed as a particle which is free to move only along the two dimensions. The two-dimensional nature of the particles is perceptible when the energy intervals between subbands are larger. This may be possible when the width of the potential well for the electrons is of the order of a nanometre. Such a quantum well for the electrons in a low-dimensional structure can be fabricated using semiconductor layers which are quite thin $\sim 10nm$.

2.5.2 Modulation doping [3,5]

The carrier concentration in a bulk may be increased to the required level only by increasing the concentration of the dopant impurities. As the free carriers are generated from the ionization of the dopants, the ionised impurities which are left behind, result in dominant ionised impurity scattering of the generated carriers. The mobility of the free carriers are thus lowered. The problem in a heterostructure can be averted to a large extent by segregating the impurities from the carriers through the process of modulation doping. As a result, higher concentration of

carriers may be realised without the associated reduction of the mobility values. Hence, the electron conductivity in the structure may be much increased along with the mobility. This in turn goes to provide higher switching speed simultaneously with higher transconductance. This is indeed much desired from the device point of view.

As an illustrative example, one may refer to a single heterojunction between wider bandgap n-AlGaAs and undoped, lower bandgap GaAs as shown in the Figure 2.6 below.

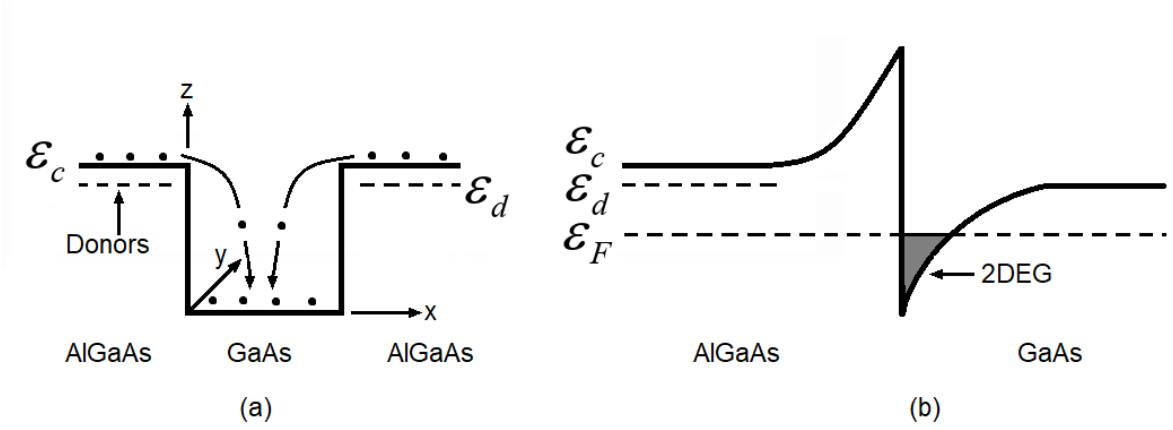

Figure 2.6 (a) Simplified view of modulation doping, showing only the conduction band. Electrons in the donor-doped AlGaAs falls into the GaAs potential well and become trapped. As a result, the undoped GaAs becomes n-type, without the scattering by ionised donors which is typical of bulk n-type material. (b) Use of a single AlGaAs/GaAs heterojunction to trap electrons in the undoped GaAs. The thin sheet of charge due to free electrons at the interface forms a two-dimensional electron gas (2DEG), which can be exploited in HEMT devices [53].

The material n-AlGaAs is neutral everywhere and the bands are flat, so long as the electrons sit on their donors in n-AlGaAs (Figure 2.6 (a)). As soon as some of the donors are ionised the electrons, thus on being released, travel around and diffuse into the smaller bandgap GaAs layer. They are hence prevented from returning to the n-AlGaAs by the potential barrier at the AlGaAs/GaAs interface. The electrons thus get confined in the nearly triangular well.

The ensemble of electrons so confined in the triangular quantum well can have only free in-plane motion (on the $x-y$ plane), but their motion along the transverse direction z is quantized. Hence the electrons of the ensemble lose one degree of freedom and thus give rise to a 2DEG.

Thus, the practical realisation of better performance of a heterostructure in respect of the higher values of switching speed, as well as of higher transconductance, has made it possible to

fabricate devices like the High electron mobility transistor (HEMT), Two-dimensional electron gas field-effect transistor (TEGFET), modulation-doped field-effect transistor (MODFET) etc. Obviously, the success of fabrication of such devices make it quite stimulating to study the physics of electron transport in quantum confined semiconductor structures.

2.5.3 Phenomena of screening [46, 50]

The free electrons which are uniformly distributed in a semiconductor sample, either collect or are removed from the region where any potential discontinuity occurs due to various lattice imperfections depending upon the sign of the discontinuity. The resulting space charge through its extra potential modifies the prevalent potential discontinuity and thus effectively screens its effect for large distances. The resulting potential is known to decay exponentially with a coefficient which is termed as the screening length α. One can calculate the screening length from the solution of the Poisson's equation.

When the electrons occupy only the lowest subband one obtains [46, 50]

$$\alpha = \left(\frac{e^2 N_i}{2 \in_{sc}} \right) \left[K_B T_L \left(1 + \mathrm{e}^{-y}\right) \ln\left(1 + \mathrm{e}^{y}\right) \right]^{-1} \tag{2.40}$$

where $y = \left(\varepsilon_F - \varepsilon_0\right) / K_B T_L$. Obviously, the effects of screening may be neglected at high temperatures and for moderate carrier concentrations. But at low lattice temperatures and for higher carrier concentrations, the effects of screening should be taken into account in the studying the transport phenomenon [50].

2.5.4 General properties

The useful semiconducting properties can be derived from heterostructures in lattice matched layers with minimum band gap and such layers are obtained from only few III-V or II-VI group semiconductors. The active regions of any 2DEG are typically at or close to the interface. In MOSFET the interface between Si-SiO_2 is not perfect and contain surface defects because Si is crystalline and SiO_2 is amorphous. The electrons confined to the inversion layer at the interface of Si-SiO_2, suffers scattering from the surface roughness and charged defects in the oxide and this results in degradation of the mobility. As such, in III-V heterostructures have nearly perfect interfaces owing to the suffocated fabrication techniques. The requirements for the two materials to form a heterostructure are: (i) they should have same crystal structure (or at least symmetry) and this is satisfied for the common III-V compounds and (ii) there is no strain in the final structure i.e., two lattice constants must be nearly identical.

The lattice constant of an alloy is usually given by linear interpolation between its constituents. This is known as Vegard's law. For example, the lattice constant of $Al_xGa_{1-x}As$ is given by $xa_{AlAs}+(1-x)a_{GaAs}$ where a is the lattice constant of the respective material. As available in the literature, the Figure 2.7 shows the lattice constant of various semiconductors against their minimum band gap, for these alloys the lattice constant changes by less than 0.15% as a function of x. Thus, it is possible to grow layers of GaAs and AlAs or any of the intermediate alloys $Al_xGa_{1-x}As$ on top of one another without significant stress. A much wider choice becomes available if the demand of lattice matching is relaxed [1, 3, 5].

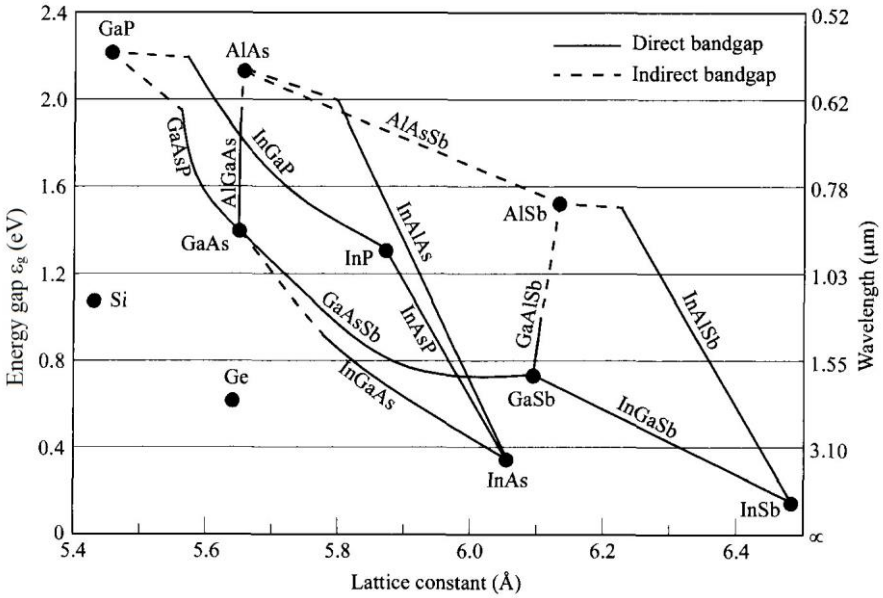

Fig. 2.7 Energy gap vs. lattice constant for some common elementary and binary semiconductors.

2.6 Some widely used structures which support 2DEG

Two-dimensional electron gas (2DEG) can be realised in a number of semiconductor structures. In many of such structures, some of the physical parameters can be controlled by varying the electric field. The structures where the carriers are confined either to the vicinity of junctions between insulators and semiconductors, or between layers of different semiconductors are some of the examples. They have at least one well-defined interface, usually sharp to the extent of a nanometre or less and the carrier concentration in these systems can be varied [2]. A few of the well-known structures which support 2DEG are now described briefly [2, 61-63].

(i) Heterostructures

(a) A single heterostructure

It has already been illustrated in the preceding paragraphs that a single heterostructure is formed when two lattice-matched semiconductors with different band gaps, work functions and electron affinities are brought together to form a junction. It is also explained there how does a single heterostructure support a 2DEG.

At equilibrium, the Fermi levels line up which results in the discontinuities in the energy bands. The band offset in the conduction band $\Delta\varepsilon_c$ and that in valance band $\Delta\varepsilon_v$ accommodate the difference in the band gap between the two semiconductors $\Delta\varepsilon_g$. Depending upon the layers of lattice-matched different semiconductors, one deposited on the top of the other, the nature of the quantum wells thus formed are different.

The widely used material pair is GaAs and $Al_xGa_{1-x}As$. The band gap of the alloy may be expressed as $\varepsilon_g = 1.424x + 1.247$ for $x < 0.45$ [62]. When x exceeds 0.45, the alloy becomes an indirect material.

Apart from the single heterostructure, there are other well-known heterostructures.

(b) Double heterostructure

A double heterostructure is formed when a small thickness of semiconductor of lower band gap is sandwiched between the two thick layers of the higher band gap material. Such heterostructure consists of two heterojunctions which confine the carriers in a nearly square quantum well. A widely used double heterostructure is AlGaAs/GaAs/AlGaAs in which the electrons accumulate in the GaAs side at the two heterointerfaces. Due to the thick barrier layer of AlGaAs, the electrons are not able to penetrate and are thus get confined in the quantum well region. This confinement results in quantisation of the electron motion perpendicular to the interface and gives rise to a subband energy structure. Since electrons are able to move freely in the plane parallel to the heterointerface, they exhibit two-dimensional characteristics, as shown in Figure 2.8.

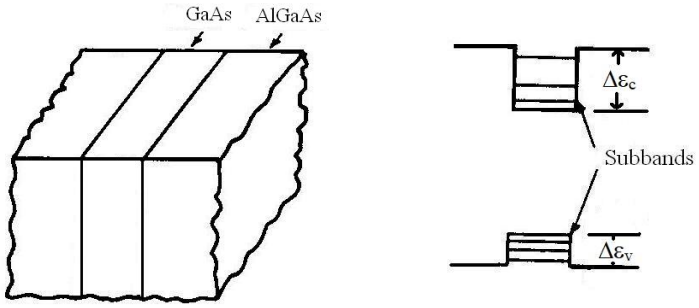

Figure 2.8 A double heterostructure and corresponding band diagram.

(c) Multiple Quantum Well (MQW) and Superlattice

A semiconductor structure having a number of alternate layers of GaAs and AlGaAs can lead to either a multiple quantum well or a superlattice. When the barrier layer is thick enough, the electronic wave function hardly penetrates into the barrier. The structure is then known as multiple quantum well. However, for narrow barrier layers, the wave functions of the adjacent wells when overlap, the electrons can move freely from one well to another and the resultant structure is a giant lattice or to speak, a superlattice.

Besides these, the advanced semiconductor technology now permits to tailor a band structure and produce the kind of variation in the potential profile as desired by the device designers.

(ii) Metal Oxide Semiconductor Field Effect Transistor (MOSFET)

A common n-channel MOSFET is a four-terminal device that consists of a p-type semiconductor substrate into which two n^+-regions, the source (S) and drain (D), are formed, usually by ion implantation. The SiO_2 gate dielectric is formed by thermal oxidation of Si to obtain a high-quality SiO_2-Si interface. The metal contact on the insulator is called the gate (G). A cross-sectional view of such a MOSFET is shown in Figure 2.9. If the gate bias voltage V_G is kept positive with respect to the substrate, the energy bands bend near the interface as shown in Figure 2.10(a). Under this condition a small bias voltage pushes the holes away from the interface between Si and SiO_2 forming a depletion region there, consisting of the negatively charged acceptor ions in the p-type material. On increasing the gate bias voltage electrons are induced, inverting the conductivity of the substrate. The bands near the interface now bend sufficiently, and the conduction band may even cross the Fermi level, resulting in accumulation of electrons in the surface region. These electrons are now confined in the Z-direction in a surface layer of small thickness by a narrow, nearly triangular potential well at the Si-SiO_2 interface. As a result, the electrons that are induced near the interface invert the conductivity

type of the substrate there and thus forming what is called an inversion layer. The electrons in the inversion layer form a system of two-dimensional electron gas. The band diagram of such a system is shown in Figure 2.10(b) and 2.10(c). Many interesting properties of this system may come up when the electron density in the inversion layer are controlled by varying the bias between the gate and the substrate.

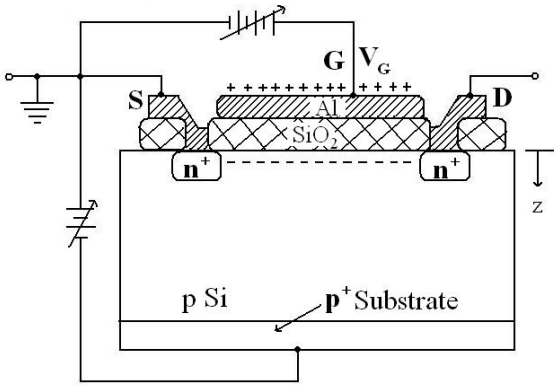

Figure 2.9 A cross-sectional view of a Metal Oxide Semiconductor Field Effect Transistor (MOSFET). The substrate is shown biased with respect to the source (S).

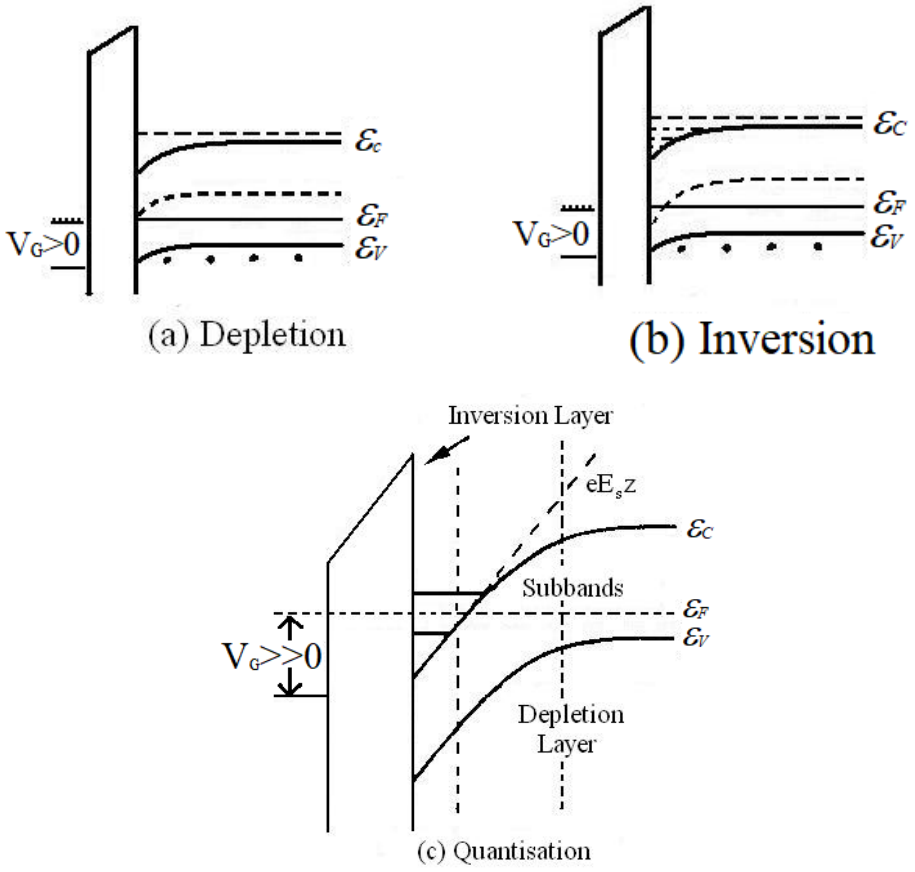

Figure 2.10 Band Diagram in a MOSFET under depletion, surface inversion and under strong inversion leading to quantisation of electron motion.

2.7 Scattering mechanisms

Different scattering mechanisms of the electrons in an ensemble of 2DEG in a semiconductor structure determine the electronic transport characteristics of the structure. These scattering mechanisms are induced by various lattice imperfections, such as impurity atoms, dislocations, and crystal defects, as well as by acoustic and optical phonons, which are brought about by the vibrations of the crystal lattice. All the scattering mechanisms just described are not always equally contribute to the process of transport. The dominant scattering mechanism depends on the prevailing experimental conditions, such as the lattice temperature, the impurity or the carrier concentration, and the crystal structure etc. For example, impurity atoms may remain neutral at very low temperatures, causing neutral impurity scattering to dominate, while ionized impurity scattering becomes more important at some higher temperatures and carrier concentrations. Remote impurity scattering can also play a role due to the non-uniform distribution of impurities in some systems.

Structural defects, such as the surface roughness, the edge and the screw dislocations, can also cause scattering, but their effects can be minimized using improved crystal growth techniques. The scattering caused by the lattice imperfections due to crystal defects or impurity atoms can be controlled taking recourse to requisite crystal growth technique, while the phonon scattering caused by the interaction of free carriers with the lattice vibrations is just intrinsic and hardly be averted.

Different types of phonon scattering mechanisms, including the deformation potential acoustic scattering, the piezoelectric scattering, and the polar optic phonon scattering become important at different temperature ranges and can have different prominence in controlling transport characteristics, depending upon the crystal structure of the semiconducting material.

A schematic diagram of different scattering mechanisms is shown in Table 2.1.

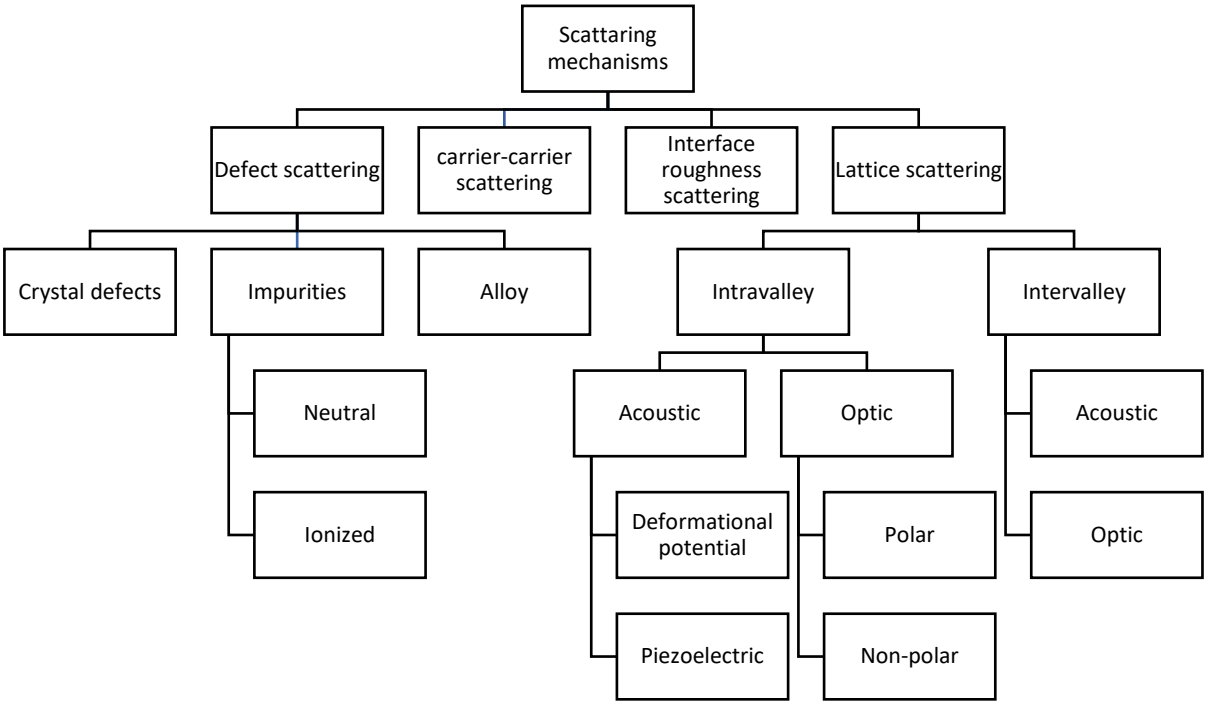

Table 2.1 Scattering Mechanisms

CHAPTER III

NON-OHMIC TWO-DIMENSIONAL ELECTRON ENSEMBLE IN A QUANTUM WELL OF A COMPOUND SEMICONDUCTOR

3.1 Introduction

The present chapter deals with the causes of the non-ohmicity of a 2DEG ensemble which is confined to a quantum well of a single heterostructure of compound semiconductors. Different types of the ensemble viz. the non-degenerate, the moderately degenerate and the highly degenerate ensembles have been considered. The interactions of the electrons with various intrinsic lattice imperfections have been taken into account.

These studies form the key to understanding the effects of the non-ohmic characteristics of the electron ensemble on the device performance.

3.1.1 Types of electron ensemble

The concentration, n, of the electrons in the conduction band may be calculated by carrying out the integral

$$n = \int_0^\infty D_2\left(\varepsilon_{\vec{k}}\right) f\left(\varepsilon_{\vec{k}}\right) d\varepsilon_{\vec{k}} \tag{3.1}$$

The density of states $D_2\left(\varepsilon_{\vec{k}}\right)$ for a two-dimensional structure have already been obtained in Eq. (2.28) and the energy distribution function $f\left(\varepsilon_{\vec{k}}\right)$ of the equilibrium electrons may be represented by the Fermi-Dirac distribution function

$$f\left(\varepsilon_{\vec{k}}\right) = \frac{1}{1+\exp\left(\dfrac{\varepsilon_{\vec{k}} - \varepsilon_F}{K_B T_L}\right)} \tag{3.2}$$

where ε_F is the Fermi energy level, and the bottom of the conduction band is taken to be at $\varepsilon_{\vec{k}} = 0$.

Hence, the concentration of the electrons may be expressed as

$$n = 2\left(\frac{2\pi g_v m_{\|}^* K_B T_L}{h^2}\right)\int_0^\infty \frac{dw}{1+\exp\left(w-\eta_D\right)} = N_c \int_0^\infty \frac{dw}{1+\exp\left(w-\eta_D\right)} = N_c F_0\left(\eta_D\right) \qquad (3.3)$$

where N_c is the effective density of states, $w = \varepsilon_{\vec{k}} / K_B T_L$ and $\eta_D = \varepsilon_F / K_B T_L$.

Nondegenerate ensemble of 2DEG

By definition, in nondegenerate semiconductors, the doping concentration are smaller than N_c and the Fermi levels are more than several $K_B T_L$ below the bottom of the conduction band. Hence η_D is negative. The Fermi function now simplifies to the Maxwellian function since one can neglect 1 in comparison to $\exp\left(w-\eta_D\right)$. Thus, one obtains

$$n = N_c \exp\left(\frac{\varepsilon_F}{K_B T_L}\right) \qquad (3.4)$$

The Fermi energy can now be expressed as

$$\varepsilon_F = -K_B T_L \ln\left(\frac{g_v m_{\|}^* K_B T_L}{\pi n \hbar^2}\right) \qquad (3.5)$$

The average thermal energy of the carriers can be obtained as

$$\left\langle \varepsilon_{\vec{k}} \right\rangle = \frac{\int_0^\infty \varepsilon_{\vec{k}} \exp\left(-\frac{\varepsilon_{\vec{k}} - \varepsilon_F}{K_B T_L}\right) d^2k}{\int_0^\infty \exp\left(-\frac{\varepsilon_{\vec{k}} - \varepsilon_F}{K_B T_L}\right) d^2k} = K_B T_L \qquad (3.6)$$

Moderately Degenerate 2DEG

For a moderately degenerate 2DEG, the concentration of the electrons is near the effective density of states N_c. The Fermi-Dirac function has to be used now instead of the simplified Boltzmann distribution function. For $\eta_D > -1$ or if ε_F is much lower than $K_B T_L$ of the band edge, one gets

$$n = N_c \ln\left[1+\exp\left(\frac{\varepsilon_F}{K_B T_L}\right)\right] \qquad (3.7)$$

The Fermi energy can now be obtained as

$$\varepsilon_F = K_B T_L \ln\left[\exp\left(\frac{\pi n\hbar^2}{g_v m_{\|}^* K_B T_L}\right) - 1\right] \tag{3.8}$$

The average thermal energy of carriers can be obtained as

$$\left\langle \varepsilon_{\vec{k}} \right\rangle = \frac{\int_0^\infty \varepsilon_{\vec{k}} \left[1+\exp\left(\frac{\varepsilon_{\vec{k}} - \varepsilon_F}{K_B T_L}\right)\right]^{-1} d^2k}{\int_0^\infty \left[1+\exp\left(\frac{\varepsilon_{\vec{k}} - \varepsilon_F}{K_B T_L}\right)\right]^{-1} d^2k} = K_B T_L \frac{F_1(\eta_D)}{F_0(\eta_D)} \tag{3.9}$$

Extremely degenerate 2DEG

For an extremely degenerate ensemble, the carrier concentration is beyond the effective density of states N_c, η_D is very large and then the Fermi function may be taken as 1. The Fermi level now moves into the conduction band and the carrier concentration may be approximated as

$$n = N_c \int_0^{\eta_D} dw = N_c \left(\frac{\varepsilon_F}{K_B T_L}\right) \tag{3.10}$$

The Fermi energy can be evaluated to be

$$\varepsilon_F = K_B T_L \left(\frac{\pi n\hbar^2}{g_v m_{\|}^* K_B T_L}\right) = \frac{\pi n\hbar^2}{g_v m_{\|}^*} \tag{3.11}$$

and the average thermal energy of carriers can be obtained as

$$\left\langle \varepsilon_{\vec{k}} \right\rangle = \frac{\int_0^{\varepsilon_F} \varepsilon_{\vec{k}} d^2k}{\int_0^{\varepsilon_F} d^2k} = \frac{1}{2}\varepsilon_F \tag{3.12}$$

3.1.2 Effects of high D.C. electric field on the energy distribution of an electron ensemble

When subjected to a high d.c. electric field, the electron ensemble is significantly perturbed from the state of thermodynamic equilibrium with the lattice atoms. As such, the energy distribution function of the electrons is consequently perturbed, and can no longer be

represented by the distribution (3.2) which is applicable only for an equilibrium ensemble, in the absence of any electric field.

In principle, the distribution function for the non-equilibrium ensemble of electrons, in the presence of the electric field, may be obtained from the solution of the Boltzmann Transport Equation (BTE). But in almost all cases, the transport equation is not amenable to an analytical solution in the presence of a high electric field, unless some simplifying assumptions are made. Furthermore, these assumptions very often compromise with the validity of the theoretical results over a rather considerable range of the prevalent experimental conditions. Hence one has to take recourse to either some numerical methods or go for some broad-based analytical method in order to obtain a reasonably valid solution of the transport equation. One of such widely used method is the use of the concept of effective electron temperature.

3.1.3 Concept of effective temperature of an electron ensemble

At any lattice temperature T_L, the free electrons of an ensemble in a semiconductor move randomly due to their thermal energy. In course of such motion, the electrons make collisions with the vibrating, host lattice atoms. As a result, there is an exchange of energy between the electron and the phonon ensembles. The rate of loss of energy through the process of phonon emission balances with the rate of gain through the process of absorption of phonons. So, the net transfer of energy in the absence of any electric field is zero under this condition.

Since the temperature difference between the two systems accounts for the amount of energy transfer, the temperature of the electron ensemble remains the same as that of the phonon ensemble. The electron ensemble thus remains in thermal equilibrium with the lattice atoms. The energy distribution of the equilibrium ensemble of electrons obeys the Fermi-Dirac distribution, and the phonon ensemble follows the Bose-Einstein distribution, both at the same lattice temperature T_L.

To make a current flow through the semiconductor, a bias field $\vec{E}$ is required. When an electric field is applied, the free carriers attain a drift velocity, which in turn produces the current J. Under this condition, the electrons begin to gain energy from the field at a rate $\vec{J}.\vec{E}$ per unit volume. Obviously, their average energy begins to grow with time. But the average energy cannot grow indefinitely. As soon as the average energy of the electrons surpasses that of the lattice atoms, the electrons start emitting more phonons per unit time. This makes the rate of loss of energy increase compared to the gain of energy through absorption of phonons. The rate

of loss increases with the growth of the average energy of the electrons. A steady state is reached for the electrons when the rate of gain of the energy from the electric field is balanced by the rate of loss due to the emission of more phonons. The electrons having small effective mass, lose energy rather slowly as a result of emission of phonons. Again, the mean free path of the electrons being quite large, the energy gained in between successive collisions may exceed what is lost to the phonon ensemble, during the same time. Under this condition, the average energy of the electrons exceed its thermal equilibrium value. As a result, now, the electron ensemble may be assumed to acquire a field dependent effective temperature $T_e(E)$, which surpasses the lattice temperature T_L i.e., $T_e(E) > T_L$. The electron ensemble then does no longer remain in thermal equilibrium with the lattice atoms [24, 55].

3.1.4 Applicability of the effective temperature approximation

Under the condition, when the concentration of the carriers is large enough, so that the carrier-carrier interaction dominates over the interaction of the carriers with the lattice imperfections, an approximate analysis of the high-field transport characteristics may be made by applying the effective temperature approximation. Such an approximate analysis is quite worthy, as because, it often provides data, which are useful for the device technologists. Moreover, the effective electron temperature approximation is known to be more justified for the low-dimensional structures where a considerably higher carrier concentration can be realised without any effective loss of the carrier mobility [2-5, 26, 55, 64].

For a theoretical analysis it is traditionally assumed that the perturbed distribution function of an ensemble of electrons in the presence of a high electric field may be symbolically written as

$$f\left(\vec{k}\right) = f_0\left(\varepsilon_{\vec{k}}\right) + k\cos\theta\, f_1\left(\varepsilon_{\vec{k}}\right) \tag{3.13}$$

where $f_0\left(\varepsilon_{\vec{k}}\right)$ is the isotropic part of the distribution function, and θ is the angle between the vectors $\vec{k}$ and $\vec{E}$. In the effective electron temperature approximation $f_0\left(\varepsilon_{\vec{k}}\right)$ is taken to be the heated Fermi-Dirac distribution of the form (3.2) with such modification as the lattice temperature T_L, now replaced by T_e, the field dependence effective temperature of the ensemble [24, 26, 55].

3.2 Method of calculation of the electron temperature characteristics

The field dependence of the effective temperature of an electron in an ensemble may be obtained from the solution of the energy balance equation of the electron-phonon system taking into account all the processes of scattering under the prevalent conditions of interest here.

3.2.1 Energy balance condition for the electron-phonon system

The energy balance condition for the electron-phonon system can be symbolically written as [24, 55]

$$\int_0^\infty \left.\frac{\partial f\left(\vec{k}\right)}{dt}\right|_{field} \varepsilon_{\vec{k}} d\vec{k} = \sum_j \int_0^\infty \left.\frac{\partial f\left(\vec{k}\right)}{dt}\right|_{collision} \varepsilon_{\vec{k}} d\vec{k} \tag{3.14}$$

Here the left side of the equation represents the rate of energy gain by the electrons from the field and the right side of the equation represents the rate of energy loss through various collision processes. $\partial f\left(\vec{k}\right)\big/dt$ is the time rate of change of the high-field distribution function $f\left(\vec{k}\right)$ of the electron ensemble given in Eq. (3.13).

3.3 Calculation of the collision integrals

The transport coefficients for an ensemble of 2DEG which is confined to a quantum well may be evaluated by using the Boltzmann transport equation. The transport equation may be expressed as [55]

$$\frac{eE}{\hbar}.\nabla_{\vec{k}} f = -\frac{A}{\left(2\pi\right)^2}\frac{2\pi}{\hbar}\int \left\{ \begin{array}{l} S\left(\vec{k},\vec{k}'\right) f\left(\vec{k}\right)\left[1-f\left(\vec{k}'\right)\right] \\ -S\left(\vec{k}',\vec{k}\right) f\left(\vec{k}'\right)\left[1-f\left(\vec{k}\right)\right] \end{array} \right\} d^2k' \tag{3.15}$$

where E is the externally applied electric field and $\left(1/2\pi\right)^2$ is the density of states for the 2DEG. A is the surface area of the ensemble of 2DEG. $S\left(\vec{k},\vec{k}'\right)$ or $S\left(\vec{k}',\vec{k}\right)$ represent the rate of transition of an electron in the wave vector space, either from $\vec{k}$ to $\vec{k}'$ or from $\vec{k}'$ to $\vec{k}$. The rates can be calculated from the perturbation theory for interaction of an electron with any lattice imperfection. d^2k is the two-dimensional element in the wave vector space. The left-hand-side gives the change in f, caused by the field E, while the right-hand-side gives the change due to scattering. In the steady-state, the two terms are balanced. The right-hand-side

term is often referred as the collision integral. The first term in the integral gives the number of electrons scattered out from the $\vec{k}$ -state to different $\vec{k}'$-states per unit time and is called the out-scattering term. The second term in the integral gives the number of electrons scattered from different $\vec{k}'$-states into the $\vec{k}$ -state per unit time, and is called the in-scattering term. The equation is solved by substituting (3.13) for $f\left(\vec{k}\right)$ and assuming the direction of E as the polar axis.

Eq. (3.15) contains symmetric and asymmetric components of the collision integrals. It follows from the well-known principle of detailed balance that the asymmetric component is essentially zero [5, 55]. Hence, the symmetric component may be obtained as

$$\frac{eE}{\hbar}\left[f_1\left(\varepsilon_{\vec{k}}\right) + k_x \frac{\partial f_1\left(\varepsilon_{\vec{k}}\right)}{\partial \varepsilon_{\vec{k}}} \frac{\partial \varepsilon_{\vec{k}}}{\partial k_x} \right] = -\frac{A}{\left(2\pi\right)^2} \frac{2\pi}{\hbar} \int \left\{ \begin{matrix} S\left(\vec{k},\vec{k}'\right) f_0\left(\vec{k}\right)\left[1 - f_0\left(\vec{k}'\right)\right] \\ -S\left(\vec{k}',\vec{k}\right) f_0\left(\vec{k}'\right)\left[1 - f_0\left(\vec{k}\right)\right] \end{matrix} \right\} d^2k' \quad (3.16)$$

It may be mentioned here that in the relaxation time approximation $f_1\left(\varepsilon_{\vec{k}}\right) = -\tau\left(\varepsilon_{\vec{k}}\right) \frac{eE\hbar}{m_{\|}^*} \frac{\partial f_0}{\partial \varepsilon_{\vec{k}}}$ [55].

Thus, Eq. (3.16) reduces to

$$\frac{e^2E^2}{m_{\|}^*} \frac{\partial}{\partial \varepsilon_{\vec{k}}} \left(\varepsilon_{\vec{k}} \tau\left(\varepsilon_{\vec{k}}\right) \frac{\partial f_0\left(\varepsilon_{\vec{k}}\right)}{\partial \varepsilon_{\vec{k}}} \right) = -\frac{A}{\left(2\pi\right)^2} \frac{2\pi}{\hbar} \int \left\{ \begin{matrix} S\left(\vec{k},\vec{k}'\right) f_0\left(\vec{k}\right)\left[1 - f_0\left(\vec{k}'\right)\right] \\ -S\left(\vec{k}',\vec{k}\right) f_0\left(\vec{k}'\right)\left[1 - f_0\left(\vec{k}\right)\right] \end{matrix} \right\} d^2k' \quad (3.17)$$

3.4 Matrix elements for various interactions of the two-dimensional electrons with lattice imperfections

The calculation of the rate of transition, like $S\left(\vec{k},\vec{k}'\right)$ for any interaction of an electron with a lattice imperfection demands the knowledge of the matrix element $\left|M\left(\vec{k},\vec{k}'\right)\right|^2$. The expression for each of them are available in the literature. For a ready reference they are listed one by one in what follows now.

(a) Deformation potential acoustic phonons

When an acoustic wave propagates in a crystal lattice, the atoms oscillate about their equilibrium positions which induces a modification or deformation in the band structure. The deformation potential is a measure of how much does the energy of an electron with a wave

vector $\vec{k}$ change as a result of some deformation of the crystal lattice. For the interaction of the electrons with the deformation potential acoustic phonons (ac), the matrix element is given by [2, 5]

$$\left|M\left(\vec{k},\vec{k}'\right)\right|_{ac}^{2}=\frac{E_a^2\hbar Q}{2Ad\rho_v u_l}\frac{1}{S\left(\vec{q}\right)}\left|G\left(q_z\right)\right|^2\begin{pmatrix}N_{\vec{Q}}\\N_{\vec{Q}}+1\end{pmatrix}\delta_{\vec{k}',\vec{k}\pm\vec{q}} \tag{3.18}$$

where E_a is the deformation potential constant, $\vec{Q}$ is the three-dimensional phonon wave vector having the component q on the $x-y$ plane and q_z is the transverse component, such that $Q^2=q^2+q_z^2$, d is the width of the layer of the lattice atoms with which the electrons can interact, ρ_v is the volume mass density.

The screening factor $S\left(\vec{q}\right)=\left(1+\alpha/q\right)$, where α is the screening length given by (2.40). As has already been said, it follows from the expression for α, that the effects of screening may be neglected at higher temperatures, and for moderately degenerate ensemble of 2DEG. But at low lattice temperatures, and for highly degenerate ensembles, the effects of screening need to be taken into account when analysing the electrical transport phenomenon.

It may be seen that for a highly degenerate ensembles at the low lattice temperatures $S\left(\vec{q}\right)$ reduces to $S\left(\vec{q}\right)=1+e^2m_{\parallel}^{*}/2\pi\in_{sc}\hbar^2q$ [2, 5].

$G\left(q_z\right)$ is the form factor that describes the extent of the conservation of the transverse component of the momentum of an electron. For the case of the infinite triangular well potential it may be taken as [65]

$$\left|G\left(q_z\right)\right|^2\approx\frac{2\pi G}{d}\left[4\delta\left(q_z\right)+\delta\left(q_z-\frac{2\pi}{d}\right)+\delta\left(q_z+\frac{2\pi}{d}\right)\right] \tag{3.19}$$

where $G=\left(d/4\right)^2\left(d/2-0.707\hbar^{2/3}/\left(144\pi em_{\perp}^{*}E_s\right)^{1/3}\right)^{-2}$.

(b) Piezoelectric acoustic phonons

If a semiconductor crystal consists of dissimilar atoms such as in compound semiconductors where the bonds are partly ionic and the unit cell does not contain a centre of symmetry (as in the zincblende lattice or the trigonal lattice), electrons may be scattered by longitudinal acoustic

waves due to piezoelectric scattering. The matrix element for the interaction of the electrons with the piezoelectric phonons (pz) is given by [2, 5]

$$\left|M\left(\vec{k},\vec{k}'\right)\right|^2_{pz} = \frac{e^2 k_m^2 \hbar u_l}{2Ad \in_{sc} Q} \frac{1}{S\left(\vec{q}\right)} \left|G\left(q_z\right)\right|^2 \begin{pmatrix} N_{\vec{Q}} \\ N_{\vec{Q}}+1 \end{pmatrix} \delta_{\vec{k}',\vec{k}\pm\vec{q}} \tag{3.20}$$

where k_m is the dimensionless piezoelectric coupling constant.

(c) Remote ionized impurity

The electrons may be scattered by the Coulomb potential induced by the ionized impurities. The most effective way to achieve high electron mobility, is to segregate the 2DEG from the ionized impurities through the process of modulation-doping, like the case of AlGaAs/GaAs heterostructures. This structure will reduce the ionized impurity scattering of the electrons of the 2DEG, because the GaAs layer is not doped intentionally. At the low temperatures the electrons of the 2DEG suffer collisions mostly with the acoustic phonons. Therefore, the remotely placed ionized impurities in AlGaAs layer serve as the source of colliding centres for the electrons. For the interaction of electrons with the remote ionized impurities (rm), the matrix element is given by [66, 67]

$$\left|M\left(\vec{k},\vec{k}'\right)\right|^2_{rm} = \frac{1}{A}\left(\frac{e^2}{2 \in_{sc} qS\left(\vec{q}\right)}\right)^2 \int \left|F\left(q,z_i\right)\right|^2 N_i^r\left(z_i\right) dz_i \tag{3.21}$$

where $N_i^r\left(z_i\right)$ is the remote ionized impurity density at a distance z_i from the 2DEG. The form factor $F\left(q,z_i\right)$ in this case may be obtained by using the Fang-Howard variational wave function $\Psi_{F-H}\left(z\right) = \left(b^3/2\right)^{1/2} z\exp\left(-bz/2\right)$, b being the variational parameter given by $\left(33m_\perp^* e^2 n_{2D}/8\hbar^2 \in_{sc}\right)^{1/3}$ [68]. Thus, the form factor may be expressed as

$$F\left(q,z_i\right) = \int_0^\infty \left|\Psi_{F-H}\left(z\right)\right|^2 \exp\left(-q\left|z-z_i\right|\right) dz = \left(\frac{b}{b+q}\right)^2 \exp\left(qz_i\right) \tag{3.22}$$

(d) Background ionized impurity

The unintentional impurities in the semiconductor material form the background ionized impurity. Electrons may be scattered by the Coulomb potential induced by such ionized impurities. To calculate the scattering rate from homogeneous background of impurities, it is

necessary to divide the sample into infinitesimal layers. Each layer may be assumed to be a δ -doped layer of remote ionized impurities at a distance of z_i from the 2DEG. For interaction of the electrons with the background ionized impurities (bg), the corresponding matrix element is given by [69, 70]

$$\left|M\left(\vec{k},\vec{k}'\right)\right|^2_{bg} = \frac{1}{A}\left(\frac{e^2}{2\in_{sc} qS\left(\vec{q}\right)}\right)^2 \frac{N_i^B}{2q}\left[F_1\left(q\right)+F_2\left(q\right)\right] \tag{3.23}$$

where $N_i^B\left(z_i\right)$ is the two-dimensional impurity concentration in the δ -doped layer, $F_1\left(q\right)$ and $F_2\left(q\right)$ are the form factors for the supplementary material adjacent to the central core material, and that for the central core material respectively. They are given by [70]

$$\begin{aligned} F_1\left(q\right) &= \left(\frac{b}{b+q}\right)^6 \\ F_2\left(q\right) &= \frac{2+24\left(q/b\right)^2+48\left(q/b\right)^3+18\left(q/b\right)^4+3\left(q/b\right)^5}{2\left(1+q/b\right)^6} \end{aligned} \tag{3.24}$$

(e) Surface roughness scattering

A two-dimensional electron gas is confined by potential barriers, which are the interfaces of SiO_2 and Si in the case of a Si-MOSFET and the AlGaAs/GaAs interfaces in the case of heterostructures. It is hardly possible to grow such surfaces with flatness of atomic order and thus the electrons may be scattered due to the surface roughness. The matrix element for the interaction of the electrons with the surface roughness (sr) is given by [67, 71]

$$\left|M\left(\vec{k},\vec{k}'\right)\right|^2_{sr} = \frac{\pi}{A}\left(\frac{e^2 n_{2D}\Delta\Lambda}{2\in_{sc} S\left(\vec{q}\right)}\right)^2 \exp\left(-q^2\Lambda^2/4\right) \tag{3.25}$$

where Δ is the average height of the roughness in the z direction, and Λ is the spatial extent of the roughness in the direction parallel to the interface.

3.5 Calculation of the rate of change of the isotropic part of the high-field distribution function of the electrons in a degenerate ensemble of 2DEG for interaction with phonons

The transition of electrons may be between the states $\left|\vec{k}\right\rangle$ and $\left|\vec{k}+\vec{q}\right\rangle$ or between the states $\left|\vec{k}\right\rangle$ and $\left|\vec{k}-\vec{q}\right\rangle$, involving either the absorption or the emission of a phonon. Using the perturbation

theory, one can express the rate of change of the isotropic part of the high-field distribution function of the electrons $\partial f_0(\vec{k})/\partial t\big|_{collision}$ in the degenerate ensemble of 2DEG for interaction with phonons. Symbolically it may be represented as

$$\left.\frac{\partial f_0(\vec{k})}{\partial t}\right|_{collision} = \sum_j \left[\frac{2\pi}{\hbar} \sum_{\vec{q}} \left[\begin{array}{l} \left|\left\langle \vec{k}, N_{\vec{q}}+1 \left| H_j' \right| \vec{k}+\vec{q}, N_{\vec{q}} \right\rangle\right|^2 \delta\left(\varepsilon_{\vec{k}} - \varepsilon_{\vec{k}+\vec{q}} + \hbar\omega_{\vec{q}}\right) f_0\left(\vec{k}+\vec{q}\right)\left(1-f_0\left(\vec{k}\right)\right) \\ -\left|\left\langle \vec{k}-\vec{q}, N_{\vec{q}}+1 \left| H_j' \right| \vec{k}, N_{\vec{q}} \right\rangle\right|^2 \delta\left(\varepsilon_{\vec{k}-\vec{q}} - \varepsilon_{\vec{k}} + \hbar\omega_{\vec{q}}\right) f_0\left(\vec{k}\right)\left(1-f_0\left(\vec{k}-\vec{q}\right)\right) \\ +\left|\left\langle \vec{k}, N_{\vec{q}}-1 \left| H_j' \right| \vec{k}-\vec{q}, N_{\vec{q}} \right\rangle\right|^2 \delta\left(\varepsilon_{\vec{k}} - \varepsilon_{\vec{k}-\vec{q}} - \hbar\omega_{\vec{q}}\right) f_0\left(\vec{k}-\vec{q}\right)\left(1-f_0\left(\vec{k}\right)\right) \\ -\left|\left\langle \vec{k}+\vec{q}, N_{\vec{q}}-1 \left| H_j' \right| \vec{k}, N_{\vec{q}} \right\rangle\right|^2 \delta\left(\varepsilon_{\vec{k}+\vec{q}} - \varepsilon_{\vec{k}} - \hbar\omega_{\vec{q}}\right) f_0\left(\vec{k}\right)\left(1-f_0\left(\vec{k}+\vec{q}\right)\right) \end{array} \right] \right] \quad (3.26)$$

It may be noted that $\sum_j$ appears due to combined interaction of the electrons with the different type of phonons and the factor $\left(1-f_0\right)$ accounts for the degeneracy of the ensemble. H_j' is the perturbation in the Hamiltonian due to j[th] type of phonons.

3.5.1 Interaction with deformation potential acoustic phonons

The rate of change of isotropic part of the high-field distribution function is calculated for the 2DEG which is confined in an infinite triangular potential well due to interaction with the deformation potential acoustic phonons using Eq. (3.26). The matrix elements for such interaction is given by Eq. (3.18). The scattering by the phonons only with the in-plane wave vector has been considered, as done in the analyses reported earlier [42, 72-75]. In such condition the form factor essentially becomes 1.

Since the 2DEG of interest here is assumed to be confined in an infinite triangular potential well, the energy dispersion relation for spherical constant energy surfaces may be taken as [42] $\varepsilon_{\vec{k}} = \hbar^2 k^2 / 2m_{\|}^* + \varepsilon_n$. Here ε_n is the nth energy eigenvalue and is given by $\left(e^2\hbar^2 E_s^2 / 2m_{\perp}^*\right)^{1/3} \gamma_n$; γ_n are the roots of the equation $A_i\left(-\gamma_n\right) = 0$, $A_i\left(z\right)$ being the Airy function.

In the electrical quantum limit, when only the lowest subband is populated at the low temperatures, the layer width d is given by [42] $d = \left(\hbar^2 \in_{sc} / 2m_{\perp}^* e^2 N_i\right)^{1/3} \gamma_0$.

The summation over the two-dimensional phonon wave vector $\vec{q}$ can be transformed into an integration over the angle $\theta_{\vec{k}\vec{q}}$, the angle between $\vec{k}$ and $\vec{q}$ and over $|\vec{q}|$. The limits of $\theta_{\vec{k}\vec{q}}$ are from 0 to 2π and the integration over $\theta_{\vec{k}\vec{q}}$ is straightforward. The limits of $|\vec{q}|$ can be obtained from the energy and momentum conservation equations of the electron-phonon system. They are given by $q = 0$ and $q = 2k \pm 2m_{\|}^{*} u_l / \hbar$. The (+) and (-) signs correspond to the processes of absorption and emission respectively. Hence one can obtain

$$\left.\frac{\partial f_0(\vec{k})}{\partial t}\right|_{\substack{\text{collision with}\\ \text{acoustic phonons}}} \equiv$$

$$\left.\frac{\partial f_0(\vec{k})}{\partial t}\right|_{\text{ac}} = \frac{2\left(E_a m_{\|}^{*}\right)^2}{d\rho_v \hbar^3}\left[\begin{array}{l} f_0(\varepsilon_{\vec{k}})\left(1-f_0(\varepsilon_{\vec{k}})\right)+\varepsilon_L f_0'(\varepsilon_{\vec{k}})\left\{1+\frac{\varepsilon_{\vec{k}}}{\varepsilon_L}+\frac{8}{\pi}\frac{\left(\varepsilon_s\varepsilon_{\vec{k}}\right)^{1/2}}{\varepsilon_L}\right\} \\ +\varepsilon_L\varepsilon_{\vec{k}} f_0''(\varepsilon_{\vec{k}})\left\{1+\frac{16}{3\pi}\frac{\left(\varepsilon_s\varepsilon_{\vec{k}}\right)^{1/2}}{\varepsilon_L}\right\}-2\varepsilon_{\vec{k}} f_0(\varepsilon_{\vec{k}}) f_0'(\varepsilon_{\vec{k}}) \\ -12\varepsilon_s\varepsilon_{\vec{k}} f_0(\varepsilon_{\vec{k}}) f_0''(\varepsilon_{\vec{k}}) \end{array}\right] \qquad (3.27)$$

where $\varepsilon_L = K_B T_L$, $\varepsilon_s = m_{\|}^{*} u_l^2 / 2$, $f_0'(\varepsilon_{\vec{k}})$ and $f_0''(\varepsilon_{\vec{k}})$ are the first order and the second order derivatives of the heated Fermi-Dirac distribution function with respect to electron energy.

3.5.2 Interaction with piezoelectric acoustic phonons

For the interaction with the piezoelectric acoustic phonons, the matrix elements as given by Eq. (3.20) may be used. Now following the same steps as those of the preceding paragraph one can calculate the rate of change of the isotropic part of the high-field distribution function for the ensemble of 2DEG confined in an infinite triangular potential well due to interaction with the piezoelectric acoustic phonons. Thus, one can obtain

$$\left.\frac{\partial f_0(\vec{k})}{\partial t}\right|_{\substack{\text{collision with}\\ \text{piezoelectric phonons}}} \equiv$$

$$\left.\frac{\partial f_0(\vec{k})}{\partial t}\right|_{pz} = \frac{e^2 k_m^2 \varepsilon_s}{d \in_{sc} \hbar}\left[\begin{array}{l} f_0'(\varepsilon_{\vec{k}})\left\{1+\frac{2}{\pi}\left(\frac{\varepsilon_s}{\varepsilon_{\vec{k}}}\right)^{1/2}\right\}+\varepsilon_L f_0''(\varepsilon_{\vec{k}})\left\{1+\frac{4}{\pi}\frac{\left(\varepsilon_s\varepsilon_{\vec{k}}\right)^{1/2}}{\varepsilon_L}\right\} \\ -2 f_0(\varepsilon_{\vec{k}}) f_0'(\varepsilon_{\vec{k}})-4\varepsilon_s f_0(\varepsilon_{\vec{k}}) f_0''(\varepsilon_{\vec{k}}) \end{array}\right] \qquad (3.28)$$

It may be noted here that $f_0\left(\varepsilon_{\vec{k}}\right)$ term in $\partial f_0\left(\vec{k}\right)/\partial t\big|_{pz}$ is absent, since its contribution turns out to be negligible in this case. Furthermore, it may also be noted that for a non-degenerate ensemble of 2DEG when one can assume $f_0\left(\varepsilon_{\vec{k}}\right) \ll 1$ and $\left(1-f_0\right)$ term in Eq. (3.26) reduces to 1. Thus, for a non-degenerate ensemble, the collision terms Eq. (3.27) and (3.28) can be reduced by omitting the terms containing the products of f_0, f_0' and f_0''.

3.6 Calculation of the rate of change of the isotropic part of the high-field distribution function of the electrons in a degenerate ensemble of 2DEG due to an applied field

The time rate of change of high-field distribution function due to an applied electric field is obtained from left-hand-side of Eq. (3.17)

$$\left.\frac{\partial f_0\left(\vec{k}\right)}{\partial t}\right|_{field} = -\frac{e^2E^2}{m_{\|}^*}\frac{\partial}{\partial \varepsilon_{\vec{k}}}\left(\frac{\varepsilon_{\vec{k}}}{p_{eff}\left(\varepsilon_{\vec{k}}\right)}\frac{\partial f_0\left(\varepsilon_{\vec{k}}\right)}{\partial \varepsilon_{\vec{k}}}\right) \tag{3.29}$$

where E is the applied electric field and $p_{eff}\left(\varepsilon_{\vec{k}}\right)$ is the effective scattering rate of an electron due to the combined interaction with the deformation potential acoustic and the piezoelectric phonons.

3.7 Calculation of the field dependence of the electron temperature of different surface layers for interaction with phonons

The field dependence of the effective electron temperature of an ensemble of 2DEG on different surface layers for interaction with phonons can be calculated from Eq. (3.14) which is the energy balance condition for the electron-phonon system.

As has already been mentioned, in the effective temperature approximation, $f_0\left(\vec{k}\right)$ for a degenerate ensemble is given by the heated Fermi-Dirac function at an effective electron temperature $T_e\left(E\right) > T_L$. Unless one makes some oversimplified approximations, the integration in Eq. (3.14) can hardly be evaluated analytically. As such, in place of the Fermi-Dirac function, here we make use of a well-tested alternative distribution which has been used in [76-78]. The use of such a distribution makes it possible to carry out the integration in Eq. (3.14) analytically without incurring any significant error. The whole energy range is split there into three regions: $0 < \varepsilon_{\vec{k}} \le \beta_1\varepsilon_F$; $\left(\beta_1 \le 1\right)$, $\beta_1\varepsilon_F < \varepsilon_{\vec{k}} \le \beta_2\varepsilon_F$; $\left(\beta_2 \ge 1\right)$ and $\beta_2\varepsilon_F \le \varepsilon_{\vec{k}} < \infty$. Here

β_1 and β_2 are chosen as $\beta_1 = 1 - K_B T_L / \varepsilon_F$ and $\beta_2 = 1 + K_B T_L / \varepsilon_F$. In the first and the third regions, the distribution is represented by a simple exponential function, whereas in the narrow intermediate region the same is assumed to be given by Karlovsky's model of linear approximation [79]. The integrals in Eq. (3.14) for these regions are now straight forward.

3.7.1 Case of a moderately degenerate layer under different conditions

For the case of a moderately degenerate layer, the effective electron temperature characteristics can be obtained by integrating the energy balance condition for electron-phonon system of Eq. (3.14) over the full energy range i.e., from 0 to ∞.

(i) When the electrons interact only with the deformation potential acoustic phonons

For the interaction with the deformation potential acoustic phonons, the scattering rate is obtained as

$$p_{ac}\left(\varepsilon_{\vec{k}}\right) = \tau_{acm}\left[1 + \frac{4}{\pi}\frac{\left(\varepsilon_s \varepsilon_{\vec{k}}\right)^{1/2}}{\varepsilon_L}\right] \tag{3.30}$$

where $\tau_{acm} = E_a^2 m_{\|}^* K_B T_L / d\rho_v \hbar^3 u_l^2$. The field term of the Eq. (3.14) for the interaction only with the deformation potential acoustic phonons can be obtained by using Eq. (3.30) in Eq. (3.29).

Now putting the collision term of Eq. (3.27) and the field term in the energy balance condition, the integrals in Eq. (3.14) can be carried out for the three energy regions. Thus, one can express the energy balance equation in the form

$$\left[I_{coll}^{ac}\right]_0^{\beta_1\varepsilon_F} + \left[I_{coll}^{ac}\right]_{\beta_1\varepsilon_F}^{\beta_2\varepsilon_F} + \left[I_{coll}^{ac}\right]_{\beta_2\varepsilon_F}^{\infty} = \left[I_{field}^{ac}\right]_0^{\beta_1\varepsilon_F} + \left[I_{field}^{ac}\right]_{\beta_1\varepsilon_F}^{\beta_2\varepsilon_F} + \left[I_{field}^{ac}\right]_{\beta_2\varepsilon_F}^{\infty} \tag{3.31}$$

The expressions of each of these integrals are given in the Appendix A.

(ii) When the electrons interact only with the piezoelectric acoustic phonons

For the interaction with the piezoelectric acoustic phonons, the scattering rate is obtained as

$$p_{pz}\left(\varepsilon_{\vec{k}}\right) = \frac{\tau_{pzm}}{\varepsilon_{\vec{k}}}\left[1 + \frac{4}{\pi}\frac{\left(\varepsilon_s \varepsilon_{\vec{k}}\right)^{1/2}}{\varepsilon_L}\right] \tag{3.32}$$

where $\tau_{pzm} = e^2 k_m^2 K_B T_L / 4d \in_{sc} \hbar$. The field term of the Eq. (3.14) for the interaction with the piezoelectric acoustic phonons can be obtained by putting Eq. (3.32), the expression for $p_{pz}\left(\varepsilon_{\vec{k}}\right)$ in the Eq. (3.29).

Now putting Eq. (3.28) for the collision term and the field term in the energy balance equation, the integrals in Eq. (3.14) can be carried out for the three energy regions. Thus, one can express the energy balance equation in the form

$$\left[I_{coll}^{pz}\right]_{0}^{\beta_1\varepsilon_F}+\left[I_{coll}^{pz}\right]_{\beta_1\varepsilon_F}^{\beta_2\varepsilon_F}+\left[I_{coll}^{pz}\right]_{\beta_2\varepsilon_F}^{\infty}=\left[I_{field}^{pz}\right]_{0}^{\beta_1\varepsilon_F}+\left[I_{field}^{pz}\right]_{\beta_1\varepsilon_F}^{\beta_2\varepsilon_F}+\left[I_{field}^{pz}\right]_{\beta_2\varepsilon_F}^{\infty} \tag{3.33}$$

The expressions of the integrals are given in the Appendix B.

(iii) For the combined interaction with both the deformation potential acoustic and the piezoelectric acoustic phonons

The effective scattering rate $p_{eff}\left(\varepsilon_{\vec{k}}\right)$ due to the combined interaction with both the deformation potential and the piezoelectric acoustic phonons may be obtained by Mattheisen's rule. Thus, one obtains

$$p_{eff}\left(\varepsilon_{\vec{k}}\right)=\frac{\tau_{pzm}}{\varepsilon_{\vec{k}}}\left[1+\frac{4}{\pi}\frac{\left(\varepsilon_s\varepsilon_{\vec{k}}\right)^{1/2}}{\varepsilon_L}\right]\left[1+\tau_n\varepsilon_{\vec{k}}\right] \tag{3.34}$$

where $\tau_n=\tau_{acm}/\tau_{pzm}$. The field term of the Eq. (3.14) for the combined interaction with both the deformation potential and the piezoelectric acoustic phonons can be obtained by using Eq. (3.34) for $p_{eff}\left(\varepsilon_{\vec{k}}\right)$ in Eq. (3.29).

Now putting the collision terms of Eq. (3.27) and (3.28) and the field term in the energy balance equation, the integrals in Eq. (3.14) can be carried out for the three energy regions. Thus, one can obtain the energy balance equation in the form

$$\left[I_{field}^{eff}\right]_{0}^{\beta_1\varepsilon_F}+\left[I_{field}^{eff}\right]_{\beta_1\varepsilon_F}^{\beta_2\varepsilon_F}+\left[I_{field}^{eff}\right]_{\beta_2\varepsilon_F}^{\infty}=\left[I_{coll}^{eff}\right]_{0}^{\beta_1\varepsilon_F}+\left[I_{coll}^{eff}\right]_{\beta_1\varepsilon_F}^{\beta_2\varepsilon_F}+\left[I_{coll}^{eff}\right]_{\beta_2\varepsilon_F}^{\infty} \tag{3.35}$$

The expressions of the integrals are given in the Appendix C.

3.7.2 Case of a highly degenerate layer of an ensemble of 2DEG under the condition of the combined interaction of the electrons with the deformation potential acoustic and the piezoelectric acoustic phonons

A sample becomes more and more degenerate when the concentration of the electrons is increased or the lattice temperature is decreased. As the degeneracy is increased the contribution of the integrals in Eq. (3.35) representing the parts of the energy balance equation

over the first $\left(0 < \varepsilon_{\vec{k}} \le \beta_1 \varepsilon_F\right)$ and the third $\left(\beta_2 \varepsilon_F \le \varepsilon_{\vec{k}} < \infty\right)$ regions will tend to be more and more insignificant. Hence, for a highly degenerate ensemble, only the integrals over the intermediate region $\left(\beta_1 \varepsilon_F < \varepsilon_{\vec{k}} \le \beta_2 \varepsilon_F\right)$ would make the principal contribution. Thus, for a highly degenerate ensemble of 2DEG, the field dependence of the effective temperature of the electrons may be obtained from Eq. (3.35) taking into account only the middle terms of both sides, in the light of Karlovsky's framework, which he used for the analysis of $I-V$ characteristic of a Tunnel diode [79]. Hence one can approximately obtain the effective electron temperature characteristics for the combined interaction of the electrons in a highly degenerate ensemble of 2DEG from

$$E^2 = \frac{\hbar^2 \tau_{pzm}}{2\pi C e^2 f\left(\eta_D, T_L\right)} \times \left[\begin{array}{l} C_{ac} \left[\begin{array}{l} \left\{ \frac{1}{8} - \frac{1}{2} C^2 \left(\eta_D \varepsilon_L\right)^2 + \frac{1}{2} C \varepsilon_L \right\} \left(\eta_D \varepsilon_L\right)^2 \left(\beta_2^2 - \beta_1^2\right) \\ -\frac{3}{4} C^2 \left(\eta_D \varepsilon_L\right)^4 \left(\beta_2^4 - \beta_1^4\right) + \frac{4}{3} C^2 \left(\eta_D \varepsilon_L\right)^4 \left(\beta_2^3 - \beta_1^3\right) \\ + \frac{16}{5\pi} C \varepsilon_s^{1/2} \left(\eta_D \varepsilon_L\right)^{5/2} \left(\beta_2^{5/2} - \beta_1^{5/2}\right) \end{array} \right] \\ + C_{pz} \left[\begin{array}{l} \frac{4}{3\pi} C \varepsilon_s^{1/2} \left(\eta_D \varepsilon_L\right)^{3/2} \left(\beta_2^{3/2} - \beta_1^{3/2}\right) - \frac{2}{3} C^2 \left(\eta_D \varepsilon_L\right)^3 \left(\beta_2^3 - \beta_1^3\right) \\ + C^2 \left(\eta_D \varepsilon_L\right)^3 \left(\beta_2^2 - \beta_1^2\right) \end{array} \right] \end{array} \right] \quad (3.36)$$

where η_D is the degeneracy parameter and is given by $\eta_D = \varepsilon_F / K_B T_L$ and the expressions for C, C_{ac}, C_{pz} and $f\left(\eta_D, T_L\right)$ are given in Appendix A, B and C.

3.7.3 Case of a non-degenerate layer of an ensemble of 2DEG

(i) When the electrons interact only with the deformation potential acoustic phonons

For a non-degenerate ensemble of 2DEG, the field dependence of the electron temperature for interaction only with the deformation potential phonons has been obtained as

$$\left[1 + 2\left(\frac{\varepsilon_s}{\pi \varepsilon_L}\right)^{1/2} \left(\frac{T_e}{T_L}\right)^{1/2}\right] \left[\frac{T_e}{T_L} - 1 - 4\left(\frac{\varepsilon_s}{\pi \varepsilon_L}\right)^{1/2} \left(\frac{T_e}{T_L}\right)^{1/2}\right] = \frac{1}{2}\left(\frac{eE\hbar^3 d \rho_v u_l}{E_a^2 m_{\|}^{*2} \varepsilon_L}\right)^2 \quad (3.37)$$

(ii) When the electrons interact only with the piezoelectric acoustic phonons

The field dependence of the electron temperature for interaction only with the piezoelectric phonons has been obtained as

$$\left(\frac{T_L}{T_e}\right)^2\left[1+2\left(\frac{\varepsilon_s}{\pi\varepsilon_L}\right)^{1/2}\left(\frac{T_e}{T_L}\right)^{1/2}\right]\left[\frac{T_e}{T_L}-1-2\left(\frac{\varepsilon_s}{\pi\varepsilon_L}\right)^{1/2}\left(\frac{T_e}{T_L}\right)^{1/2}\right]=\left(\frac{4E\in_{sc} d\hbar}{ek_m^2 m_{\|}^* u_l}\right)^2 \qquad (3.38)$$

(iii) For the combined interaction with both the deformation potential acoustic and the piezoelectric acoustic phonons

For the combined interaction of the electrons in a non-degenerate ensemble of 2DEG, with the deformation potential acoustic and the piezoelectric acoustic phonons, carrying out a straight forward analysis, one can obtain the field dependence of the effective electron temperature from

$$C_f\left[\frac{\varepsilon_e^2}{\tau_n}-\frac{\varepsilon_e}{\tau_n^2}+\frac{1}{\tau_n^3}\exp\left(\frac{1}{\tau_n\varepsilon_e}\right)E_1\left(\frac{1}{\tau_n\varepsilon_e}\right)\right]=$$
$$\varepsilon_L^2\left[C_{ac}\varepsilon_L\left(\frac{T_e}{T_L}\right)^2\left\{\frac{T_e}{T_L}-1-4\left(\frac{\varepsilon_s}{\pi\varepsilon_L}\right)^{1/2}\left(\frac{T_e}{T_L}\right)^{1/2}\right\}+C_{pz}\left(\frac{T_e}{T_L}\right)\left\{\frac{T_e}{T_L}-1-2\left(\frac{\varepsilon_s}{\pi\varepsilon_L}\right)^{1/2}\left(\frac{T_e}{T_L}\right)^{1/2}\right\}\right] \qquad (3.39)$$
$$\times\left[1+2\left(\frac{\varepsilon_s}{\pi\varepsilon_L}\right)^{1/2}\left(\frac{T_e}{T_L}\right)^{1/2}\right]$$

where $E_1(z)$ is the exponential integral function [51].

3.8 Results for the field dependence of the effective electron temperature for the quantum confined surface layers of 2DEG in InSb, GaAs and GaN, with different levels of degeneracy, and their comparison with the theoretical and the experimental results which are available from other studies

Considering a degenerate ensemble of non-equilibrium 2DEG, confined in a quantum well of a compound semiconductor an approximate analysis has been made here for the field dependence of the effective electron temperature. An assessment of the effects of degeneracy and that of the piezoelectric interaction of the electrons, on the field dependence can be made from the present analysis. It may be noted that the dependence of the effective electron temperature on the electric field is quite complex under the prevalent conditions of interest here.

The assessment of the effects of degeneracy and that of the piezoelectric interaction of the non-equilibrium electrons on the effective electron temperature characteristics has been made through a comparison of the characteristics obtainable from the present analysis with the available theoretical and experimental results. Three compounds, which are quite important for the device purpose, namely InSb, GaAs and GaN have been considered. The values of the material parameters for the compounds are given in Table 3.1. It may be kept in mind that $m_{\|}^{*} = m_{\perp}^{*} = m^{*}$ for each compound which have been considered here. The numerical values of T_e for different values of the electric field are calculated for these compounds from the present analysis and are plotted in Figures 3.1, 3.2, 3.3, 3.4, 3.5 and 3.6.

In each figure, the characteristics drawn with solid lines correspond to the case when the degeneracy of the ensemble has been taken into account. Whereas, the characteristics which have been obtained without taking the degeneracy factor into account, have been plotted with dashed lines. Apart from that, there are two sets of curves. One set corresponds to the conditions when the electrons make combined interaction with the piezoelectric and the deformation potential acoustic phonons and the other set corresponds to the interaction only with deformation potential acoustic phonons.

Table 3.1: Material parameters

Physical Parameters	InSb	GaAs	GaN
Deformation potential, E_a (eV)	20.0	12.0	8.0
Acoustic velocity, u_l $(\times 10^3\ m.s^{-1})$	3.7	5.22	5.0
Density, ρ_v $(\times 10^3\ kg.m^{-1})$	5.78	5.31	6.1
Static dielectric constant, $\in_{sc}$	17.51	12.91	9.5
Piezoelectric coupling constant, k_m	0.027	0.052	0.18
Effective-mass ratio $\left(m^{*}/m_0\right)$	0.014	0.072	0.2

m_0 being the free electron mass

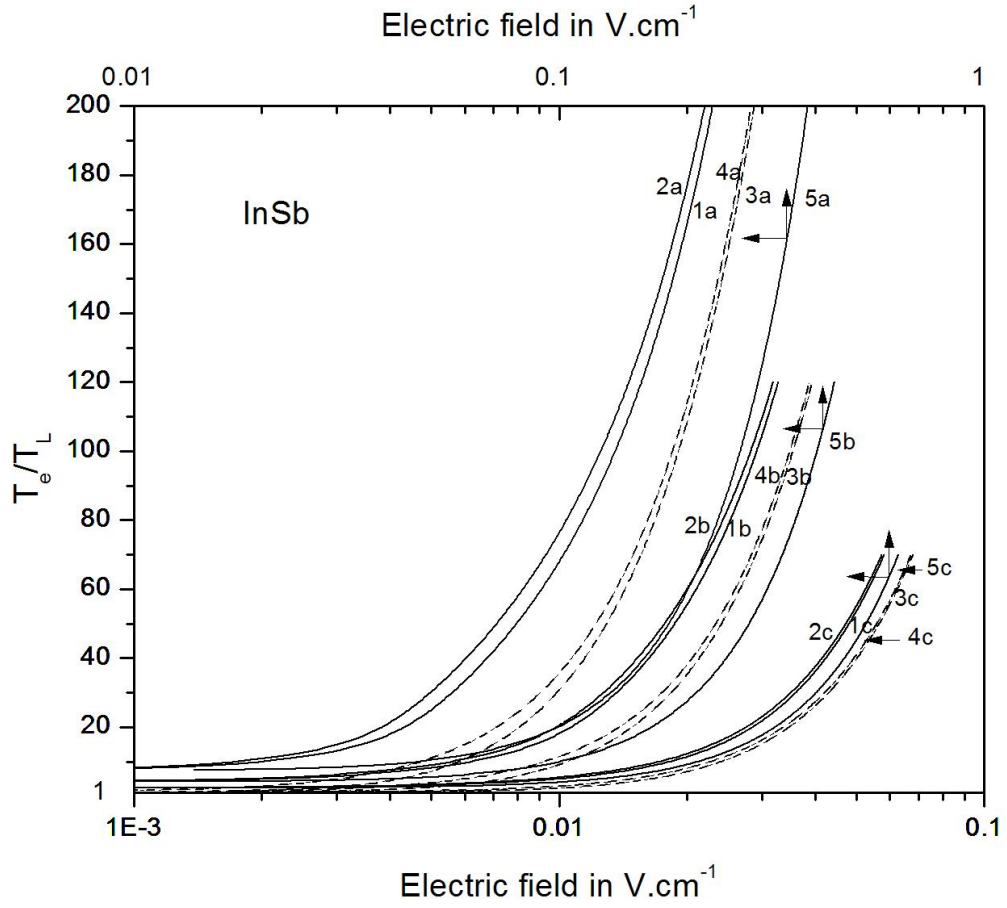

Figure 3.1 Dependence of the normalized electron temperature upon the electric field in InSb for different lattice temperatures and different levels of degeneracy when the layer concentration is taken to be $2.5\times10^{13}\ m^{-2}$. Curves marked a, b and c are obtained at the lattice temperatures of 2, 4, and 10*K*, which correspond to $\eta_D = 18.93$, 9.16 and 2.86 respectively. Solid curves are obtained considering degeneracy and dashed curves are obtained when degeneracy is not taken into account. The curves 1 and 3 represent the dependence for combined interactions with deformation potential acoustic and piezoelectric phonons, and the curves 2 and 4 are obtained for interaction only with deformation potential acoustic phonons. Curve 5 have been obtained for $N_i = 1.0\times10^{16}\ m^{-2}$ [80], i.e., for a highly degenerate specimen from the present theoretical analysis.

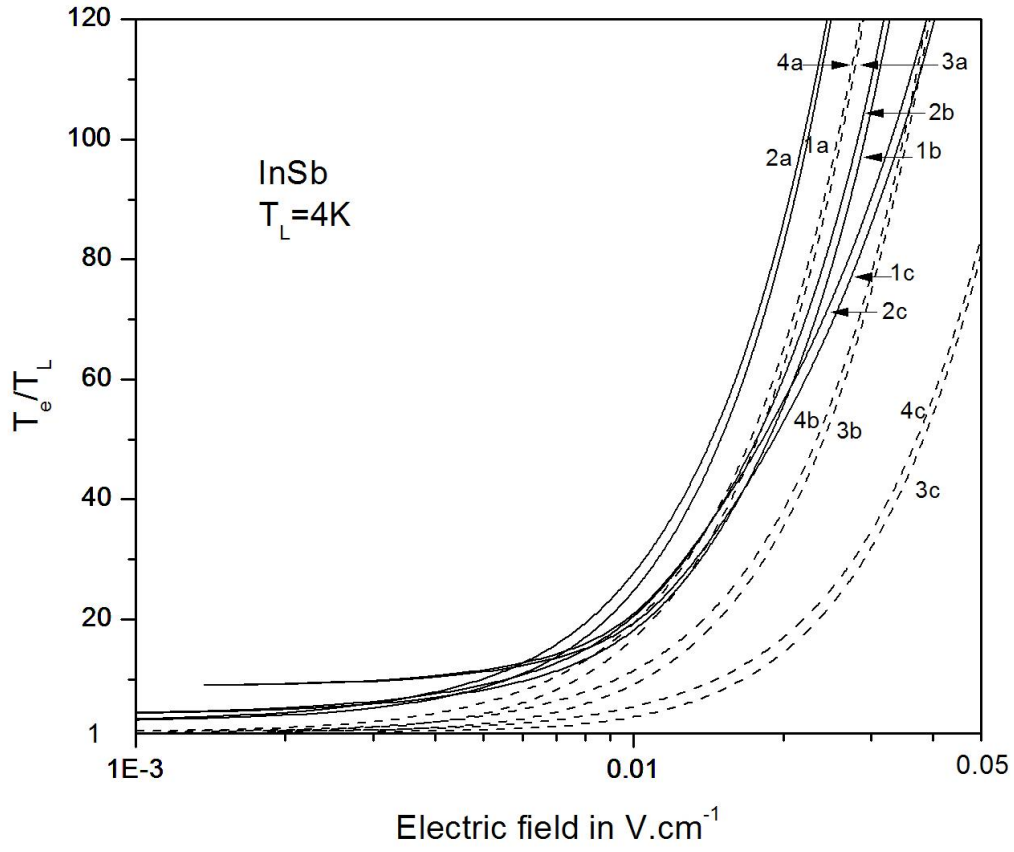

Figure 3.2 Dependence of the normalized electron temperature upon the electric field in InSb for different values of the layer concentration, at a fixed lattice temperature of 4*K*. The curves a, b and c are obtained for layer concentrations of $1.0\times10^{13}\ m^{-2}$, $2.5\times10^{13}\ m^{-2}$ and $1.0\times10^{14}\ m^{-2}$ respectively, corresponding to $\eta_D = 4.98$, 9.16 and 25.8. Solid curves are obtained considering degeneracy and dashed curves are obtained when degeneracy is not taken into account. The curves 1 and 3 represent the dependence for combined interactions with deformation potential acoustic and piezoelectric phonons, and the curves 2 and 4 are obtained for interaction only with deformation potential acoustic phonons.

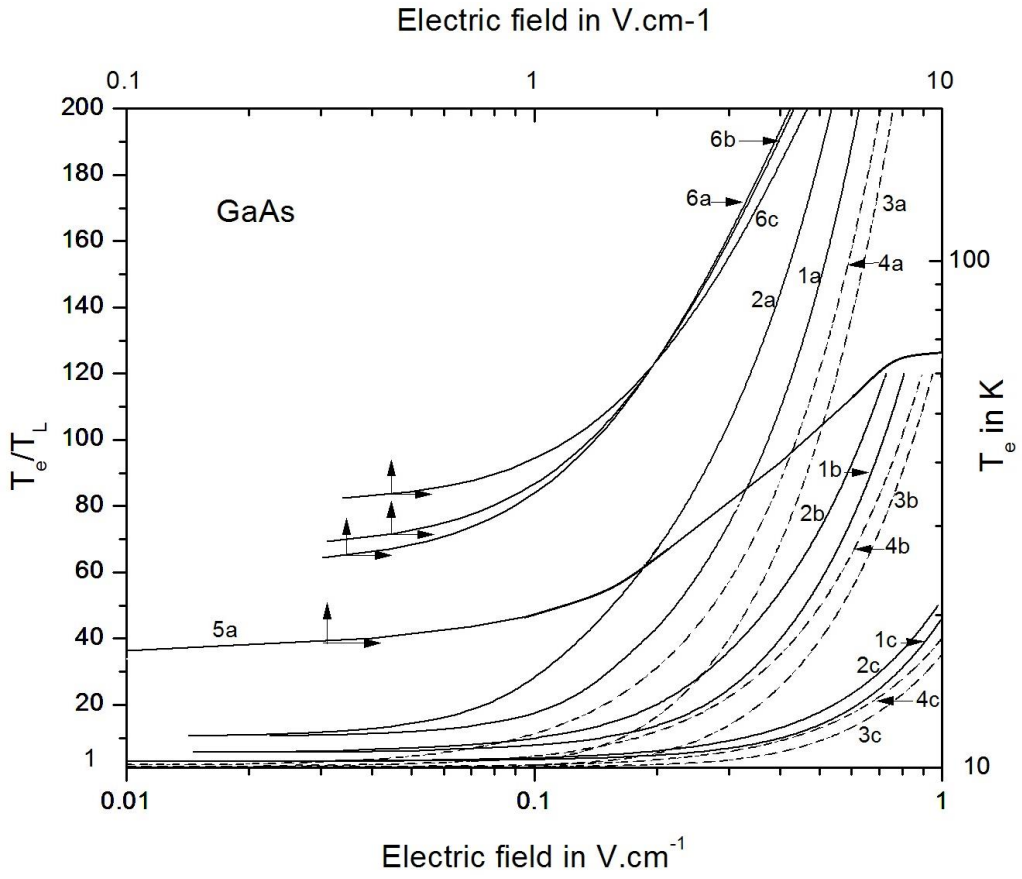

Figure 3.3 Dependence of the normalized electron temperature upon the electric field in GaAs for different lattice temperatures and different levels of degeneracy when the layer concentration is taken to be $5.0\times10^{13}\ m^{-2}$. Curves marked a, b and c are obtained at the lattice temperatures of 2, 4, and 10*K*, which correspond to $\eta_D = 19.6$, 9.79 and 3.91 respectively. Solid curves are obtained considering degeneracy and dashed curves are obtained when degeneracy is not taken into account. The curves 1 and 3 represent the dependence for combined interactions with deformation potential acoustic and piezoelectric phonons, and the curves marked 2 and 4 are obtained for interaction only with deformation potential acoustic phonons. Curves 5 and 6 have been obtained for $N_i = 7.0\times10^{15}\ m^{-2}$, i.e., for a highly degenerate specimen. Curve 5 represent the average experimental characteristic at $T_L = 2K$ [81], and curves 6 are obtained from the present theoretical analysis.

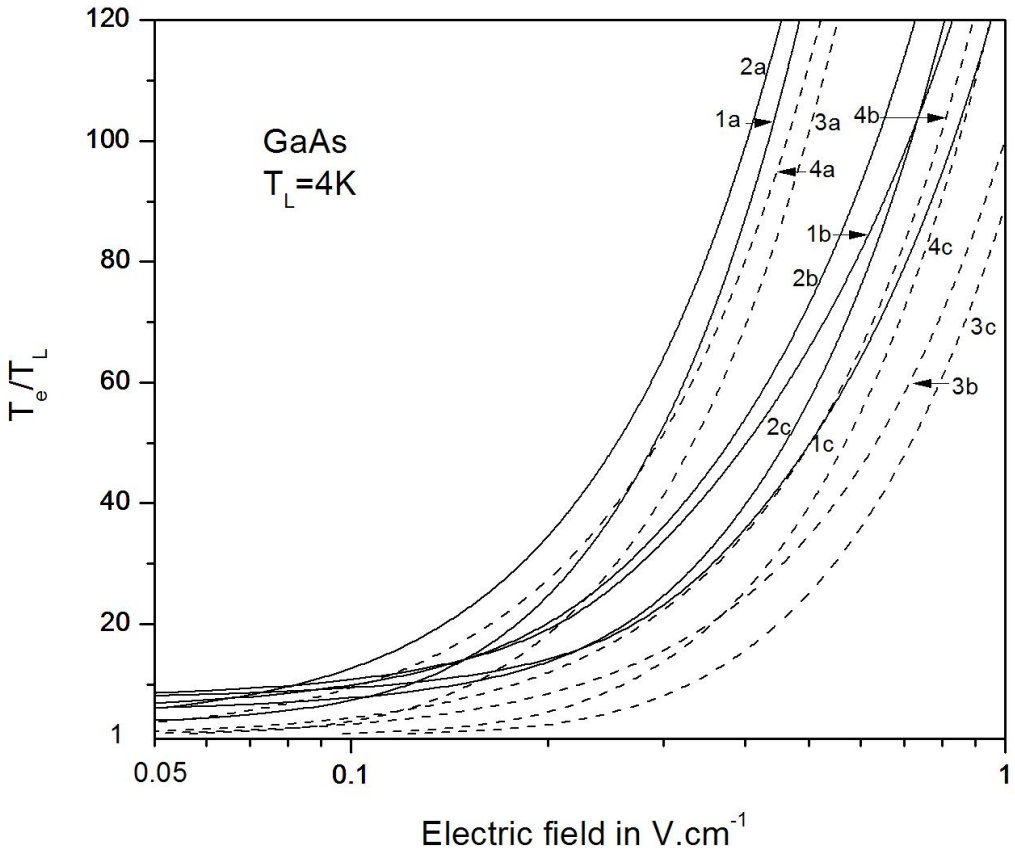

Figure 3.4 Dependence of the normalized electron temperature upon the electric field in GaAs for different values of the layer concentration at a fixed lattice temperature of 4*K*. The curves a, b and c are obtained for layer concentrations of $1.0\times10^{13}\ m^{-2}$, $5.0\times10^{13}\ m^{-2}$ and $1.0\times10^{14}\ m^{-2}$ respectively, corresponding to $\eta_D = 3.28$, 9.79 and 15.75. Solid curves are obtained considering degeneracy and dashed curves are obtained when degeneracy is not taken into account. The curves 1 and 3 represent the dependence for combined interactions with deformation potential acoustic and piezoelectric phonons, and the curves marked 2 and 4 are obtained for interaction only with deformation potential acoustic phonons.

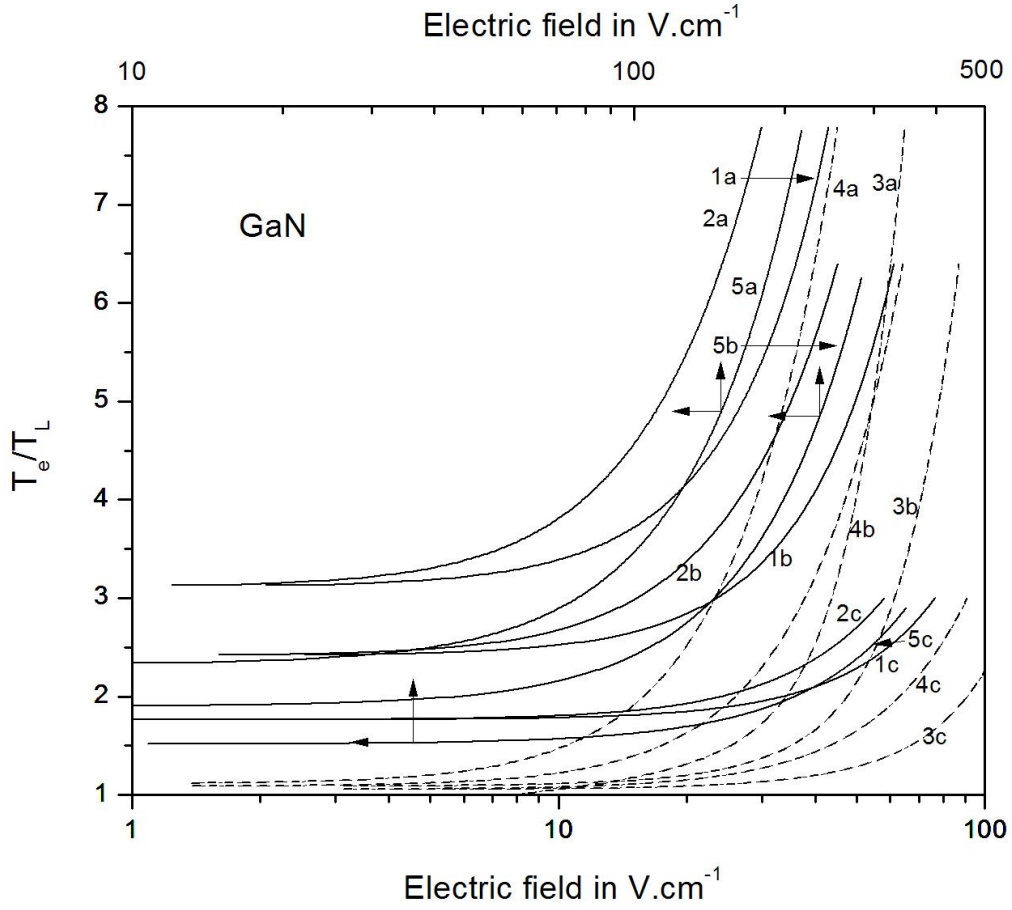

Figure 3.5 Dependence of the normalized electron temperature upon the electric field in GaN for different lattice temperatures and different levels of degeneracy when the layer concentration is taken to be $2.0\times10^{15}\ m^{-2}$. Curves marked a, b and c are obtained at the lattice temperatures of 77, 125 and 300*K*, which correspond to $\eta_D = 5.3$, 3.26 and 1.36 respectively. Solid curves are obtained considering degeneracy and dashed curves are obtained when degeneracy is not taken into account. The curves 1 and 3 represent the dependence for combined interactions with deformation potential acoustic and piezoelectric phonons, and the curves marked 2 and 4 are obtained for interaction only with deformation potential acoustic phonons. Curve 5 have been obtained for $N_i = 1.27\times10^{17}\ m^{-2}$ [82], i.e., for a highly degenerate specimen from the present theoretical analysis.

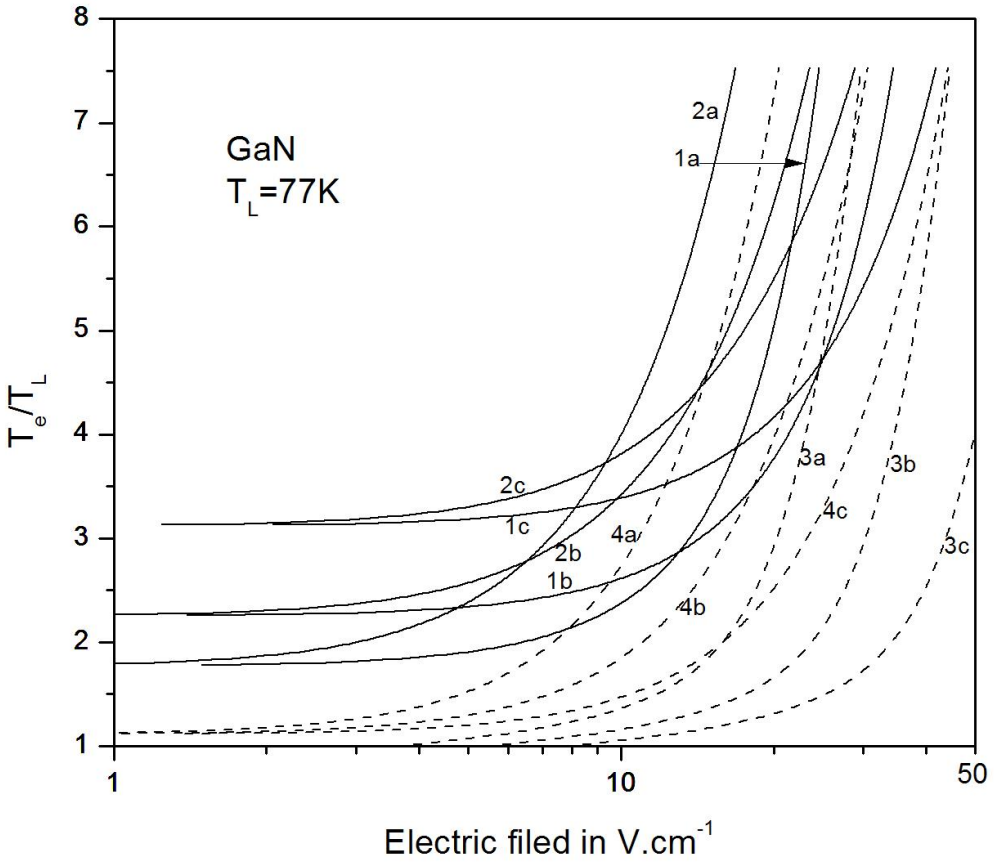

Figure 3.6 Dependence of the normalized electron temperature upon the electric field in GaN for different values of the layer concentration at a fixed lattice temperature of 77*K*. The curves a, b and c are obtained for layer concentrations of 2.0×10^{14} m^{-2}, 6.7×10^{14} m^{-2} and 2.0×10^{15} m^{-2} respectively, corresponding to $\eta_D = 1.1,\ 2.5$ and 5.3. Solid curves are obtained considering degeneracy and dashed curves are obtained when degeneracy is not taken into account. The curves 1 and 3 represent the dependence for combined interactions with deformation potential acoustic and piezoelectric phonons, and the curves marked 2 and 4 are obtained for interaction only with deformation potential acoustic phonons.

3.9 Discussions

Figure 3.1 shows the effective electron temperature-field characteristics for an ensemble of 2DEG in a quantum well of InSb with a layer concentration of $N_i = 2.5\times10^{13}\ m^{-2}$ at the lattice temperatures of 2, 4 and 10*K* corresponding to the degeneracy parameter $\eta_D = 18.93$, 9.16 and 2.86 respectively. Figure 3.2 on the other hand shows the similar characteristics which are obtained at a fixed lattice temperature, $T_L = 4K$ and for different values of N_i ; $N_i = 1.0\times10^{13}\ m^{-2}$, $2.5\times10^{13}\ m^{-2}$ and $1.0\times10^{14}\ m^{-2}$.

Similar sets of the characteristics which follow from the present analysis for an ensemble of 2DEG in a quantum well of GaAs have been plotted in Figures 3.3 and 3.4 respectively.

Figure 3.3 has been obtained for a layer concentration of $N_i = 5.0\times10^{13}\ m^{-2}$ at the lattice temperatures of 2, 4 and 10*K*, the corresponding values of the degeneracy parameter η_D being 19.6, 9.79 and 3.91 respectively. Apart from that the characteristics which follow from the present analysis for a highly degenerate ensemble with $N_i = 7.0\times10^{15}\ m^{-2}$ at $T_L = 2K$ along with the experimentally observed characteristics [81] under the similar prevalent conditions have also been plotted in the same Figure 3.3.

Figure 3.4 depicts similar characteristics as that of Figure 3.2 at a fixed T_L of 4*K* and for three different values of the layer concentration N_i, namely $1.0\times10^{13}\ m^{-2}$, $5.0\times10^{13}\ m^{-2}$ and $1.0\times10^{14}\ m^{-2}$, for an ensemble of 2DEG in the quantum well of GaAs.

GaN, nowadays proves to be a quite important compound from the device point of view, although it possesses significantly different values of the physical parameters, like the piezoelectric coupling constant, effective mass and the deformation potential constant etc. compared to those of InSb and GaAs. As such, it is observed that the electron ensemble in a quantum well of GaN gets heated up for a considerably higher value of the electric field and at higher lattice temperatures, compared to the other two compounds. Figure 3.5 shows the electron temperature characteristics for a non-equilibrium ensemble of 2DEG in a well of GaN at $T_L = 77$, 125 and $300K$, the layer concentration N_i being $2.0\times10^{15}\ m^{-2}$. Hence the corresponding degeneracy parameters come out to be $\eta_D = 5.3$, 3.26 and 1.36 respectively. In Figure 3.6 the characteristics for a non-equilibrium ensemble of 2DEG in a well of GaN has

been presented at a fixed lattice temperature of $T_L = 77K$ and for $N_i = 2.0\times10^{14}\ m^{-2}$, $6.7\times10^{14}\ m^{-2}$ and $2.0\times10^{15}\ m^{-2}$ which correspond to $\eta_D = 1.1, 2.5, 5.3$ respectively.

Comparing the solid curves with the dashed ones for any lattice temperature, it may be noted that, particularly for the higher fields, the qualitative nature of the $T_e/T_L - E$ characteristics nearly remains the same irrespective of whether the degeneracy of the ensemble is taken into account or not. But at any field, whatsoever, the degeneracy significantly raises the electron temperature, and the rise is effected more, the lower the lattice temperature is. The rate of rise of the temperature picks up fast as the field increases.

The interaction with piezoelectric phonons tends to decrease the electron temperature at any field without much change in the qualitative nature of the characteristics. Moreover, as expected, the electron temperature at any field is effected more the higher is the value of the piezoelectric coupling constant of the material or the lower is the lattice temperature.

It may be mentioned here that the experimentally reported values of the concentration of the electrons are sometimes larger than what have been considered in the present work. For example, in [80], an investigation has been carried out on the weak antilocalisation effect in InSb thin films, in which some quasi-two-dimensional features have been found for the samples used in the investigation. The electron concentration as reported there has been $\sim10^{16}\ m^{-2}$. Similarly, the effects of GaN interlayer on the transport properties of 2DEG confined in the lattice matched AlInN/AlN/GaN heterostructures have been studied in [82]. The electron concentration as reported there has been $\sim10^{17}\ m^{-2}$. As such, considering these higher values of the electron concentration for InSb and GaN, the field dependence of the effective electron temperature have also been calculated from (3.36), and the characteristics are represented here by the curves 5a, 5b and 5c in Figures 3.1 and 3.5 for InSb and GaN respectively. The curves also display the effect, that the degeneracy significantly raises the electron temperature at any field, and the rise is more the lower the lattice temperature is. Moreover, the rate of rise of the effective electron temperature, for such higher values of the concentration of electrons, also picks up fast with the increase of the electric field as one obtains for the lower values of the concentration, when the field dependence of the effective electron temperature is calculated from (3.35).

From Figures 3.1 and 3.3 one can note that the electron ensemble attains the same values of T_e/T_L in the quantum well of GaAs at a higher electric field, compared to that for the well of

InSb. For example, at the lattice temperature of 2*K*, T_e/T_L rises to about 120 at an electric field of $\sim 0.015\ V/cm$ for InSb, whereas, a higher electric field $\sim 0.3\ V/cm$ is required in case of GaAs for the same rise of T_e/T_L. This is principally because of the higher values of the effective mass of GaAs $\left(m^* = 0.072m_0\right)$ compared to that of InSb $\left(m^* = 0.014m_0\right)$. Apart from that, when the lattice temperature is quite low $\sim 2K$, the interaction with piezoelectric phonons in any semiconductor would dominate over that with deformation acoustics phonons in determining the characteristics of the effective electron temperature. The piezoelectric coupling constant for GaAs is almost the double of that of InSb. As such, the scattering rate due to interaction with the piezoelectric phonons would be more in GaAs than in InSb. Hence the dominating interaction with the piezoelectric phonons under the prevalent condition would make the electron temperature lower in the wells of GaAs than that of InSb at any electric field.

The prevalent conditions for which the analysis has been developed here are accessible in the laboratory. There are ample experimental data available in the literature for the dependence of the effective electron temperature on the electric field for the bulk semiconductor structures [26]. But the present theoretical analysis deals with the dependence of the effective electron temperature of a degenerate ensemble of 2DEG upon the electric field in a quantum well of a compound semiconductor at low lattice temperatures. The scarcity of the corresponding experimental data in the literature makes it hardly possible to make a conclusive comparison of the present theoretical results with the experimental observations. However, the experimental data on the field dependence of the effective temperature of the electrons, for the sample quantum well of GaAs-AlGaAs with $N_i = 7.0\times10^{15}\ m^{-2}$ at the lattice temperature of 2K, are available only in [81]. As has been said earlier, the data on the effective electron temperature characteristic have been obtained there indirectly from the high energy slope of the experimentally observed photoluminescence spectra. Such experimental data has been presented by the curve 5a in Figure 3.3. The experimental sample being highly degenerate, the theoretical results which are presented by the curves 6a, 6b and 6c in the same Figure have been obtained from (3.36), which follow from the approximate analysis made here under the condition of high degeneracy. Obviously a much conclusive comparison of the theoretical data which are obtained here with the experimental observations could not be made. But, from a just cursory comparison of the results of our approximate theoretical analysis with the experimental curve 5a in Figure 3.3, one can note some qualitative similarity, particularly for the lower values of the electric field. The quantitative difference by a scale factor may be

attributed to our chosen values of the material parameter, which are not quoted in [81]. At higher fields, however, other interactions should come into play and make the rise of the electron temperature quite slow with the electric field.

However, the results that have been obtained from the present approximate analysis indicate that none of the contributions, either of the degeneracy or of the piezoelectric interaction is negligibly small in determining the electron temperature characteristics at low lattice temperatures.

CHAPTER IV

ENERGY LOSS RATE AND NON-OHMIC MOBILITY OF A DEGENERATE TWO-DIMENSIONAL ENSEMBLE IN A QUANTUM WELL OF COMPOUND SEMICONDUCTORS

4.1 Introduction

In the presence of a high electric field, a number of innovative and technologically important features of the electrical transport characteristics are exhibited by an electron ensemble in any semiconductor structure. The value of the electric field at which such features may be observed depends upon T_L, the lattice temperature.

It is well known that under the condition, when the lattice temperature is low $(T_L \leq 20K)$, an apparently low electric field $\sim$ a fraction of $volt/cm$, may turn out to be effectively high, and the innovative features which can hardly be contemplated at higher temperatures for really low fields, may now be observed.

One of the high-field features being that the structure turns out to be non-ohmic. The electron mobility does no longer remain independent of the field. It is found that the drift velocity of the electrons may decrease, and even the saturation of the velocity may be observed with the increase of the field. Over a region of the high-field, the phenomenon, like the negative differential resistivity (NDR) may also be exhibited. Such a feature in the high-field characteristics suggests its importance for the fabrication of the devices, like microwave oscillator and harmonic generator etc.

Since the operating conditions of many devices usually extend to this region, the switching speed and the transconductance now significantly depend on such high-field-velocity characteristics.

Apart from that, as has already been mentioned earlier, in the presence of an effectively high electric field $\vec{E}$, the average energy of a non-equilibrium electron exceeds its average thermal value. Hence these electrons can be assumed to have attained a field dependent effective temperature $T_e(E) > T_L$. This leads to a growth of the number of phonons with time.

The average energy loss rate (ELR) of a carrier of an equilibrium ensemble is obviously zero. But in the presence of a high electric field the ELR for an electron of the non-equilibrium ensemble, as a result of the growth of the phonon number, assumes a finite value, so as to maintain the energy balance of the electron-phonon system. This finite ELR now controls the electrical transport in the structure under the prevailing condition.

The ELR characteristics provide some knowledge like that of the energy band structure of the material, and also of the interaction which the electrons may undergo with the lattice imperfections. This in turn could suggest the suitability of a material for the device purpose.

In the present chapter we make an attempt to study some of the aspects of the average ELR and the non-ohmic mobility characteristics of the electrons in a degenerate ensemble of 2DEG which is confined in a quantum well of compound semiconductors at the low and at some other lattice temperatures.

Due account of the some of the low temperature features which have been described in the paragraph 1.2.2 has been taken into account in the study that is made here.

In place of the Fermi-Dirac distribution function for the ensemble, a well-tested alternative form of the distribution function has been used here to make the study analytically tractable. Numerical results as have been obtained here for the wells in InSb, GaAs and GaN are compared with the available theoretical and experimental data. The theoretical results that are obtained here appear to be in reasonable qualitative agreement with the available experimental data.

4.2 Brief review of the studies on the energy loss rate of electrons in quantized surface layer

The study of energy loss rate (ELR) of electrons in semiconductor structures has attracted considerable interest for many years [2, 24]. The problem of ELR has been studied by Hess and Sah [43] in a non-degenerate ensemble of 2DEG under the condition of high temperature when the traditional equipartition approximation holds good. Using Maxwellian approximation, they obtained the electron temperature dependence of the average ELR when the carriers interact with intravalley acoustic mode lattice vibrations. The same problem has been studied by Nakamura [83] for Si (100) inversion layers when the carriers interact with both the acoustic and the optical phonons and also considering the full subband structure of the electron energy spectrum. Ferry [84] studied the problem of ELR considering a degenerate

statistic for an ensemble of 2DEG and found that the form of the relaxation rate is relatively insensitive to the detailed form of the distribution. His results seem to be compatible with those of Nakamura [83] for scattering within the lowest subband.

At higher lattice temperatures, when the polar optical phonon scattering dominates, the energy loss rate of the electrons in 2DEG system has been investigated by many [85, 86]. Straw et al. [87] have studied the energy relaxation for non-degenerate ensembles in quantum wells. Using mobility-temperature thermoelectric technique, they experimentally determined the power loss per electron as a function of the electron temperature. In the region below 30*K*, which has been referred there as the acoustic phonon region, the power loss is found to be proportional to $\left(T_e - T_L\right)$.

Reports on some experimental and theoretical studies on the characteristics of 2DEG systems at low lattice temperatures are also available in the literature. Suresha and Naik [88] have studied the problem of ELR in a degenerate two-dimensional hot electron gas in Si inversion layer of MOSFET structure in the range of electron temperature $0.15K < T_e < 1.7K$ when the carriers interact predominantly with the acoustic phonons. They have shown that the ELR is proportional to T_e^5 when the screening effect is taken into account.

The study of ELR in 2DEG systems formed on III-V compound semiconductors at low lattice temperatures have also been made [85, 89-93]. Considering a heterostructure like $Ga_{0.47}In_{0.53}As/InP$, the ELR of hot carriers in quantum well of width 154Å and 14Å have been measured by Westland et al. [94]. They have found that the ELR is considerably lower than what one obtains on considering the unscreened carrier-LO phonon interaction. The discrepancy has been attributed to the presence of a non-equilibrium phonon distribution. The magnitude of the effect have been dependent upon the well width. Using the non-equilibrium Green's function approach, the ELR have been studied theoretically by Tao, Ting and Singh [95]. They suggested a possible explanation for the dramatic enhancement of the loss rate of the non-equilibrium electrons in the GaAs/GaAlAs quantum wells when the lattice temperature is low enough. The average ELR of hot carriers in AlGaN/GaN quantum well have been theoretically obtained by Katti at al. [96]. They have obtained the results at the lattice temperature of 4.2*K* for a degenerate ensemble of 2DEG considering the interactions with the deformation potential acoustic phonons, the piezoelectric phonons and the polar optical phonons. They have also considered the effect of hot phonons. The results thus obtained when

compared with the experimental data seem to match well. Experimental study of average ELR of hot carriers in AlGaN/GaN at high temperature have been carried out by Balkan at al. [97]. The electron energy loss rate is determined from the electron temperature dependence of the power loss using the power balance equations.

Using Shubnikov-de-Hass effect, Daniels et al. [98] have investigated the energy loss rate in a series of modulation doped GaAs/AlGaAs single and multiple quantum well structures at low lattice temperature when the carriers interact with acoustic phonons. They have found how does the energy loss rate depend upon the electron temperature. Their results seem to agree well with the experimental results in the range of electron temperature $2.2K < T_e < 8K$. Apart from that, Santra and Sarkar [99] have studied the effects of non-parabolicity of the energy band on the ELR of the hot electrons in narrow gap semiconductors in the extreme quantum limit at low temperatures. They have shown that the ELR gets enhanced due to the non-parabolicity of band structure.

The theory of ELR of an electron due to interaction with the acoustic mode lattice vibrations in a non-degenerate 2DEG has been developed under the condition of low lattice temperature, when the approximations of the traditional theory are not valid [100]. The dependence of the ELR upon the carrier energy, the lattice temperature, and the impurity concentration is obtained in a 2DEG in Si. On comparing the results with that of Hess and Sah it has been observed that the effect of the finite energy of the acoustic phonons on the ELR is quite significant at the low temperatures.

In an almost impurity-free 2DEG, a high carrier concentration may result in a Fermi level $\varepsilon_F \geq K_B T_L$ at the low temperatures. Under these conditions the ensemble of 2DEG can hardly be regarded as non-degenerate. As has already been said, one of the much important transport parameters that determines the high-field effects in any semiconductor structure is the average ELR of a carrier of the ensemble. Hence in the next section, we develop the theory of ELR due to interaction with the deformation potential acoustic and the piezoelectric phonons, considering a degenerate ensemble of 2DEG which is confined to a quantum well of a heterostructure, under the condition of low lattice temperature. Some of the specific features of the low lattice temperature has been taken into account. The numerical results are obtained for some quantum confined degenerate ensembles in InSb, GaAs and GaN.

4.3 Method of calculation of the energy loss rate of the electrons in surface layers of compound semiconductors

The average rate of loss of energy of an electron of an ensemble for any interaction may be symbolically represented as [101]

$$\left\langle \frac{d\varepsilon_{\vec{k}}}{dt} \right\rangle = \int \varepsilon_{\vec{k}} \left(\frac{df_0}{dt} \right)_{coll} d\vec{k} \Big/ \int f_0 d\vec{k} \tag{4.1}$$

With the help of the perturbation theory, the rate of change of the spherical part of the distribution function $\left(df_0/dt\right)_{coll}$ for degenerate ensemble of 2DEG has been obtained in Eq. (3.27) and (3.28) for the interaction of electrons with the deformation potential acoustic and the piezoelectric phonons respectively. Obviously, the results reduce for the case of a non-degenerate ensemble when one assumes that $f_0\left(\varepsilon_{\vec{k}}\right) \ll 1$ and so that the $\left(1-f_0\right) \sim 1$. As has been explained there the collision terms in Eq. (3.27) and (3.28) reduce for the case of a non-degenerate ensemble by omitting the terms containing the products of f_0, f_0' and f_0''.

4.4 Calculation of the rate of loss of energy of non-equilibrium 2DEG in different surface layers

The average energy loss of a non-equilibrium electron in an ensemble of 2DEG has been obtained under different levels of degeneracy and for the interactions of the electrons with the deformation potential acoustic and the piezoelectric phonons.

4.4.1 Case of a moderately degenerate layer under different conditions

As has already been said, a well-tested model distribution function for $f_0\left(\varepsilon_{\vec{k}}\right)$ has been used here in place of the heated Fermi-Dirac distribution function for the electrons of the ensemble, for the case of a moderately degenerate layer. The average rate of energy loss of the non-equilibrium electrons can be obtained by integrating the Eq. (4.1) over the entire energy range.

(i) When the electrons interact only with the deformation potential acoustic phonons

Now considering the interaction of the electrons with the deformation potential acoustic phonons (ac.) one can obtain the average ELR for moderately degenerate 2DEG as

$$\left\langle \frac{d\varepsilon_{\bar{k}}}{dt} \right\rangle_{ac.}^{\text{deg.}} = C_{ac}^{ELR} \left(I_d\right)^{-1} \left[\left(I_1^{ac}\right)_0^{\beta_1 \varepsilon_F} + \left(I_2^{ac}\right)_{\beta_1 \varepsilon_F}^{\beta_2 \varepsilon_F} + \left(I_3^{ac}\right)_{\beta_2 \varepsilon_F}^{\infty} \right] \tag{4.2}$$

where $C_{ac}^{ELR} = 2\left(E_a m_{\|}^{*}\right)^2 \Big/ d\rho_v \hbar^3$ and the expressions for other symbols are given in Appendix D.

(ii) When the electrons interact only with the piezoelectric acoustic phonons

Now considering the interaction of the electrons with the piezoelectric acoustic phonons (pz.) one can obtain the average ELR for moderately degenerate 2DEG as

$$\left\langle \frac{d\varepsilon_{\bar{k}}}{dt} \right\rangle_{\text{pz.}}^{\text{deg.}} = C_{pz}^{ELR} \left(I_d\right)^{-1} \left[\left(I_1^{pz}\right)_0^{\beta_1 \varepsilon_F} + \left(I_2^{pz}\right)_{\beta_1 \varepsilon_F}^{\beta_2 \varepsilon_F} + \left(I_3^{pz}\right)_{\beta_2 \varepsilon_F}^{\infty} \right] \tag{4.3}$$

where $C_{pz}^{ELR} = e^2 k_m^2 \varepsilon_s \big/ d \in_{sc} \hbar$ and the expressions for other symbols are given in Appendix D.

(iii) For the combined interaction with both the deformation potential acoustic and the piezoelectric acoustic phonons

The effective average ELR of an electron of the non-equilibrium, degenerate ensemble $\left\langle d\varepsilon_{\bar{k}} \big/ dt \right\rangle_{eff.}^{\text{deg.}}$ for the combined interaction with the deformation potential acoustic and the piezoelectric phonons can be obtained from the sum of the expressions given in Eq. (4.2) and (4.3).

It may be mentioned here that the dependence of the average ELR of an electron on the effective electron temperature T_e, hence on the electric field, have already been calculated using the field dependence of T_e under the identical conditions. Use has been made of the $T_e\left(E\right) - E$ characteristics as given in Eq. (3.31), (3.33) and (3.35) for the interaction of the electrons with the deformation potential acoustic phonons, the piezoelectric acoustic phonons, and the combined interactions respectively.

4.4.2 Case of a highly degenerate surface layer for the combined interaction of the electrons with both the deformation potential acoustic and the piezoelectric acoustic phonons

As has already been mentioned, for the case of the highly degenerate ensemble, the contribution of the integrals in Eq. (4.2) and (4.3) representing the parts of the energy balance equation over

the first $\left(0 < \varepsilon_{\vec{k}} \le \beta_1 \varepsilon_F\right)$ and the third $\left(\beta_2 \varepsilon_F \le \varepsilon_{\vec{k}} < \infty\right)$ regions will tend to be more and more insignificant. Hence, for a highly degenerate ensemble, only the integrals over the intermediate region $\left(\beta_1 \varepsilon_F < \varepsilon_{\vec{k}} \le \beta_2 \varepsilon_F\right)$ would make the principal contribution. Thus, for a highly degenerate ensemble of 2DEG, the average ELR for the combined interaction of the electrons can be obtained considering only the integrals $\left(I_2^{ac}\right)_{\beta_1\varepsilon_F}^{\beta_2\varepsilon_F}$ and $\left(I_2^{pz}\right)_{\beta_1\varepsilon_F}^{\beta_2\varepsilon_F}$ for the intermediate energy range as given in Eq. (4.2) and (4.3).

4.4.3 Case of a non-degenerate surface layer under different conditions

In order to study the effects of degeneracy of the ensemble on the average ELR characteristics, the loss rate for a non-degenerate (non-deg) ensemble needs to be known.

One may assume that the spherical part $f_0\left(\varepsilon_{\vec{k}}\right)$ of the high field distribution function for the non-degenerate ensemble is given by the heated Maxwellian distribution function at the field dependent effective temperature T_e of the ensemble.

(i) When the electrons interact only with the deformation potential acoustic phonons

The analysis for the average ELR characteristics considering a non-degenerate ensemble of 2DEG for the intrinsic interaction of the electrons with the deformation potential acoustic phonons (ac.) has already been obtained in Ref. [102]. The result is quoted here for a ready reference

$$\left\langle \frac{d\varepsilon_{\vec{k}}}{dt} \right\rangle_{ac.}^{\text{non-deg.}} = \frac{2E_a^2 m_{\parallel}^{*2} K_B T_L}{\hbar^3 \rho_v d}\left[1 - \frac{T_e}{T_L} + 4\left(\frac{\varepsilon_s}{\pi K_B T_L}\right)^{1/2}\left\{\left(\frac{T_e}{T_L}\right)^{1/2} - 1\right\}\right] \tag{4.4}$$

(ii) When the electrons interact only with the piezoelectric acoustic phonons

Now considering the interaction of the electrons only with the piezoelectric acoustic phonons (pz.) one can obtain the average ELR for non-degenerate 2DEG as

$$\left\langle \frac{d\varepsilon_{\vec{k}}}{dt} \right\rangle_{\text{pz.}}^{\text{non-deg.}} = \frac{2e^2 k_m^2 \varepsilon_s}{d \in_{sc} \hbar}\left(\frac{T_L}{T_e}\right)\left[1 - \frac{T_e}{T_L} + 2\left(\frac{\varepsilon_s}{\pi K_B T_L}\right)^{1/2}\left\{\left(\frac{T_e}{T_L}\right)^{1/2} - 1\right\}\right] \tag{4.5}$$

(iii) For the combined interaction with both the deformation potential acoustic and the piezoelectric acoustic phonons

The effective average ELR of the non-equilibrium electrons $\left\langle d\varepsilon_{\vec{k}}/dt\right\rangle_{eff.}^{non-\deg.}$ for the combined interaction with the deformation potential acoustic and the piezoelectric phonons can be obtained from the sum of the expressions given in Eq. (4.4) and (4.5).

It may be mentioned here that the dependence of the average ELR of an electron on the effective electron temperature T_e, hence on the electric field, have already been calculated using the field dependence of T_e under the identical conditions. Use has been made here of the $T_e(E)-E$ characteristics as given in Eq. (3.37), (3.38) and (3.39) for the interaction of the electrons with the deformation potential acoustic phonons, the piezoelectric acoustic phonons and the combined interactions respectively.

4.5 Results for the dependence of average ELR of an electron in a non-equilibrium ensemble of 2DEG upon the normalised electron temperature on the surface layers of InSb, GaAs and GaN with different levels of degeneracy

Considering a degenerate ensemble of non-equilibrium 2DEG which is confined in an infinite triangular potential well of a compound semiconductor, an approximate analysis has been made here to study the effects of some of the low temperature features on the characteristics of the average ELR of an electron of the ensemble. The low temperature features which have been considered here are the degeneracy of the ensemble and the interaction of the electrons with the piezoelectric phonons in the compound semiconductor material.

For an application of the above formulation, we have considered here degenerate ensembles of 2DEG, which is confined to the wells of the semiconductor compounds like InSb, GaAs and GaN, which are quite important for the device purpose. It may be pointed out here that for all the three compounds $m_{\|}^{*}=m_{\perp}^{*}=m^{*}$. The values of the material parameters are given in Table 3.1.

The variation of the average ELR of an electron with the effective electron temperature for these compounds, as obtained from the present analysis, are shown in Figures 4.1, 4.2 and 4.3.

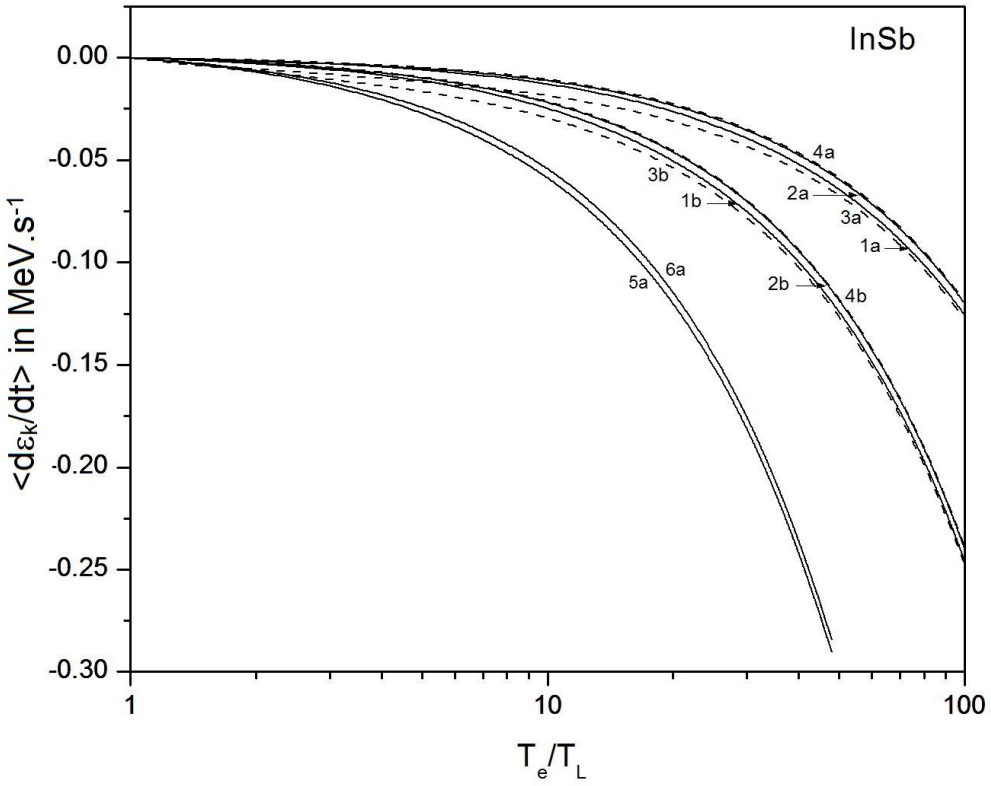

Figure 4.1 Dependence of the average energy loss rate of a non-equilibrium electron in an ensemble of 2DEG which is confined in a quantum well of InSb, upon the normalized electron temperature T_e/T_L at different lattice temperatures and for different levels of degeneracy η_D. Curves marked a and b are obtained at the lattice temperatures of 2*K* and 4*K* respectively, the corresponding values of η_D being 51.6 and 25.8 respectively for a layer concentration $N_i = 1.0\times10^{14}\ m^{-2}$. Solid curves are obtained considering the degeneracy of the ensemble and dashed curves are obtained when the degeneracy is not taken into account. The curves 1, 3 and 5 represent the dependence for the combined interaction of the electrons with the acoustic and the piezoelectric phonons, and the curves 2, 4 and 6 are obtained for interaction only with the acoustic phonons. Curve 5a and 6a have been obtained for a highly degenerate specimen at the same lattice temperature 2*K*, when $N_i = 1.0\times10^{16}\ m^{-2}$ or $\eta_D = 1891$ [80].

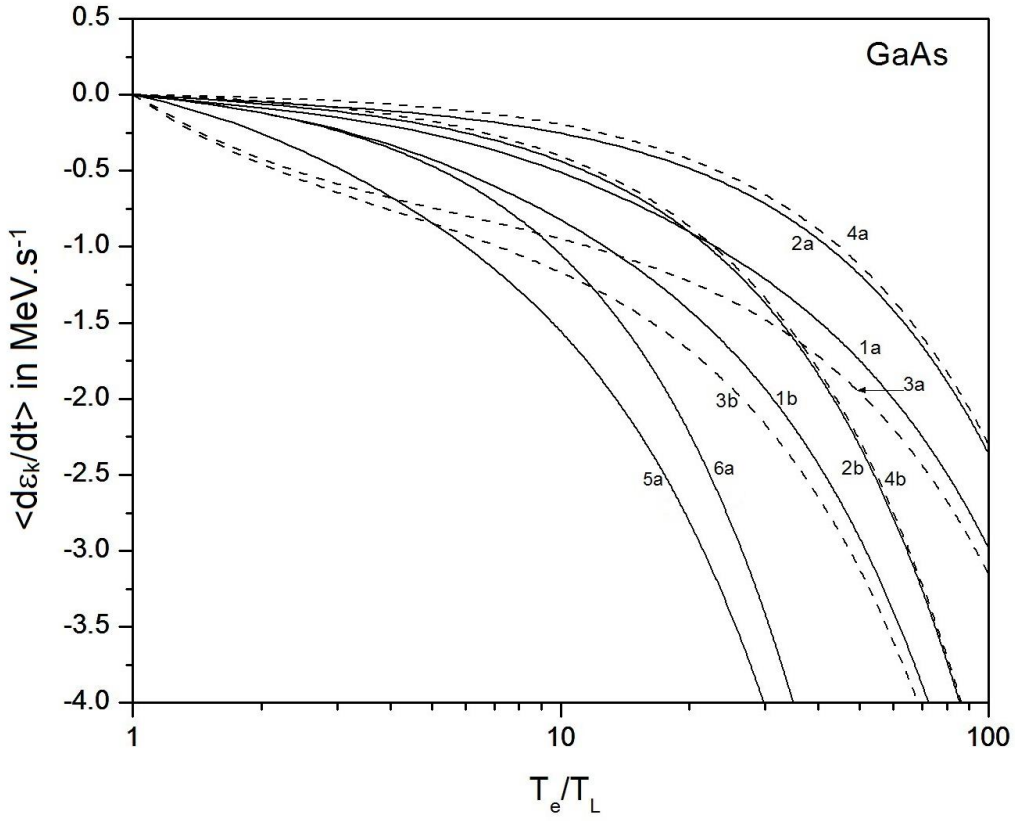

Figure 4.2 Dependence of the average energy loss rate of a non-equilibrium electron in an ensemble of 2DEG which is confined in a quantum well of GaAs, upon the normalized electron temperature T_e/T_L at different lattice temperatures and for different levels of degeneracy η_D. Curves marked a and b are obtained at the lattice temperatures of 2*K* and 4*K* respectively, the corresponding values of η_D being 31.5 and 15.75 respectively for a layer concentration $N_i = 1.0\times10^{14}\ m^{-2}$. Solid curves are obtained considering the degeneracy of the ensemble and dashed curves are obtained when the degeneracy is not taken into account. The curves 1, 3 and 5 represent the dependence for the combined interaction of the electrons with the acoustic and the piezoelectric phonons, and the curves 2, 4 and 6 are obtained for interaction only with the acoustic phonons. Curve 5a and 6a have been obtained for a highly degenerate specimen at the same lattice temperature 2*K* when $N_i = 7.0\times^{15}\ m^{-2}$ or $\eta_D = 637.5$ [81].

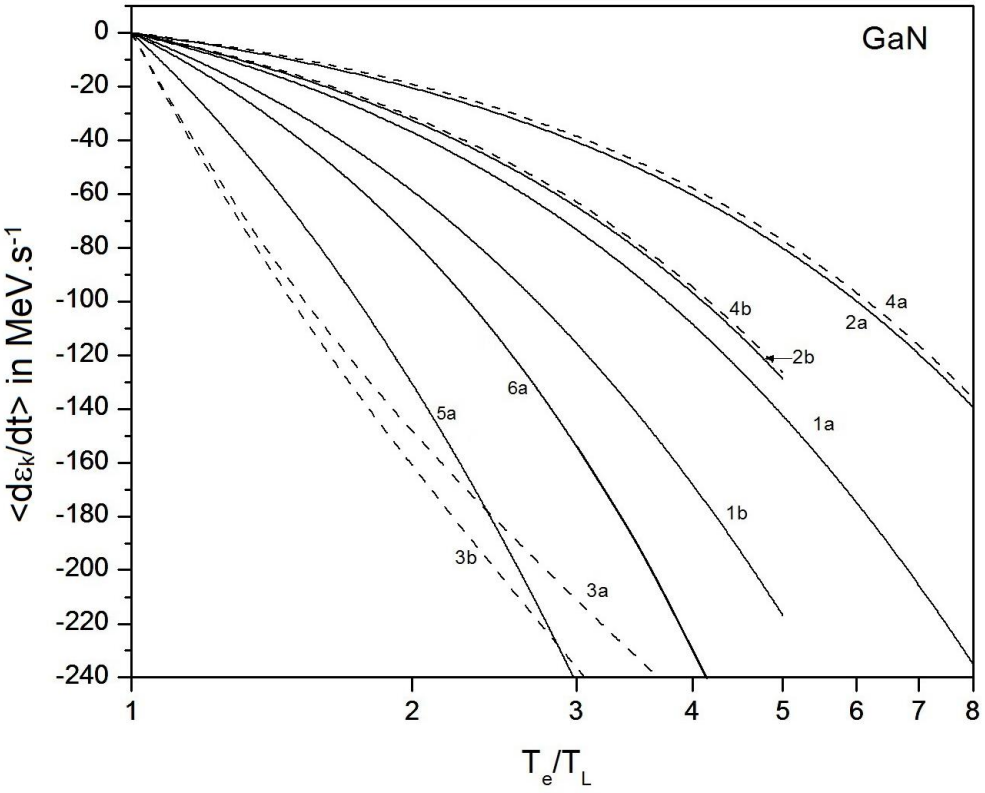

Figure 4.3 Dependence of the average energy loss rate of a non-equilibrium electron in an ensemble of 2DEG which is confined in a quantum well of GaN, upon the normalized electron temperature T_e/T_L at different lattice temperatures and for different levels of degeneracy η_D. Curves marked a and b are obtained at the lattice temperatures of 77*K* and 125*K* respectively, the corresponding values of η_D being 5.3 and 3.26 respectively for a layer concentration $N_i = 2.0\times10^{15}\ m^{-2}$. Solid curves are obtained considering the degeneracy of the ensemble and dashed curves are obtained when the degeneracy is not taken into account. The curves 1, 3 and 5 represent the dependence for the combined interaction of the electrons with the acoustic and the piezoelectric phonons, and the curves 2, 4 and 6 are obtained for interaction only with the acoustic phonons. Curve 5a and 6a have been obtained for a highly degenerate specimen at the same lattice temperatures 77*K* when $N_i = 1.0\times^{17}\ m^{-2}$ or $\eta_D = 85.10$ [82].

4.6 Discussions

In additional to InSb and GaAs, GaN has also been chosen for our study. This compound is quite different from the others, in that, it has significantly higher values of the piezoelectric coupling constant and the effective mass and lower values of the deformation potential constant and the static dielectric constant. Moreover, it has come up as a potentially important material from the device point of view. However, the electrons in GaN demand quite higher values of the electric field and of the lattice temperature so as to be significantly heated up. Comparing the Figure 4.3 with Figure 4.1 and 4.2, one can see that the average ELR of an electron in a well of GaN is much higher than that of the other two compounds.

On comparing the solid curves with the dashed ones for any lattice temperature, it is seen that the degeneracy factor effects significant changes in the average ELR of the carriers. It may be seen from Figures 4.1-4.3 that, irrespective of the type of the ensemble, the average ELR of an electron almost monotonically decreases with the increase of the effective temperature of an electron, and the rate of decrease gradually increases. But in general, the degeneracy tends to decrease the value of ELR. The effects of degeneracy are seen to be more pronounced for GaAs and GaN compared to that for InSb. However, for any compound the discrepancy between the values of ELR for the degenerate and the non-degenerate ensembles tends to decrease as T_e increases more and more. Furthermore, it is also seen that the interaction with the piezoelectric phonons tends to increase the average rate of energy loss of the carriers with the rise of T_e/T_L. As has already been said, it is observed that the average ELR is affected more, when the value of the piezoelectric coupling constant of the material is higher or the lattice temperature is lower. This is because the interaction with the piezoelectric phonons gets stronger in any material, on lowering the lattice temperature.

4.7 Brief review of the studies on the non-ohmic mobility characteristics of electrons in quantized surface layer

Investigations on the non-ohmic mobility characteristics of electrons in quantised surface layers have been made by several workers. Fang and Fowler [103] studied experimentally the variation of carrier mobility with the field and the lattice temperature in silicon inversion layers. The density of the electrons has been less than about $2\times10^{12}\ cm^{-2}$. The mobility was found to increase with the field and the temperature near the liquid-helium temperatures. The measurement of the electron drift velocity for different surface orientations and substrate doping in the temperature regime 4.2K to 300K has been carried out. Depending upon the low field mobility, the drift velocity was found to saturate for fields greater than a few times $10^4\ V/cm$, and was found to be lower than the reported bulk values. The electric field dependence of the mobility of electrons and holes were calculated theoretically by Hess and Sah [43] using Maxwellian distribution function and taking into account a repopulation of the carriers among the different valleys in an n-channel silicon inversion layer. The formulations for the energy loss rate were also presented considering scattering due to the optical and the acoustic phonons. Taking the subband structure of the electron energy spectrum into account the energy losses per electron to both acoustic and optical phonons were calculated for Si (100) inversion layer by Nakamura [83]. Apart from that using the energy balance method, the electron mobility variations in Si inversion layer with applied electric field was also studied. Similar investigations on the high-field transport for both the electrons and the holes in silicon inversion layers were carried out by many others [101,104-106].

Ferry [107] calculated the characteristics of the high-field mobility and the carrier velocities in the (100)-silicon quantum inversion layers for interaction with the intervalley and acoustic phonons at 300K and 77K using a drifted Maxwellian distribution function, and taking into account the repopulation of the carriers among the various subbands. The calculated velocity-field data were found to be in good agreement with the experimental results of Fang and Fowler [103]. Some experimental aspects of the hot-electron transport in MOS structures were reviewed by Hess [108]. Basu and Roy [109] calculated the warm electron coefficient of a 2DEG in Si-MOSFET's at low temperatures in the framework of effective electron temperature approximation. Unlike previous workers, negative values of the coefficient were also obtained along with the positive values. Sivan et al. [110] studied the ballistic transport of hot electrons in a high mobility 2DEG system over distances as large as two micrometres, along with the tunnelling through a barrier induced in the 2DEG. The effects of the various inelastic scattering

mechanisms were studied experimentally. Dmitriev et al. [111] calculated the dependence of the electron temperature and the drift velocity on the applied electric field for a 2DEG system in elementary semiconductors under the condition of high electron concentrations when the electron distribution function was governed by the electron-electron collisions. In the one valley approximation, they showed that the electron temperature tends to increase endlessly at a certain value of the electric field.

Price [112] developed the theory of high-field electron mobility in GaAs heterolayers at low temperatures. The 2DEG structure has been assumed to be highly degenerate. The scattering is assumed to be predominantly elastic. The inelastic scattering which seemed to control the electron heating is by the acoustic mode phonons, both deformation and piezoelectric. Lei, Birman and Ting developed a non-Boltzmann theory of the steady-state transport for 2DEG systems in a strong electric field. The electron temperature, impurity and phonon-limited mobilities were determined solely from the force and energy balance equations. The theory was applied to obtain the ohmic and non-linear transport characteristics in GaAs-GaAlAs heterojunctions at low temperatures [113]. Using the technique of Monte Carlo simulation, Tomizawa et al. [114] studied the velocity-field characteristics under the stationary and the non-stationary conditions at a modulation-doped AlGaAs/GaAs heterostructure. In contrast to the bulk materials, they found a steeper increase in the velocity for the 2DEG system, closely dependent on the low-field high mobility and hence suggested that the high mobility could be effectively utilized in a high-speed logic application of such heterostructure devices. Inoue et al. [115] made a simulation study of the hot-electron effects in InP/n-AlInAs heterostructures considering the electron-electron scattering and the screening by the high-density of the electrons.

Some measurements were made to determine the electron temperature and the mobility as functions of the electric field of a modulation doped GaAs-GaAlAs heterojunction. The electron mobility in such systems was found to be strongly depended on the electric field strength, and the hot-electron effects were observable at a low field $\sim 10\ V/cm$. The decrease of high-field mobility with increasing electron temperature was found to be much more rapid than the decrease of the low-field mobility with the lattice temperature. The high-field mobility characteristics were explained in terms of the field-induced electron heating and the temperature dependence of the low-field mobility [81, 116, 117].

Weng and Wu [118-120] computed the mobility of a 2DEG in GaAs-AlGaAs heterojunction through numerically solving the energy balance equation. Instead of the displaced Fermi function a new expression for the distribution function and a renormalized phonon frequency were used in the computation. The agreement between their theory and the experiments seemed to improve by such changes.

The problems on the hot-electrons in the low-dimensional structures were dealt by Ridley in some details [32]. Reviews were made on the principal aspects of the hot-electron phenomena like the negative-differential-resistance, as well as the other instabilities associated with the parallel transport. Apart from that, the ballistic transport and the phenomenon of impact ionization are also reassessed. A review on the real space transfer effects with reference to the contribution of non-local mechanisms to the non-linear transport in semiconductor structures was made by Gribnikov et al. [121].

In the next section, the non-ohmic mobility characteristics, which follow subsequently from the energy balance equation are obtained. Apart from that, the same non-ohmic mobility characteristics which follow directly from the expression for the current density under the same prevalent conditions have also been obtained. The numerical results have been evaluated for the quantum confined ensemble of 2DEG in the compounds like InSb, GaAs and GaN, which are largely used for the device purpose. It may be mentioned here that in the region of low lattice temperatures, the average thermal energy of the electrons is so limited that they can hardly excite optical mode lattice vibrations. Hence, the number of optical phonons would be negligibly small. As such, the effects of interaction of the carriers with the optical phonons on the transport characteristics at the low lattice temperatures would be quite insignificant. Hence such interaction has not been taken into account.

4.8 Method of calculation of non-ohmic mobility characteristics

The non-ohmic mobility characteristics have been obtained following two methods: (i) the energy balance equation of the electron-phonon system and (ii) from the current density of the non-equilibrium carriers.

First Method:

4.9 Calculation of non-ohmic mobility characteristics of an ensemble of 2DEG from the expression for the average ELR

The above theoretical analysis for the average ELR of a non-equilibrium electron in any ensemble, degenerate or non-degenerate, can be directly used, to obtain $\mu(T_e)$, the dependence of the non-ohmic mobility on the effective electron temperature T_e. Now, from the knowledge of the dependence of the effective electron temperature T_e upon the electric field E, one can find the experimentally measurable, non-ohmic mobility characteristics $\mu(E)$ of the ensemble under the similar prevalent conditions.

It follows from the power balance equation of the electron-phonon system that [24]

$$\mu(E) = -\frac{1}{eE^2}\left\langle \frac{d\varepsilon_{\vec{k}}}{dt} \right\rangle \tag{4.6}$$

For the case of a moderately degenerate ensemble, the non-ohmic mobility $\mu_{ac}^{\deg}(T_e)$ and $\mu_{pz}^{\deg}(T_e)$ due to interaction of electrons with the deformation potential acoustic phonons and the piezoelectric phonons can be obtained using the corresponding values of average ELR of electron given in Eq. (4.2) and (4.3). Obviously, the effective mobility $\mu_{eff}^{\deg}(T_e)$ due to the combined interaction of the electrons with the deformation potential acoustic and the piezoelectric phonons is obtained from the sum of the averages of ELR given by Eq. (4.2) and (4.3).

For the case of a highly degenerate ensemble, the effective non-ohmic mobility due to the combined interaction of the electrons with the deformation potential acoustic and the piezoelectric phonons is obtained from the sum of only the intermediate terms $\left(I_2^{ac}\right)_{\beta_1\varepsilon_F}^{\beta_2\varepsilon_F}$ and $\left(I_2^{pz}\right)_{\beta_1\varepsilon_F}^{\beta_2\varepsilon_F}$ in the square brackets of Eq. (4.2) and (4.3).

Similarly, for a non-degenerate ensemble, the non-ohmic mobility $\mu_{ac}^{non-\deg}(T_e)$ and $\mu_{pz}^{non-\deg}(T_e)$ due to interaction of the electrons with the deformation potential acoustic phonons and the piezoelectric phonons can obtained using the corresponding values of average ELR of electrons

given in Eq. (4.4) and (4.5). Obviously, the effective mobility $\mu_{eff}^{non-\deg}\left(T_e\right)$ due to the combined interaction of electrons with the deformation potential acoustic and the piezoelectric phonons is obtained from the sum of the averages of ELR given by Eq. (4.4) and (4.5).

It may be noted here that the expressions for $\left\langle d\varepsilon_{\vec{k}}/dt\right\rangle_{ac/pz}^{\deg.}$ are quite complex compared to that of $\left\langle d\varepsilon_{\vec{k}}/dt\right\rangle_{ac/pz}^{non-\deg}$.

Thus, for a non-degenerate ensemble, the expressions for $\mu_{ac}\left(T_e\right)$ and the $\mu_{pz}\left(T_e\right)$ can be easily combined, and thus one get $\mu_{eff}^{non-\deg}\left(T_e\right)$ as

$$\mu_{eff}^{non-\deg}\left(T_e\right)=\left(\mu_0\right)_{eff}\left(\frac{T_L}{T_e}\right)^2\frac{\left[1+2\left(\frac{\varepsilon_s}{\pi K_B T_L}\right)^{1/2}\right]}{\left[1+2\left(\frac{\varepsilon_s}{\pi K_B T_L}\right)^{1/2}\left(\frac{T_e}{T_L}\right)^{1/2}\right]}\times\frac{\left[\frac{\left(K_B T_e\right)^2}{\tau_n}-\frac{K_B T_e}{\tau_n^2}+\frac{1}{\tau_n^3}\exp\left(\frac{1}{\tau_n K_B T_e}\right)E_1\left(\frac{1}{\tau_n K_B T_e}\right)\right]}{\left[\frac{\left(K_B T_L\right)^2}{\tau_n}-\frac{K_B T_L}{\tau_n^2}+\frac{1}{\tau_n^3}\exp\left(\frac{1}{\tau_n K_B T_L}\right)E_1\left(\frac{1}{\tau_n K_B T_L}\right)\right]} \tag{4.7}$$

where $\left(\mu_0\right)_{eff}$, is the effective mobility at low fields. It is given by $\left(\mu_0\right)_{eff}=\frac{e}{m_{\|}^{*}\tau_{pzm}\left(K_B T_L\right)^2}\frac{\left[\frac{\left(K_B T_L\right)^2}{\tau_n}-\frac{K_B T_L}{\tau_n^2}+\frac{1}{\tau_n^3}\exp\left(\frac{1}{\tau_n K_B T_L}\right)E_1\left(\frac{1}{\tau_n K_B T_L}\right)\right]}{\left[1+2\left(\frac{\varepsilon_s}{\pi K_B T_L}\right)^{1/2}\right]}$, $E_1\left(z\right)$ is the exponential integral function [51], τ_{acm} and τ_{pzm} are the energy independent parts of the momentum relaxation times for the acoustic and the piezoelectric interactions respectively.

Second Method:

4.10 Calculation of non-ohmic mobility characteristics of 2DEG from the expression for the current density

The non-ohmic effective mobility characteristics $\mu(E)$ under the conditions of interest here, can also be calculated from the expression for the current density $\vec{J}$. One can calculate $\vec{J}$ by carrying out the integral in (2.38)

$$\vec{J} \equiv ne\mu(E)\vec{E} = -e^2 \int \nabla_{\vec{k}} \varepsilon_{\vec{k}} \left(\vec{k}.\overleftrightarrow{M}.\vec{E}\right) \tau\left(\varepsilon_{\vec{k}}\right) \frac{\partial f_0}{\partial \varepsilon_{\vec{k}}} d\vec{k} \tag{4.8}$$

where n is the concentration of the electrons in the ensemble of 2DEG.

The integration in (4.8) can be carried out analytically for the parabolic energy dispersion law of a 2DEG. The reciprocal effective mass tensor, $\overleftrightarrow{M}$ then reduces to the scalar $1/m_{\|}^*$, $m_{\|}^*$ being the in-plane component of the effective mass. The integrand may be expressed in polar coordinates taking the direction of the applied field $\vec{E}$ as the reference axis x. Thus, for any individual interaction one can obtain the corresponding mobility from

$$\mu(E) = -\frac{e}{m_{\|}^*} \int_0^\infty \varepsilon_{\vec{k}} \tau\left(\varepsilon_{\vec{k}}\right) \frac{\partial f_0}{\partial \varepsilon_{\vec{k}}} d\varepsilon_{\vec{k}} \Bigg/ \int_0^\infty f_0 d\varepsilon_{\vec{k}} \tag{4.9}$$

4.10.1 Case of a moderately degenerate layers under different conditions

(i) When the electrons interact only with the deformation potential acoustic phonons

For the interaction of electrons only with the deformation potential acoustic phonons, the relaxation time $\tau_{ac}\left(\varepsilon_{\vec{k}}\right)$ have already been obtained in Eq. (3.30) under the similar conditions. Now, using the alternative form of f_0 which has been described in paragraph 3.7, one can carry out the integration in (4.9) for a degenerate ensemble of 2DEG and obtain the expression for $\mu_{ac}^{\deg}(E)$ as

$$\mu_{ac}^{\deg}(E) = -\frac{e}{m_{\|}^* I_d} \left[\left(I_\mu^{ac}\right)_0^{\beta_1 \varepsilon_F} + \left(I_\mu^{ac}\right)_{\beta_1 \varepsilon_F}^{\beta_2 \varepsilon_F} + \left(I_\mu^{ac}\right)_{\beta_2 \varepsilon_F}^{\infty} \right] \tag{4.10}$$

The expressions for symbols are given in Appendix E.

(ii) When the electrons interact only with the piezoelectric acoustic phonons

For the interaction of electrons only with the piezoelectric acoustic phonons, the relaxation time $\tau_{pz}\left(\varepsilon_{\vec{k}}\right)$ have already been obtained in Eq. (3.32) under the similar conditions. Now, using again the alternative form of f_0, one can carry out the integration in (4.9) for a degenerate ensemble of 2DEG and obtain the expression for $\mu_{pz}^{\deg}\left(E\right)$ as

$$\mu_{pz}^{\deg}\left(E\right)=-\frac{e}{m_{||}^{*}I_d}\left[\left(I_{\mu}^{pz}\right)_{0}^{\beta_1\varepsilon_F}+\left(I_{\mu}^{pz}\right)_{\beta_1\varepsilon_F}^{\beta_2\varepsilon_F}+\left(I_{\mu}^{pz}\right)_{\beta_2\varepsilon_F}^{\infty}\right] \tag{4.11}$$

The expressions for symbols are given in Appendix E.

(iii) For the combined interaction with both the deformation potential acoustic and the piezoelectric acoustic phonons

For the combined interaction of the electrons with deformation potential acoustic and piezoelectric phonons, the effective mobility $\mu_{eff}^{\deg}\left(E\right)$ can be obtained using Matthiessen's rule which is given by $\mu_{eff}^{\deg}\left(E\right)=\left(1/\mu_{ac}^{\deg}\left(E\right)+1/\mu_{pz}^{\deg}\left(E\right)\right)^{-1}$. Here the expressions for $\mu_{ac}^{\deg}\left(E\right)$ and $\mu_{pz}^{\deg}\left(E\right)$ are given in Eq. (4.10) and (4.11).

4.10.2 Case of a highly degenerate layer for the combined interaction of the electrons with both the deformation potential acoustic and the piezoelectric acoustic phonons

For the case of a highly degenerate ensemble, the effective non-ohmic mobility due to the combined interaction of the electrons with the deformation potential acoustic and the piezoelectric phonons have been obtained taking the values of integration of the intermediate region, viz. $\left(I_{\mu}^{ac}\right)_{\beta_1\varepsilon_F}^{\beta_2\varepsilon_F}$ and $\left(I_{\mu}^{pz}\right)_{\beta_1\varepsilon_F}^{\beta_2\varepsilon_F}$ in (4.10) and (4.11).

4.10.3 Case of a non-degenerate layers under different conditions

For a non-degenerate ensemble of 2DEG, the integral (4.9) may be evaluated using the heated Maxwellian function, at an effective electron temperature T_e.

(i) When the electrons interact only with the deformation potential acoustic phonons

The non-ohmic mobility characteristics $\mu_{ac}^{non-\deg}\left(E\right)$ for the interaction of the electrons with deformation potential acoustic phonons has already been obtained in [102] from the average

ELR. It is easy to see that as expected the same result follows from the expression for the current density.

(ii) When the electrons interact only with the piezoelectric acoustic phonons

The expression for $\mu_{pz}^{non-\deg}(E)$ is not available in the literature. Hence it has been calculated here. The calculation gives

$$\mu_{pz}^{non-\deg}(E) = (\mu_0)_{pz}\left(\frac{T_e}{T_L}\right)\frac{\left[1+2\left(\frac{\varepsilon_s}{\pi K_B T_L}\right)^{1/2}\right]}{\left[1+2\left(\frac{\varepsilon_s}{\pi K_B T_L}\right)^{1/2}\left(\frac{T_e}{T_L}\right)^{1/2}\right]} \tag{4.12}$$

where the low field mobility only for the interaction with the piezoelectric phonons $(\mu_0)_{pz}$, is given by $(\mu_0)_{pz} = \left(8d \in_{sc} \hbar / e m_{\|}^{*} k_m^2\right) \Big/ \left[1+2\left(\frac{\varepsilon_s}{\pi K_B T_L}\right)^{1/2}\right]$.

(iii) For the combined interaction with both the deformation potential acoustic and the piezoelectric acoustic phonons

The effective mobility for the non-degenerate ensemble under the condition when the electrons interact with both the acoustic and the piezoelectric phonons, turns out to be

$$\mu_{eff}^{non-\deg}(E) = \frac{(\mu_0)_{ac}(\mu_0)_{pz}\left(\frac{T_e}{T_L}\right)}{(\mu_0)_{ac}+(\mu_0)_{pz}\left(\frac{T_e}{T_L}\right)} \times \frac{\left[1+2\left(\frac{\varepsilon_s}{\pi K_B T_L}\right)^{1/2}\right]}{\left[1+2\left(\frac{\varepsilon_s}{\pi K_B T_L}\right)^{1/2}\left(\frac{T_e}{T_L}\right)^{1/2}\right]} \tag{4.13}$$

Here $(\mu_0)_{ac} = \left(e\hbar^3 d\rho_v u_l^2 / E_a^2 m_{\|}^{*2} K_B T_L\right) \Big/ \left[1+2\left(\frac{\varepsilon_s}{\pi K_B T_L}\right)^{1/2}\right]$.

4.11 Results for the field dependence of non-ohmic mobility of the non-equilibrium electrons which are confined to the quantum wells on the surface layers of InSb, GaAs and GaN with different levels of degeneracy

To observe the consequence of the effective high-field, on the mobility it is normalised to its zero-field mobility μ_0. The results for the quantum confined ensembles of 2DEG on the surfaces of InSb, GaAs and GaN with different levels of degeneracy, using both the methods have been plotted in Figures 4.4, 4.5 and 4.6.

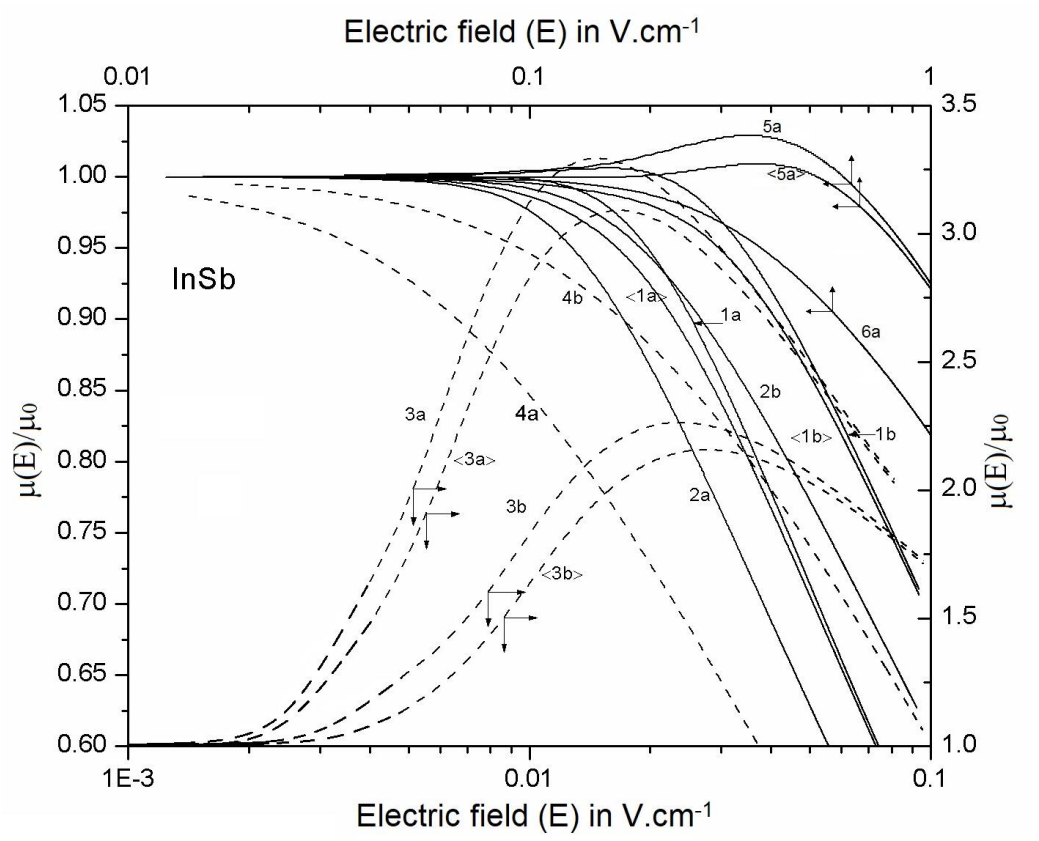

Figure 4.4 Dependence of the normalized non-ohmic mobility of the non-equilibrium carriers upon the electric field in InSb at different lattice temperatures and for different levels of degeneracy η_D when the layer concentration N_i is taken to be $1.0\times10^{14}\ m^{-2}$. Curves marked a and b are obtained at the lattice temperatures of 2*K* and 4*K* respectively, the corresponding values of η_D being 51.6 and 25.8 respectively. Solid curves are obtained considering the degeneracy and dashed curves are obtained when the degeneracy is not taken into account. The curves 1, 3 and 5 represent the dependence for the combined interaction of the electrons with the acoustic and the piezoelectric phonons, and the curves 2, 4 and 6 are obtained for interaction only with the acoustic phonons. Curves marked with < > are obtained from the solution of the energy balance equation for the electron-phonon system, whereas other curves follow from the expression for the current density. Curves 5a and 6a have been obtained for a highly degenerate specimen at the same lattice temperature 2*K* when $N_i = 1.0\times10^{16}\ m^{-2}$ or $\eta_D = 1891$ [80].

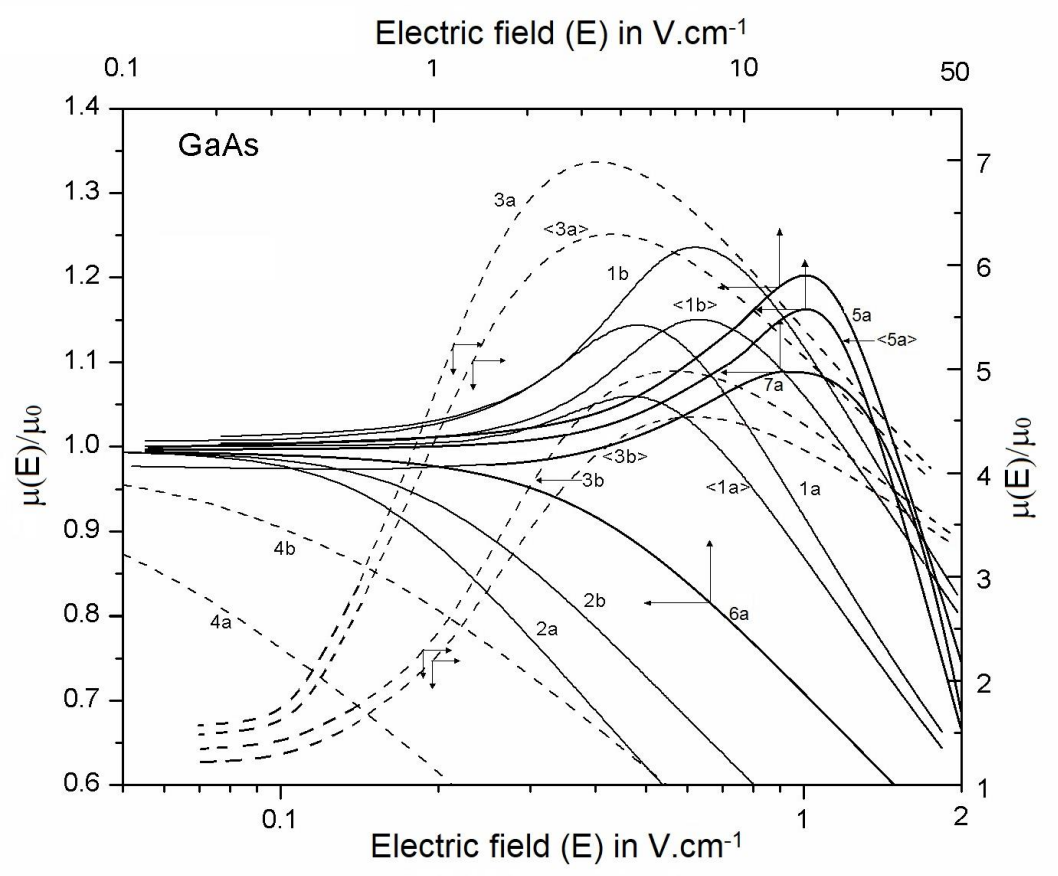

Figure 4.5 Dependence of the normalized non-ohmic mobility of the non-equilibrium carriers upon the electric field in GaAs at different lattice temperatures and for different levels of degeneracy η_D when the layer concentration N_i is taken to be $1.0\times10^{14}\ m^{-2}$. Curves marked a and b are obtained at the lattice temperatures of 2*K* and 4*K* respectively, the corresponding values of η_D being 31.5 and 15.75 respectively. Solid curves are obtained considering the degeneracy and dashed curves are obtained when the degeneracy is not taken into account. The curves 1, 3 and 5 represent the dependence for the combined interaction of the electrons with the acoustic and the piezoelectric phonons, and the curves 2, 4 and 6 are obtained for interaction only with the acoustic phonons. Curves marked with < > are obtained from the solution of the energy balance equation for the electron-phonon system, whereas other curves follow from the expression for the current density. Curves 5a, 6a and 7a have been obtained for a highly degenerate specimen at the same lattice temperatures 2*K* when $N_i = 7.0\times10^{15}\ m^{-2}$ or $\eta_D = 637.5$. Curve 7a represents the average experimental characteristics [81].

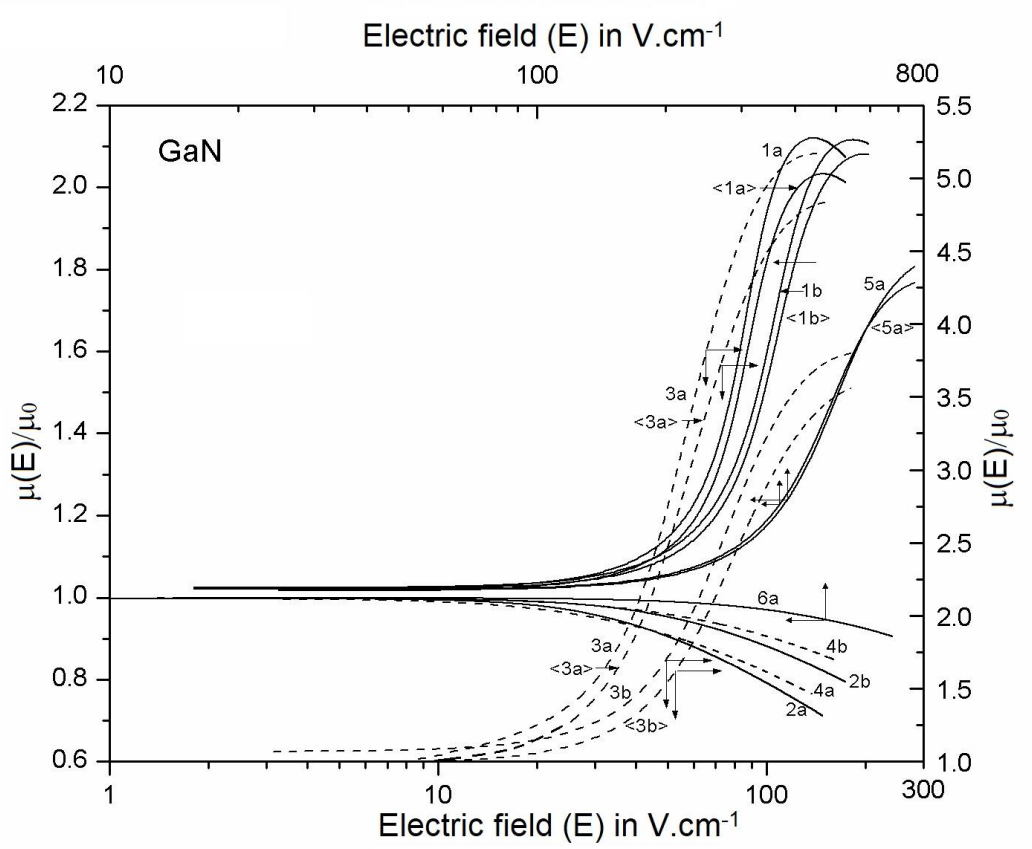

Figure 4.6 Dependence of the normalized non-ohmic mobility of the non-equilibrium carriers upon the electric field in GaN at different lattice temperatures and for different levels of degeneracy η_D when the layer concentration N_i is taken to be $2.0\times10^{15}\ m^{-2}$. Curves marked a and b are obtained at the lattice temperatures of 77*K* and 125*K*, the corresponding values of η_D being 5.3 and 3.26 respectively. Solid curves are obtained considering the degeneracy and dashed curves are obtained when the degeneracy is not taken into account. The curves 1, 3 and 5 represent the dependence for the combined interaction of the electrons with the acoustic and the piezoelectric phonons, and the curves 2, 4 and 6 are obtained for interaction only with the acoustic phonons. Curves marked with < > are obtained from the solution of the energy balance equation for the electron-phonon system, whereas other curves follow from the expression for the current density. Curves 5a and 6a have been obtained for a highly degenerate specimen at the same lattice temperature 77*K* when $N_i = 1.0\times10^{17}\ m^{-2}$ or $\eta_D = 85.10$ [82].

4.12 Discussions

From Figures 4.4, 4.5 and 4.6, the effects of the electric field on the non-ohmic mobility can be clearly understood, as each curves showing the field dependence of the normalized non-ohmic mobility $\mu(E)/\mu_0$ deviates from 1 when the field increases. It can be noted that as the electric field increases, the mobility curves attain a maximum value for certain electric field and then drop sharply for higher fields under the condition when the electrons make combined interaction with the acoustic and the piezoelectric phonons. On the other hand, the mobility due only to acoustic interaction falls off quite linearly with the increase of the field. It may also be noted that the non-ohmic mobility characteristic which follows from the two different methods show qualitative similarities, but are quantitatively different in nature.

It is to be noted here that the experimental data under the identical conditions of interest here are rather scarce in the literature. However, some data on the non-ohmic mobility characteristics in a quantum well of GaAs are available, and are represented by the curve 7a in Figure 4.5. A comparison of this average experimental curve with the curve 5a which follows from the present theory, under the condition of high degeneracy, shows that the qualitative agreement between them is quite reasonable. The small discrepancy between them may be ascribed to the non-availability of the parameter values of the experimental sample.

The results that have been obtained here from the present theoretical analysis reveals the practical importance of the contribution of the piezoelectric interaction and of the degeneracy, in determining the average ELR of a non-equilibrium electron and the non-ohmic mobility characteristics of a degenerate ensemble of 2DEG at the low lattice temperatures. The predictions which follow from the results of the present analysis are quite interesting from the device point of view.

CHAPTER V

MICROWAVE HARMONIC GENERATION IN A QUANTUM WELL OF COMPOUND SEMICONDUCTORS

5.1 Introduction

It has already been discussed in Chapter IV that the relation between the current density and the applied d.c. electric field for an ensemble of 2DEG in a semiconductor structure when subjected to a high electric field turns nonlinear. The field for the onset of this nonlinearity depends upon the lattice temperature and the type of the material. When the lattice temperature is low, $\left(T_L \leq 20K\right)$ an apparently low electric field $\sim$ a fraction of a $volt/cm$ may turn out to be convincingly high, and such nonlinearity may indeed be observed.

This electrical nonlinearity may be exploited for the generation of higher harmonics in the semiconductor structure when a microwave field is applied in conjunction with the d.c. bias field. The output at higher harmonics can be conveniently controlled by varying the d.c. field in some cases.

The cause of the electrical nonlinearity under the high-field condition is usually attributed to the field dependence of the mobility of the non-equilibrium carriers. However, at low lattice temperatures, the electrical nonlinearity sometimes may also occur due to the impact ionization of the impurity atoms by the energetic non-equilibrium electrons, and to their thermal recombination. The ionization and recombination probabilities are dependent upon the carrier energy, hence upon the electric field. As a result, the dynamical equilibrium between the free electrons and the ionization and recombination centres may shift as the effective electron temperature exceeds that of the lattice atoms in the presence of a convincingly high electric field. Hence, the concentration n of the free electrons may also turn field dependent, thus causing additional nonlinearity in the $\vec{J} - \vec{E}$ characteristics. Thus, in general, the electrical conductivity in the presence of a high electric field may be represented as $\sigma\left(E\right) = n\left(E\right)e\mu\left(E\right)$ [24, 26, 122-124].

Some studies on the characteristics of harmonic generation in low dimensional semiconductor structures due to their optical nonlinearity have already been made [125-129]. The reports on

the studies of the efficiency of second harmonic generation (SHG) due to the electrical nonlinearity of the bulk semiconductor structures are also available in the literature [130-145]. But the study of the same phenomenon, due to the electrical nonlinearity of the low dimensional structures is scarce in the literature.

In this chapter, we make an attempt to analyse the dependence of the efficiency η of generation of the second harmonic current upon the bias field E_0 for modulation doped heterostructures of compound semiconductor at the low lattice temperatures. The efficiency characteristics of the second harmonic generation are obtained for some widely used heterostructures of the compounds like InSb, GaAs, and GaN.

5.2 Brief review of the studies on the characteristics of Harmonic Generation in semiconductor structures

Seeger [138] has performed an experiment on the microwave frequency multiplication in Ge around room temperature at power levels of several kilowatt. For a fundamental frequency of 9.4 GHz, he has observed a yield of about 1% of third harmonic power. The result is in conformity with the calculations based on the observed deviation from the Ohm's law. Kobayashi et. al. [139] has performed the same experiment also at room temperature and at liquid nitrogen temperature.

For a theoretical analysis of the second harmonic generation (SHG) in a non-degenerate bulk semiconductor, P.K. Kaw has considered the d.c. electric field of arbitrary strength and made use of the Boltzmann transport equation technique to describe the motion of the carriers inside the material [130]. The carriers have been assumed to be scattered only through the acoustic mode lattice vibrations. For sufficiently strong d.c. fields, the generated second harmonic has been found to decrease with the increase of the d.c. fields obeying the simple power law. Moreover, for some optimum value of the d.c. field the generation seems to be more efficient.

It has been shown by Das that the efficiency of SHG arising from the nonlinear current-voltage characteristics should be derivable from a direct perturbation of the characteristics around the biased voltage [131]. It has been pointed out that this different derivation of the results is of preeminent practical importance as one can now easily calculate the efficiency from the experimental d.c. $J - E_0$ characteristics for any material, thus considerably simplifying the estimation in actual experiment.

Chattopadhyay and Nag have developed an approximate theory for the third harmonic generation in GaAs which is subjected to a large high frequency sinusoidal electric field [140]. The ratio of the third harmonic to the fundamental frequency currents has been found to be 0.22 and 0.15 for a field of amplitude $6.7\ KV/cm$ at the fundamental frequencies of 100 GHz and 450 GHz respectively.

The generation of the second harmonic of high frequency electromagnetic waves in anisotropic semiconductors has been theoretically investigated by Sodha and Gupta. D.C. electric fields of arbitrary strength has been considered and it has been assumed that the acoustic, nonpolar optical phonon and intervalley scatterings are the dominant type of scattering under the prevailing conditions of interest there. It has been observed that when the frequency of the wave is much greater than the effective collision frequency (i.e., the I.R. region), the generated second harmonic is proportional to the applied d.c. field [141]. This is in contrast to the range of microwave frequency when the generation is most efficient at some optimum d.c. field. The calculation of the anisotropy and the magnitude of the efficiency of SHG for the [100], [110] and [111] directions have been reported, in the case of bulk structure of n-Ge.

Yamamoto and Iwasawa have made an estimation of the efficiency of SHG in nonpolar, non-degenerate semiconductor, assuming a hyperbolic equation for the nonlinear velocity-electric-field relations in the temperature range between 77 and $300K$ [142]. Their calculation has predicted a maximum efficiency of about 5% in n-Ge and n-Si for some optimum bias field.

It has been shown by Mukhopadhyay et. al. that II-VI compound semiconductors seem to be more suitable for harmonic generation under the high-field condition than the elemental semiconductors or the III-V compound semiconductors [143-145]. Using a nonlinear analytical approximation for the velocity-field characteristics of the material the efficiency of SHG in II-VI compounds have been calculated for a lattice temperature of $77K$.

5.3 Method of calculation of the efficiency of SHG in an ensemble of 2DEG

We consider a degenerate layer of an ensemble of two-dimensional electron gas (2DEG) which is confined in an infinite triangular quantum well of a modulation doped heterostructure of a compound semiconductor at a low lattice temperature. For the analysis that follows the specific low temperature features which have been taken into account includes the degeneracy of the electron ensemble and their interaction with the piezoelectric acoustic phonons. The intrinsic interaction of the ensemble with the deformation potential acoustic phonons is also taken into account. The ensemble exhibits electrical nonlinearity when subjected to an effectively high

bias field E_0. When an a.c. field of microwave frequency f ($=\omega/2\pi$, ω being the angular frequency) is superimposed at the input. The current harmonics of higher frequencies may be generated at the output due to the nonlinear $J-E_0$ characteristics of the ensemble.

The analysis requires the knowledge of the dependence of the non-ohmic mobility, and also of its first and second order derivatives upon the bias field E_0 for the electron ensemble under consideration here. The required high-field mobility characteristics of the similar ensemble in a modulation-doped heterostructure, under the identical conditions of interest here have already been obtained in Chapter IV.

The total field E at any instant t may now be written as

$$E = E_0 + E_1 \exp\left(-i\omega t\right) \tag{5.1}$$

The resultant current density J due to the electrical nonlinearity of the ensemble may then be expressed as

$$J = \sum_{m=0}^{\infty} J_m \exp\left(-im\omega t\right) \tag{5.2}$$

where J_m is the amplitude of the mth harmonic.

The effective momentum relaxation time $\left(\tau_m\right)_{eff}$ for the combined interaction of the electrons with the deformation potential acoustic and the piezoelectric phonons, at the low lattice temperatures of interest here is $\sim 10^{-12}$ sec. It is well known that the energy relaxation time $\tau_e \sim \left(u_{th}/u_l\right)^2 \tau_m$, where u_{th} is the average thermal velocity of the electrons and u_l is the acoustic velocity [24]. When the lattice temperature is low, τ_e is almost of the same order as that of τ_m. So, at the microwave frequency around the x-band, $\omega\tau_e < 1$ [130]. Thus, the relaxation time being quite small, the free carriers can follow the input microwave signal quite exactly. Hence, one can derive the characteristics of SHG due to the electrical nonlinearity of the structure, from a direct perturbation of the d.c. $J-E_0$ characteristics, around the bias field [131].

By definition, the efficiency η of the second harmonic generation is given by the ratio $\left|J_2\right|/\left|J_1\right|$, where J_1 and J_2 are respectively the fundamental and the second harmonic components of

the current density. Hence while calculating the efficiency of generation of the second harmonic current, the series for J in (5.2) may be truncated at m=2.

If the input microwave field is small $\left(E_1 \ll E_0\right)$, then neglecting the higher order terms one may obtain

$$\eta = \frac{E_1 E_0 D^2\sigma\left(E_0\right) + 2E_1 D\sigma\left(E_0\right)}{4\left[E_0 D\sigma\left(E_0\right) + \sigma\left(E_0\right)\right]} \tag{5.3}$$

where the operator $D \equiv d/dE_0$.

When confined in the quantum well of the modulation-doped heterostructure, the electrons are mainly segregated from the impurity atoms. As such, the concentration of the electrons now hardly depends upon the field i.e., $n\left(E_0\right) \equiv n$. Hence

$$\sigma\left(E_0\right) = ne\mu\left(E_0\right) \tag{5.4}$$

As said earlier, $\mu\left(E_0\right)$ for a similar ensemble of 2DEG, under the identical conditions as those which are being considered here, has already been obtained in Chapter IV. The expressions for $\mu\left(E_0\right)$ involve the field-dependent effective temperature of the electron ensemble $T_e\left(E_0\right)$. The pertinent $T_e\left(E_0\right) - E_0$ characteristics for the semiconductor structure under consideration here have also been calculated in Chapter III.

5.4 Results for the dependence of the efficiency of SHG upon the biased field in quantum surface layers of InSb, GaAs and GaN with different levels of degeneracy

The theory is now used to investigate the characteristics of the efficiency of SHG for the degenerate ensembles on the quantum surfaces of InSb, GaAs and GaN under various conditions, in respect of the lattice temperature T_L and the level of degeneracy η_D of the ensemble.

It follows from (5.3) and (5.4) that the results for the $\eta - E_0$ characteristics evolve collectively from the field dependences of the factors like the non-ohmic mobility $\mu\left(E_0\right)$ and its first and second order derivatives $d\mu\left(E_0\right)/dE_0$ and $d^2\mu\left(E_0\right)/dE_0^2$. As is already said the results of the

field dependence of $\mu(E_0)$ for the degenerate layers of the three compounds, under the similar conditions and in the same framework have already been obtained in Chapter IV. Hence, we make use of the same results.

The analytical expression for the $\mu(E_0)$, and consequently its graphical representation, as obtained in Chapter IV is quite complex. As such, the field dependence of the derivatives of the mobility could hardly be calculated analytically. Hence, we take recourse to the numerical technique of finite differences [146, 147] to calculate these derivatives.

These factors, viz. the non-ohmic mobility and its two derivatives are entangled in the expression (5.3) for the efficiency η, in such a way, that it is hardly possible to single out any specific aspect of the resultant $\eta - E_0$ characteristics, that may have been produced solely by any of these three factors alone. However, it may be expected that all the complexities exhibited by the non-ohmic mobility characteristics and by its derivatives would make the $\eta - E_0$ characteristics quite complex under any contemplated conditions.

Figures 5.1a, 5.1b, 5.2a, 5.2b, 5.3a and 5.3b depict $\eta - E_0$ characteristics for the degenerate ensembles of 2DEG which are confined in an infinite triangular quantum well of some widely used compounds like InSb, GaAs, and GaN. The numerical values of η for any E_0 are obtained here using the values of the material parameters given in Table 3.1. The calculations have been carried out for $E_1/E_0 = 0.1$. The maximum error involved in the numerical calculation of the derivates of $\mu(E_0)$ has been estimated to be less than 0.5%.

The characteristics are obtained for various conditions, in respect of the level of degeneracy η_D, the dominant interaction of the carriers, and the lattice temperature. The results are shown by the curves in Figures 5.1, 5.2, and 5.3 respectively for the degenerate ensembles on the surfaces of InSb, GaAs, and GaN. The solid curves are obtained considering the degeneracy (deg.) of the ensemble, and the dashed curves are obtained for the non-degenerate (nd.) ones. The curve numbers in any figure are also subscripted accordingly. The figure numbers are again suffixed differently for different lattice temperatures T_L, for which the curves are drawn. For the ensembles of 2DEG on InSb and GaAs the suffix 'a' corresponds to $T_L = 2K$ and 'b' to $T_L = 4K$. Whereas in the case of the ensemble in GaN, the suffix 'a' corresponds to $T_L = 77K$ and 'b' to $T_L = 125K$.

It is important to mention here that the d.c. bias field that may turn out to be effectively high and is thus able to set in the electrical nonlinearity in a semiconductor structure, depends upon the lattice temperature T_L. It is well-known that the electrical nonlinearity in InSb and GaAs may be exhibited at the low lattice temperatures $\left(T_L \leq 20K\right)$, for d.c. bias fields of the order of a fraction of $volt/cm$. As has already been said, apart from these two compounds, the study of the harmonic generation characteristics for GaN is also obtained. GaN is well known to possess much different values of the material parameters. The significantly higher values of the piezoelectric coupling constant and effective mass, along with the much lower values of the deformation potential constant and the static dielectric constant, make this compound an interesting material from the device point of view. However, it is also well known that the electron ensemble in this material requires quite a high value of the electric field and the lattice temperature, to exhibit significant nonlinearity in the electrical characteristics. As such, the values of T_L for GaN have been chosen to be $77K$ and $125K$.

To reveal clearly how does the degeneracy of the ensemble effect changes in the second harmonic generation characteristics of a layer of any material, the results that may be obtained for a non-degenerate ensemble have also been added in each figure.

Moreover, to note the changes in the generation characteristics of any surface layer due to the interaction of the ensemble with the piezoelectric phonons, two $\eta - E_0$ characteristics are given in each figure. One, due to the combined interaction with the deformation potential acoustic and the piezoelectric phonons (curves labelled as 1) and another due to the intrinsic interaction of the electrons, only with the deformation potential acoustic phonons (curves labelled as 2).

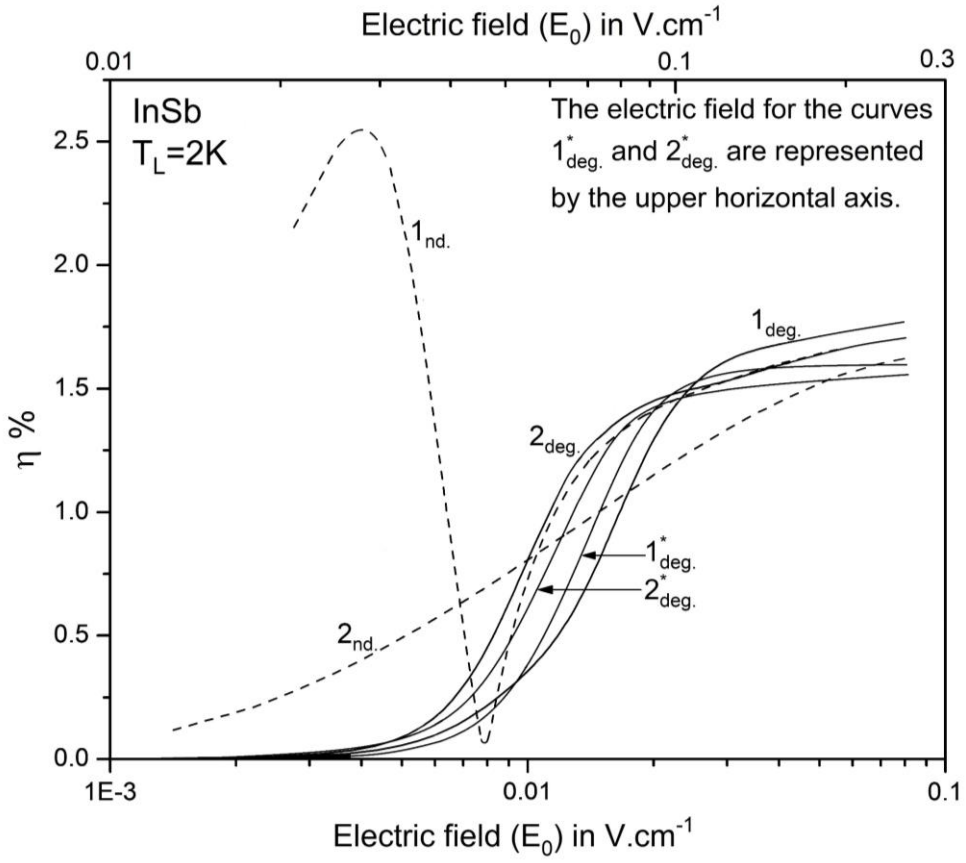

Figure 5.1a Dependence of the efficiency of SHG η upon the bias field E_0 of a non-equilibrium ensemble of 2DEG which is confined in a quantum well of InSb at the lattice temperature of 2*K* and with a layer concentration $n = 1.0 \times 10^{14}\ m^{-2}$. The level of degeneracy $\eta_D = 51.6$. The solid curves are obtained considering the degeneracy of the ensemble and the dashed curves are obtained when the degeneracy is not taken into account. The curves marked 1 represent the dependence for the combined interaction of the electrons with the acoustic and the piezoelectric phonons, and the curves marked 2 are obtained for interaction only with the acoustic phonons. Curves with * marks have been obtained for a highly degenerate specimen, when $n = 1.0 \times 10^{16}\ m^{-2}$ or $\eta_D = 1891$ [80].

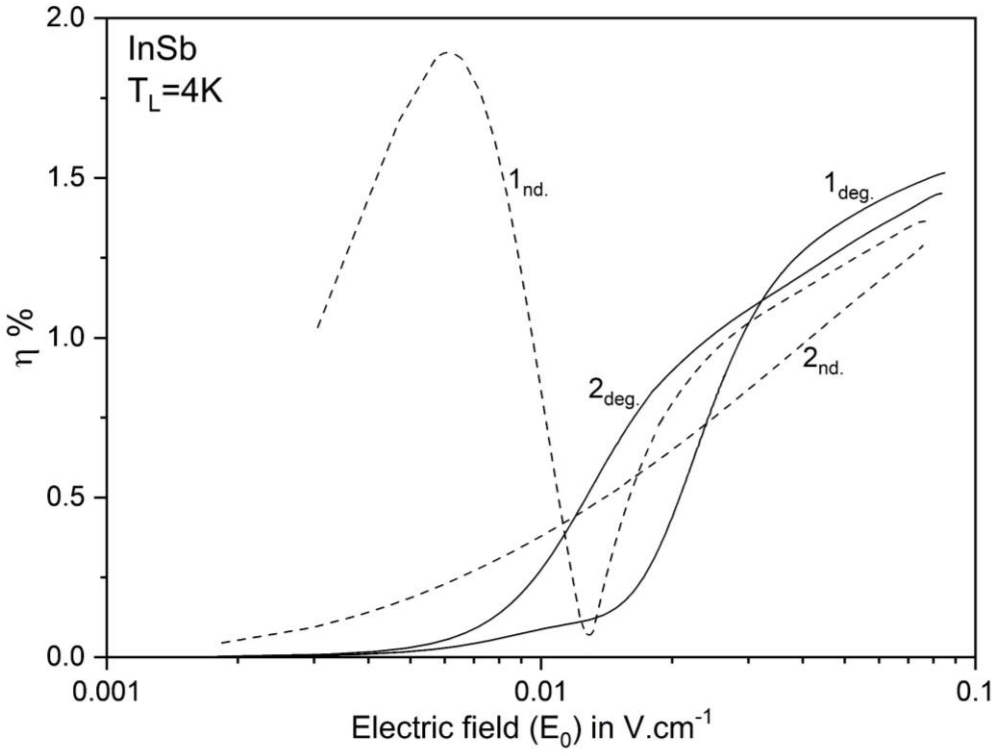

Figure 5.1b Dependence of the efficiency of SHG η upon the bias field E_0 of a non-equilibrium ensemble of 2DEG which is confined in a quantum well of InSb at the lattice temperature of 4*K* and with a layer concentration $n = 1.0 \times 10^{14}\ m^{-2}$. The level of degeneracy $\eta_D = 25.8$. The solid curves are obtained considering the degeneracy of the ensemble and the dashed curves are obtained when the degeneracy is not taken into account. The curves marked 1 represent the dependence for the combined interaction of the electrons with the acoustic and the piezoelectric phonons, and the curves marked 2 are obtained for interaction only with the acoustic phonons.

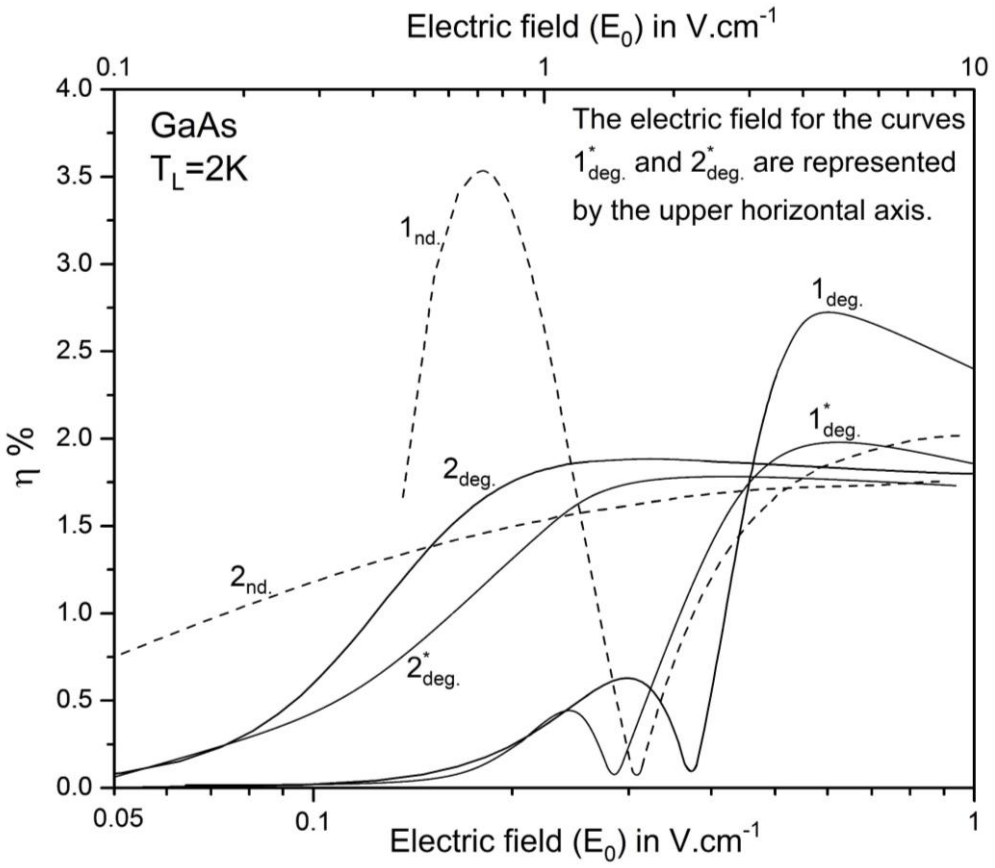

Figure 5.2a Dependence of the efficiency of SHG η upon the bias field E_0 of a non-equilibrium ensemble of 2DEG which is confined in a quantum well of GaAs at the lattice temperature of 2*K* and with a layer concentration $n = 1.0 \times 10^{14}\ m^{-2}$. The level of degeneracy $\eta_D = 31.5$. The solid curves are obtained considering the degeneracy of the ensemble and the dashed curves are obtained when the degeneracy is not taken into account. The curves marked 1 represent the dependence for the combined interaction of the electrons with the acoustic and the piezoelectric phonons, and the curves marked 2 are obtained for interaction only with the acoustic phonons. Curves with * marks have been obtained for a highly degenerate specimen, when $n = 7.0 \times 10^{15}\ m^{-2}$ or $\eta_D = 637.5$ [81].

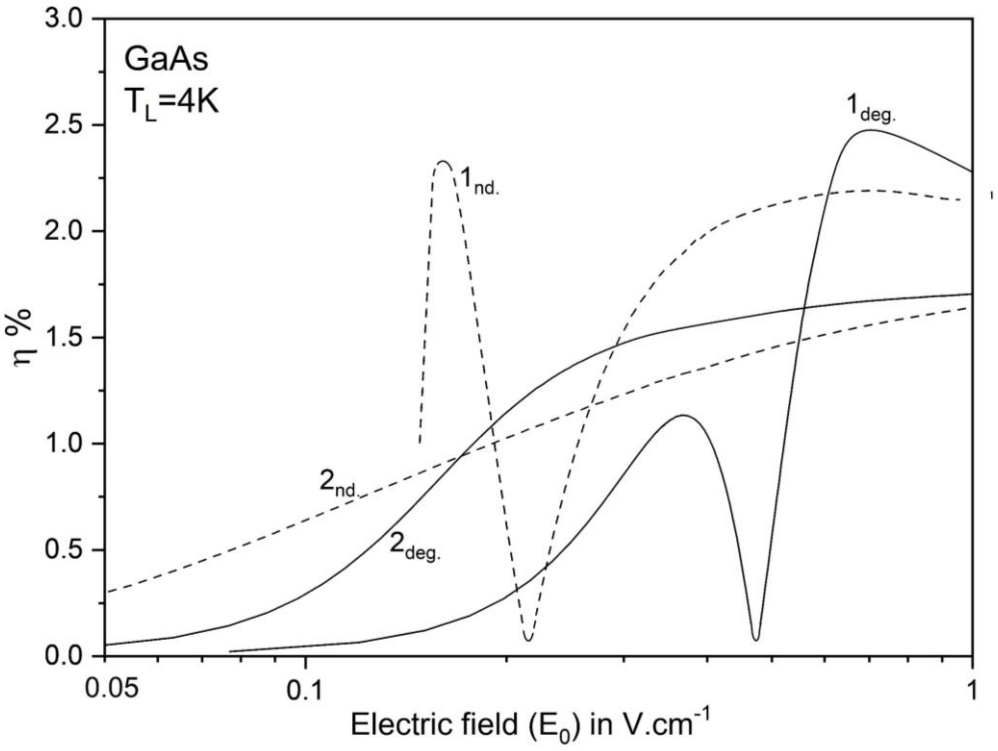

Figure 5.2b Dependence of the efficiency of SHG η upon the bias field E_0 of a non-equilibrium ensemble of 2DEG which is confined in a quantum well of GaAs at the lattice temperature of 4*K* and with a layer concentration $n = 1.0 \times 10^{14}\ m^{-2}$. The level of degeneracy $\eta_D = 15.75$. The solid curves are obtained considering the degeneracy of the ensemble and the dashed curves are obtained when the degeneracy is not taken into account. The curves marked 1 represent the dependence for the combined interaction of the electrons with the acoustic and the piezoelectric phonons, and the curves marked 2 are obtained for interaction only with the acoustic phonons.

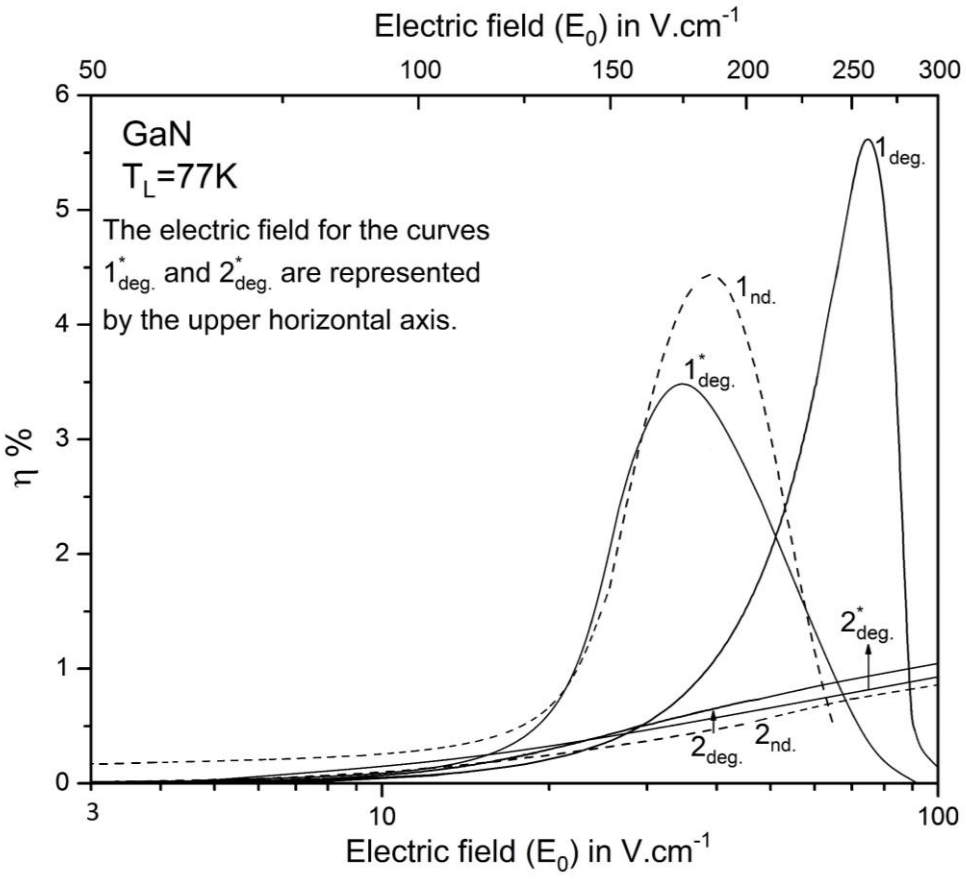

Figure 5.3a Dependence of the efficiency of SHG η upon the bias field E_0 of a non-equilibrium ensemble of 2DEG which is confined in a quantum well of GaN at the lattice temperature of 77*K* and with a layer concentration $n = 2.0\times10^{15}\ m^{-2}$. The level of degeneracy $\eta_D = 5.3$. The solid curves are obtained considering the degeneracy of the ensemble and the dashed curves are obtained when the degeneracy is not taken into account. The curves marked 1 represent the dependence for the combined interaction of the electrons with the acoustic and the piezoelectric phonons, and the curves marked 2 are obtained for interaction only with the acoustic phonons. Curves with * marks have been obtained for a highly degenerate specimen, when $n = 1.0\times10^{17}\ m^{-2}$ or $\eta_D = 85.10$ [82].

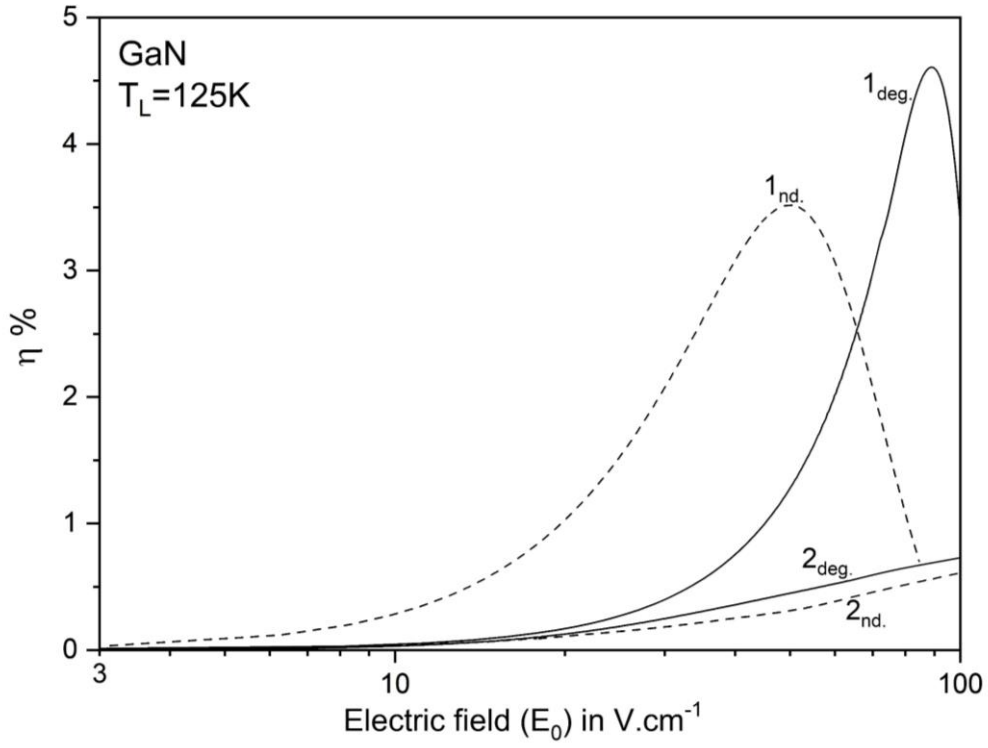

Figure 5.3b Dependence of the efficiency of SHG η upon the bias field E_0 of a non-equilibrium ensemble of 2DEG which is confined in a quantum well of GaN at the lattice temperature of 125K and with a layer concentration $n = 2.0\times10^{15}\ m^{-2}$. The level of degeneracy $\eta_D = 3.26$. The solid curves are obtained considering the degeneracy of the ensemble and the dashed curves are obtained when the degeneracy is not taken into account. The curves marked 1 represent the dependence for the combined interaction of the electrons with the acoustic and the piezoelectric phonons, and the curves marked 2 are obtained for interaction only with the acoustic phonons.

5.5 Discussions

The effects of some of the low-temperature features, like that of the degeneracy of the electron ensemble, and of their piezoelectric interaction, on the characteristics of the microwave harmonic generation in the degenerate ensembles of 2DEG which are confined to the quantum wells of InSb, GaAs and GaN in some heterostructures may be observed from the present study.

It may be seen from the figures that the $\eta - E_0$ characteristics which follow from the present analysis for the quantum confined ensembles of 2DEG in the heterostructures of interest here seem to be quite interesting.

Generally speaking, for the degenerate layers, the efficiency η, in the low-field regime, slowly increases with E_0 for any compound, irrespective of the prevalent conditions. However, the rate of increase of η at any lattice temperature is different for the surface layers of different materials. Again, for the layer of any material, the rate of increase of η is also susceptible to changes with the change of the lattice temperature.

As E_0 increases, the characteristics turn out to be more and more complex. Moreover, the widely different values of E_a, k_m, and $m*$, make the characteristics significantly different for the modulation-doped heterostructures of different materials at higher fields.

The effects of the contemplated low temperature features on the field dependence of η of the heterostructure of any material can be revealed from a comparison of the different curves for the corresponding material.

The material parameters for InSb are not much different from those of GaAs. The electrical nonlinearity in these materials is exhibited starting from a field, which is of the order of a small fraction of a $volt/cm$ at the lattice temperatures of $2K$ and $4K$. A small regime of the nonlinearity up to a few tenths of a $volt/cm$ for the surface layers of InSb, and up to a few $volt/cm$ for the GaAs layers has been considered here.

On the other hand, as has been said already, the wells of GaN is known to start exhibiting electrical nonlinearity from a considerably higher field, that too at a higher lattice temperature. Hence, in this case, the range of electric field that has been considered here lies between 10.0 $volt/cm$ up to 300 $volt/cm$ at the lattice temperatures of $77K$ and $125K$.

In order to make the discussion more comprehensive, the results for the surface layers of the three compounds InSb, GaAs, and GaN may be compared.

From the Figures. 5.1a, 5.2a, and 5.3a, it may be noted that the consideration of the degeneracy of the layers brings in significant qualitative, as well as quantitative changes in the $\eta - E_0$ characteristics of the layer of any material, irrespective of the type of interaction of the electrons, either only with the deformation potential acoustic phonons or for the case of combined interaction. The effected changes are more profound for the layers of InSb and GaAs than that of GaN.

Now the efficiency starts increasing with the field quite slowly, then the rate of increase picks up and for higher fields, the efficiency eventually tends to a saturation value. This saturation value is little higher for the layers of GaAs than that for the InSb layers. At the higher fields, η for the layers of GaN also tends to a saturation value, which turns out to be quite low.

Interestingly, under the condition of the combined interaction of the electrons the $\eta - E_0$ characteristics exhibit some extrema for the layers of Gallium (Ga) compounds. But under the same condition, no such extrema are observed for the layer of InSb. However, for the layers of the Ga compounds the efficiency again tends to a saturation value for the higher fields.

It seems quite pertinent to mention here that the $\eta - E_0$ characteristics of the non-degenerate ensembles for the combined scattering of the electrons also exhibit a few extrema usually at the lower fields. The values of the maximum efficiency are the highest for the wells of GaN, and the same is lower for GaAs and still lower for InSb. Comparing with the similar curves in Figures. 5.1b, 5.2b, and 5.3b, one can note that the maximum value of η is now lower for higher lattice temperatures. The electric field at which the maximum of η occurs, except for GaAs shifts towards the higher fields as the lattice temperature increases. For the layer of GaAs there is hardly any such shift. But, when the interaction only with the deformation potential acoustic phonons is taken into account, the efficiency characteristics for the same non-degenerate ensembles of 2DEG get quite flat and hardly any maximum of the efficiency may occur.

As the field increases, the rate of increase of η with E_0 decreases and eventually η tends to a saturation value. The saturation value of η under this condition is the highest for the layer

of InSb and the lowest for the layer of GaN. For the layer of GaAs, the saturation value is little less than that of InSb layer.

Again, comparing the curves $1_{deg.}$ with $2_{deg.}$ for any material, it may be noted that the piezoelectric interaction of the electrons is more dominant in the low-field regime. As such, the value of η is lowered in this regime, compared to its value under the condition when the electronic interaction only with the deformation potential acoustic phonons is taken into account. Moreover, as expected, for considerably higher fields, where the value of η tends to saturate, the influence of the piezoelectric interaction is hardly perceptible. As a result, the curve $2_{deg.}$ asymptotically follows the curve $1_{deg.}$ as E_0 increases.

The piezoelectric coupling constant of GaAs is 0.052, whereas that for InSb is 0.027, which is almost half of that of GaAs. As a result, one can note from the Figures. 5.2a and 5.2b that, in the lower field regime, where the piezoelectric interaction dominates, the values of η for GaAs, as given by the curve $1_{deg.}$ are much lower than that given by the curve $2_{deg.}$ as compared to what is observed for the layers of InSb.

The value of k_m for GaN is 0.18, which is much higher than that of GaAs. The Figures. 5.3a and 5.3b show that, for the wells in GaN, the $\eta - E_0$ characteristics have some qualitative similarity with that of the wells of GaAs. It is also interesting to note that the characteristics for the wells of GaAs and GaN, though start like that of InSb, but as E_0 increases, they exhibit one or a few extrema at the intermediate fields, and beyond which η again tends to a saturation value.

On comparing the Figures. 5.1a with 5.1b, 5.2a with 5.2b, and 5.3a with 5.3b, one can note that some little variation of the lattice temperature results in quite perceptible qualitative as well as quantitative changes in the $\eta - E_0$ characteristics of the layers of any material. The changes are most pronounced for the layers of InSb compared to those of the layers of the Ga compounds.

A comparison of the two sets of curves $1_{deg.}$ and $1_{nd.}$ for any material highlight that the degeneracy of the ensemble effect quite marked changes in the $\eta - E_0$ characteristics, under the more realistic condition when the electrons make combined interaction with the deformation potential acoustic and the piezoelectric phonons. Hence the interaction with the

piezoelectric phonons extensively controls the shape of the efficiency characteristics for the non-degenerate ensembles.

The results that are obtained here, could not be compared with the experimental data, as there is a dearth of the same in the literature. However, the results seem to be interesting and prompt further work through the refinement of the present analysis.

CHAPTER VI

GALVANOMAGNETIC PHENOMENA IN A TWO-DIMENSIONAL ENSEMBLE OF ELECTRONS IN A QUANTUM WELL OF A HETEROSTRUCTURE OF COMPOUND SEMICONDUCTORS

6.1 Introduction

In the presence of an electric field $\vec{E}$, an electron experiences a force $e\vec{E}$. So far, the present thesis have been dealing with the response of an electron of an ensemble of 2DEG, in a semiconductor heterostructure, to the electric field $\vec{E}$ only. However, when the electron is subjected simultaneously to an electric field $\vec{E}$ and a magnetic field $\vec{B}$, the electron experiences a Lorentz force $e\left[\vec{E}+\frac{1}{\hbar}\nabla_{\vec{k}}\varepsilon_{\vec{k}}\times\vec{B}\right]$. In response to the Lorentz force, the ensemble of electrons in a semiconductor structure exhibits galvanomagnetic phenomenon. It is well-known that there are a number of semiconductor devices whose working principle is controlled by the Lorentz force.

The knowledge of the Hall mobility at any temperature proves to be one of the important galvanomagnetic coefficients from the viewpoint of device application. Hence, the study of the Hall mobility characteristics of a structure is of considerable interest [55]. A number of well-known reports on the various aspects of the galvanomagnetic effects in the quasi-two-dimensional (Q2D), quantum-confined structures, are available in the literature [148-154].

At the low lattice temperatures, as a consequence of the weaker interaction of the electrons with the phonons and due to modulation doping of the structure, the values of the mobility in Q2D are significantly enhanced. Hence, similar structures are quite useful for the fabrication of high-speed devices [2, 3, 5]. As such, some detailed studies on the characteristics of the Hall mobility in quantum wells, at the low lattice temperatures is quite important.

6.2 Brief review of the studies on the Hall mobility of two-dimensional electrons in quantum well structures

The temperature dependence of the conductivity and Hall mobility in the quantum wells in the GaAs/InGaAs/GaAs heterostructure with different concentrations of delta doping impurity in

the well plane has been studied in [148] in some details, over a wide range of temperature, from 4K to 400K. In order to facilitate a comparison, the structures with the delta doped adjacent barrier have also been considered there. The comparison of the experimental results with what the theory predicts, exhibits quite a good agreement if the contribution of the electron transport due to the states of the impurity band formed by the delta impurity under the bottom of the lower subband is taken into account.

A theoretical study of the hole mobility in a narrow Si/SiGe quantum well has been made in [149]. The valence band in such a narrow well with high Ge content is distinguished by a light mass and by a large subband separation. The results reveal that such a narrow quantum well could yield high mobilities $\sim 10^3 \ cm^2/V.s$ around the room temperature and $\sim 10^4 \ cm^2/V.s$ at the low temperatures. Hence narrow Si/SiGe quantum wells provide greatly improved p-channel MOSFETs.

An experimental study of the Hall mobility in anti-modulation doped GaAs/AlGaAs quantum wells in the temperature range of 10K to 100K and beyond, has been made in [150]. The study offers the first evidence that the ionized impurity scattering in uniformly doped quantum wells is greater than that in a similarly doped bulk semiconductor.

It is worth mentioning here that apart from these, there are also a number of reports which serve as a valuable source of the experimental data and provide a good theoretical review of the problems related to the galvanomagnetic phenomena in Q2D structures of GaAs, GaN and InSb materials [151-154].

Considering an ensemble of Q2D, which, for the sake of mathematical simplicity, is assumed, to be confined in a simple square well potential in GaAs heterostructure, the galvanomagnetic coefficients in the presence of a non-quantising magnetic field, have been analysed in [154], for the ohmic field region, under the condition of low lattice temperature $T_L \leq 40K$ ignoring some needful details. The interactions of electrons with the screened deformation potential, both acoustic and piezoelectric and with the ionized impurities have been considered there. Furthermore, the calculations have been carried out without due regard to some of the important low-temperature features [155]. Such as, in place of the true phonon distribution, the simple equipartition approximation has been used, and the inelasticity of the electron-phonon interaction has also been neglected. The agreement of the theoretically obtained temperature dependence of the Hall mobility with the available experimental results have been brought about by choosing a fitting value for the ionized impurity concentration.

Obviously, all these interesting reports [148-155] leave enough scope for further studies on the galvanomagnetic phenomena in Q2D structures.

For the analysis that will follow shortly, an area A of a degenerate ensemble of 2DEG, which is confined to an infinite triangular potential well along the $z-$direction of a heterostructure is considered. The ensemble is subjected simultaneously to an electric field $\vec{E}$ and a non-quantizing magnetic field $\vec{B}$ along the x and z axes respectively. Hence, the electrons of the ensemble move freely on the $x-y$ plane, parallel to the interface. But their motion along the z direction is quantized due to the presence of the potential well.

A comprehensive analysis of the Hall mobility characteristics of the ensemble is carried out here considering the two cases, viz. (i) the case of an ohmic ensemble and (ii) the case of a non-ohmic ensemble.

6.2.1 (i) The case of an ohmic ensemble

In the present case, some comprehensive refinement of the analysis on the temperature dependence of the Hall mobility which has been reported in [154] is undertaken. The refinements involve, taking into account some of the salient features which have been ignored in [154]. These include the inelasticity of the electron-phonon interactions, and the true phonon distribution instead of using the equipartition approximation. Moreover, in place of the quite hypothetical square well potential as assumed in [154], the more realistic quantum well viz. the infinite triangular well potential has been considered. Apart from that, the interactions which have been ignored in [154], like that with the remote impurities and with the interface roughness, have also been considered. The Ridley's momentum conservation approximation (MCA) [156] as modified for the triangular potential well [65] has been used for the transverse component of the electron momentum.

The numerical results have been obtained for the Q2D in some widely used heterostructures like AlGaAs/GaAs, AlGaN/GaN, and AlInSb/InSb. The results of the present analysis motivate one to make more comprehensive studies on the galvanomagnetic coefficients for the ohmic as well as for the non-ohmic ensembles of Q2D at the low lattice temperatures.

6.2.2 Method of calculation of temperature dependence of Hall mobility for an ohmic and degenerate ensemble of Q2D in a modulation-doped heterostructure

The barrier potential, energy eigenvalues and the width d of the layer of the lattice atoms with which the electrons can interact in infinite triangular potential well has already been described in Chapter 2 Section 2.3.2. It may be mentioned here that under the condition of low lattice temperature of interest here, only the lowest subband is populated.

The energy distribution function $f(\vec{k})$ of the carriers of the ensemble in the presence of the magnetic field may be represented as [55, 157]

$$f(\vec{k}) = f_0(\varepsilon_{\vec{k}}) - \left(\frac{e\hbar E}{m_{\|}^*}\frac{\partial f_0}{\partial \varepsilon_{\vec{k}}}\right)\left[k_x \xi_x(\varepsilon_{\vec{k}}) - \omega_B k_y \xi_y(\varepsilon_{\vec{k}})\right] \tag{6.1}$$

where $f_0(\varepsilon_{\vec{k}})$ is the equilibrium Fermi-Dirac distribution function, ω_B is the cyclotron resonance frequency given by $\omega_B = eB/m_{\|}^*$. $\xi_x(\varepsilon_{\vec{k}})$ and $\xi_y(\varepsilon_{\vec{k}})$ are the perturbation functions. It follows from the Boltzmann transport equation that

$$\xi_x(\varepsilon_{\vec{k}}) = P(\varepsilon_{\vec{k}})\xi_y(\varepsilon_{\vec{k}}) = \frac{P(\varepsilon_{\vec{k}})}{P^2(\varepsilon_{\vec{k}}) + \omega_B^2} \tag{6.2}$$

$P(\varepsilon_{\vec{k}})$ represents the net scattering rate of an electron due to the prevalent interactions with the lattice imperfections. It follows from the perturbation theory that for any interaction 'i' [2, 3, 5, 24]

$$P_i(\varepsilon_{\vec{k}}) = \frac{2\pi}{\hbar}\sum_Q \left|M(\vec{k},\vec{k}')\right|_i^2 \delta(\varepsilon_{\vec{k}} - \varepsilon_{\vec{k}'})(1-\cos\theta_{\vec{k}})\left[1 - f_0(\varepsilon_{\vec{k}})\right] \tag{6.3}$$

where Q is the three-dimensional phonon wave vector having the component q on the $x-y$ plane and q_z is the transverse component; hence, $Q^2 = q^2 + q_z^2$; $\left|M(\vec{k},\vec{k}')\right|_i^2$ is the matrix element for the transition of an electron from the wave vector state $\vec{k}$ to the state $\vec{k}'$ due to the interaction of an electron with the ith imperfection, $\theta_{\vec{k}}$ is the scattering angle between the initial state $\vec{k}$ and the final state $\vec{k}'$. Obviously, the net scattering rate is the sum of those due interaction of the electrons with the (a) deformation potential acoustic (ac) and (b) piezoelectric

(pz) phonons, (c) remote impurities (rm), (d) background impurities (bg) and (e) surface roughness (sr), i.e.

$$P\left(\varepsilon_{\vec{k}}\right)=\sum_{i}P_{i}\left(\varepsilon_{\vec{k}}\right),\ \text{where i=ac, pz, rm, bg, sr} \tag{6.4}$$

It is well known that the presence of the magnetic field $\vec{B}$ the mobility of the ensemble turns out to be anisotropic. Thus, the Hall mobility μ_H can be expressed as [154, 157]

$$\mu_H=\frac{\mu_{xx}(0)\left|\mu_{xy}\right|}{B\left(\mu_{xx}^2+\mu_{xy}^2\right)} \tag{6.5}$$

where the components of the anisotropic mobility μ_{xx} and μ_{xy} are given by

$$\mu_{xx}=\frac{e}{\pi n_{2D}\hbar^2}\int_0^\infty\left(-\frac{\partial f_0}{\partial\varepsilon_{\vec{k}}}\right)\xi_x\left(\varepsilon_{\vec{k}}\right)\varepsilon_{\vec{k}}\,d\varepsilon_{\vec{k}} \tag{6.6}$$

$$\mu_{xy}=\frac{e\omega_B}{\pi n_{2D}\hbar^2}\int_0^\infty\left(-\frac{\partial f_0}{\partial\varepsilon_{\vec{k}}}\right)\xi_y\left(\varepsilon_{\vec{k}}\right)\varepsilon_{\vec{k}}\,d\varepsilon_{\vec{k}} \tag{6.7}$$

$\mu_{xx}(0)$ being the value of μ_{xx} in the absence of the magnetic field.

6.2.3 The transition probability for interaction with different lattice imperfections

Thus, the Hall mobility may be calculated once the integrations (6.6) and (6.7) are carried out. The integrands there, involve the perturbation functions $\xi_x\left(\varepsilon_{\vec{k}}\right)$ and $\xi_y\left(\varepsilon_{\vec{k}}\right)$. From (6.2) it may be seen that these functions may be calculated when the transition probability $P_i\left(\varepsilon_{\vec{k}}\right)$ for any interaction of an electron is known. The calculation of $P_i\left(\varepsilon_{\vec{k}}\right)$ requires the knowledge of the matrix elements $\left|M\left(\vec{k},\vec{k}'\right)\right|_i^2$ for the same interaction. These matrix elements for various interactions are given in Chapter III Section 3.4. As has been proposed the transition probabilities for different interactions can now be calculated from the expression like (6.3) under the condition of low lattice temperature, by incorporating the low temperature features. This apart, some additional interactions, all of which have been ignored in [154] have also been taken into account.

The matrix elements for interaction with the phonons involve the phonon population $N_{\vec{Q}}$. As said earlier, under the condition when the lattice temperature is low, $N_{\vec{Q}}$ can no longer be approximated by the equipartition law. The true $N_{\vec{Q}}$ at the low lattice temperatures may be represented by the Laurent expansion [25] given in Chapter I Section 1.2.2.

Again, when the lattice temperature is low, the average thermal energy of the electrons turns out to be comparable with $\hbar\omega_{\vec{Q}}$, the energy of a phonon. As such, the interaction with the phonons can no longer be assumed to be elastic. Hence, the phonon energy has to be taken into account in the energy balance equation of the electron-phonon system.

6.2.3.1 Deformation potential acoustic scattering

For the interaction of the electrons with the deformation potential acoustic phonons, the matrix element and the form factor that describes the extent of the conservation of the transverse component of the momentum of an electron are given in Chapter III Section 3.4.

It may be noted here that for the interaction with deformation potential acoustic phonons $\left\langle \cos\theta_{\vec{k}} \right\rangle = 0$, hence $1-\cos\theta_{\vec{k}} \approx 1$ [24].

Now, in order to carry out the integration (6.3) one has to know the limits of the magnitude of the phonon vector $\vec{q}$. They are obtained here from the physically realistic solutions of the energy and momentum conservation equations for the electron-phonon system. In taking due account of the phonon energy, the processes of absorption (ab.) and emission (em.) of the phonons are needed to be considered separately. The calculated values of the limits of the magnitude of the phonon wave vector $\vec{q}$ are given in Table 6.1.

Thus, one can obtain

$$P_{ac}\left(\varepsilon_{\vec{k}}\right) = \frac{A_{ac}}{\varepsilon_{\vec{k}}^{1/2}}\left(\Psi_m^{ab}\left(\varepsilon_{\vec{k}}\right) + \Psi_m^{em}\left(\varepsilon_{\vec{k}}\right)\right) \tag{6.8}$$

where $A_{ac} = E_a^2\left(2m_{\|}^*\right)^{1/2}\left(K_B T_L\right)^2 G \Big/ 2\pi\rho_v d\left(\hbar u_l\right)^3$.

$\Psi_m^{ab}\left(\varepsilon_{\vec{k}}\right)$ and $\Psi_m^{em}\left(\varepsilon_{\vec{k}}\right)$ are some modulating functions which are related to the processes of absorption and emission respectively. Depending upon the lattice temperature, these functions

assume different complex forms in different ranges of the energy $\varepsilon_{\vec{k}}$. The expressions for these modulating functions are given in Appendix F.

Table 6.1: The calculated values of the limits of q, the magnitude of the phonon wave vector

Electron energy range	Value of q_z	Approximation of x	Lower limits of q	Upper limits of q
$\varepsilon_{\vec{k}} > \varepsilon_s$ Absorption	$q_z = 0$	Nil	$x_1^{ab} = 0$	$x_2^{ab} = \lambda\left(\sqrt{\varepsilon_{\vec{k}}} + \sqrt{\varepsilon_s}\right)$
	$q_z = \pm\frac{2\pi}{d}$	$x < s$	$x_3^{ab} = \frac{\lambda}{2}\left(\sqrt{\varepsilon_{\vec{k}} + sK_BT_L} - \sqrt{\varepsilon_{\vec{k}}}\right)$	$x_4^{ab} = \frac{\lambda}{2}\left(\sqrt{\varepsilon_{\vec{k}} + sK_BT_L} + \sqrt{\varepsilon_{\vec{k}}}\right)$
		$x > s$	$x_1^{ab} = 0$	$x_2^{ab} = \lambda\left(\sqrt{\varepsilon_{\vec{k}}} + \sqrt{\varepsilon_s}\right)$
$\varepsilon_{\vec{k}} > \varepsilon_s$ and $\varepsilon_{\vec{k}} > sK_BT_L$ Absorption and emission	$q_z = 0$	Nil	$x_1^{em} = 0$	$x_2^{em} = \lambda\left(\sqrt{\varepsilon_{\vec{k}}} - \sqrt{\varepsilon_s}\right)$
	$q_z = \pm\frac{2\pi}{d}$	$x < s$	$x_3^{em} = \frac{\lambda}{2}\left(\sqrt{\varepsilon_{\vec{k}}} - \sqrt{\varepsilon_{\vec{k}} - sK_BT_L}\right)$	$x_4^{em} = \frac{\lambda}{2}\left(\sqrt{\varepsilon_{\vec{k}}} + \sqrt{\varepsilon_{\vec{k}} - sK_BT_L}\right)$
		$x > s$	$x_1^{em} = 0$	$x_2^{em} = \lambda\left(\sqrt{\varepsilon_{\vec{k}}} - \sqrt{\varepsilon_s}\right)$

6.2.3.2 Piezoelectric acoustic phonons scattering

For the interaction of the electrons with the piezoelectric acoustic phonons, the matrix element and the form factor are given in Chapter III Section 3.4.

For the case of piezoelectric scattering, $1-\cos\theta_{\vec{k}} \approx q^2/2k^2$ [24]. Now, proceeding in the same manner as that followed for the case of deformation potential acoustic scattering, one obtains

$$P_{pz}\left(\varepsilon_{\vec{k}}\right) = \frac{A_{pz}}{\varepsilon_{\vec{k}}^{3/2}}\left(\Phi_m^{ab}\left(\varepsilon_{\vec{k}}\right) + \Phi_m^{em}\left(\varepsilon_{\vec{k}}\right)\right) \tag{6.9}$$

where $A_{pz} = \left(ek_mK_BT_L\right)^2 G\Big/4\pi\hbar\in_{sc} du_l\left(2m_{\|}^*\right)^{1/2}$ and $\Phi_m^{ab}\left(\varepsilon_{\vec{k}}\right)$ and $\Phi_m^{em}\left(\varepsilon_{\vec{k}}\right)$ are some other modulating functions. The complex expressions for these functions over different ranges of the energy $\varepsilon_{\vec{k}}$ also depend upon the lattice temperature T_L. These expressions are given in Appendix G.

6.2.3.3 Remote ionized impurity scattering

For the interaction of the electrons with the remote ionized impurities, the matrix element and the form factor are given in Chapter III Section 3.4.

Let the spacer thickness be d_s and the thickness of the supplementary material at the sides of the heterostructure be L. Then, one can obtain assuming a uniform density N_i^r and for a large value of L

$$P_{rm}\left(\varepsilon_{\vec{k}}\right)=\frac{m_{\|}^{*}e^{4}N_{i}^{r}}{16\pi\in_{sc}^{2}\hbar^{3}k^{3}}\int_{0}^{2k}\frac{1}{q}\left(\frac{b}{b+q}\right)^{6}\frac{1}{S\left(\vec{q}\right)^{2}}\exp\left(-2qd_{s}\right)\frac{1}{\sqrt{1-\left(q/2k\right)^{2}}}dq \qquad (6.10)$$

6.2.3.4 Background ionized impurity scattering

For the interaction of the electrons with the background ionized impurities, the matrix element and the form factor are given in Chapter III Section 3.4.

Hence applying the matrix element in (6.3), one can obtain

$$P_{bg}\left(\varepsilon_{\vec{k}}\right)=\frac{m_{\|}^{*}e^{4}N_{i}^{B}}{16\pi\in_{sc}^{2}\hbar^{3}k^{3}}\int_{0}^{2k}\frac{1}{q}\left[F_{1}\left(q\right)+F_{2}\left(q\right)\right]\frac{1}{S\left(\vec{q}\right)^{2}}\frac{1}{\sqrt{1-\left(q/2k\right)^{2}}}dq \qquad (6.11)$$

6.2.3.5 Surface roughness scattering

For the interaction of the electrons with the surface roughness, the matrix element is given in Chapter III Section 3.4.

Hence applying the matrix element in (6.3), one can obtain

$$P_{sr}\left(\varepsilon_{\vec{k}}\right)=\left(\frac{e^{2}n_{2D}\Delta\Lambda}{2\in_{sc}}\right)^{2}\frac{m_{\|}^{*}}{2\hbar^{3}k^{3}}\int_{0}^{2k}q^{2}\frac{1}{S\left(\vec{q}\right)^{2}}\exp\left(-q^{2}\Lambda^{2}/4\right)\frac{1}{\sqrt{1-\left(q/2k\right)^{2}}}dq \qquad (6.12)$$

6.2.4 Results for the dependence of Hall mobility of an ohmic degenerate ensemble of Q2D upon the lattice temperature in AlGaAs/GaAs, AlGaN/GaN and AlInSb/InSb heterostructures

The lattice temperature dependence of the Hall mobility of the Q2D that is under consideration here, can be calculated from (6.2) and (6.4-6.12). Thus, the mobility characteristics are obtained for some widely used heterostructures like AlGaAs/GaAs, AlGaN/GaN, and AlInSb/InSb. The

values of the material parameters that have been used for the numerical calculations are quoted in Table 6.2 from [151-153, 158, 159]. It may be mentioned here, that the most of the parameter values are collected from the available references which are cited at the top of the Table 6.2. However, the values of Δ, the height of the roughness and of Λ, the spatial extent of the roughness for GaN end InSb heterostructures are selected from the given set of the possible values quoted in [152] and [153] respectively. But, only for GaAs, these values are scarcely available in the literature. Hence, in this case, as the usual practice [159], some fairly workable values for them are chosen so that our theoretical results are reasonably supported by the experimental data [151].

It may also be noted that for all the compounds of consideration here, $m_{\|}^{*} = m_{\perp}^{*} = m^{*}$. Moreover, it may be seen from the calculation of Hall-ratio $\left(= \mu_H / \mu_{xx}(0)\right)$, that it remains quite near to unity over the range of the low lattice temperatures of interest here, $T_L \leq 40K$, for all the three ensembles of Q2D considered here. Hence, the values of the Hall mobility for each of them hardly differ from the values of their drift mobility for the present range of the lattice temperature.

The mobility characteristics for the three separate heterostructures have been obtained from the present analysis. As can be seen from Table 6.2, the material parameters for the three structures are quite different from each other. The theoretical results thus obtained here have been compared with the available experimental data.

The characteristic variation of the Hall mobility with the lattice temperature for the three heterostructures, viz. AlGaAs/GaAs, AlGaN/GaN, and AlInSb/InSb as obtained from the present analysis are plotted in Figures 6.1, 6.2 and 6.3 respectively. The Hall mobility characteristics due to each individual interaction of the electrons have been plotted separately in each figure, with the labels that identify the interaction like ac, pz, etc. The significance of each level has been explained earlier. Apart from that the label “overall” attached to a characteristic curve signifies that the same characteristic has been obtained when all the interactions of the electrons are taken into account. Moreover, the curve with the level “expt” represents the characteristic that follows from the experimental data. Hence, the relative contribution of any interaction in controlling the overall characteristic of the Hall mobility for any heterostructure can be assessed from the respective figure which is drawn for the same structure.

Table 6.2 Material parameters [151-153, 158, 159]

Physical Parameters	**GaAs**	**GaN**	**InSb**
Deformation potential, $E_a\left(eV\right)$	12.0	8.0	20.0
Acoustic velocity, $u_l\left(\times 10^3\ m.s^{-1}\right)$	5.22	5.0	3.7
Density, $\rho_v\left(\times 10^3\ kg.m^{-3}\right)$	5.31	6.1	5.78
Static dielectric constant, $\in_{sc}$	12.91	9.5	17.51
Piezoelectric coupling constant, k_m	0.052	0.18	0.027
Effective mass ratio, $\left(m^*/m_0\right)$	0.072	0.2	0.014
Spacer width, $d_s\left(\text{Å}\right)$	300	333	300
Remote ionized impurities, $N_i^r\left(m^{-3}\right)$	3.4×10^{23}	3×10^{24}	1×10^{23}
Background ionized impurities, $N_i^B\left(m^{-3}\right)$	1×10^{20}	1×10^{20}	1×10^{20}
Average height of roughness, $\Delta\left(\text{Å}\right)$	2.1225	10	17
Spatial extent of roughness, $\Lambda\left(\text{Å}\right)$	15	95	95
Two-dimensional electron concentration, $n_{2D}\left(m^{-2}\right)$	6×10^{15}	1×10^{17}	5.1×10^{15}
Well width, $d\left(\text{Å}\right)$	92.4	95	186.39
Fermi level energy, $\varepsilon_F\left(meV\right)$	97.63	562.18	185.63
Ground state energy, $\varepsilon_0\left(meV\right)$	77.62	442.19	98.13

m_0 being the free electron mass

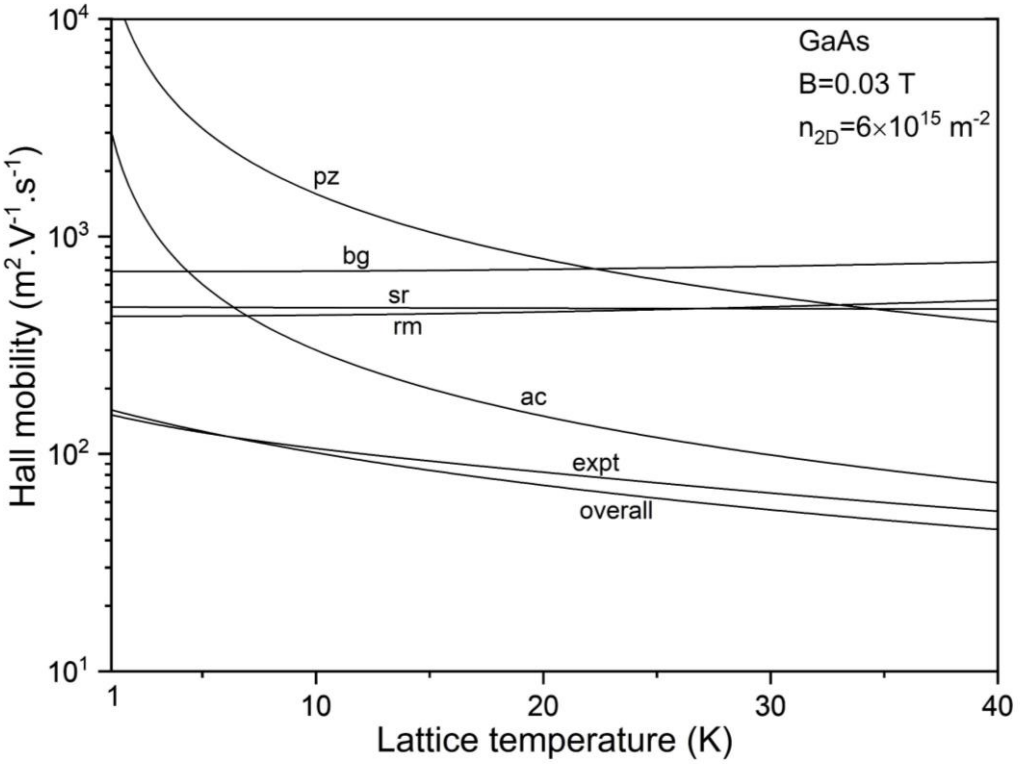

Figure 6.1 Dependence of the Hall mobility of a degenerate Q2D in the AlGaAs/GaAs heterostructure upon the lattice temperature for $B = 0.03\ T$ and $n_{2D} = 6\times10^{15}\ m^{-2}$. The curve with the label "expt" represents the experimental results which have been reported in [151].

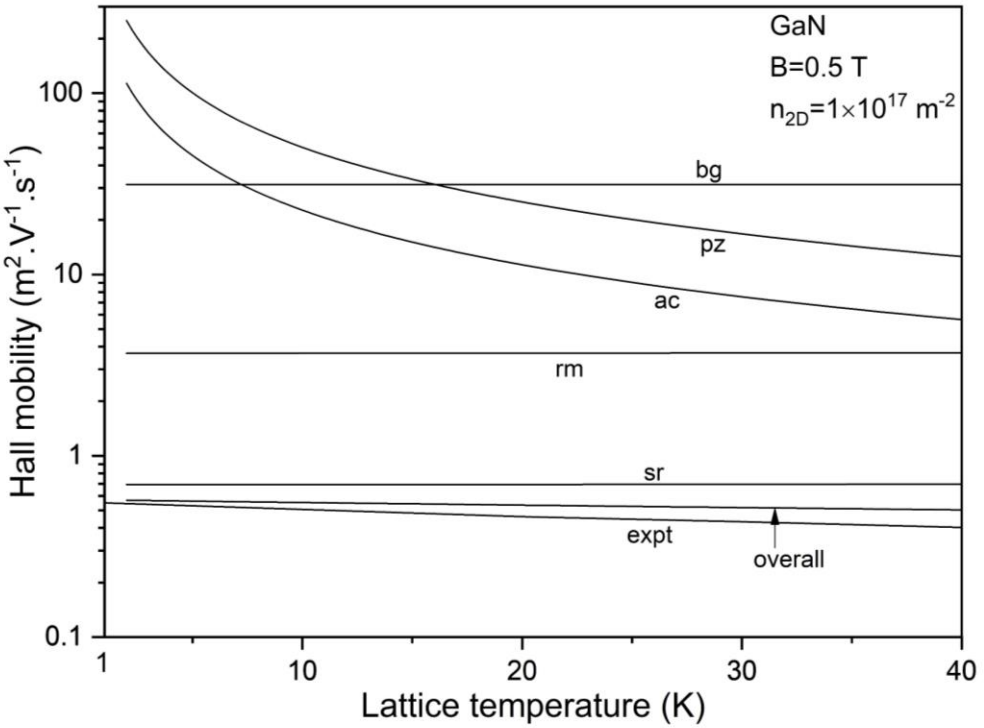

Figure 6.2 Dependence of the Hall mobility of a degenerate Q2D in the AlGaN/GaN heterostructure upon the lattice temperature for $B = 0.5\ T$ and $n_{2D} = 1\times10^{17}\ m^{-2}$. The curve with the label "expt" represents the experimental results which have been reported in [152].

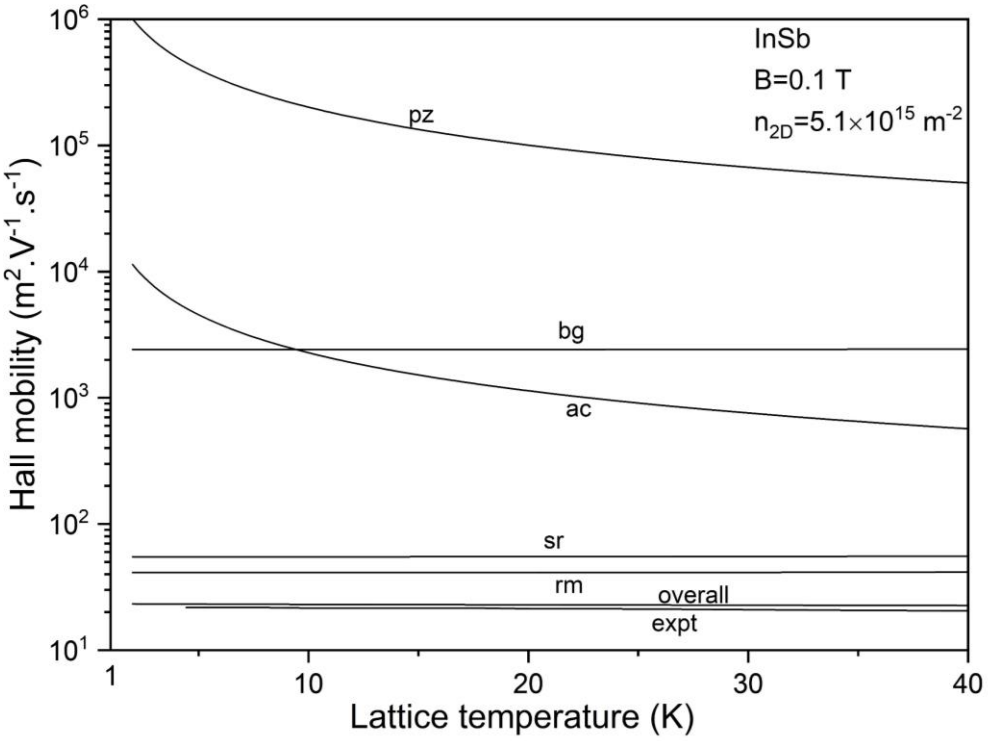

Figure 6.3 Dependence of the Hall mobility of a degenerate Q2D in the AlInSb/InSb heterostructure upon the lattice temperature for $B = 0.1\ T$ and $n_{2D} = 5.1\times10^{15}\ m^{-2}$. The curve with the label "expt" represents the experimental results which have been reported in [153].

6.2.5 Discussions

It may be noted that the characteristics obtained for the three heterostructures are qualitatively much similar to each other. However, with a view to make the discussion more knowledgeable, the characteristics as obtained for the three heterostructures may be compared.

The piezoelectric coupling constant k_m for GaAs and InSb are of the same order, but in the case of GaN it assumes a distinctly higher value. The mobility for interaction only with the piezoelectric phonons $(\mu_H)_{pz}$ attains the highest value at the low temperature: $(\mu_H)_{pz} \sim 10^4\ m^2.V^{-1}.s^{-1}$ for GaAs, and $\sim 10^6\ m^2.V^{-1}.s^{-1}$ for InSb and it assumes the least value $\sim 10^{-2}\ m^2.V^{-1}.s^{-1}$ for GaN for temperatures around 1K or so. It may be noted that for each structure, the mobility falls with the rise of temperature, initially at a fast rate, then the rate falls gradually. The qualitative picture of variation of $(\mu_H)_{ac}$ for interaction only with the deformation potential acoustic phonons is similar to that of $(\mu_H)_{pz}$. But quantitatively, it reaches a value $\sim 2\times10^3\ m^2.V^{-1}.s^{-1}$ for GaAs, $\sim 10^4\ m^2.V^{-1}.s^{-1}$ for InSb and $\sim 10^2\ m^2.V^{-1}.s^{-1}$ for GaN. $(\mu_H)_{ac}$ falls with the rise of temperature in each case following the same pattern as that of $(\mu_H)_{pz}$. For interaction only with background impurities, the mobility $(\mu_H)_{bg}$ hardly depends upon the temperature. However, it remains more or less constant at a value $\sim 7\times10^3\ m^2.V^{-1}.s^{-1}$ for GaAs, at $\sim 2\times10^3\ m^2.V^{-1}.s^{-1}$ for InSb, whereas for GaN it assumes a value $\sim 30\ m^2.V^{-1}.s^{-1}$. For interaction only with the remote impurities, the mobility $(\mu_H)_{rm}$ like the $(\mu_H)_{bg}$ is hardly dependent upon the temperature. However, for each it assume a much lower value: $(\mu_H)_{rm} \sim 700\ m^2.V^{-1}.s^{-1}$ for GaAs, $\sim 40\ m^2.V^{-1}.s^{-1}$ for InSb and in case of GaN it assumes a value $\sim 4\ m^2.V^{-1}.s^{-1}$ only. For the interaction only with surface roughness, the mobility $(\mu_H)_{sr}$ in each case is almost independent of the lattice temperature. $(\mu_H)_{sr}$ assumes a value $\sim 500\ m^2.V^{-1}.s^{-1}$ for GaAs and is $\sim 60\ m^2.V^{-1}.s^{-1}$ for InSb, whereas for GaN it is only $\sim 0.7\ m^2.V^{-1}.s^{-1}$.

The resultant overall mobility $(\mu_H)_{total}^{-1} = (\mu_H)_{ac}^{-1} + (\mu_H)_{pz}^{-1} + (\mu_H)_{rm}^{-1} + (\mu_H)_{bg}^{-1} + (\mu_H)_{sr}^{-1}$, assumes the highest values at the low temperature. It is $\sim 10^2\ m^2.V^{-1}.s^{-1}$ for GaAs and is $\sim 25\ m^2.V^{-1}.s^{-1}$ for InSb. In case of GaN it is $\sim 0.6\ m^2.V^{-1}.s^{-1}$. There is just a little fall of the overall mobility

with the rise of the lattice temperature for InSb and GaN. However, in the case of GaAs, there is a quite perceptible fall of the overall mobility with the rise of temperature.

The agreement of the characteristics of the overall mobility with the experimental prediction is quite satisfactory.

One can note that the contribution of the interactions with the remote ionized impurities and with the surface roughness in controlling the overall Hall mobility is hardly negligible. They, no doubt, bring in important changes in the characteristics. The significant improvement in the agreement of the overall characteristics that follow from the present analysis with the experimental data is quite noteworthy.

6.3.1 (ii) The case of a non-ohmic ensemble

Now let us consider the case of a non-ohmic ensemble of 2DEG. The semiconductor structure along with all the prevailing conditions remain the same as that of the preceding case. A study will now follow to assess the changes effected for the overall Hall mobility of the non-ohmic ensemble relative to that for the case of the ohmic ensemble as the applied electric field is increased. But before proceeding any further, a few features of a non-ohmic ensemble need to be elaborated.

As has already been mentioned that the two-dimensional electron ensemble in a heterostructure exhibits high electron mobility due to the segregation of the impurities from the electron ensemble. Hence, such high-speed systems are used to fabricate a number of low-dimensional devices [2, 3, 5, 160-164]. However, such high mobility system is not always effective, but could be invalidated in many cases, especially when the electrons in an ensemble are accelerated appreciably under the external applied electric field [165]. As a results of the high electric field, the electrons gain energy from the field and attain a field dependent effective electron temperature $T_e(E) > T_L$ in the steady state. This may eventually result in a reduction of the electron mobility, hence, effect the switching speed of the device. Such phenomena is of great importance for the device applications and also for extracting information about the electron-phonon interaction.

6.3.2 Method of calculation of the Hall mobility of a non-ohmic ensemble of Q2D in a modulation-doped heterostructure

The Hall mobility μ_H for the non-ohmic ensemble can be obtained from the Eq. (6.5). The components of the anisotropic mobilities, μ_{xx} and μ_{xy} are given by the Eq. (6.6) and (6.7). It may be noted here that in the presence of an effectively high-field, $f_0\left(\varepsilon_{\vec{k}}\right)$ in the Eq. (6.6) and (6.7) is given by the heated Fermi-Dirac distribution function at an effective electron temperature $T_e\left(E\right)$. Hence, the Hall mobility may be calculated once the integrals for μ_{xx} and μ_{xy} are carried out. The integrands there, involve the perturbation functions $\xi_x\left(\varepsilon_{\vec{k}}\right)$ and $\xi_y\left(\varepsilon_{\vec{k}}\right)$ which are obtained considering the net scattering processes $P\left(\varepsilon_{\vec{k}}\right)$. It is to be mentioned here that the scattering rates for different lattice imperfections viz. for the deformation potential acoustic phonons, the piezoelectric acoustic phonons, the remote ionized impurities, the background ionized impurities and the surface roughness have already been obtained in Eq. (6.8), (6.9), (6.10), (6.11) and (6.12) respectively.

The expressions for the anisotropic mobilities involve $T_e\left(\vec{E}\right)$, the effective temperature of the electron ensemble, which depend upon the heating field $\vec{E}$. The $T_e\left(\vec{E}\right)-E$ characteristics for the semiconductor heterostructure of consideration here, have been calculated from the energy balance equation of the electron-phonon system [24]

$$e\mu E^2 = \left\langle \frac{d\varepsilon_{\vec{k}}}{dt} \right\rangle \tag{6.13}$$

The rate of loss of energy $d\varepsilon_{\vec{k}}/dt$ for the electron may be obtained from the perturbation theory by summing up over all the possible emission and absorption processes. For any, say, the i[th] scattering process one can use [2, 24]

$$\frac{d\varepsilon_{\vec{k}}}{dt} = \frac{2\pi}{\hbar}\sum_{\vec{Q}} \hbar\omega_{\vec{Q}} \left|M\left(\vec{k},\vec{k}'\right)\right|_i^2 \delta\left(\varepsilon_{\vec{k}} - \varepsilon_{\vec{k}'} \pm \hbar\omega_{\vec{Q}}\right)\left[1 - f_0\left(\varepsilon_{\vec{k}}\right)\right] \tag{6.14}$$

And the average rate of loss of energy $\left\langle d\varepsilon_{\vec{k}}/dt \right\rangle$ for the non-equilibrium electrons may be obtained by taking the average of the energy loss of an electron over the energy distribution of the electrons.

The collisions with the impurities being elastic in nature, the electrons hardly lose any energy through such collisions. As such, the electrons primarily lose energy through phonons scatterings. At low temperature $T_L \le 20K$ and over the range of the electric field for which electron temperature $T_e(E)$ does not exceed $30K$, the average thermal energy of the electrons would not be sufficient enough to excite optical mode lattice vibrations. Thus, the electrons lose energy through the interaction with the deformation potential acoustic and the piezoelectric phonons in any compound semiconductor structure at the low lattice temperatures.

6.3.3 Energy loss rate of the non-equilibrium electrons due to interaction with the deformation potential acoustic phonons

The energy loss of the non-equilibrium electrons due to interaction with the deformation potential acoustic phonons can be obtained from Eq. (6.14) using the matrix element and the form factor which are given in Chapter III Section 3.4.

Now, in order to carry out the integration (6.14) one has to know the limits of the magnitude of the phonon wave vector $\vec{q}$. They are obtained in the usual way from the physically realistic solutions of the energy and momentum conservation equations for the electron-phonon system. In taking due account of the phonon energy, the processes of absorption (ab.) and emission (em.) of the phonons are needed to be considered separately [155]. The calculated values of the limits of the magnitude of the phonon wave vector $\vec{q}$ are given in Table 6.1.

Thus, one can obtain

$$\left(\frac{d\varepsilon_{\vec{k}}}{dt}\right)_{ac} = \frac{\varepsilon_{ac}}{\varepsilon_{\vec{k}}^{1/2}}\left(\Theta_m^{ab}\left(\varepsilon_{\vec{k}}\right) + \Theta_m^{em}\left(\varepsilon_{\vec{k}}\right)\right) \tag{6.15}$$

where $\varepsilon_{ac} = E_a^2\left(2m_{\|}^*\right)^{1/2}\left(K_B T_L\right)^3 G \Big/ 2\pi\rho_v d\left(\hbar u_l\right)^3$. $\Theta_m^{ab}\left(\varepsilon_{\vec{k}}\right)$ and $\Theta_m^{em}\left(\varepsilon_{\vec{k}}\right)$ are some modulating functions which are related to the processes of absorption and emission respectively. Depending upon the lattice temperature, these functions assume different complex forms in different ranges of the electron energy $\varepsilon_{\vec{k}}$. The expressions for the modulating functions are given in Appendix H.

6.3.4 Energy loss rate of the non-equilibrium electrons due to the interaction with the piezoelectric acoustic phonons

The energy loss rate of the non-equilibrium electrons due to the interaction with the piezoelectric acoustic phonons, can be obtained from Eq. (6.14) using the matrix element and the form factor which are given in Chapter III Section 3.4.

Now, proceeding in the same manner as that followed for the case of the deformation potential acoustic phonon, one may obtain

$$\left(\frac{d\varepsilon_{\vec{k}}}{dt}\right)_{pz} = \frac{\varepsilon_{pz}}{\varepsilon_{\vec{k}}^{1/2}}\left(\Pi_m^{ab}\left(\varepsilon_{\vec{k}}\right) + \Pi_m^{em}\left(\varepsilon_{\vec{k}}\right)\right) \tag{6.16}$$

where $\varepsilon_{pz} = \left(ek_m\right)^2 \left(2m_{\|}^*\right)^{1/2} u_l K_B T_L G \Big/ 2\pi \in_{sc} \hbar d$. $\Pi_m^{ab}\left(\varepsilon_{\vec{k}}\right)$ and $\Pi_m^{em}\left(\varepsilon_{\vec{k}}\right)$ are some other modulating functions which are related to the processes of absorption and emission respectively. The complex expressions for these functions over different ranges of the energy $\varepsilon_{\vec{k}}$, also depend upon the lattice temperature T_L. These expressions are given in Appendix I.

Now, the net average energy loss rate of the non-equilibrium electrons due to the interactions with the deformation potential acoustic and the piezoelectric acoustic phonons are obtained by taking the average of the energy loss of an electron over the energy distribution of the electrons. It may be mentioned here that due to complex nature of the energy loss rate given by Eq. (6.15) and (6.16), the average energy loss rate are obtained using the method of numerical integration [146, 147]. Obviously, the effective average energy loss of the non-equilibrium electrons is given by the sum of the averages of the two energy losses.

6.3.5 Results for the field dependence of the Hall mobility of a non-ohmic degenerate Q2D in AlGaAs/GaAs, AlGaN/GaN and AlInSb/InSb heterostructures

The Hall mobility of a non-ohmic ensemble of 2DEG, as given by Eq. (6.5) involves the field-dependent effective temperature of the electron ensemble $T_e\left(\vec{E}\right)$. The field-dependent effective temperature of the electrons can be calculated from (6.13) and thus the field-dependence of the Hall mobility can be obtained.

The dependence of the normalized Hall mobility of the non-ohmic ensemble of 2DEG, and their effective electron temperature, upon the heating electric field in the channels of AlGaAs/GaAs, AlGaN/GaN, and AlInSb/InSb heterostructures are obtained at different lattice temperatures and have been plotted in Figures 6.4, 6.5 and 6.6. The values of the material parameters that have been used for the numerical calculations are quoted in Table 6.2.

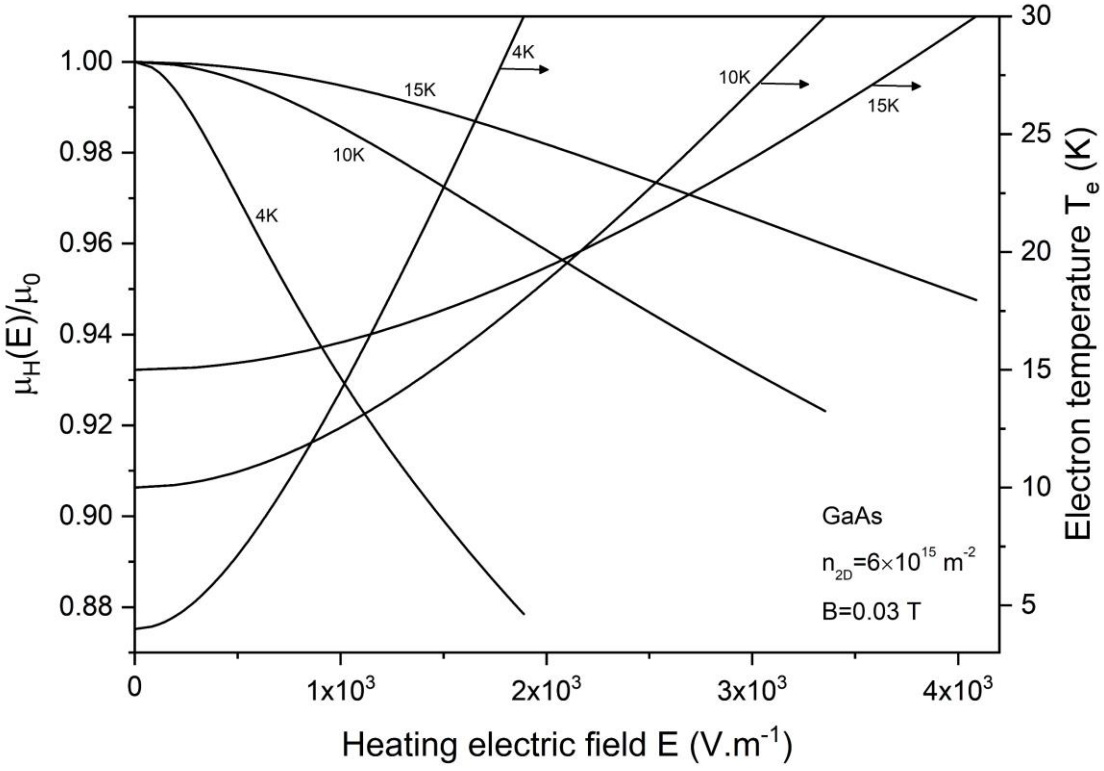

Figure 6.4 Dependence of the normalized Hall mobility and the effective temperature of an electron in the Q2D which is confined in the quantum well of AlGaAs/GaAs heterostructure, upon the heating electric field E, for $B = 0.03\ T$, $n_{2D} = 6\times10^{15}\ m^{-2}$, $N_i^r = 3.4\times10^{23}\ m^{-3}$, $N_i^B = 1\times10^{20}\ m^{-3}$ and $d = 9.241\ nm$ at the lattice temperature of $4K$, $10K$ and $15K$.

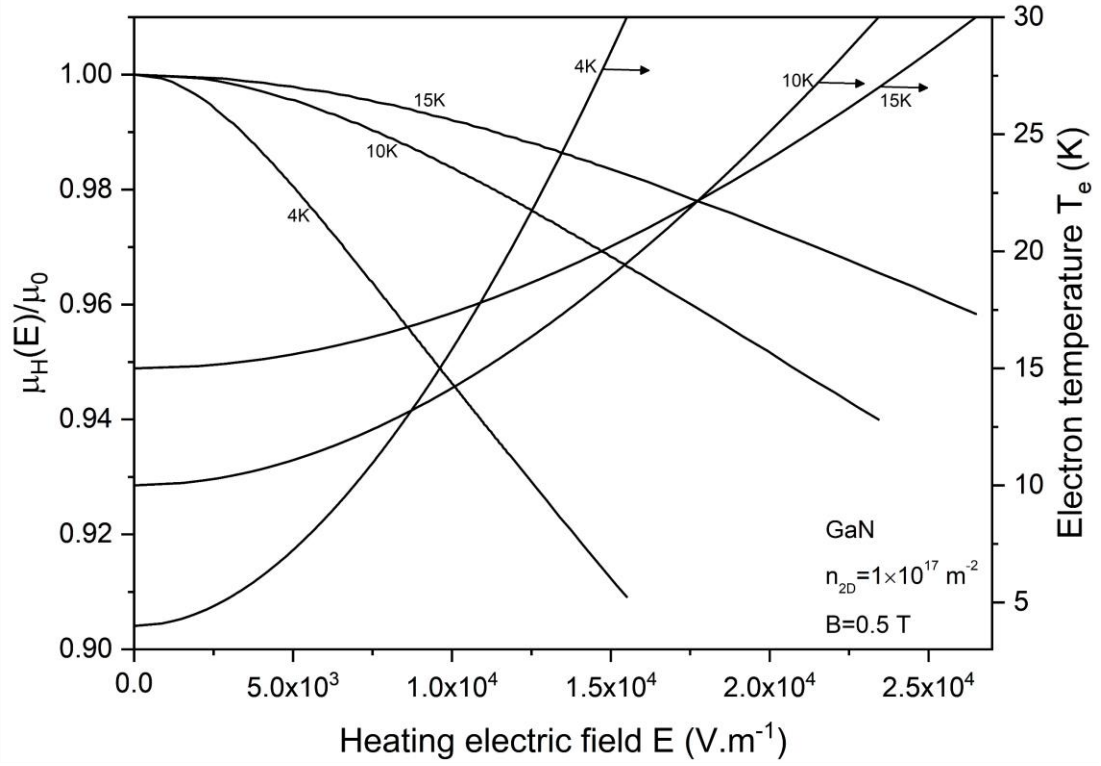

Figure 6.5 Dependence of the normalized Hall mobility and the effective temperature of an electron in the Q2D which is confined in the quantum well of AlGaN/GaN heterostructure, upon the heating electric field E, for $B = 0.5\ T$, $n_{2D} = 1\times10^{17}\ m^{-2}$, $N_i^r = 3\times10^{24}\ m^{-3}$, $N_i^B = 1\times10^{20}\ m^{-3}$ and $d = 2.3235\ nm$ at the lattice temperature of $4K$, $10K$ and $15K$.

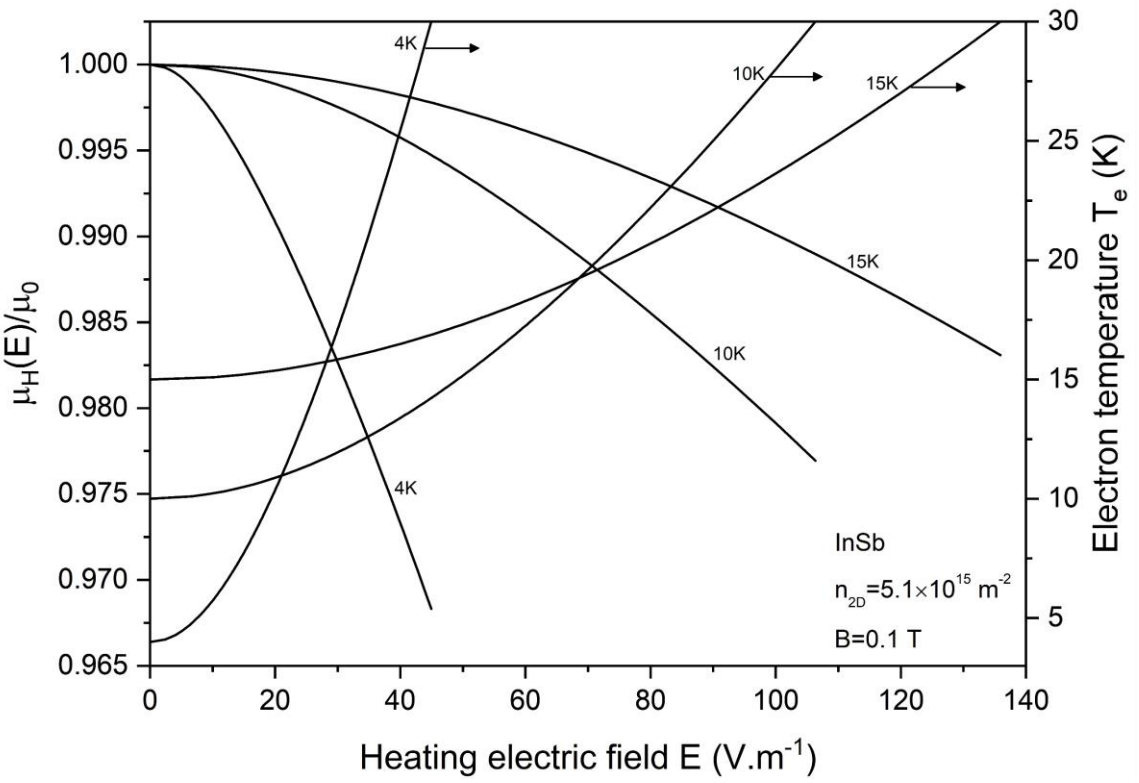

Figure 6.6 Dependence of the normalized Hall mobility and the effective temperature of an electron in the Q2D which is confined in the quantum well of AlInSb/InSb heterostructure, upon the heating electric field E, for $B = 0.1\ T$, $n_{2D} = 5.1\times10^{15}\ m^{-2}$, $N_i^r = 1\times10^{23}\ m^{-3}$, $N_i^B = 1\times10^{20}\ m^{-3}$ and $d = 18.64\ nm$ at the lattice temperature of $4K$, $10K$ and $15K$.

6.3.6 Discussions

To observe the effects of the high-field on the Hall mobility, it is normalized to its zero-field value μ_0. The values of μ_0 for the 2DEG in the heterostructure of AlGaAs/GaAs, at $T_L = 4K$, $10K$ and $15K$ are obtained as $55.28\ m^2.V^{-1}.s^{-1}$ $46.30\ m^2.V^{-1}.s^{-1}$ and $41.04\ m^2.V^{-1}.s^{-1}$ respectively. The values of μ_0 for the 2DEG in the heterostructure of AlGaN/GaN at $T_L = 4K$, $10K$ and $15K$ are obtained as $0.47\ m^2.V^{-1}.s^{-1}$, $0.45\ m^2.V^{-1}.s^{-1}$ and $0.43\ m^2.V^{-1}.s^{-1}$ respectively. The values of μ_0 for the 2DEG in the heterostructure of AlInSb/InSb at $T_L = 4K$, $10K$ and $15K$ are obtained as $22.58\ m^2.V^{-1}.s^{-1}$, $22.25\ m^2.V^{-1}.s^{-1}$ and $22.01\ m^2.V^{-1}.s^{-1}$ respectively.

It may be noted here that the lattice temperature and the heating electric fields for each material are such that the electron temperature is always below $30K$. Within the electric field range of our consideration, the effects of the high-field on the Hall mobility can be clearly understood as $\mu_H(E)/\mu_0$ drops from 1 as the field increases. This nonlinearity in the Hall mobility is due to the rise of the electron temperature with the heating field.

In the case of AlGaAs/GaAs heterostructure, the maximum drop of 12.15% of $\mu_H(E)$ occurs at the lattice temperature of $4K$. An increase of the lattice temperature to $10K$ and $15K$ results in a decrease of the maximum drop by 7.69% and 5.24% respectively. Whereas in the case of AlGaN/GaN heterostructure, the maximum drop of 9.1% of $\mu_H(E)$ occurs at the lattice temperature of $4K$. The maximum drop decreases by 6% and 4.16% as T_L is increased to $10K$ and $15K$ respectively. Similarly, in the case of AlInSb/InSb heterostructure, the maximum drop of $\mu_H(E)$ is 3.17% that occurs at the lattice temperature of $4K$. The maximum drop in $\mu_H(E)$ now decreases by 2.31% and 1.69% as T_L is increased to $10K$ and $15K$ respectively. Hence, such changes in the Hall mobility effect the corresponding changes in the values of the transconductance, and that in turn changes the switching speed of a transistor operating under the high-field condition.

To study the effects of lattice temperature on the Hall mobility and the electron temperature, the curves for each material have been plotted at different lattice temperatures of $4K$, $10K$ and $15K$. It is interesting to note that at the lower lattice temperatures, in each material the electrons get heated up rapidly at a lower field to attain an electron temperature $T_e = 30K$,

which results in a rapid decrease of the Hall mobility than what is observed at the higher temperatures where higher field is required to attain T_e of $30K$ and the rate of fall of the Hall mobility drops.

Appendix A

$$\left[I_{coll}^{ac}\right]_0^{\beta_1\varepsilon_F} =$$

$$C_{ac}\sum_{m=1}^{\infty}(-1)^m\left[\begin{array}{l}\dfrac{1}{m}\exp(-x)\left[\begin{array}{l}\left\{\exp(x\beta_1)(x\beta_1-1)+1\right\}\left(\varepsilon_e\varepsilon_L-\varepsilon_e^2/m\right)+\\ \left\{\exp(x\beta_1)\left((x\beta_1)^2-2x\beta_1+2\right)-2\right\}\left(\varepsilon_e\varepsilon_L-12\varepsilon_s\varepsilon_e-\varepsilon_e^2/m\right)+\\ \dfrac{8}{\pi}\dfrac{\varepsilon_e^{3/2}\varepsilon_s^{1/2}}{m^{1/2}}\left\{\dfrac{2}{3}(x\beta_1)^{5/2}-\dfrac{7}{3}(x\beta_1)^{3/2}+\dfrac{7}{2}(x\beta_1)^{1/2}-\dfrac{7\sqrt{\pi}}{4}erfi\left(\sqrt{x\beta_1}\right)\right\}\end{array}\right]\\ +\displaystyle\sum_{n=1}^{\infty}\frac{(-1)^n}{(m+n)^2}\exp(-y)\left[\begin{array}{l}-\varepsilon_e^2\left\{\exp(y\beta_1)(y\beta_1-1)+1\right\}-\\ \dfrac{2n\varepsilon_e}{(m+n)}\left(\varepsilon_e+6n\varepsilon_s\right)\left\{\exp(y\beta_1)\left((y\beta_1)^2-2y\beta_1+2\right)-2\right\}\end{array}\right]\end{array}\right] \tag{A.1}$$

$$\left[I_{coll}^{ac}\right]_{\beta_1\varepsilon_F}^{\beta_2\varepsilon_F} = C_{ac}\left[\begin{array}{l}\left\{\dfrac{1}{8}-\dfrac{1}{2}C^2(\eta_D\varepsilon_L)^2+\dfrac{1}{2}C\varepsilon_L\right\}(\eta_D\varepsilon_L)^2(\beta_2^2-\beta_1^2)\\ +\dfrac{4}{3}C^2(\eta_D\varepsilon_L)^4(\beta_2^3-\beta_1^3)-\dfrac{3}{4}C^2(\eta_D\varepsilon_L)^4(\beta_2^4-\beta_1^4)\\ +\dfrac{16}{5\pi}C\varepsilon_s^{1/2}(\eta_D\varepsilon_L)^{5/2}(\beta_2^{5/2}-\beta_1^{5/2})\end{array}\right] \tag{A.2}$$

$$\left[I_{coll}^{ac}\right]_{\beta_2\varepsilon_F}^{\infty} =$$

$$C_{ac}\sum_{m=1}^{\infty}(-1)^{m+1}\left[\begin{array}{l}\dfrac{1}{m}\exp(x)\left[\begin{array}{l}\exp(-x\beta_2)(x\beta_2+1)\left(\varepsilon_e^2/m-\varepsilon_L\varepsilon_e\right)\\ +\exp(-x\beta_2)\left((x\beta_2)^2+2x\beta_2+2\right)\left(\varepsilon_L\varepsilon_e-\varepsilon_e^2/m\right)\\ +\dfrac{8}{\pi}\dfrac{\varepsilon_e^{3/2}\varepsilon_s^{1/2}}{m^{1/2}}\left\{\dfrac{2}{3}\Gamma(7/2,x\beta_2)-\Gamma(5/2,x\beta_2)\right\}\end{array}\right]\\ +\displaystyle\sum_{n=1}^{\infty}\frac{(-1)^{n+1}}{(m+n)^2}\exp(y)\exp(-y\beta_2)\left[\begin{array}{l}\dfrac{2n\varepsilon_e}{(m+n)}\left(\varepsilon_e-6n\varepsilon_s\right)\times\\ \left((y\beta_2)^2+2y\beta_2+2\right)-\varepsilon_e^2(y\beta_2+1)\end{array}\right]\end{array}\right] \tag{A.3}$$

$$\left[I_{field}^{ac}\right]_0^{\beta_1\varepsilon_F} = C_{ac}^f\left[\begin{array}{l}\dfrac{(\eta_D\beta_1T_n)^2\varepsilon_e}{\left[1+\dfrac{4}{\pi}(\eta_D\beta_1\varepsilon_{sL})^{1/2}\right]}\displaystyle\sum_{m=1}^{\infty}(-1)^m m\exp\left(x(\beta_1-1)\right)\\ -\dfrac{\varepsilon_e}{\left[1+\dfrac{8}{3\pi}(\eta_D\beta_1\varepsilon_{sL})^{1/2}\right]}\displaystyle\sum_{m=1}^{\infty}\frac{(-1)^m}{m}\exp(-x)\left\{\exp(x\beta_1)\left((x\beta_1-1)+1\right)\right\}\end{array}\right] \tag{A.4}$$

$$\left[I_{field}^{ac}\right]_{\beta_1\varepsilon_F}^{\beta_2\varepsilon_F} = C_{ac}^{f} C \left[\begin{array}{l} \left(\eta_D\varepsilon_L\right)^2\left(\dfrac{\beta_2^2}{\left[1+x_2^{1/2}\right]}-\dfrac{\beta_1^2}{\left[1+x_1^{1/2}\right]}\right)-\dfrac{2\left(\eta_D\varepsilon_L\right)^{3/2}}{3a_{sL}^{1/2}}\left(\beta_2^{3/2}-\beta_1^{3/2}\right) \\ +\dfrac{\left(\eta_D\varepsilon_L\right)}{a_{sL}}\left(\beta_2-\beta_1\right)-\dfrac{2\left(\eta_D\varepsilon_L\right)^{1/2}}{a_{sL}^{3/2}}\left(\beta_2^{1/2}-\beta_1^{1/2}\right)+\dfrac{2}{a_{sL}^{2}}\ln\left(\dfrac{1+x_2^{1/2}}{1+x_1^{1/2}}\right) \end{array} \right] \tag{A.5}$$

$$\left[I_{field}^{ac}\right]_{\beta_2\varepsilon_F}^{\infty} = C_{ac}^{f} \left[\begin{array}{l} \dfrac{\left(\eta_D\beta_2T_n\right)^2\varepsilon_e}{\left[1+\dfrac{4}{\pi}\left(\eta_D\beta_2\varepsilon_{sL}\right)^{1/2}\right]}\displaystyle\sum_{m=1}^{\infty}\left(-1\right)^{m+1}m\exp\left(x\left(1-\beta_2\right)\right) \\ -\dfrac{\varepsilon_e}{\left[1+\dfrac{4}{\pi}\dfrac{\varepsilon_s^{1/2}\left\langle\varepsilon_{\vec{k}}^{1/2}\right\rangle}{\varepsilon_L}\right]}\displaystyle\sum_{m=1}^{\infty}\frac{\left(-1\right)^{m+1}}{m}\exp\left(x\left(1-\beta_2\right)\right)\left(x\beta_2+1\right) \end{array} \right] \tag{A.6}$$

where $C_{ac}=\dfrac{4\pi E_a^2 m_{\|}^{*3}}{d\rho_v\hbar^5}$; $C_{ac}^{f}=\dfrac{2\pi e^2E^2d\rho_v\hbar u_l^2}{E_a^2m_{\|}^{*}K_BT_L}$; $x=m\eta_D\dfrac{T_L}{T_e}$; $y=\left(m+n\right)\eta_D\dfrac{T_L}{T_e}$; $T_n=\dfrac{T_L}{T_e}$; $\varepsilon_{sL}=\dfrac{\varepsilon_s}{\varepsilon_L}$; $a_{sL}=\dfrac{16}{\pi^2}\dfrac{\varepsilon_s}{\varepsilon_L^2}$; $x_2=a_{sL}\beta_2\eta_D\varepsilon_L$; $x_1=a_{sL}\beta_1\eta_D\varepsilon_L$; $\left\langle\varepsilon_{\vec{k}}^{1/2}\right\rangle$ is average electron energy in a respective region. $C=\dfrac{\exp\left(\omega_1\right)-\exp\left(\omega_2\right)}{\left[1+\exp\left(\omega_1\right)\right]\left[1+\exp\left(\omega_2\right)\right]\left(\beta_2-\beta_1\right)\eta_D\varepsilon_L}$ here $\omega_1=\left(\beta_1-1\right)\eta_DT_n$ and $\omega_2=\left(\beta_2-1\right)\eta_DT_n$. $erfi\left(z\right)$ is the imaginary error function and $\Gamma\left(s,x\right)$ is the incomplete Gamma function [51].

Appendix B

$$\left[I_{coll}^{pz}\right]_{0}^{\beta_1\varepsilon_F}=C_{pz}\sum_{m=1}^{\infty}(-1)^m\left[\begin{array}{l}\exp(-x)\left[\begin{array}{l}\left\{\exp(x\beta_1)(x\beta_1-1)+1\right\}(\varepsilon_L-4\varepsilon_s-\varepsilon_e/m)\\+\dfrac{2}{\pi}\left(\dfrac{\varepsilon_e\varepsilon_s}{m}\right)^{1/2}\left\{2(x\beta_1)^{3/2}-2(x\beta_1)^{1/2}+\sqrt{\pi}erfi\left(\sqrt{x\beta_1}\right)\right\}\end{array}\right]\\-\displaystyle\sum_{n=1}^{\infty}(-1)^n\frac{2n}{(m+n)^2}\exp(-y)\left\{\exp(y\beta_1)(y\beta_1-1)+1\right\}(\varepsilon_e+2n\varepsilon_s)\end{array}\right] \tag{B.1}$$

$$\left[I_{coll}^{pz}\right]_{\beta_1\varepsilon_F}^{\beta_2\varepsilon_F}=C_{pz}\left[\begin{array}{l}\dfrac{4}{3\pi}C\varepsilon_s^{1/2}(\eta_D\varepsilon_L)^{3/2}(\beta_2^{3/2}-\beta_1^{3/2})-\dfrac{2}{3}C^2(\eta_D\varepsilon_L)^3(\beta_2^3-\beta_1^3)\\+C^2(\eta_D\varepsilon_L)^3(\beta_2^2-\beta_1^2)\end{array}\right] \tag{B.2}$$

$$\left[I_{coll}^{pz}\right]_{\beta_2\varepsilon_F}^{\infty}=C_{pz}\sum_{m=1}^{\infty}(-1)^{m+1}\left[\begin{array}{l}\exp(x)\left[\begin{array}{l}\exp(-x\beta_2)(x\beta_2+1)(\varepsilon_L-\varepsilon_e/m)+\\\dfrac{2}{\pi}\left(\dfrac{\varepsilon_e\varepsilon_s}{m}\right)^{1/2}\left\{2\Gamma(5/2,x\beta_2)-\Gamma(3/2,x\beta_2)\right\}\end{array}\right]\\+\displaystyle\sum_{n=1}^{\infty}(-1)^{n+1}\frac{2n}{(m+n)^2}\exp(y)\exp(-y\beta_2)(y\beta_2+1)(\varepsilon_e-2n\varepsilon_s)\end{array}\right] \tag{B.3}$$

$$\left[I_{field}^{pz}\right]_{0}^{\beta_1\varepsilon_F}=C_{pz}^{f}\left[\begin{array}{l}\dfrac{(\eta_D\beta_1T_n)^3\varepsilon_e^2}{\left[1+\dfrac{4}{\pi}(\eta_D\beta_1\varepsilon_{sL})^{1/2}\right]}\displaystyle\sum_{m=1}^{\infty}(-1)^m m\exp(x(\beta_1-1))-\\\dfrac{\varepsilon_e^2}{\left[1+\dfrac{8}{3\pi}(\eta_D\beta_1\varepsilon_{sL})^{1/2}\right]}\displaystyle\sum_{m=1}^{\infty}\frac{(-1)^m}{m^2}\exp(-x)\left\{\exp(x\beta_1)\left(\left((x\beta_1)^2-2x\beta_1+2\right)-2\right)\right\}\end{array}\right] \tag{B.4}$$

$$\left[I_{field}^{pz}\right]_{\beta_1\varepsilon_F}^{\beta_2\varepsilon_F}=C_{pz}^{f}C\left[\begin{array}{l}(\eta_D\varepsilon_L)^3\left(\dfrac{\beta_2^3}{\left[1+x_2^{1/2}\right]}-\dfrac{\beta_1^3}{\left[1+x_1^{1/2}\right]}\right)-\dfrac{2(\eta_D\varepsilon_L)^{5/2}}{5a_{sL}^{1/2}}(\beta_2^{5/2}-\beta_1^{5/2})\\+\dfrac{(\eta_D\varepsilon_L)^2}{2a_{sL}}(\beta_2^2-\beta_1^2)-\dfrac{2(\eta_D\varepsilon_L)^{3/2}}{3a_{sL}^{3/2}}(\beta_2^{3/2}-\beta_1^{3/2})+\dfrac{(\eta_D\varepsilon_L)}{a_{sL}^2}(\beta_2-\beta_1)\\-\dfrac{2(\eta_D\varepsilon_L)^{1/2}}{a_{sL}^{5/2}}(\beta_2^{1/2}-\beta_1^{1/2})+\dfrac{2}{a_{sL}^3}\ln\left(\dfrac{1+x_2^{1/2}}{1+x_1^{1/2}}\right)\end{array}\right] \tag{B.5}$$

$$\left[I_{field}^{pz}\right]_{\beta_2\varepsilon_F}^{\infty} = C_{pz}^{f}\left[\begin{array}{l}\dfrac{\left(\eta_D\beta_2 T_n\right)^3\varepsilon_e^2}{\left[1+\dfrac{4}{\pi}\left(\eta_D\beta_2\varepsilon_{sL}\right)^{1/2}\right]}\displaystyle\sum_{m=1}^{\infty}(-1)^{m+1}\,m\exp\left(x\left(1-\beta_2\right)\right) \\ +\dfrac{\varepsilon_e^2}{\left[1+\dfrac{4}{\pi}\dfrac{\varepsilon_s^{1/2}\left\langle\varepsilon_{\vec{k}}^{1/2}\right\rangle}{\varepsilon_L}\right]}\displaystyle\sum_{m=1}^{\infty}\frac{(-1)^{m+1}}{m^2}\exp\left(x\left(1-\beta_2\right)\right)\left(\left(x\beta_2\right)^2+2x\beta_2+2\right)\end{array}\right] \tag{B.6}$$

where $C_{pz}=\dfrac{2\pi m_{\|}^{*}e^2k_m^2\varepsilon_s}{d\in_{sc}\hbar^3}$; $C_{pz}^{f}=\dfrac{2\pi e^2E^2}{\hbar^2\tau_{pzm}}$. It may be noted that the expressions for all symbols are given in Appendix A.

Appendix C

$$\left[I_{coll}^{eff}\right]_{0}^{\beta_1\varepsilon_F}=\left[I_{coll}^{ac}\right]_{0}^{\beta_1\varepsilon_F}+\left[I_{coll}^{pz}\right]_{0}^{\beta_1\varepsilon_F} \tag{C.1}$$

$$\left[I_{coll}^{eff}\right]_{\beta_1\varepsilon_F}^{\beta_2\varepsilon_F}=\left[I_{coll}^{ac}\right]_{\beta_1\varepsilon_F}^{\beta_2\varepsilon_F}+\left[I_{coll}^{pz}\right]_{\beta_1\varepsilon_F}^{\beta_2\varepsilon_F} \tag{C.2}$$

$$\left[I_{coll}^{eff}\right]_{\beta_2\varepsilon_F}^{\infty}=\left[I_{coll}^{ac}\right]_{\beta_2\varepsilon_F}^{\infty}+\left[I_{coll}^{pz}\right]_{\beta_2\varepsilon_F}^{\infty} \tag{C.3}$$

$$\left[I_{field}^{eff}\right]_{0}^{\beta_1\varepsilon_F}= C_f\left[\begin{array}{l}\dfrac{\left(\eta_D\beta_1T_n\right)^3\varepsilon_e^2}{\left[1+\dfrac{4}{\pi}\left(\eta_D\beta_1\varepsilon_{sL}\right)^{1/2}\right]\left[1+y_1\right]}\displaystyle\sum_{m=1}^{\infty}\left(-1\right)^m m\exp\left(x\left(\beta_1-1\right)\right)- \\ \dfrac{1}{\left[1+\dfrac{8}{3\pi}\left(\eta_D\beta_1\varepsilon_{sL}\right)^{1/2}\right]}\displaystyle\sum_{m=1}^{\infty}\left(-1\right)^m\exp\left(-x\beta_1\right)\left[\begin{array}{l}\dfrac{1}{\tau_n}\left(\dfrac{\varepsilon_e}{m}\right)\left\{\exp\left(x\beta_1\right)\left(x\beta_1-1\right)+1\right\} \\ -\dfrac{1}{\tau_n^2}\left\{\exp\left(x\beta_1\right)-1\right\}+ \\ \dfrac{m}{\varepsilon_e\tau_n^3}\exp\left(-u\right)\left\{E_i\left(x\beta_1+u\right)-E_i\left(u\right)\right\}\end{array}\right]\end{array}\right] \tag{C.4}$$

$$\left[I_{field}^{eff}\right]_{\beta_1\varepsilon_F}^{\beta_2\varepsilon_F}= C_f C\left[\begin{array}{l}\dfrac{\left(\eta_D\beta_2\varepsilon_L\right)^3}{\left[1+\dfrac{4}{\pi}\left(\eta_D\beta_2\varepsilon_{sL}\right)^{1/2}\right]\left[1+y_2\right]}-\dfrac{\left(\eta_D\beta_1\varepsilon_L\right)^3}{\left[1+\dfrac{4}{\pi}\left(\eta_D\beta_1\varepsilon_{sL}\right)^{1/2}\right]\left[1+y_1\right]} \\ -\dfrac{1}{\tau_n^2\left(\tau_n+a_{sL}\right)}\ln\left(\dfrac{1+y_2}{1+y_1}\right)-\dfrac{2x_2^{1/2}}{3a_{sL}^2\tau_n^2}\left(\tau_n x_2+3\tau_n-3a_{sL}\right) \\ +\dfrac{2x_1^{1/2}}{3a_{sL}^2\tau_n^2}\left(\tau_n x_1+3\tau_n-3a_{sL}\right)+\dfrac{\eta_D\varepsilon_L}{a_{sL}\tau_n}\left(\beta_2-\beta_1\right) \\ +\dfrac{2}{a_{sL}^2\left(\tau_n+a_{sL}\right)}\ln\left(\dfrac{1+x_2^{1/2}}{1+x_1^{1/2}}\right)-\dfrac{2a_{sL}^{1/2}}{\tau_n^{5/2}\left(\tau_n+a_{sL}\right)}\left(\tan^{-1}y_2^{1/2}-\tan^{-1}y_1^{1/2}\right)\end{array}\right] \tag{C.5}$$

$$\left[I_{field}^{eff}\right]_{\beta_2\varepsilon_F}^{\infty}= C_f\left[\begin{array}{l}\dfrac{\left(\eta_D\beta_2T_n\right)^3{\varepsilon_e}^2}{\left[1+\dfrac{4}{\pi}\left(\eta_D\beta_2\varepsilon_{sL}\right)^{1/2}\right]\left[1+y_2\right]}\displaystyle\sum_{m=1}^{\infty}\left(-1\right)^{m+1}m\exp\left(x\left(1-\beta_2\right)\right)+ \\ \dfrac{1}{\left[1+\dfrac{4}{\pi}\dfrac{\varepsilon_s^{1/2}\left\langle\varepsilon_k^{1/2}\right\rangle}{\varepsilon_L}\right]}\displaystyle\sum_{m=1}^{\infty}\left(-1\right)^{m+1}\exp\left(x\right)\left[\begin{array}{l}\dfrac{1}{\tau_n}\left(\dfrac{\varepsilon_e}{m}\right)\exp\left(-x\beta_2\right)\left(x\beta_2+1\right) \\ -\dfrac{1}{\tau_n^2}\exp\left(-x\beta_2\right) \\ +\dfrac{m}{\varepsilon_e\tau_n^3}\exp\left(u\right)E_1\left(x\beta_2+u\right)\end{array}\right]\end{array}\right] \tag{C.6}$$

where $C_f = 2\pi \frac{e^2 E^2}{\hbar^2 \tau_{pzm}}$; $y_1 = \tau_n \eta_D \beta_1 \varepsilon_L$; $y_2 = \tau_n \eta_D \beta_2 \varepsilon_L$ and $u = m/\tau_n \varepsilon_e$. $E_i(z)$ and $E_1(z)$ are exponential integral functions. They may be expressed as $E_i(z) = \gamma + \ln(z) + \sum_{k=1}^{\infty} \frac{z^k}{k.k!}$ and $E_1(z) = -\gamma - \ln(z) - \sum_{k=1}^{\infty} \frac{(-1)^k z^k}{k.k!}$ respectively; $\gamma =$ Euler's constant=0.57721 [51] and $f(\eta_D, T_L) = \left[I_{field}^{eff} \right]_{\beta_1 \varepsilon_F}^{\beta_2 \varepsilon_F} \Big/ C_f C$. It may be noted that the expressions for all symbols are given in Appendix A.

Appendix D

$$\left(I_1^{ac}\right)_0^{\beta_1\varepsilon_F} = \left[I_{coll}^{ac}\right]_0^{\beta_1\varepsilon_F} \Big/ C_{ac} \tag{D.1}$$

$$\left(I_2^{ac}\right)_{\beta_1\varepsilon_F}^{\beta_2\varepsilon_F} = \left[I_{coll}^{ac}\right]_{\beta_1\varepsilon_F}^{\beta_2\varepsilon_F} \Big/ C_{ac} \tag{D.2}$$

$$\left(I_3^{ac}\right)_{\beta_2\varepsilon_F}^{\infty} = \left[I_{coll}^{ac}\right]_{\beta_2\varepsilon_F}^{\infty} \Big/ C_{ac} \tag{D.3}$$

$$\left(I_1^{pz}\right)_0^{\beta_1\varepsilon_F} = \left[I_{coll}^{pz}\right]_0^{\beta_1\varepsilon_F} \Big/ C_{pz} \tag{D.4}$$

$$\left(I_2^{pz}\right)_{\beta_1\varepsilon_F}^{\beta_2\varepsilon_F} = \left[I_{coll}^{pz}\right]_{\beta_1\varepsilon_F}^{\beta_2\varepsilon_F} \Big/ C_{pz} \tag{D.5}$$

$$\left(I_3^{pz}\right)_{\beta_2\varepsilon_F}^{\infty} = \left[I_{coll}^{pz}\right]_{\beta_2\varepsilon_F}^{\infty} \Big/ C_{pz} \tag{D.6}$$

$$\begin{aligned} I_d = {} & \beta_1\eta_D\varepsilon_L + \varepsilon_e\sum_{m=1}^{\infty}\frac{(-1)^m}{m}\exp(-x)\left\{\exp(x\beta_1)-1\right\} + \eta_D\varepsilon_L\left\{\frac{1}{2}-C\eta_D\varepsilon_L\right\}(\beta_2-\beta_1) \\ & + \frac{1}{2}C(\eta_D\varepsilon_L)^2(\beta_2^2-\beta_1^2) + \varepsilon_e\sum_{m=1}^{\infty}\frac{(-1)^{m+1}}{m}\exp(x)\exp(-x\beta_2) \end{aligned} \tag{D.7}$$

Here the expressions for $\left[I_{coll}^{ac}\right]_0^{\beta_1\varepsilon_F}$, $\left[I_{coll}^{ac}\right]_{\beta_1\varepsilon_F}^{\beta_2\varepsilon_F}$, $\left[I_{coll}^{ac}\right]_{\beta_2\varepsilon_F}^{\infty}$ and C_{ac} are given in Appendix A and the expressions for $\left[I_{coll}^{pz}\right]_0^{\beta_1\varepsilon_F}$, $\left[I_{coll}^{pz}\right]_{\beta_1\varepsilon_F}^{\beta_2\varepsilon_F}$, $\left[I_{coll}^{pz}\right]_{\beta_2\varepsilon_F}^{\infty}$ and C_{pz} are given in Appendix B. It may be noted that the expressions for all other symbols are given in Appendix A.

Appendix E

$$\left(I_{\mu}^{ac}\right)_{0}^{\beta_1\varepsilon_F} = \mu^{ac}\frac{\varepsilon_e}{\left[1+\frac{8}{3\pi}\left(\eta_D\beta_1\varepsilon_{sL}\right)^{1/2}\right]}\sum_{m=1}^{\infty}\frac{(-1)^m}{m}\exp(-x)\left\{\exp(x\beta_1)\left((x\beta_1-1)+1\right)\right\} \quad \text{(E.1)}$$

$$\left(I_{\mu}^{ac}\right)_{\beta_1\varepsilon_F}^{\beta_2\varepsilon_F} = \mu^{ac}C\left[\begin{array}{l}\frac{2\left(\eta_D\varepsilon_L\right)^{3/2}}{3a_{sL}^{1/2}}\left(\beta_2^{3/2}-\beta_1^{3/2}\right)+\frac{\left(\eta_D\varepsilon_L\right)}{a_{sL}}\left(\beta_2-\beta_1\right)+\frac{2\left(\eta_D\varepsilon_L\right)^{1/2}}{a_{sL}^{3/2}}\left(\beta_2^{1/2}-\beta_1^{1/2}\right)\\ -\frac{2}{a_{sL}^2}\ln\left(\frac{1+x_2^{1/2}}{1+x_1^{1/2}}\right)\end{array}\right] \quad \text{(E.2)}$$

$$\left(I_{\mu}^{ac}\right)_{\beta_2\varepsilon_F}^{\infty} = \mu^{ac}\frac{-\varepsilon_e}{\left[1+\frac{4}{\pi}\frac{\varepsilon_s^{1/2}\left\langle\varepsilon_{\vec{k}}^{1/2}\right\rangle}{\varepsilon_L}\right]}\sum_{m=1}^{\infty}\frac{(-1)^{m+1}}{m}\exp\left(x\left(1-\beta_2\right)\right)\left(x\beta_2+1\right) \quad \text{(E.3)}$$

$$\left(I_{\mu}^{pz}\right)_{0}^{\beta_1\varepsilon_F} = \mu^{pz}\frac{\varepsilon_e^2}{\left[1+\frac{8}{3\pi}\left(\eta_D\beta_1\varepsilon_{sL}\right)^{1/2}\right]}\sum_{m=1}^{\infty}\frac{(-1)^m}{m^2}\exp(-x)\left\{\exp(x\beta_1)\left(\left((x\beta_1)^2-2x\beta_1+2\right)-2\right)\right\}$$

(E.4)

$$\left(I_{\mu}^{pz}\right)_{\beta_1\varepsilon_F}^{\beta_2\varepsilon_F} = \mu^{pz}C\left[\begin{array}{l}\frac{2\left(\eta_D\varepsilon_L\right)^{5/2}}{5a_{sL}^{1/2}}\left(\beta_2^{5/2}-\beta_1^{5/2}\right)-\frac{\left(\eta_D\varepsilon_L\right)^2}{2a_{sL}}\left(\beta_2^2-\beta_1^2\right)+\frac{2\left(\eta_D\varepsilon_L\right)^{3/2}}{3a_{sL}^{3/2}}\left(\beta_2^{3/2}-\beta_1^{3/2}\right)\\ -\frac{\left(\eta_D\varepsilon_L\right)}{a_{sL}^2}\left(\beta_2-\beta_1\right)+\frac{2\left(\eta_D\varepsilon_L\right)^{1/2}}{a_{sL}^{5/2}}\left(\beta_2^{1/2}-\beta_1^{1/2}\right)-\frac{2}{a_{sL}^3}\ln\left(\frac{1+x_2^{1/2}}{1+x_1^{1/2}}\right)\end{array}\right] \quad \text{(E.5)}$$

$$\left(I_{\mu}^{pz}\right)_{\beta_2\varepsilon_F}^{\infty} = \mu^{pz}\frac{-\varepsilon_e^2}{\left[1+\frac{4}{\pi}\frac{\varepsilon_s^{1/2}\left\langle\varepsilon_{\vec{k}}^{1/2}\right\rangle}{\varepsilon_L}\right]}\sum_{m=1}^{\infty}\frac{(-1)^{m+1}}{m^2}\exp\left(x\left(1-\beta_2\right)\right)\left(\left(x\beta_2\right)^2+2x\beta_2+2\right) \quad \text{(E.6)}$$

Here $\mu^{ac}=\frac{d\rho_v\hbar^3u_l^2}{E_a^2m_{\|}^*K_BT_L}$ and $\mu^{pz}=\frac{4d\hbar\in_{sc}}{e^2k_m^2K_BT_L}$. It may be noted that the expressions for all symbols are given in Appendix A.

Appendix F

In the temperature range $T_L < T_c$, one can see that $\varepsilon_{cr}^{ab,em} < \varepsilon_1^{ab,em}$:

For the energy range $\varepsilon_{\vec{k}} \le \varepsilon_{cr}^{ab} < \varepsilon_1^{ab}$:

$$\Psi_m^{ab} = \sum_{m=0}^{\infty} \frac{B_m}{m!} \left\{ 2\left[I_{m+1} \right]_{x_1^{ab}}^{x_2^{ab}} + \sum_{r=o}^{m/2} {}^{m/2}C_r s^{m-2r} \left[J_r \right]_{x_3^{ab}}^{x_4^{ab}} \text{(m even) or } \sum_{r=o}^{\infty} \binom{m/2}{r} s^{m-2r} \left[J_r \right]_{x_3^{ab}}^{x_4^{ab}} \text{ (m odd)} \right\} \tag{F.1}$$

For the energy range $\varepsilon_{cr}^{ab} < \varepsilon_{\vec{k}} \le \varepsilon_1^{ab}$ and $\varepsilon_{cr}^{ab} < \varepsilon_1^{ab} < \varepsilon_{\vec{k}}$:

$$\Psi_m^{ab} = \sum_{m=0}^{\infty} \frac{B_m}{m!} \left\{ 2\left[I_{m+1} \right]_{x_1^{ab}}^{\bar{x}} + \sum_{r=o}^{m/2} {}^{m/2}C_r s^{m-2r} \left[J_r \right]_{x_3^{ab}}^{\bar{x}} \text{(m even) or } \sum_{r=o}^{\infty} \binom{m/2}{r} s^{m-2r} \left[J_r \right]_{x_3^{ab}}^{\bar{x}} \text{ (m odd)} \right\} \tag{F.2}$$

For the energy range $\varepsilon_{\vec{k}} \le \varepsilon_{cr}^{em} < \varepsilon_1^{em}$:

$$\Psi_m^{em} = \begin{cases} \sum_{m=0}^{\infty} \frac{B_m}{m!} \left\{ 2\left[I_{m+1} \right]_{x_1^{em}}^{x_2^{em}} + \sum_{r=o}^{m/2} {}^{m/2}C_r s^{m-2r} \left[J_r \right]_{x_3^{em}}^{x_4^{em}} \text{(m even) or } \sum_{r=o}^{\infty} \binom{m/2}{r} s^{m-2r} \left[J_r \right]_{x_3^{em}}^{x_4^{em}} \text{ (m odd)} \right\} \\ +2\left[I_2 \right]_{x_1^{em}}^{x_2^{em}} + \sum_{r=o}^{\infty} \binom{1/2}{r} s^{1-2r} \left[J_r \right]_{x_3^{em}}^{x_4^{em}} \end{cases} \tag{F.3}$$

For the energy range $\varepsilon_{cr}^{em} < \varepsilon_{\vec{k}} \le \varepsilon_1^{em}$:

$$\Psi_m^{em} = \begin{cases} \sum_{m=0}^{\infty} \frac{B_m}{m!} \left\{ 2\left[I_{m+1} \right]_{x_1^{em}}^{\bar{x}} + \sum_{r=o}^{m/2} {}^{m/2}C_r s^{m-2r} \left[J_r \right]_{x_3^{em}}^{\bar{x}} \text{(m even) or } \sum_{r=o}^{\infty} \binom{m/2}{r} s^{m-2r} \left[J_r \right]_{x_3^{em}}^{\bar{x}} \text{ (m odd)} \right\} \\ +2\left[I_2 \right]_{x_1^{em}}^{x_2^{em}} + \sum_{r=o}^{\infty} \binom{1/2}{r} s^{1-2r} \left[J_r \right]_{x_3^{em}}^{x_4^{em}} \end{cases} \tag{F.4}$$

For the energy range $\varepsilon_{cr}^{em} < \varepsilon_1^{em} < \varepsilon_{\vec{k}}$:

$$\Psi_m^{em} = \begin{cases} \sum_{m=0}^{\infty} \frac{B_m}{m!} \left\{ 2\left[I_{m+1} \right]_{x_1^{em}}^{\bar{x}} + \sum_{r=o}^{m/2} {}^{m/2}C_r s^{m-2r} \left[J_r \right]_{x_3^{em}}^{\bar{x}} \text{(m even) or } \sum_{r=o}^{\infty} \binom{m/2}{r} s^{m-2r} \left[J_r \right]_{x_3^{em}}^{\bar{x}} \text{ (m odd)} \right\} \\ +2\left[I_2 \right]_{x_1^{em}}^{x_2^{em}} + \sum_{r=o}^{\infty} \binom{1/2}{r} \left\{ s^{1-2r} \left[J_r \right]_{x_3^{em}}^{s} + s^{2r} \left[I_{2-2r} \right]_{s}^{x_2^{em}} \right\} \end{cases} \tag{F.5}$$

In the temperature range $T_L > T_c$, it follows that $\varepsilon_1^{ab,em} < \varepsilon_{cr}^{ab,em}$:

For the energy range $\varepsilon_{\vec{k}} \le \varepsilon_1^{ab} < \varepsilon_{cr}^{ab}$:

$$\Psi_m^{ab} = \sum_{m=0}^{\infty} \frac{B_m}{m!} \left\{ 2\left[I_{m+1} \right]_{x_1^{ab}}^{x_2^{ab}} + \sum_{r=o}^{m/2} {}^{m/2}C_r s^{m-2r} \left[J_r \right]_{x_3^{ab}}^{x_4^{ab}} \text{ (m even) or } \sum_{r=o}^{\infty} \binom{m/2}{r} s^{m-2r} \left[J_r \right]_{x_3^{ab}}^{x_4^{ab}} \text{ (m odd)} \right\} \tag{F.6}$$

For the energy range $\varepsilon_1^{ab} < \varepsilon_{\vec{k}} \le \varepsilon_{cr}^{ab}$:

$$\Psi_m^{ab} = \sum_{m=0}^{\infty} \frac{B_m}{m!} \left\{ \begin{array}{l} 2\left[I_{m+1} \right]_{x_1^{ab}}^{x_2^{ab}} + \sum_{r=o}^{m/2} {}^{m/2}C_r s^{m-2r} \left\{ \left[J_r \right]_{x_3^{ab}}^{s} + \left[I_{2r+1} \right]_{s}^{x_2^{ab}} \right\} \text{(m even)} \\ \text{or } \sum_{r=o}^{\infty} \binom{m/2}{r} \left\{ s^{m-2r} \left[J_r \right]_{x_3^{ab}}^{s} + s^{2r} \left[\mathrm{I}_{m+1-2r} \right]_{s}^{x_2^{ab}} \right\} \text{(m odd)} \end{array} \right\} \tag{F.7}$$

For the energy range $\varepsilon_1^{ab} < \varepsilon_{cr}^{ab} < \varepsilon_{\vec{k}}$:

$$\Psi_m^{ab} = \sum_{m=0}^{\infty} \frac{B_m}{m!} \left\{ \begin{array}{l} 2\left[I_{m+1} \right]_{x_1^{ab}}^{\bar{x}} + \sum_{r=o}^{m/2} {}^{m/2}C_r s^{m-2r} \left\{ \left[J_r \right]_{x_3^{ab}}^{s} + \left[I_{2r+1} \right]_{s}^{\bar{x}} \right\} \text{ (m even)} \\ \text{or } \sum_{r=o}^{\infty} \binom{m/2}{r} \left\{ s^{m-2r} \left[J_r \right]_{x_3^{ab}}^{s} + s^{2r} \left[I_{m+1-2r} \right]_{s}^{\bar{x}} \right\} \text{ (m odd)} \end{array} \right\} \tag{F.8}$$

For the energy range $\varepsilon_{\vec{k}} \le \varepsilon_1^{em} < \varepsilon_{cr}^{em}$:

$$\Psi_m^{em} = \left\{ \begin{array}{l} \sum_{m=0}^{\infty} \frac{B_m}{m!} \left\{ 2\left[I_{m+1} \right]_{x_1^{em}}^{x_2^{em}} + \sum_{r=o}^{m/2} {}^{m/2}C_r s^{m-2r} \left[J_r \right]_{x_3^{em}}^{x_4^{em}} \text{ (m even) or } \sum_{r=o}^{\infty} \binom{m/2}{r} s^{m-2r} \left[J_r \right]_{x_3^{em}}^{x_4^{em}} \text{ (m odd)} \right\} \\ +2\left[I_2 \right]_{x_1^{em}}^{x_2^{em}} + \sum_{r=o}^{\infty} \binom{1/2}{r} s^{1-2r} \left[J_r \right]_{x_3^{em}}^{x_4^{em}} \end{array} \right. \tag{F.9}$$

For the energy range $\varepsilon_1^{em} < \varepsilon_{\vec{k}} \le \varepsilon_{cr}^{em}$:

$$\Psi_m^{em} = \left\{ \begin{array}{l} \sum_{m=0}^{\infty} \frac{B_m}{m!} \left\{ \begin{array}{l} 2\left[I_{m+1} \right]_{x_1^{em}}^{x_2^{em}} + \sum_{r=o}^{m/2} {}^{m/2}C_r s^{m-2r} \left\{ \left[J_r \right]_{x_3^{em}}^{s} + \left[I_{2r+1} \right]_{s}^{x_2^{em}} \right\} \text{ (m even)} \\ \text{or } \sum_{r=o}^{\infty} \binom{m/2}{r} \left\{ s^{m-2r} \left[J_r \right]_{x_3^{em}}^{s} + s^{2r} \left[I_{m+1-2r} \right]_{s}^{x_2^{em}} \right\} \text{ (m odd)} \end{array} \right. \\ +2\left[I_2 \right]_{x_1^{em}}^{x_2^{em}} + \sum_{r=o}^{\infty} \binom{1/2}{r} \left\{ s^{1-2r} \left[J_r \right]_{x_3^{em}}^{s} + s^{2r} \left[I_{2-2r} \right]_{s}^{x_2^{em}} \right\} \end{array} \right. \tag{F.10}$$

For the energy range $\varepsilon_1^{em} < \varepsilon_{cr}^{em} < \varepsilon_{\bar{k}}$:

$$\Psi_m^{em} = \begin{Bmatrix} \sum_{m=0}^{\infty} \frac{B_m}{m!} \begin{Bmatrix} 2\left[I_{m+1}\right]_{x_1^{em}}^{\bar{x}} + \sum_{r=o}^{m/2} {}^{m/2}C_r s^{m-2r} \left\{ \left[J_r\right]_{x_3^{em}}^{s} + \left[I_{2r+1}\right]_{s}^{\bar{x}} \right\} \text{ (m even)} \\ \text{or } \sum_{r=o}^{\infty} \binom{m/2}{r} \left\{ s^{m-2r} \left[J_r\right]_{x_3^{em}}^{s} + s^{2r} \left[I_{m+1-2r}\right]_{s}^{\bar{x}} \right\} \text{(m odd)} \end{Bmatrix} \\ +2\left[I_2\right]_{x_1^{em}}^{x_2^{em}} + \sum_{r=o}^{\infty} \binom{1/2}{r} \left\{ s^{1-2r} \left[J_r\right]_{x_3^{em}}^{s} + s^{2r} \left[I_{2-2r}\right]_{s}^{x_2^{em}} \right\} \end{Bmatrix} \tag{F.11}$$

Here $T_c = \frac{2\pi\hbar u_l}{dK_B\bar{x}}$; $x = \frac{\hbar u_l q}{K_B T_L}$; $\bar{x} = \left(\overline{X}^2 - \frac{\pi^4}{75}\right)^{1/2}$; $\varepsilon_{cr}^{ab} = \left(\frac{\bar{x}}{\lambda} - \sqrt{\varepsilon_s}\right)^2$; $\varepsilon_1^{ab} = \left(\frac{s}{\lambda} - \sqrt{\varepsilon_s}\right)^2$;

$\varepsilon_{cr}^{em} = \left(\frac{\bar{x}}{\lambda} + \sqrt{\varepsilon_s}\right)^2$; $\varepsilon_1^{em} = \left(\frac{s}{\lambda} + \sqrt{\varepsilon_s}\right)^2$; $\varepsilon_s = m^* u_l^2/2$; $\lambda = \frac{4\sqrt{\varepsilon_s}}{K_B T_L}$; $s = \frac{2\pi\hbar u_l}{dK_B T_L}$.

$\left[I_m\right]_{x_1}^{x_2} = I_m(x_2) - I_m(x_1)$;

$$I_m^{ab(em)}(x) = \int \frac{x^m dx}{(x+\beta)\sqrt{R^{ab(em)}(x)}} = K_{m-1}^{ab(em)}(x) - \beta I_{m-1}^{ab(em)}(x);$$

$$I_{-m}^{ab(em)}(x) = \int \frac{x^{-m} dx}{(x+\beta)\sqrt{R^{ab(em)}(x)}} = \frac{1}{\beta}\left[L_{-m}^{ab(em)}(x) - I_{-(m-1)}^{ab(em)}(x)\right];$$

$$K_m^{ab(em)}(x) = \int \frac{x^m dx}{\sqrt{R^{ab(em)}(x)}} = \frac{x^{m-1}}{mc}\sqrt{R^{ab(em)}(x)} - \frac{(2m-1)b^{ab(em)}}{2mc} K_{m-1}(x) - \frac{(m-1)a}{mc} K_{m-2}(x);$$

$$L_{-m}^{ab(em)}(x) = \int \frac{x^{-m} dx}{\sqrt{R^{ab(em)}(x)}} = -\frac{\sqrt{R^{ab(em)}(x)}}{(m-1)ax^{m-1}} - \frac{(2m-3)b^{ab(em)}}{2(m-1)a} L_{-(m-1)}(x) - \frac{(m-2)c}{(m-1)a} L_{-(m-2)}(x);$$

$$K_0^{ab(em)}(x) = \frac{-1}{\sqrt{-c}} \sin^{-1}\left(\frac{2cx + b^{ab(\text{em})}}{\sqrt{-\Delta^{ab(\text{em})}}}\right) \text{ for } c < 0 \text{ and } \Delta < 0;$$

$$L_{-1}^{ab(em)}(x) = \begin{cases} \frac{1}{\sqrt{a}} \cosh^{-1}\left(\frac{2a + b^{ab(\text{em})}x}{x\sqrt{-\Delta^{ab(\text{em})}}}\right) \text{ for } a > 0 \text{ and } \Delta < 0 \\ \frac{1}{\sqrt{-a}} \sin^{-1}\left(\frac{2a + b^{ab(\text{em})}x}{x\sqrt{-\Delta^{ab(\text{em})}}}\right) \text{ for } a < 0 \text{ and } \Delta < 0 \end{cases}.$$

Here $a = 1 - \frac{\varepsilon_s}{\varepsilon_{\vec{k}}}$; $b^{ab} = -b^{em} = \frac{K_B T_L}{\varepsilon_{\vec{k}}}$; $c = -\frac{\left(K_B T_L\right)^2}{16 \varepsilon_s \varepsilon_{\vec{k}}}$; $R^{ab(em)}\left(x\right) = a + b^{ab(em)} x + c x^2$;

$\Delta^{ab(em)} = 4ac - \left(b^{ab(em)}\right)^2$ and $\beta = \frac{e^2 m^* u_l}{2\pi\hbar \in_{sc} K_B T_L}$.

$$I_0^{ab(em)}\left(t\right) = \begin{cases} -\frac{1}{\sqrt{c_t^{ab(em)}}} \ln\left(2\sqrt{c_t^{ab(em)} R_t^{ab(em)}} + 2c_t^{ab(em)} t + b_t^{ab(em)}\right) \text{ for } c_t^{ab(em)} > 0 \\ \frac{1}{\sqrt{-c_t^{ab(em)}}} \sin^{-1}\left(\frac{2c_t^{ab(em)} t + b_t^{ab(em)}}{\sqrt{-\Delta_t^{ab(\mathrm{em})}}}\right) \text{ for } c_t^{ab(em)} < 0 \end{cases};$$

$$I_{-1}^{ab(em)}\left(t\right) = -\frac{1}{\beta} I_0^{ab(em)}\left(t\right) + \frac{1}{\beta} L_{-1}^{ab(em)}\left(x\right).$$

Here $t = \frac{1}{x+\beta}$; $a_t = c$; $b_t^{ab(em)} = b^{ab(em)} - 2\beta c$; $c_t^{ab(em)} = a - b^{ab(em)}\beta + c\beta^2$;

$\Delta_t^{ab(\mathrm{em})} = 4a_t c_t^{ab(\mathrm{em})} - \left(b_t^{ab(\mathrm{em})}\right)^2$; $R_t^{ab(em)}\left(t\right) = a_t + b_t^{ab(em)} t + c_t^{ab(em)} t^2$.

$\left[J_m\right]_{x_1}^{x_2} = J_m\left(x_2\right) - J_m\left(x_1\right)$;

$$J_m\left(x\right) = \begin{cases} \int \frac{x^{2m+2} dx}{\left(x+\beta\right)\sqrt{R_1^{ab(\mathrm{em})}\left(x\right)}} \approx \left(\frac{x}{x+\beta}\right) \int \frac{x^{2m+1} dx}{\sqrt{R_1^{ab(\mathrm{em})}\left(x\right)}} \\ = \frac{1}{2}\left(\frac{x}{x+\beta}\right)\left(\frac{x^{2m-2}}{mc_1}\sqrt{R_1^{ab(\mathrm{em})}\left(x\right)} - \frac{\left(2m-1\right) b_1^{ab(em)}}{2mc_1} J_{m-1}\left(x\right) - \frac{\left(m-1\right) a_1}{mc_1} J_{m-2}\left(x\right)\right) \end{cases};$$

$$J_0^{ab(em)}\left(x\right) \approx \frac{1}{2}\left(\frac{x}{x+\beta}\right) \frac{-1}{\sqrt{-c_1}} \sin^{-1}\left(\frac{2c_1 x^2 + b_1^{ab(\mathrm{em})}}{\sqrt{-\Delta_1^{ab(\mathrm{em})}}}\right).$$

Here $a_1 = \left(a-1\right)s^2$; $b_1^{ab(\mathrm{em})} = a + s b^{ab(\mathrm{em})}$; $c_1 = c$; $R_1^{ab(\mathrm{em})}\left(x\right) = a_1 + b_1^{ab(\mathrm{em})} x^2 + c_1 x^4$;

$\Delta_1^{ab(\mathrm{em})} = 4a_1 c_1 - \left(b_1^{ab(\mathrm{em})}\right)^2$.

Appendix G

In the temperature range $T_L < T_c$, one can see that $\varepsilon_{cr}^{ab,em} < \varepsilon_1^{ab,em}$:

For the energy range $\varepsilon_{\vec{k}} \le \varepsilon_{cr}^{ab} < \varepsilon_1^{ab}$:

$$\Phi_m^{ab} = \sum_{m=0}^{\infty} \frac{B_m}{m!} \left\{ \begin{array}{l} 2\left[I_{m+1}\right]_{x_1^{ab}}^{x_2^{ab}} + \sum_{r=o}^{(m-2)/2} {}^{(m-2)/2}C_r s^{m-2-2r} \left[J_{r+1}\right]_{x_3^{ab}}^{x_4^{ab}} \text{(m even \& m} \ge 2) \\ \text{or } \sum_{r=o}^{\infty} \binom{(m-2)/2}{r} s^{m-2-2r} \left[J_{r+1}\right]_{x_3^{ab}}^{x_4^{ab}} \text{(m odd, inc. m=0)} \end{array} \right\} \tag{G.1}$$

For the energy range $\varepsilon_{cr}^{ab} < \varepsilon_{\vec{k}} \le \varepsilon_1^{ab}$ and $\varepsilon_{cr}^{ab} < \varepsilon_1^{ab} < \varepsilon_{\vec{k}}$:

$$\Phi_m^{ab} = \sum_{m=0}^{\infty} \frac{B_m}{m!} \left\{ \begin{array}{l} 2\left[I_{m+1}\right]_{x_1^{ab}}^{\bar{x}} + \sum_{r=o}^{(m-2)/2} {}^{(m-2)/2}C_r s^{m-2-2r} \left[J_{r+1}\right]_{x_3^{ab}}^{\bar{x}} \text{(m even \& m} \ge 2) \\ \text{or } \sum_{r=o}^{\infty} \binom{(m-2)/2}{r} s^{m-2-2r} \left[J_{r+1}\right]_{x_3^{ab}}^{\bar{x}} \text{(m odd, inc. m=0)} \end{array} \right\} \tag{G.2}$$

For the energy range $\varepsilon_{\vec{k}} \le \varepsilon_{cr}^{em} < \varepsilon_1^{em}$:

$$\Phi_m^{em} = \left\{ \begin{array}{l} \sum_{m=0}^{\infty} \frac{B_m}{m!} \left\{ \begin{array}{l} 2\left[I_{m+1}\right]_{x_1^{em}}^{x_2^{em}} + \sum_{r=o}^{(m-2)/2} {}^{(m-2)/2}C_r s^{m-2-2r} \left[J_{r+1}\right]_{x_3^{em}}^{x_4^{em}} \text{(m even \& m} \ge 2) \\ \text{or } \sum_{r=o}^{\infty} \binom{(m-2)/2}{r} s^{m-2-2r} \left[J_{r+1}\right]_{x_3^{em}}^{x_4^{em}} \text{(m odd, inc. m=0)} \end{array} \right\} \\ +2\left[I_2\right]_{x_1^{em}}^{x_2^{em}} + \sum_{r=o}^{\infty} \binom{-1/2}{r} s^{-1-2r} \left[J_{r+1}\right]_{x_3^{em}}^{x_4^{em}} \end{array} \right. \tag{G.3}$$

For the energy range $\varepsilon_{cr}^{em} < \varepsilon_{\vec{k}} \le \varepsilon_1^{em}$:

$$\Phi_m^{em} = \left\{ \begin{array}{l} \sum_{m=0}^{\infty} \frac{B_m}{m!} \left\{ \begin{array}{l} 2\left[I_{m+1}\right]_{x_1^{em}}^{\bar{x}} + \sum_{r=o}^{(m-2)/2} {}^{(m-2)/2}C_r s^{m-2-2r} \left[J_{r+1}\right]_{x_3^{em}}^{\bar{x}} \text{(m even \& m} \ge 2) \\ \text{or } \sum_{r=o}^{\infty} \binom{(m-2)/2}{r} s^{m-2-2r} \left[J_{r+1}\right]_{x_3^{em}}^{\bar{x}} \text{ (m odd, inc. m=0)} \end{array} \right\} \\ +2\left[I_2\right]_{x_1^{em}}^{x_2^{em}} + \sum_{r=o}^{\infty} \binom{-1/2}{r} s^{-1-2r} \left[J_{r+1}\right]_{x_3^{em}}^{x_4^{em}} \end{array} \right. \tag{G.4}$$

For the energy range $\varepsilon_{cr}^{em} < \varepsilon_1^{em} < \varepsilon_{\vec{k}}$:

$$\Phi_m^{em} = \begin{cases} \sum_{m=0}^{\infty} \frac{B_m}{m!} \begin{cases} 2\left[I_{m+1}\right]_{x_1^{em}}^{\bar{x}} + \sum_{r=o}^{(m-2)/2} {}^{(m-2)/2}C_r s^{m-2-2r} \left[J_{r+1}\right]_{x_3^{em}}^{\bar{x}} \text{(m even \& m} \geq 2) \\ \text{or } \sum_{r=o}^{\infty} \binom{(m-2)/2}{r} s^{m-2-2r} \left[J_{r+1}\right]_{x_3^{em}}^{\bar{x}} \text{ (m odd, inc. m=0)} \end{cases} \\ +2\left[I_2\right]_{x_1^{em}}^{x_2^{em}} + \sum_{r=o}^{\infty} \binom{-1/2}{r} \left\{ s^{-1-2r} \left[J_{r+1}\right]_{x_3^{em}}^{s} + s^{2r} \left[I_{2-2r}\right]_{s}^{x_2^{em}} \right\} \end{cases} \quad \text{(G.5)}$$

In the temperature range $T_L > T_c$, it follows that $\varepsilon_1^{ab,em} < \varepsilon_{cr}^{ab,em}$:

For the energy range $\varepsilon_{\vec{k}} \leq \varepsilon_1^{ab} < \varepsilon_{cr}^{ab}$:

$$\Phi_m^{ab} = \sum_{m=0}^{\infty} \frac{B_m}{m!} \begin{cases} 2\left[I_{m+1}\right]_{x_1^{ab}}^{x_2^{ab}} + \sum_{r=o}^{(m-2)/2} {}^{(m-2)/2}C_r s^{m-2-2r} \left[J_{r+1}\right]_{x_3^{ab}}^{x_4^{ab}} \text{(m even \& m} \geq 2) \\ \text{or } \sum_{r=o}^{\infty} \binom{(m-2)/2}{r} s^{m-2-2r} \left[J_{r+1}\right]_{x_3^{ab}}^{x_4^{ab}} \text{ (m odd, inc. m=0)} \end{cases} \quad \text{(G.6)}$$

For the energy range $\varepsilon_1^{ab} < \varepsilon_{\vec{k}} \leq \varepsilon_{cr}^{ab}$:

$$\Phi_m^{ab} = \sum_{m=0}^{\infty} \frac{B_m}{m!} \begin{cases} 2\left[I_{m+1}\right]_{x_1^{ab}}^{x_2^{ab}} + \sum_{r=o}^{(m-2)/2} {}^{(m-2)/2}C_r s^{m-2-2r} \left\{ \left[J_{r+1}\right]_{x_3^{ab}}^{s} + \left[I_{2r+3}\right]_{s}^{x_2^{ab}} \right\} \text{(m even \& m} \geq 2) \\ \text{or } \sum_{r=o}^{\infty} \binom{(m-2)/2}{r} \left\{ s^{m-2-2r} \left[J_{r+1}\right]_{x_3^{ab}}^{s} + s^{2r} \left[\mathrm{I}_{m+1-2r}\right]_{s}^{x_2^{ab}} \right\} \text{(m odd, inc. m=0)} \end{cases} \quad \text{(G.7)}$$

For the energy range $\varepsilon_1^{ab} < \varepsilon_{cr}^{ab} < \varepsilon_{\vec{k}}$:

$$\Phi_m^{ab} = \sum_{m=0}^{\infty} \frac{B_m}{m!} \begin{cases} 2\left[I_{m+1}\right]_{x_1^{ab}}^{\bar{x}} + \sum_{r=o}^{(m-2)/2} {}^{(m-2)/2}C_r s^{m-2-2r} \left\{ \left[J_{r+1}\right]_{x_3^{ab}}^{s} + \left[I_{2r+3}\right]_{s}^{\bar{x}} \right\} \text{(m even \& m} \geq 2) \\ \text{or } \sum_{r=o}^{\infty} \binom{(m-2)/2}{r} \left\{ s^{m-2-2r} \left[J_{r+1}\right]_{x_3^{ab}}^{s} + s^{2r} \left[I_{m+1-2r}\right]_{s}^{\bar{x}} \right\} \text{(m odd, inc. m=0)} \end{cases} \quad \text{(G.8)}$$

For the energy range $\varepsilon_{\vec{k}} \leq \varepsilon_1^{em} < \varepsilon_{cr}^{em}$:

$$\Phi_m^{em} = \begin{cases} \sum_{m=0}^{\infty} \frac{B_m}{m!} \begin{cases} 2\left[I_{m+1}\right]_{x_1^{em}}^{x_2^{em}} + \sum_{r=o}^{(m-2)/2} {}^{(m-2)/2}C_r s^{m-2-2r} \left[J_{r+1}\right]_{x_3^{em}}^{x_4^{em}} \text{(m even \& m} \geq 2) \\ \text{or } \sum_{r=o}^{\infty} \binom{(m-2)/2}{r} s^{m-2-2r} \left[J_{r+1}\right]_{x_3^{em}}^{x_4^{em}} \text{ (m odd, inc. m=0)} \end{cases} \\ +2\left[I_2\right]_{x_1^{em}}^{x_2^{em}} + \sum_{r=o}^{\infty} \binom{-1/2}{r} s^{-1-2r} \left[J_{r+1}\right]_{x_3^{em}}^{x_4^{em}} \end{cases} \quad \text{(G.9)}$$

For the energy range $\varepsilon_1^{em} < \varepsilon_{\bar{k}} \le \varepsilon_{cr}^{em}$:

$$\Phi_m^{em} = \begin{cases} \sum_{m=0}^{\infty} \frac{B_m}{m!} \begin{cases} 2\left[I_{m+1}\right]_{x_1^{em}}^{x_2^{em}} + \sum_{r=o}^{(m-2)/2} {}^{(m-2)/2}C_r s^{m-2-2r} \left\{ \left[J_{r+1}\right]_{x_3^{em}}^{s} + \left[I_{2r+3}\right]_{s}^{x_2^{em}} \right\} \text{ (m even \& m} \ge 2) \\ \text{or } \sum_{r=o}^{\infty} \binom{(m-2)/2}{r} \left\{ s^{m-2-2r} \left[J_{r+1}\right]_{x_3^{em}}^{s} + s^{2r} \left[I_{m+1-2r}\right]_{s}^{x_2^{em}} \right\} \text{ (m odd, inc. m=0)} \end{cases} \\ +2\left[I_2\right]_{x_1^{em}}^{x_2^{em}} + \sum_{r=o}^{\infty} \binom{-1/2}{r} \left\{ s^{-1-2r} \left[J_{r+1}\right]_{x_3^{em}}^{s} + s^{2r} \left[I_{2-2r}\right]_{s}^{x_2^{em}} \right\} \end{cases}$$

(G.10)

For the energy range $\varepsilon_1^{em} < \varepsilon_{cr}^{em} < \varepsilon_{\bar{k}}$:

$$\Phi_m^{em} = \begin{cases} \sum_{m=0}^{\infty} \frac{B_m}{m!} \begin{cases} 2\left[I_{m+1}\right]_{x_1^{em}}^{\bar{x}} + \sum_{r=o}^{(m-2)/2} {}^{(m-2)/2}C_r s^{m-2-2r} \left\{ \left[J_{r+1}\right]_{x_3^{em}}^{s} + \left[I_{2r+3}\right]_{s}^{\bar{x}} \right\} \text{ (m even \& m} \ge 2) \\ \text{or } \sum_{r=o}^{\infty} \binom{(m-2)/2}{r} \left\{ s^{m-2-2r} \left[J_{r+1}\right]_{x_3^{em}}^{s} + s^{2r} \left[I_{m+1-2r}\right]_{s}^{\bar{x}} \right\} \text{ (m odd, inc. m=0)} \end{cases} \\ +2\left[I_2\right]_{x_1^{em}}^{x_2^{em}} + \sum_{r=o}^{\infty} \binom{-1/2}{r} \left\{ s^{-1-2r} \left[J_{r+1}\right]_{x_3^{em}}^{s} + s^{2r} \left[I_{2-2r}\right]_{s}^{x_2^{em}} \right\} \end{cases}$$

(G.11)

It may be noted here that expressions for all the symbols are given in Appendix F.

Appendix H

When $\varepsilon_{\vec{k}} \le \varepsilon_s$:

In the temperature range: $T_L < T_c$ one can see that $\varepsilon_{cr}^{ab,em} < \varepsilon_1^{ab,em}$:

For the energy range: $\varepsilon_{\vec{k}} \le \varepsilon_{cr}^{ab} < \varepsilon_1^{ab}$:

$$\Theta_m^{ab} = \sum_{m=0}^{\infty} \frac{B_m}{m!} \left\{ \begin{array}{l} 2\left[I_{m+1}\right]_{x_{\min}^{ab}}^{x_2^{ab}} + \sum_{r=o}^{\infty} \binom{(m+1)/2}{r} s^{m+1-2r} \left[J_r\right]_{x_3^{ab}}^{x_4^{ab}} \text{(m even)} \\ \text{or} \sum_{r=o}^{(m+1)/2} {}^{(m+1)/2}C_r s^{m+1-2r} \left[J_r\right]_{x_3^{ab}}^{x_4^{ab}} \text{(m odd)} \end{array} \right\} \quad \text{(H.1)}$$

In the temperature range: $T_L > T_c$ one can see that $\varepsilon_1^{ab,em} < \varepsilon_{cr}^{ab,em}$:

For the energy range: $\varepsilon_{\vec{k}} < \varepsilon_1^{ab} \le \varepsilon_{cr}^{ab}$:

$$\Theta_m^{ab} = \text{H.1} \quad \text{(H.2)}$$

For the energy range: $\varepsilon_1^{ab} < \varepsilon_{\vec{k}} \le \varepsilon_{cr}^{ab}$:

$$\Theta_m^{ab} = \sum_{m=0}^{\infty} \frac{B_m}{m!} \left\{ \begin{array}{l} 2\left[I_{m+1}\right]_{x_{\min}^{ab}}^{x_2^{ab}} + \sum_{r=o}^{\infty} \binom{(m+1)/2}{r} \left(s^{m+1-2r} \left[J_r\right]_{x_3^{ab}}^{s} + s^{2r} \left[I_{m+1-2r}\right]_{s}^{x_2^{ab}} \right) \text{(m even)} \\ \text{or} \sum_{r=o}^{(m+1)/2} {}^{(m+1)/2}C_r s^{m+1-2r} \left(\left[J_r\right]_{x_3^{ab}}^{s} + \left[I_{2r}\right]_{s}^{x_2^{ab}} \right) \text{(m odd)} \end{array} \right\} \quad \text{(H.3)}$$

When $\varepsilon_{\vec{k}} > \varepsilon_s$:

In the temperature range: $T_L < T_c$:

Absorption process: For the energy range: $\varepsilon_{\vec{k}} \le \varepsilon_{cr}^{ab} < \varepsilon_1^{ab}$:

$$\Theta_m^{ab} = \sum_{m=0}^{\infty} \frac{B_m}{m!} \left\{ \begin{array}{l} 2\left[I_{m+1}\right]_{x_1^{ab}}^{x_2^{ab}} + \sum_{r=o}^{\infty} \binom{(m+1)/2}{r} s^{m+1-2r} \left[J_r\right]_{x_3^{ab}}^{x_4^{ab}} \text{(m even) or} \\ \sum_{r=o}^{(m+1)/2} {}^{(m+1)/2}C_r s^{m+1-2r} \left[J_r\right]_{x_3^{ab}}^{x_4^{ab}} \text{(m odd)} \end{array} \right\} \quad \text{(H.4)}$$

For the energy range: $\varepsilon_{cr}^{ab} < \varepsilon_{\vec{k}} \le \varepsilon_1^{ab}$ and $\varepsilon_{cr}^{ab} < \varepsilon_1^{ab} < \varepsilon_{\vec{k}}$:

$$\Theta_m^{ab} = \sum_{m=0}^{\infty} \frac{B_m}{m!} \left\{ \begin{array}{l} 2\left[I_{m+1}\right]_{x_1^{ab}}^{\bar{x}} + \sum_{r=o}^{\infty} \binom{(m+1)/2}{r} s^{m+1-2r} \left[J_r\right]_{x_3^{ab}}^{\bar{x}} \text{(m even)} \\ \text{or} \sum_{r=o}^{(m+1)/2} {}^{(m+1)/2}C_r s^{m+1-2r} \left[J_r\right]_{x_3^{ab}}^{\bar{x}} \text{(m odd)} \end{array} \right\} \quad \text{(H.5)}$$

Emission process: For the energy range: $\varepsilon_{\vec{k}} \le \varepsilon_{cr}^{em} < \varepsilon_1^{em}$:

$$\Theta_m^{em} = \begin{cases} \sum_{m=0}^{\infty} \frac{B_m}{m!} \begin{cases} 2\left[I_{m+1}\right]_{x_1^{em}}^{x_2^{em}} + \sum_{r=o}^{\infty} \binom{(m+1)/2}{r} s^{m+1-2r} \left[J_r\right]_{x_3^{em}}^{x_4^{em}} \text{ (m even)} \\ \text{or } \sum_{r=o}^{(m+1)/2} {}^{(m+1)/2}C_r s^{m+1-2r} \left[J_r\right]_{x_3^{em}}^{x_4^{em}} \text{ (m odd)} \end{cases} \\ +2\left[I_2\right]_{x_1^{em}}^{x_2^{em}} + \left[J_1\right]_{x_3^{em}}^{x_4^{em}} + s^2 \left[J_0\right]_{x_3^{em}}^{x_4^{em}} \end{cases} \quad \text{(H.6)}$$

For the energy range: $\varepsilon_{cr}^{em} < \varepsilon_{\vec{k}} \le \varepsilon_1^{em}$:

$$\Theta_m^{em} = \begin{cases} \sum_{m=0}^{\infty} \frac{B_m}{m!} \begin{cases} 2\left[I_{m+1}\right]_{x_1^{em}}^{\bar{x}} + \sum_{r=o}^{\infty} \binom{(m+1)/2}{r} s^{m+1-2r} \left[J_r\right]_{x_3^{em}}^{\bar{x}} \text{ (m even)} \\ \text{or } \sum_{r=o}^{(m+1)/2} {}^{(m+1)/2}C_r s^{m+1-2r} \left[J_r\right]_{x_3^{em}}^{\bar{x}} \text{ (m odd)} \end{cases} \\ +2\left[I_2\right]_{x_1^{em}}^{x_2^{em}} + \left[J_1\right]_{x_3^{em}}^{x_4^{em}} + s^2 \left[J_0\right]_{x_3^{em}}^{x_4^{em}} \end{cases} \quad \text{(H.7)}$$

For the energy range: $\varepsilon_{cr}^{em} < \varepsilon_1^{em} < \varepsilon_{\vec{k}}$:

$$\Theta_m^{em} = \begin{cases} \sum_{m=0}^{\infty} \frac{B_m}{m!} \begin{cases} 2\left[I_{m+1}\right]_{x_1^{em}}^{\bar{x}} + \sum_{r=o}^{\infty} \binom{(m+1)/2}{r} s^{m+1-2r} \left[J_r\right]_{x_3^{em}}^{\bar{x}} \text{ (m even)} \\ \text{or } \sum_{r=o}^{(m+1)/2} {}^{(m+1)/2}C_r s^{m+1-2r} \left[J_r\right]_{x_3^{em}}^{\bar{x}} \text{ (m odd)} \end{cases} \\ +2\left[I_2\right]_{x_1^{em}}^{x_2^{em}} + \left[J_1\right]_{x_3^{em}}^{s} + s^2 \left[J_0\right]_{x_3^{em}}^{s} + \left[I_2\right]_{s}^{x_2^{em}} + s^2 \left[I_0\right]_{s}^{x_2^{em}} \end{cases} \quad \text{(H.8)}$$

In the temperature range: $T_L > T_c$:

Absorption process: For the energy range: $\varepsilon_{\vec{k}} \le \varepsilon_1^{ab} < \varepsilon_{cr}^{ab}$:

$$\Theta_m^{ab} = \sum_{m=0}^{\infty} \frac{B_m}{m!} \begin{cases} 2\left[I_{m-1}\right]_{x_1^{ab}}^{x_2^{ab}} + \sum_{r=o}^{\infty} \binom{(m+1)/2}{r} s^{m+1-2r} \left[J_r\right]_{x_3^{ab}}^{x_4^{ab}} \text{ (m even)} \\ \text{or } \sum_{r=o}^{(m+1)/2} {}^{(m+1)/2}C_r s^{m+1-2r} \left[J_r\right]_{x_3^{ab}}^{x_4^{ab}} \text{ (m odd)} \end{cases} \quad \text{(H.9)}$$

For the energy range: $\varepsilon_1^{ab} < \varepsilon_{\vec{k}} \le \varepsilon_{cr}^{ab}$:

$$\Theta_m^{ab} = \sum_{m=0}^{\infty} \frac{B_m}{m!} \begin{cases} 2\left[I_{m+1}\right]_{x_1^{ab}}^{x_2^{ab}} + \sum_{r=o}^{\infty} \binom{(m+1)/2}{r} \left(s^{m+1-2r} \left[J_r\right]_{x_3^{ab}}^{s} + s^{2r} \left[I_{m+1-2r}\right]_{s}^{x_2^{ab}} \right) \text{(m even)} \\ \text{or } \sum_{r=o}^{(m+1)/2} {}^{(m+1)/2}C_r s^{m+1-2r} \left(\left[J_r\right]_{x_3^{ab}}^{s} + \left[I_{2r}\right]_{s}^{x_2^{ab}} \right) \text{(m odd)} \end{cases} \quad \text{(H.10)}$$

For the energy range: $\varepsilon_1^{ab} < \varepsilon_{cr}^{ab} < \varepsilon_{\vec{k}}$:

$$\Theta_m^{ab} = \sum_{m=0}^{\infty} \frac{B_m}{m!} \left\{ \begin{array}{l} 2\left[I_{m+1}\right]_{x_1^{ab}}^{\bar{x}} + \sum_{r=o}^{\infty} \binom{(m+1)/2}{r} \left(s^{m+1-2r} \left[J_r\right]_{x_3^{ab}}^{s} + s^{2r} \left[I_{m+1-2r}\right]_{s}^{\bar{x}} \right) \text{(m even)} \\ \text{or} \sum_{r=o}^{(m+1)/2} {}^{(m+1)/2}C_r s^{m+1-2r} \left(\left[J_r\right]_{x_3^{ab}}^{s} + \left[I_{2r}\right]_{s}^{\bar{x}} \right) \text{(m odd)} \end{array} \right\} \tag{H.11}$$

Emission process: For the energy range: $\varepsilon_{\vec{k}} \le \varepsilon_1^{em} < \varepsilon_{cr}^{em}$:

$$\Theta_m^{em} = \left\{ \begin{array}{l} \sum_{m=0}^{\infty} \frac{B_m}{m!} \left\{ \begin{array}{l} 2\left[I_{m+1}\right]_{x_1^{em}}^{x_2^{em}} + \sum_{r=o}^{\infty} \binom{(m+1)/2}{r} s^{m+1-2r} \left[J_r\right]_{x_3^{em}}^{x_4^{em}} \text{ (m even)} \\ \text{or} \sum_{r=o}^{(m+1)/2} {}^{(m+1)/2}C_r s^{m+1-2r} \left[J_r\right]_{x_3^{em}}^{x_4^{em}} \text{ (m odd)} \end{array} \right\} \\ +2\left[I_2\right]_{x_1^{em}}^{x_2^{em}} + \left[J_1\right]_{x_3^{em}}^{x_4^{em}} + s^2 \left[J_0\right]_{x_3^{em}}^{x_4^{em}} \end{array} \right. \tag{H.12}$$

For the energy range: $\varepsilon_1^{em} < \varepsilon_{\vec{k}} \le \varepsilon_{cr}^{em}$:

$$\Theta_m^{em} = \left\{ \begin{array}{l} \sum_{m=0}^{\infty} \frac{B_m}{m!} \left\{ \begin{array}{l} 2\left[I_{m+1}\right]_{x_1^{em}}^{x_2^{em}} + \sum_{r=o}^{\infty} \binom{(m+1)/2}{r} \left(s^{m+1-2r} \left[J_r\right]_{x_3^{em}}^{s} + s^{2r} \left[I_{m+1-2r}\right]_{s}^{x_2^{em}} \right) \text{ (m even)} \\ \text{or} \sum_{r=o}^{(m+1)/2} {}^{(m+1)/2}C_r s^{m+1-2r} \left(\left[J_r\right]_{x_3^{em}}^{s} + \left[I_{2r}\right]_{s}^{x_2^{em}} \right) \text{ (m odd)} \end{array} \right\} \\ +2\left[I_2\right]_{x_1^{em}}^{x_2^{em}} + \left[J_1\right]_{x_3^{em}}^{s} + s^2 \left[J_0\right]_{x_3^{em}}^{s} + \left[I_2\right]_{s}^{x_2^{em}} + s^2 \left[I_0\right]_{s}^{x_2^{em}} \end{array} \right. \tag{H.13}$$

For the energy range: $\varepsilon_1^{em} < \varepsilon_{cr}^{em} < \varepsilon_{\vec{k}}$:

$$\Theta_m^{em} = \left\{ \begin{array}{l} \sum_{m=0}^{\infty} \frac{B_m}{m!} \left\{ \begin{array}{l} 2\left[I_{m+1}\right]_{x_1^{em}}^{\bar{x}} + \sum_{r=o}^{\infty} \binom{(m+1)/2}{r} \left(s^{m+1-2r} \left[J_r\right]_{x_3^{em}}^{s} + s^{2r} \left[I_{m+1-2r}\right]_{s}^{\bar{x}} \right) \text{ (m even)} \\ \text{or} \sum_{r=o}^{(m+1)/2} {}^{(m+1)/2}C_r s^{m+1-2r} \left(\left[J_r\right]_{x_3^{em}}^{s} + \left[I_{2r}\right]_{s}^{\bar{x}} \right) \text{ (m odd)} \end{array} \right\} \\ +2\left[I_2\right]_{x_1^{em}}^{x_2^{em}} + \left[J_1\right]_{x_3^{em}}^{s} + s^2 \left[J_0\right]_{x_3^{em}}^{s} + \left[I_2\right]_{s}^{x_2^{em}} + s^2 \left[I_0\right]_{s}^{x_2^{em}} \end{array} \right. \tag{H.14}$$

It may be noted here that expressions for all the symbols are given in Appendix F.

Appendix I

When $\varepsilon_{\vec{k}} \le \varepsilon_s$:

In the temperature range: $T_L < T_c$ one can see that $\varepsilon_{cr}^{ab,em} < \varepsilon_1^{ab,em}$:

For the energy range: $\varepsilon_{\vec{k}} \le \varepsilon_{cr}^{ab} < \varepsilon_1^{ab}$:

$$\Pi_m^{ab} = \sum_{m=0}^{\infty} \frac{B_m}{m!} \left\{ \begin{array}{l} 2\left[I_{m-1}\right]_{x_{\min}^{ab}}^{x_2^{ab}} + \sum_{r=o}^{\infty} \binom{(m-1)/2}{r} s^{m-1-2r} \left[J_r\right]_{x_3^{ab}}^{x_4^{ab}} \text{(m even)} \\ \text{or} \sum_{r=o}^{(m-1)/2} {}^{(m-1)/2}C_r s^{m-1-2r} \left[J_r\right]_{x_3^{ab}}^{x_4^{ab}} \text{ (m odd)} \end{array} \right\} \quad \text{(I.1)}$$

In the temperature range: $T_L > T_c$ one can see that $\varepsilon_1^{ab,em} < \varepsilon_{cr}^{ab,em}$:

For the energy range: $\varepsilon_{\vec{k}} < \varepsilon_1^{ab} \le \varepsilon_{cr}^{ab}$:

$$\Pi_m^{ab} = \text{I.1} \quad \text{(I.2)}$$

For the energy range: $\varepsilon_1^{ab} < \varepsilon_{\vec{k}} \le \varepsilon_{cr}^{ab}$:

$$\Pi_m^{ab} = \sum_{m=0}^{\infty} \frac{B_m}{m!} \left\{ \begin{array}{l} 2\left[I_{m-1}\right]_{x_{\min}^{ab}}^{x_2^{ab}} + \sum_{r=o}^{\infty} \binom{(m-1)/2}{r} \left(s^{m-1-2r} \left[J_r\right]_{x_3^{ab}}^{s} + s^{2r} \left[I_{m-1-2r}\right]_{s}^{x_2^{ab}} \right) \text{(m even)} \\ \text{or} \sum_{r=o}^{(m-1)/2} {}^{(m-1)/2}C_r s^{m-1-2r} \left(\left[J_r\right]_{x_3^{ab}}^{s} + \left[I_{2r}\right]_{s}^{x_2^{ab}} \right) \text{(m odd)} \end{array} \right\} \quad \text{(I.3)}$$

When $\varepsilon_{\vec{k}} > \varepsilon_s$:

In the temperature range: $T_L < T_c$:

Absorption process: For the energy range: $\varepsilon_{\vec{k}} \le \varepsilon_{cr}^{ab} < \varepsilon_1^{ab}$:

$$\Pi_m^{ab} = \sum_{m=0}^{\infty} \frac{B_m}{m!} \left\{ \begin{array}{l} 2\left[I_{m-1}\right]_{x_1^{ab}}^{x_2^{ab}} + \sum_{r=o}^{\infty} \binom{(m-1)/2}{r} s^{m-1-2r} \left[J_r\right]_{x_3^{ab}}^{x_4^{ab}} \text{(m even) or} \\ \sum_{r=o}^{(m-1)/2} {}^{(m-1)/2}C_r s^{m-1-2r} \left[J_r\right]_{x_3^{ab}}^{x_4^{ab}} \text{ (m odd)} \end{array} \right\} \quad \text{(I.4)}$$

For the energy range: $\varepsilon_{cr}^{ab} < \varepsilon_{\vec{k}} \le \varepsilon_1^{ab}$ and $\varepsilon_{cr}^{ab} < \varepsilon_1^{ab} < \varepsilon_{\vec{k}}$:

$$\Pi_m^{ab} = \sum_{m=0}^{\infty} \frac{B_m}{m!} \left\{ \begin{array}{l} 2\left[I_{m-1}\right]_{x_1^{ab}}^{\bar{x}} + \sum_{r=o}^{\infty} \binom{(m-1)/2}{r} s^{m-1-2r} \left[J_r\right]_{x_3^{ab}}^{\bar{x}} \text{(m even)} \\ \text{or} \sum_{r=o}^{(m-1)/2} {}^{(m-1)/2}C_r s^{m-1-2r} \left[J_r\right]_{x_3^{ab}}^{\bar{x}} \text{ (m odd)} \end{array} \right\} \quad \text{(I.5)}$$

Emission process: For the energy range: $\varepsilon_{\vec{k}} \le \varepsilon_{cr}^{em} < \varepsilon_1^{em}$:

$$\Pi_m^{em} = \begin{cases} \sum_{m=0}^{\infty} \frac{B_m}{m!} \begin{cases} 2\left[I_{m-1}\right]_{x_1^{em}}^{x_2^{em}} + \sum_{r=o}^{\infty} \binom{(m-1)/2}{r} s^{m-1-2r} \left[J_r\right]_{x_3^{em}}^{x_4^{em}} \text{(m even)} \\ \text{or } \sum_{r=o}^{(m-1)/2} {}^{(m-1)/2}C_r s^{m-1-2r} \left[J_r\right]_{x_3^{em}}^{x_4^{em}} \text{(m odd)} \end{cases} \\ +2\left[I_0\right]_{x_1^{em}}^{x_2^{em}} + \left[J_0\right]_{x_3^{em}}^{x_4^{em}} \end{cases} \quad \text{(I.6)}$$

For the energy range: $\varepsilon_{cr}^{em} < \varepsilon_{\vec{k}} \le \varepsilon_1^{em}$:

$$\Pi_m^{em} = \begin{cases} \sum_{m=0}^{\infty} \frac{B_m}{m!} \begin{cases} 2\left[I_{m-1}\right]_{x_1^{em}}^{\bar{x}} + \sum_{r=o}^{\infty} \binom{(m-1)/2}{r} s^{m-1-2r} \left[J_r\right]_{x_3^{em}}^{\bar{x}} \text{(m even)} \\ \text{or } \sum_{r=o}^{(m-1)/2} {}^{(m-1)/2}C_r s^{m-1-2r} \left[J_r\right]_{x_3^{em}}^{\bar{x}} \text{ (m odd)} \end{cases} \\ +2\left[I_2\right]_{x_1^{em}}^{x_2^{em}} + \left[J_0\right]_{x_3^{em}}^{x_4^{em}} \end{cases} \quad \text{(I.7)}$$

For the energy range: $\varepsilon_{cr}^{em} < \varepsilon_1^{em} < \varepsilon_{\vec{k}}$:

$$\Pi_m^{em} = \begin{cases} \sum_{m=0}^{\infty} \frac{B_m}{m!} \begin{cases} 2\left[I_{m-1}\right]_{x_1^{em}}^{\bar{x}} + \sum_{r=o}^{\infty} \binom{(m-1)/2}{r} s^{m-1-2r} \left[J_r\right]_{x_3^{em}}^{\bar{x}} \text{(m even)} \\ \text{or } \sum_{r=o}^{(m-1)/2} {}^{(m-1)/2}C_r s^{m-1-2r} \left[J_r\right]_{x_3^{em}}^{\bar{x}} \text{ (m odd)} \end{cases} \\ +2\left[I_2\right]_{x_1^{em}}^{x_2^{em}} + \left[J_0\right]_{x_3^{em}}^{s} + \left[I_0\right]_{s}^{x_2^{em}} \end{cases} \quad \text{(I.8)}$$

In the temperature range: $T_L > T_c$:

Absorption process: For the energy range: $\varepsilon_{\vec{k}} \le \varepsilon_1^{ab} < \varepsilon_{cr}^{ab}$:

$$\Pi_m^{ab} = \sum_{m=0}^{\infty} \frac{B_m}{m!} \begin{cases} 2\left[I_{m-1}\right]_{x_1^{ab}}^{x_2^{ab}} + \sum_{r=o}^{\infty} \binom{(m-1)/2}{r} s^{m-1-2r} \left[J_r\right]_{x_3^{ab}}^{x_4^{ab}} \text{ (m even)} \\ \text{or } \sum_{r=o}^{(m-1)/2} {}^{(m-1)/2}C_r s^{m-1-2r} \left[J_r\right]_{x_3^{ab}}^{x_4^{ab}} \text{ (m odd)} \end{cases} \quad \text{(I.9)}$$

For the energy range: $\varepsilon_1^{ab} < \varepsilon_{\vec{k}} \le \varepsilon_{cr}^{ab}$:

$$\Pi_m^{ab} = \sum_{m=0}^{\infty} \frac{B_m}{m!} \begin{cases} 2\left[I_{m-1}\right]_{x_1^{ab}}^{x_2^{ab}} + \sum_{r=o}^{\infty} \binom{(m-1)/2}{r} \left(s^{m-1-2r} \left[J_r\right]_{x_3^{ab}}^{s} + s^{2r} \left[I_{m-1-2r}\right]_{s}^{x_2^{ab}} \right) \text{(m even)} \\ \text{or } \sum_{r=o}^{(m-1)/2} {}^{(m-1)/2}C_r s^{m-1-2r} \left(\left[J_r\right]_{x_3^{ab}}^{s} + \left[I_{2r}\right]_{s}^{x_2^{ab}} \right) \text{(m odd)} \end{cases} \quad \text{(I.10)}$$

For the energy range: $\varepsilon_1^{ab} < \varepsilon_{cr}^{ab} < \varepsilon_{\vec{k}}$:

$$\Pi_m^{ab} = \sum_{m=0}^{\infty} \frac{B_m}{m!} \left\{ \begin{array}{l} 2\left[I_{m-1}\right]_{x_1^{ab}}^{\bar{x}} + \sum_{r=o}^{\infty} \binom{(m-1)/2}{r} \left(s^{m-1-2r} \left[J_r\right]_{x_3^{ab}}^{s} + s^{2r} \left[I_{m-1-2r}\right]_{s}^{\bar{x}} \right) \text{(m even)} \\ \text{or} \sum_{r=o}^{(m-1)/2} {}^{(m-1)/2}C_r s^{m-1-2r} \left(\left[J_r\right]_{x_3^{ab}}^{s} + \left[I_{2r}\right]_{s}^{\bar{x}} \right) \text{(m odd)} \end{array} \right\} \tag{I.11}$$

Emission process: For the energy range: $\varepsilon_{\vec{k}} \le \varepsilon_1^{em} < \varepsilon_{cr}^{em}$:

$$\Pi_m^{em} = \left\{ \begin{array}{l} \sum_{m=0}^{\infty} \frac{B_m}{m!} \left\{ \begin{array}{l} 2\left[I_{m-1}\right]_{x_1^{em}}^{x_2^{em}} + \sum_{r=o}^{\infty} \binom{(m-1)/2}{r} s^{m-1-2r} \left[J_r\right]_{x_3^{em}}^{x_4^{em}} \text{ (m even)} \\ \text{or} \sum_{r=o}^{(m-1)/2} {}^{(m-1)/2}C_r s^{m-1-2r} \left[J_r\right]_{x_3^{em}}^{x_4^{em}} \text{ (m odd)} \end{array} \right\} \\ +2\left[I_0\right]_{x_1^{em}}^{x_2^{em}} + \left[J_0\right]_{x_3^{em}}^{x_4^{em}} \end{array} \right. \tag{I.12}$$

For the energy range: $\varepsilon_1^{em} < \varepsilon_{\vec{k}} \le \varepsilon_{cr}^{em}$:

$$\Pi_m^{em} = \left\{ \begin{array}{l} \sum_{m=0}^{\infty} \frac{B_m}{m!} \left\{ \begin{array}{l} 2\left[I_{m-1}\right]_{x_1^{em}}^{x_2^{em}} + \sum_{r=o}^{\infty} \binom{(m-1)/2}{r} \left(s^{m-1-2r} \left[J_r\right]_{x_3^{em}}^{s} + s^{2r} \left[I_{m-1-2r}\right]_{s}^{x_2^{em}} \right) \text{ (m even)} \\ \text{or} \sum_{r=o}^{(m-1)/2} {}^{(m-1)/2}C_r s^{m-1-2r} \left(\left[J_r\right]_{x_3^{em}}^{s} + \left[I_{2r}\right]_{s}^{x_2^{em}} \right) \text{ (m odd)} \end{array} \right\} \\ +2\left[I_0\right]_{x_1^{em}}^{x_2^{em}} + \left[J_0\right]_{x_3^{em}}^{s} + \left[I_0\right]_{s}^{x_2^{em}} \end{array} \right. \tag{I.13}$$

For the energy range: $\varepsilon_1^{em} < \varepsilon_{cr}^{em} < \varepsilon_{\vec{k}}$:

$$\Pi_m^{em} = \left\{ \begin{array}{l} \sum_{m=0}^{\infty} \frac{B_m}{m!} \left\{ \begin{array}{l} 2\left[I_{m-1}\right]_{x_1^{em}}^{\bar{x}} + \sum_{r=o}^{\infty} \binom{(m-1)/2}{r} \left(s^{m-1-2r} \left[J_r\right]_{x_3^{em}}^{s} + s^{2r} \left[I_{m-1-2r}\right]_{s}^{\bar{x}} \right) \text{ (m even)} \\ \text{or} \sum_{r=o}^{(m-1)/2} {}^{(m+1)/2}C_r s^{m-1-2r} \left(\left[J_r\right]_{x_3^{em}}^{s} + \left[I_{2r}\right]_{s}^{\bar{x}} \right) \text{ (m odd)} \end{array} \right\} \\ +2\left[I_0\right]_{x_1^{em}}^{x_2^{em}} + \left[J_0\right]_{x_3^{em}}^{s} + \left[I_0\right]_{s}^{x_2^{em}} \end{array} \right. \tag{I.14}$$

It may be noted here that expressions for all the symbols are given in Appendix F.

References

[1] S.M. Sze and K.K. Ng, *Physics of Semiconductor Devices*, John Wiley & Sons, lnc., New Delhi, 2007.

[2] T. Ando, A.B. Fowler and F. Stern, Rev. Mod. Phys. 54, 437 (1982).

[3] J.H. Davies, *The Physics of Low-Dimensional Semiconductors*, Cambridge University Press, Cambridge, 1998.

[4] V.V. Mitin, V.A. Kachelap and M.A. Stroscio, *Introduction to Nanoelectronics: Science, Nanotechnology, Engineering and Applications*, Cambridge University Press, Cambridge, 2008.

[5] B.R. Nag, *Physics of Quantum Well devices*, Kluwer Academic Publisher, Dordrecht, 2000.

[6] L. Esaki and R. Tsu, IBM J. Res. Dev. 14, 61 (1970).

[7] H.L. Störmer, R. Dingle, A.C. Gossard, W. Wiegmann and M.D. Sturge, Solid State Commun. 29, 705 (1979).

[8] M. Notomi, M. Naganuma, T. Nishida, T. Tamamura, H. Iwamura, S. Nojima and M. Okamoto, Appl. Phys. Lett. 58, 720 (1991).

[9] P. Ils, M. Michel, A. Forchel, I. Gyuro, M. Klenk and E. Zielinski, Appl. Phys. Lett. 64, 496 (1994).

[10] E. Kapon, S. Simhony, R. Bhat and D.M. Hwang, Appl. Phys. Lett. 55, 2715 (1989).

[11] Y. Hasegawa, T. Egawa, T. Jimbo and M. Umeno, J. Cryst. Growth 145, 728 (1994).

[12] T. Umeda, K. Kumakura, J. Motohisa and T. Fukui, Physica E 2, 714 (1998).

[13] A. Tukiainen, J. Tommila, A. Aho, A. Schramm, J. Viheriala, R. Ahorinta, M. Dumitrescu, M. Pessa and M. Guina, J. Cryst. Growth 323, 201 (2011).

[14] T. Mimura, S. Hiyamizu, T. Fuzi and K. Nanbu, Jpn. J. Appl. Phys. 19, L225 (1980).

[15] M.S. Shur and L.F. Eastman, IEEE Trans. Electron Devices ED-26, 1677 (1979).

[16] L. Pfeiffer, K.W. West, H.L. Störmer and K.W. Baldwin, Appl. Phys. Lett. 55, 1888 (1989).

[17] T. Saku, Y. Horikoshi and Y. Tokura, Jpn. J. Appl. Phys. 35, 34 (1996).

[18] V. Umansky, R. de-Picciotto and M. Heiblum, Appl. Phys. Lett. 71, 683 (1997).

[19] C.J. Beenakker, Phys. Rev. B 44, 1646 (1991).

[20] E. Pazy, I. D'Amico, P. Zanardi and F. Rossi, Phys. Rev. B 64, 195320 (2001).

[21] D.L. Huffaker, G. Park, Z. Zou, O.B. Shchekin and D.G. Deppe, Appl. Phys. Lett. 73, 2564 (1998).

[22] T. Yoshie, A. Scherer, H. Chen, D. Huffaker and D. Deppe, Appl. Phys. Lett. 79, 114 (2001).

[23] S.J. Xu, S.J. Chua, T. Mei, X.C. Wang, X.H. Zhang, G. Karunasiri, W.J. Fan, C.H. Wang, J. Jiang, S. Wang and X.G. Xie, Appl. Phys. Lett. 73, 3153 (1998).

[24] E.M. Conwell, *High Field Transport in Semiconductors*, Academic Press, New York, 1967.

[25] C. Jacoboni and L. Reggiani, Rev. Mod. Phys. 55, 645 (1983).

[26] G. Bauer, *Springer Tracts in Modern Physics*, Vol. 74, Springer, New York, 1974.

[27] K. Greipel and U. Rossler, Semicond. Sci. Technol. 7, 487 (1992).

[28] K. Hess, H. Morkoc, H. Shichijo and B.G. Streetman, Appl. Phys. Lett. 35, 469 (1979).

[29] K. v. Klitzing, G. Dorda and M. Pepper, Phys. Rev. Lett. 45, 494 (1980).

[30] D.C. Tsui, H.L. Störmer and A.C. Gossard, Phys. Rev. Lett. 48, 1559 (1982).

[31] K. Hirakawa and H. Sakaki, J. Appl. Phys. 63, 803 (1988).

[32] B.K. Ridley, Rep. Prog. Phys. 54, 169 (1991).

[33] J. Shah, *Hot carriers in semiconductor nanostructures: Physics and Applications*, Academic Press, USA, 1992.

[34] X.L. Lei and N.J.M. Horing, Int. J. Mod. Phys. B 6, 805 (1992).

[35] X.F. Wang and X.L. Lei, J. Phys.: Condens. Matter 6, 5667 (1994).

[36] N. Balkan, R. Gupta, M.E. Daniels, B.K. Ridley and M. Emeny, Semicond. Sci. Technol. 5, 986 (1990).

[37] H. Celik, M. Cankurtaran, N. Balkan and A. Bayrakli, Semicond. Sci. Technol. 17, 18 (2002).

[38] C. Bulutay, B.K. Ridley and N.A. Zakhleniuk, Phys. Rev. B 68, 115205 (2003).

[39] C.E. Martinez, N.M. Stanton, A.J. Kent, M.L. Williams, I. Harrison, H. Tang, J.B. Webb and J.A Bardwell, Semicond. Sci. Technol. 21, 1580 (2006).

[40] J.Z. Zhang, J. Appl. Phys. 115, 203704 (2014).

[41] S. Kawaji, J. Phys. Soc. Jpn. 27, 906 (1969).

[42] C.Y. Wu and G. Thomas, Phys. Rev. B 9, 1724 (1974).

[43] K. Hess and C.T. Sah, J. Appl. Phys. 45, 1254 (1974).

[44] P.K. Basu and B.R. Nag, Phys. Rev. B 22, 4849 (1980).

[45] P.K. Basu and B.R. Nag, J. Phys. C: Solid State Phys. 14, 1519 (1981).

[46] F. Stern and W.E. Howard, Phys. Rev. 163, 816 (1967).

[47] A.B. Fowler, F.F. Fang, W.E. Howard and P.J. Stiles, Phys. Rev. Lett. 16, 901 (1966).

[48] F.F. Fang and A.B. Fowler, Phys. Rev. 169, 619 (1968).

[49] D.J. Bishop, D.C. Tusi and R.C. Dynes, Phys. Rev. Lett. 44, 1153 (1980).

[50] B.K. Ridley, *Quantum Processes in Semiconductors*, Clarendon Press, Oxford, 1993.

[51] M. Abramowitz and I.A. Stegun, *Handbook of Mathematical Functions with Formulas, Graphs, and Mathematical Tables*, Dover Publications Inc., New York, 1972.

[52] D.J. Griffiths, *Introduction to Quantum Mechanics*, Pearson, India, 2013.

[53] B.G. Streetman and S.K. Banerjee, *Solid State Electronic Devices*, Sixth Edition, Pearson Education, New Jersey, USA, 2006.

[54] J.S. Blakemore, *Semiconductor Statistics*, Pergamon Press, Oxford, 1962.

[55] B.R. Nag, *Theory of Electrical Transport in Semiconductors*, Pergamon Press, Oxford, 1972.

[56] L. Esaki and R. Tsu, Internal Report RC 2418, IBM Research, March 26, 1969.

[57] R.D. Dupuis, P.D. Dapkus, N. Holonyak, E.A. Rezek and R. Chin, Appl. Phys. Lett. 32, 295 (1978).

[58] T.C.L.G. Sollner, W.D. Goodhue, P.E. Tannenwald, C.D. Parker and D.D. Peck, Appl. Phys. Lett. 43, 588 (1983).

[59] N. Yokoyama, K. Imamura, T. Ohshima, H. Nishi, S. Muto, K. Kondo and S. Hiyamizu, Jpn. J. Appl. Phys. 23, L311 (1984).

[60] N. Yokoyama, K. Imamura, T. Ohshima, H. Nishi, S. Muto, K. Kondo and S. Hiyamizu, Tech. Dig. IEEE IEDM, 532 (1984).

[61] B.R. Nag and P.K. Basu in: S. Guha (Ed.), *Physics of Semiconductors*, Proceedings of the Fourth Topical Seminar, Indian Physics Association, Bombay, 1981, Tata Institute of Fundamental Research, Bombay, India, 1981.

[62] P.K. Basu, *Theory of Optical Processes in Semiconductors: Bulk and Microstructures*, Clarendon Press, Oxford, 1997.

[63] S. Dutta, *Electronic Transport in Mesoscopic System*, Cambridge University Press, Cambridge, 1995.

[64] B. Roy, S. Bhattacharyya and D.P. Bhattacharya, Appl. Phys. A 125: 223 (2019).

[65] J. Lee and M.O. Vassel, Jpn. J. Appl. Phys. 23, 1086 (1984).

[66] J. Lee, H.N. Spector and V.K. Arora, J. Appl. Phys. 54, 6995 (1983).

[67] T. Ando, J. Phys. Soc. Jpn. 51, 3900 (1982).

[68] F.F. Fang and W.E. Howard, Phys. Rev. Lett. 16, 797 (1966).

[69] A. Gold, Appl, Phys. Lett. 54, 2100 (1989).

[70] S.J. MacLeod, K. Chan, T.P. Martin, A.R. Hamilton, A. See, A.P. Micolich, M. Aagesen and P.E. Lindelof, Phys. Rev. B 80, 035310 (2009).

[71] D. Zanato, S. Gökden, N. Balkan, B.K. Ridley and W.J. Schaff, Semicond. Sci. Technol. 19, 427 (2004).

[72] S. Nag and D.P. Bhattacharya, Phys. B 404, 4207 (2009).

[73] D.K. Ferry, Surf. Sci. 57, 218 (1976).

[74] P.K. Basu and B.R. Nag, J. Phys. C Solid State Phys. 14, 1519 (1981).

[75] S.S. Paul, A.K. Ghorai and D. P. Bhattacharya, Phys. Rev. B 48, 18268 (1993).

[76] B. Das, A Basu, J. Das and D.P. Bhattacharya, Phys. B 474, 21 (2015).

[77] A. Basu, B. Das, T.R. Middya and D.P. Bhattacharya, J. Phys. Chem. Sol. 100, 9 (2017).

[78] A. Basu, B. Das, T.R. Middya and D.P. Bhattacharya, Phil. Mag. 98, 803 (2018).

[79] J. Karlovsky, Phys. Rev. 127, 419 (1962).

[80] R. Yang, K.N. Gao, Y.H. Zhang, P.P. Chen, G. Yu, L.M. Wei, T. Lin, N. Dai and J.H. Chu, J. Appl. Phys. 109, 063703 (2011).

[81] J. Shah, A. Pinczuk, H.L. Störmer, A.C. Gossard and W. Wiegmann, Appl. Phys. Lett. 42(1), 55 (1983).

[82] F. Wu, K.N. Gao, Z.Q. Li, T. Lin and W.Z. Zhou, J. Appl. Phys. 117, 155701 (2015).

[83] K. Nakamura, Surf. Sci. 58, 48 (1976).

[84] D.K. Ferry, Solid State Commun. 22, 127 (1977).

[85] P.K. Basu and S. Kundu, Appl. Phys. Lett. 47, 264 (1985).

[86] J.R. Senna and S. Das Sarma, Solid State Commun. 64,1397 (1987).

[87] A. Straw, A.J. Vickers, N. Balkan and J.S. Roberts, Superlattices and Microstructures 10, 203 (1991).

[88] K. Suresha and P.S. Naik, Phys. of Low-Dimensional Structures 9-10, 39 (2001).

[89] S.S. Kubakaddi and B.G. Mulimani, Phys. Lett. A 103, 141 (1984).

[90] Y. Ma, R. Fletcher, E. Zaremba, M. D'Iorio, C.T. Foxon and J.J. Harris, Phys. Rev. B 43, 9033 (1991).

[91] S.S. Kubakaddi, K. Suresha and B.G. Mulimani, Physica E 18, 475 (2003).

[92] A.M. Kreshchuk, S.V. Novikov, I.G. Savel'ev, T.A. Polyanskaya, B. Podor, G. Remenyi and G. Kovacs, Acta Physica Polonica A 94, 415 (1998).

[93] C. Prasad, D.K. Ferry and H.H. Wieder, Superlattices and Microstructures 34, 475 (2003).

[94] D.J. Westland, J.F. Ryan, M.D. Scott, J.I. Davies and J.R. Riffat, Solid-State Electronics 31, 431 (1988).

[95] Z.C. Tao, C.S. Ting and M. Singh, Phys. Rev. Lett. 70, 2467 (1993).

[96] V.S. Kattia and S.S. Kubakaddi, Phys. E 44, 156 (2011).

[97] N. Balkan, M.C. Arikan, S. Gokden, V. Tilak, B. Schaff and R.J. Shealy, J. Phys.: Condens. Matter 14, 3457 (2002).

[98] M.E. Daniels, B.K. Ridley and M. Emeny, Solid-State Electronics 32, 1207 (1989).

[99] K. Santra and C.K. Sarkar, J. Phys. Chem. Solids 52, 1051 (1991).

[100] D.P. Bhattacharya and S.N. Patra, Physica B 269, 206 (1999).

[101] K. Hess and C.T. Sah, Phys. Rev. B 10, 3375 (1974).

[102] S. Nag and D.P. Bhattacharya, J. Phys. Chem. Sol. 70, 1150 (2009).

[103] F.F. Fang and A.B. Fowler, J. Appl. Phys. 41, 1825 (1970).

[104] Y. Katayama, I. Yoshida, N. Kotera and K.F. Komatsubara, Appl. Phys. Lett. 20, 31 (1972).

[105] K. Hess, A. Neugroschel, C.C. Shiue and C.T. Sah, J. Appl. Phys. 46, 1721 (1975).

[106] T. Sato, Y. Takeishi, H. Tango, H. Ohnuma and Y. Okamoto, J. Phys. Soc. Jpn. 31, 1846 (1971).

[107] D.K. Ferry, Phys. Rev. B 14, 5364 (1976).

[108] K. Hess, Solid-State Electronics 21, 123 (1978).

[109] P.K. Basu and J.B. Roy, Physica Status Solidi (b) 121, 743 (1984).

[110] U. Sivan, A. Palevski, M. Heiblum and C.P. Umbach, Solid-St Electron. 33, 979 (1990).

[111] A.P. Dmitriev, V. Yu. Kachorovskii and M.S. Shur, J. Appl. Phys. 89, 3793 (2001).

[112] P.J. Price, J. Appl. Phys. 53, 6863 (1982).

[113] X.L. Lei, J.L. Birman and C.S. Ting, J. Appl. Phys. 58, 2270 (1985).

[114] M. Tomizawa, K. Yokoyama and A. Yoshii, IEEE Electron Device Lett. 5, 464 (1984).

[115] M. Inoue, H. Hayashi, G. Sasaki and S. Nakajima, Physica B+C 134, 327 (1985).

[116] T.J. Drummond, M. Keever, W. Kopp, H. Morkoc, K. Hess, B.G. Streetman and A.Y. Cho, Electronics Lett. 17, 545 (1981).

[117] J. Shah, A. Pinczuk, H.L. Störmer, A.C. Gossard and W. Wiegmann, Appl. Phys. Lett. 44, 322 (1984).

[118] Ming-Qi Weng and Hang-Sheng Wu, Acta Phys. Sin. 8, 682 (1999).

[119] Hang-Sheng Wu and Ming-Qi Weng, Phys. Stat. Sol. (b) 214, 107 (1999).

[120] Ming-Qi Weng and Hang-Sheng Wu, Phys. Stat. Sol. (b) 221, 831 (2000).

[121] Z.S. Gribnikov, K. Hess and G.A. Kosinovsky, J. Appl. Phys. 77, 1337 (1995).

[122] C. Jacoboni, *Theory of Electron Transport in Semiconductors*, Springer Series in Solid Sate Sciences, Vol. 165, Springer, Berlin, Heidelberg, 2010.

[123] V.L. Bonch-Bruevich and E.G. Landsberg, Phys. Stat. Sol. 29, 9 (1968).

[124] Z.S. Kachlishvili, Phys. Stat. Sol. (a) 33, 15 (1976).

[125] O.A. Aktsipetrov, A.A. Fedyanin, E.D. Mishina, A.N. Rubtsor, C.W. van Hasselt and M.A.C. Devillers, Phys. Rev. B 54, 1825 (1996).

[126] G. Lüpke, Surf. Sci. Rep. 35, 75 (1999).

[127] I.I. Maglevanny, V.A. Smolar and T.I. Karyakina, Superlattices Microstruct. 118, 29 (2018).

[128] O.A. Aktsipetrov and A.A. Fedyanin, Thin Solid Films 294, 235 (1997).

[129] O.A. Aktsipetrov, P.V. Elyutin, A.A. Fedyanin, A.A. Nikulin and A.N. Rubtsor, Surf. Sci. 325, 343 (1995).

[130] P.K. Kaw, J. Appl. Phys. 40, 793 (1969).

[131] P. Das, J. Appl. Phys. 40, 4206 (1969).

[132] S.S. Paul and D.P. Bhattacharya, Solid State Commun. 56, 527 (1985).

[133] S.S. Paul and D.P. Bhattacharya, J. Appl. Phys. 64, 4554 (1988).

[134] T.K. Pramanik and D.P. Bhattacharya, Solid State Commun. 59, 737 (1986).

[135] T.K. Pramanik and D.P. Bhattacharya, J. Appl. Phys. 69, 2555 (1991).

[136] S.N. Patra and D.P. Bhattacharya, J. Phys. Chem. Solids 57, 165 (1996).

[137] S.N. Patra and D.P. Bhattacharya, Physica B 216, 121 (1995).

[138] K. Seeger, J. Appl. Phys. 34, 1608 (1963).

[139] S. Kobayashi, S. Yabuki and M. Akoi, Jpn. J. Appl. Phys. 2, 127 (1963).

[140] D. Chattopadhyay and B.R. Nag, Int. J. Electronics 27, 443 (1969).

[141] M.S. Sodha and B.M. Gupta, Phys. Stat. Sol. 37, 311 (1970).

[142] H. Yamamoto and H. Iwasawa, Proc. IEEE 61, 504 (1973).

[143] D. Mukhopadhyay and S. Dey, Proc. IEEE 68, 746 (1980).

[144] D. Mukhopadhyay and S. Dey, Czech J. Phys. B 30, 469 (1980).

[145] A. Choudhury and D. Mukhopadhyay, Phys. Stat. Sol. (b) 113, K49 (1982).

[146] J.B. Scarborough, *Numerical Mathematical Analysis*, sixth ed., Oxford & IBH Publishing, 2005.

[147] C.F. Gerald, P.O. Wheatley, *Applied Numerical Analysis*, seventh ed., Pearson, India, 2008.

[148] V.V. Vainberg, A.S. Pylypchuk, N.V. Baidus and B.N. Zvonkov, Semiconductor Physics, Quantum Electronics & Optoelectronics, 16(2), 152 (2013).

[149] B. Laikhtman and R.A. Kiehl, Phys. Rev. B 47, 10515 (1993).

[150] W.T. Masselink, Phys. Rev. Lett. 66, 1513 (1991).

[151] K. Hirakawa and H. Sakaki, Phys. Rev. B 33, 8291 (1986).

[152] S. Gökden. Phys, Stat. Sol. (a) 200, 369 (2003).

[153] J.M.S. Orr, A.M. Gilbertson, M. Fearn, O.W. Croad, C.J. Storey, L. Buckle, M.T. Emeny, P.D. Buckle and T. Ashley, Phys. Rev. B 77, 165334 (2008).

[154] P.K. Ghosh and D. Chattopadhyay, Phys. Rev. B 48, 17177 (1993).

[155] C. Canali, C. Jacoboni, F. Nava, G. Ottaviani and A. Alberigi-Quaranta. Phys. Rev. B 12, 2265 (1975).

[156] B.K. Ridley, J. Phys. C: Solid State Phys. 15, 5899 (1982).

[157] S. Wang, *Fundamentals of Semiconductor Theory and Device Physics*, Prentice Hall, Englewood Cliffs, 1989.

[158] S. Tiwari, *Compound Semiconductor Device Physics*, Academic Press, New York, 1992.

[159] B.R. Nag, *Electron Transport in Compound Semiconductors*, Springer, Berlin, 1980.

[160] H. Daembkes, *Modulation-Doped Field-Effect Transistors: Principles, Design and Technology*, IEEE Press, Piscataway, New Jersey, 1991.

[161] H. Morkoc, H. Unlu and G. Ji, *Principles and Technology of MODFETs: Principles, Design and Technology*, Volumes 1 and 2, Wiley, New York, 1991.

[162] C.Y. Chang and F. Kai, *GaAs High-Speed Devices*, John Wiley & Sons, New York, 1991.

[163] M. Golio and D.M. Kingsriter, *RF and Microwave Semiconductor Devices Handbook*, CRC Press, Boca Raton, Florida, 2002.

[164] U.K. Mishra, P. Parikh and Y.F. Wu, Proc. IEEE 90, 1022 (2002).

[165] J.M. Redwing, M.A. Tischler, J.S. Flynn, S. Elhamri, M. Ahoujja, R.S. Newrock and W.C. Mitchel, Appl. Phys. Lett. 69, 963 (1996).